IntechOpen

Organic Rankine Cycle Technology for Heat Recovery

Edited by Enhua Wang

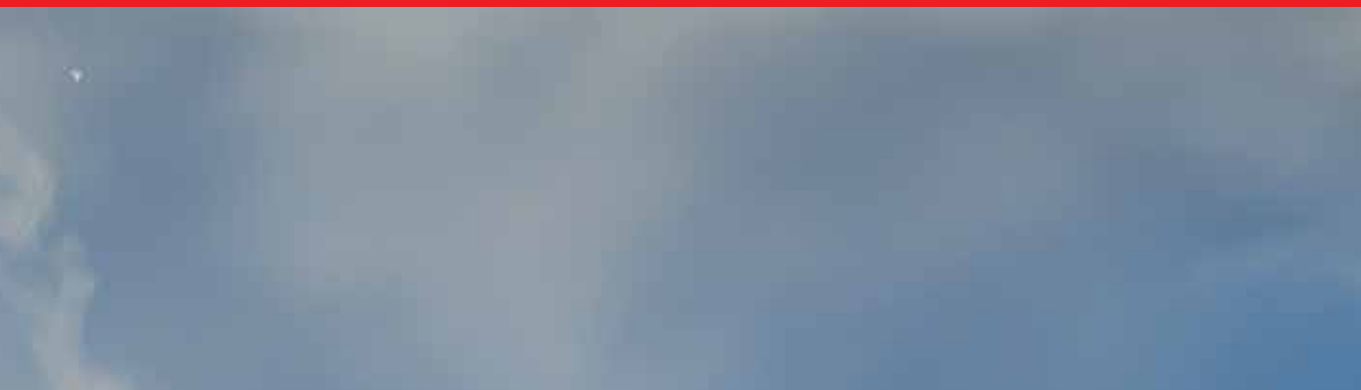

ORGANIC RANKINE CYCLE TECHNOLOGY FOR HEAT RECOVERY

Edited by **Enhua Wang**

Organic Rankine Cycle Technology for Heat Recovery
http://dx.doi.org/10.5772/intechopen.74127
Edited by Enhua Wang

Contributors

Bin Xu, Adamu Yebi, Zoran Filipi, Silvia Lasala, Romain Privat, Jean-Noel Jaubert, Junjiang Bao, Daejoong Kim, Deokhan Kim, Byung Ho Park, Kilsung Kwon, Longnan Li, Mohsen Assadi, Yaser Mollayi, Fuhaid Alshammari, Apostolos Pesyridis, Muhammad Usman, Davide Ziviani, Rémi Dickes, Vicent Lemort, James E. Braun, Eckhard A. Groll, Yiji Lu, Anthony Paul Roskilly, Xiaoli Yu, Frank Willems, Emanuel Feru, Srajan Goyal

Notice

First published in London, United Kingdom, 2018 by IntechOpen
eBook (PDF) Published by IntechOpen, 2019
IntechOpen is the global imprint of INTECHOPEN LIMITED, registered in England and Wales, registration number: 11086078, The Shard, 25th floor, 32 London Bridge Street
London, SE19SG – United Kingdom
Printed in Croatia

British Library Cataloguing-in-Publication Data
A catalogue record for this book is available from the British Library

Additional hard and PDF copies can be obtained from orders@intechopen.com

Organic Rankine Cycle Technology for Heat Recovery
Edited by Enhua Wang

p. cm.

Print ISBN 978-1-78984-347-7

Online ISBN 978-1-78984-348-4

eBook (PDF) ISBN 978-1-83881-773-2

Meet the editor

Enhua Wang has been an Associate Professor of energy and power engineering at the Beijing Institute of Technology since 2016, teaching courses on internal combustion engines. He attained his bachelor and master degrees at the Department of Automotive Engineering, Tsinghua University, in 2000 and 2003. In 2013, he received his PhD degree from the Beijing University of Technology in the field of engine combustion, conservation, and emissions control. He received a postdoctoral fellowship at the State Key Laboratory of Automotive Safety and Energy, Tsinghua University. In 2015, he worked at the School of Engineering, Glasgow University, as a research associate for one year. His research topics are organic Rankine cycle technology, simulation and control of the internal combustion engine, and hybrid-electric powertrains.

Contents

Preface

Utilization of low-grade heat energy, especially for medium and small power applications, is critical for a sustainable energy development strategy in our world. The organic Rankine cycle using a working fluid with a low boiling point can recover various kinds of low-grade heat energy effectively, which has great potential for industrial waste heat recovery such as internal combustion engines, combined heat and power systems. The energy efficiency can be enhanced and emissions can be decreased evidently by employment of organic Rankine cycle systems. Recently, with the progress of thermodynamic simulation technology, working fluids with good system performance and environmental properties are analyzed. Meanwhile, with the help of advanced software, methodologies for system design and optimization of organic Rankine cycle systems are developed. Rapid progress in computer-aided design and manufacturing technology makes it possible to design organic Rankine cycle systems for various applications.

This book on organic Rankine cycle technology presents nine chapters on research activities covering a wide range of current issues on the organic Rankine cycle: working fluid selection, component design, system analysis and optimization, dynamic modeling and control, system integration and testing, etc. In practice, these aspects must be taken into account together in order to fully utilize the potential of an organic Rankine cycle system. The contributions in this book have been separated into three sections. The first section deals with working fluid selection and component design mainly focused on expanders of organic Rankine cycles. The second section is related to dynamic modeling of organic Rankine cycles, starting from internal combustion engines to industrial power plants. The third section discusses industrial applications, including heat energy recovery from internal combustion engines, LNG cold energy recovery, and waste water heat energy utilization.

A comprehensive analysis of the technologies and applications of organic Rankine cycle systems is beyond the aim of the book. However, the content of this volume can be useful for scientists and students to broaden their knowledge of technologies and applications of organic Rankine cycle systems

I would like to thank IntechOpen Publisher for inviting me to be the editor of this volume, Ms. Maja Bozicevic, and the whole publishing process staff for their help in coordinating the reviews, editing, and printing of the book.

Enhua Wang
Associate Professor of Energy and Power Engineering
Beijing Institute of Technology, China

Section 1

Technologies

Chapter 1

Inert and Reactive Working Fluids for Closed Power Cycles: Present Knowledge, Applications and Open Researches

Silvia Lasala, Romain Privat and Jean-Noël Jaubert

Additional information is available at the end of the chapter

http://dx.doi.org/10.5772/intechopen.79290

Abstract

The possibility of selecting the working fluid of a closed power cycle represents one of the most important levers to maximise the efficiency and to optimise the design of this technology. This chapter is intended to provide a description of the present state of knowledge on the effects that fluid thermo-physical properties, such as molecular complexity and molecular mass, have on the design and performance of cycle components. With a view to allow for accounting for multicomponent inert and reactive working fluids along the optimisation process, the chapter then presents the main outstanding scientific barriers which need to be overcome.

Keywords: closed thermodynamic cycle, working fluid, inert and reactive mixture, thermodynamic properties, transformations, thermal stability

1. Introduction

The history of power production systems has been marked by the deployment of two main technologies: the water cycle and the open gas cycle. Both the engines owe their development to the possible exploitation of the traditional high-grade heat sources (i.e. characterised by a high maximum temperature and a huge thermal power), represented by the heat of combustion of fossil fuels. The achievement of a minimum acceptable efficiency level of these technologies requires the availability of a high thermal power, in the case of water cycles, and the achievement of a sufficiently high maximum temperature of the gaseous working fluid, in the case of gas cycles.

Nowadays, the recognised necessity of reducing the environmental impact of power 'production' processes has imposed the exploitation of non-traditional heat sources either recovered from industrial processes or made available by renewable energies (geothermal, biomass and solar thermal energy). These are typically characterised by a lower thermal power and a lower maximum temperature than thermal sources generated by the combustion of fossil fuels.

The efficient and economical recovery of these low-temperature thermal energies is made possible by the use of closed cycles in which the working fluid can be properly selected. Depending on the heat capacities of both the thermal source to be exploited and the cold sink where cycle heat is discharged, the use of different working fluids might be indeed more or less convenient, in terms of both energy conversion efficiency and components design.

Together with the optimisation of the cycle configuration ('process-design' approach), the possibility to define the optimal working fluid for each application ('product-design' approach) represents the greatest degree of flexibility to reduce the irreversibilities of any of these energy conversion processes and, thus, to maximise their efficiency.

Despite the pivotal role represented by the optimal selection of the working fluid, the scientific knowledge level on physicochemical thermodynamic and transport properties, thermal stability and environmental characteristics of fluids do merely allow the reliable utilisation of pure-component fluids.

This chapter aims, firstly, to present a review of the present knowledge level on this topic and, secondly, to highlight the main scientific gaps which currently limit the assessment of the energy potential of closed cycles operating with inert and reactive mixtures as working fluids.

2. The state of the art on working fluids for closed power cycles

Two main criteria exist to differentiate between working fluids, depending on whether they are pure or multicomponent, inert or reactive fluids. According to these classifications, inert fluids may be pure or multicomponent (typically binary) fluids, while reactive fluids may only be multicomponent fluids, as they are mixtures by definition. The advantage represented by the use of optimal inert fluids mainly lies in the possibility of reducing the irreversibilities occurring along the cycle; differently, reactive fluids may allow the substantial increase of the energy 'produced' during fluid expansion, thanks to the conversion of the chemical energy (other than the physical one) of the reactive fluid.

2.1. Inert pure fluids

Nowadays, pure fluids are mainly used as working fluids, among which water represents the pioneer for power cycles. Even now, water is the fluid which is mostly used in a closed thermodynamic cycle, in particular, in the Rankine cycle. The thermodynamic conversion of non-traditional thermal sources (geothermal, biomass, solar thermal and industrial waste heat recovery) is associated to a wide variety of powers, thermal grades and physical states of the

heat sources (liquid, gaseous or two-phase streams) which generally make the use of water cycles unsuitable. The thermodynamic properties of water, in fact, entail the necessity of adopting complex and expensive plant configurations, preventing from their use in low-temperature and low-power applications [1]. In these cases, the design of simple turbines and the occurrence of a single-phase vapour expansion are aspects of primary importance which direct the use of molecules being more complex and heavier than water, currently represented by organic fluids (hydrocarbons, fluorocarbons and siloxanes) [2].

Organic fluids are most conveniently used as subcritical working fluids in power production plants designed to recover heat wasted by industrial processes and many other low-medium-temperature applications. Organic fluids are used up to 400 °C, due to their limited thermal stability. Macchi has presented [2] a 'grey zone' of applications, characterised by an heat source temperature of 300–400 °C and a power output of 8–50 MW, where organic fluids could compete with water cycles.

Furthermore, the production of high-power outputs is conveniently associated with the use of either water or CO_2 cycles, giving preference to CO_2 for the high-temperature applications represented by solar energy (solar tower technology) and nuclear energy (IV generation of nuclear reactors) [3].

Moreover, it is worth highlighting that, besides the already attested application of high-temperature CO_2 power cycles, this technology may also be considered as a viable solution for the exploitation of medium-temperature heat sources (300–600 °C), competing with organic fluids and water [1].

The optimal choice between fluids for power systems designed to exploit medium-temperature and low-medium heat sources is thus not straightforward. The preferential use of a specific fluid in a particular range of power outputs and source temperatures results, in fact, from the techno-economical optimisation of these technologies, which maximises their efficiency and minimises their costs according to the specific constraints imposed by each application. Thermodynamic properties (in particular, specific molar heat capacities and critical properties) and the molar mass of each fluid influence the performance of the thermodynamic cycle and the design of components.

The nature of a selected pure working fluid does influence the performance of power cycles in the way its thermo-physical properties affect the thermodynamics of the cycle, turbomachines and heat exchanger efficiencies. Subsections 2.1.1 and 2.1.2 briefly introduce the foundations of such a statement.

2.1.1. Effect of fluid molecular complexity and mass on the performance and design of turbomachines

A preliminary classification of working fluids can be performed according to their molecular weight (first criterion) and to their molecular complexity (second criterion), the latter being related to the degrees of freedom of the molecule and, thus, to their molar heat capacity.

In general, one could erroneously think that more complex molecules are characterised, at all time, by a higher molecular weight. Although this is observable in the majority of cases, such a

conclusion is not universally correct. For example, carbon dioxide is characterised by a higher molecular complexity and a lower molecular weight with respect to krypton. This is shown in **Table 1**. The same table allows another similar comparison, between perfluorohexane and 1-undecanol, the former being heavier and molecularly simpler than the latter.

Molecular complexity influences the design and performance of a thermodynamic cycle, in such a way that complexity affects the degree of freedom of the molecule itself and, thus, the change in the thermodynamic properties of the fluid in response to energy interactions with the environment. In particular, a higher molecular complexity entails a lower adiabatic index, $\gamma = c_p/c_v$ (see **Table 1**) and, thus, a weaker temperature modification of the fluid, at a given pressure ratio, and a more important pressure change, at a fixed temperature ratio. Along an isentropic compression or expansion of molecules in the ideal gas state, temperature and pressure ratios are related by means of the molecular complexity:

$$T_2/T_1 = (P_2/P_1)^{\frac{\gamma-1}{\gamma}} = (v_2/v_1)^{1-\gamma} \tag{1}$$

By way of example, **Table 1** reports the temperature (or molar volume) and pressure changes, for each considered fluid, resulting from, respectively, pressure and temperature modifications. It can be observed, from **Table 1**, that complex molecules lead to compressions and expansions characterised by high optimal pressure ratios, high molar volume ratios and, thus, poorer turbomachine efficiencies.

Considering the expansion or the compression of different fluids characterised by equal temperature profiles, it is possible to state that turbomachines specific work, w, results to be proportional to the mass heat capacity of the fluid, $\bar{c}_p$, and, thus, to its molecular complexity, γ, and molar weight, M:

$$w \propto \bar{c}_p = \frac{\gamma}{\gamma\text{-}1}\frac{R}{M} \tag{2}$$

The axial size of turbomachines is influenced by the molecular complexity and the molar mass: as the maximum enthalpy change per stage of a turbomachine is limited, the higher the

Fluid	**He**	**Kr**	**CO_2**	**CH_4**	**C_6F_{14}**	**$C_{11}H_{24}O$**
	Helium	**Krypton**	**Carbon dioxide**	**Methane**	**Perfluorohexane**	**1-Undecanol**
M (g/mol)	3.02	83.8	44.01	16.05	338.04	172.31
$c^{\bullet}_{v,T=298.15\ K}/R(-)$	1.500	1.500	3.479	3.291	30.474	31.009
$c^{\bullet}_{p,T=298.15\ K}/R\ (-)$	2.500	2.500	4.479	4.291	31.474	32.009
$\gamma^{\bullet} = c^{\bullet}_p/c^{\bullet}_v$	1.667	1.667	1.287	1.304	1.033	1.032
$\theta^{\bullet} = (\gamma^{\bullet}\text{-}1)/\gamma^{\bullet}$	0.400	0.400	0.223	0.233	0.032	0.031
T_2/T_1; v_2/v_1 (with $P_2/P_1 = 4$)	1.74; 0.44	1.74; 0.44	1.48; 0.37	1.41; 0.35	1.06; 0.26	1.06; 0.26
P_2/P_1 (with $T_2/T_1 = 1.25$)	1.75	1.75	2.72	2.61	1122.28	1264.85

Table 1. Main characteristics of working fluids characterised by different molecular weight and molecular complexity.

specific heat capacity resulting from more complex or lighter molecules, the higher the number of stages of the turbomachine.

Moreover, it is possible to show that the radial dimensions of turbomachines depend only on the molecular complexity, the pressure and the temperature of the fluid. In particular, and contrary to axial extension, cross-sectional areas are minimised by the use of complex molecules that would reduce the volumetric flow of the stream.

To reduce the design complexity of turbomachines and to increase their efficiency (limiting the number of stages, the variation of volumetric flow and avoiding the occurrence of supersonic conditions), it is thus preferable to adopt **simple and heavy fluids**. The higher radial dimensions of turbomachines that would result from the use of simple molecules could be reduced by an increasing fluid pressure.

It is worth highlighting that the molecular complexity determines, in particular, the inclination of saturation vapour curve in the T-s diagram: the increase in temperature or in pressure results, respectively, in an increase or a decrease in saturated-vapour entropy. Depending on whether the influence of temperature or that of pressure overrides, the saturated-vapour curve slopes positively or negatively in the T-s plane (**Figure 2(a)** and **(c)**). In the case of (c), which concerns complex molecules, the expansion of saturated-vapour fluids in saturated Rankine cycles favourably occurs in the superheated vapour phase (the so-called 'dry' expansion), avoiding the inefficient expansion of the fluid in the two-phase region. Herein, a simple approach to allow for distinguishing between these two families of fluids is presented.

Assuming, for simplicity, that the vapour behaves as a perfect gas, it is possible to write that

$$ds_{gas}^{sat} = c_p^{\bullet} \frac{dT}{T} - R \frac{dP^{sat}}{P^{sat}} \tag{3}$$

Considering the Antoine equation for saturation pressure, $ln(P^{sat}) = A - B/T$, and its differential form:

$$\frac{dP^{sat}}{P^{sat}} = \frac{B}{T^2} dT \tag{4}$$

and substituting it into Eq. (3), it is possible to deduce

$$\frac{ds_{gas}^{sat}}{dT} = \frac{1}{T}\left(c_p^{\bullet} - R\frac{B}{T}\right) \tag{5}$$

or, defining $B^* = B/T_c$,

$$\frac{ds_{gas}^{sat}}{dT} = \frac{1}{T}\left(c_p^{\bullet} - R\frac{B^*}{T_r}\right) \tag{6}$$

Equation (6) shows that when the combination of $c_p^{\bullet}$ and of T_r of the fluid is such that $c_p^{\bullet} = R \cdot B^*/T_r$, the saturation vapour curve is vertical in the plane T-s. Practically, it is possible to observe the existence of an average value for B^* common to most of fluids. Considering Antoine equation in the reduced variables, $ln\left(P_r^{sat}\right) = A^* - B^*/T_r$, and letting it pass through the

critical point (P_r = 1, T_r = 1), it follows that $A^* = B^*$; optimising B^* for different fluids in the reduced temperature domain $T_r \in (0.75; 1)$, it is possible to observe that, for most common fluids, $B^* \sim 7$ (see **Figure 1**).

A very rough criterion to distinguish between fluids characterised by positively or negatively sloped saturation vapour curves consists in considering the saturation vapour curve in the temperature range identified by $T_r \in [0.65; 0.85]$ and comparing the perfect gas heat capacity of the fluid, $c_p^\bullet$, calculated at the intermediate temperature defined by $0.75 \cdot T_c$, with the two limits $R \cdot B^*/T_r = 70$ J/mol/K (with $B^* = 7$ and $T_r = 0.85$) and $R \cdot B^*/T_r = 90$ J/mol/K (with $B^* = 7$ and $T_r = 0.65$): fluids having a $c_p^\bullet$ ($T_r = 0.75$) > 90 J/mol/K are typically characterised by a retrograde saturation vapour curve, while fluids having $c_p^\bullet(T_r = 0.75) < 70$ J/mol/K most likely have a non-retrograde saturation vapour curve. Fluids with $c_p^\bullet(T_r = 0.75) \in [70$ J/mol/K; 90 J/mol/K] have, in general, quasi-isentropic saturation vapour curves (**Figure 2(b)**).

Beside the positive effect that the use of complex molecules has on dry expansions, they also entail the convenient similar gradient of vapour and liquid isobars, in the T-s plane (see **Figure 2**). Complex fluids are thus particularly suitable to exploit variable temperature heat sources.

2.1.2. Effect of fluid molecular complexity and mass on the performance and design of heat exchangers

The nature of the working fluid also affects the design of heat exchangers. Two aspects have to be considered in sizing heat exchangers: the capacity of the adopted fluid to exchange heat and the mechanical power consumed by compressors to enable the fluid flowing through the heat exchanger.

It is possible to show [4] that the most important parameter of an optimal heat transfer fluid is the molar mass, which should preferably be low (**light molecule**) to allow the maximisation of heat exchange coefficients. Heavy molecules would instead entail the adoption of heavy and expensive heat exchangers.

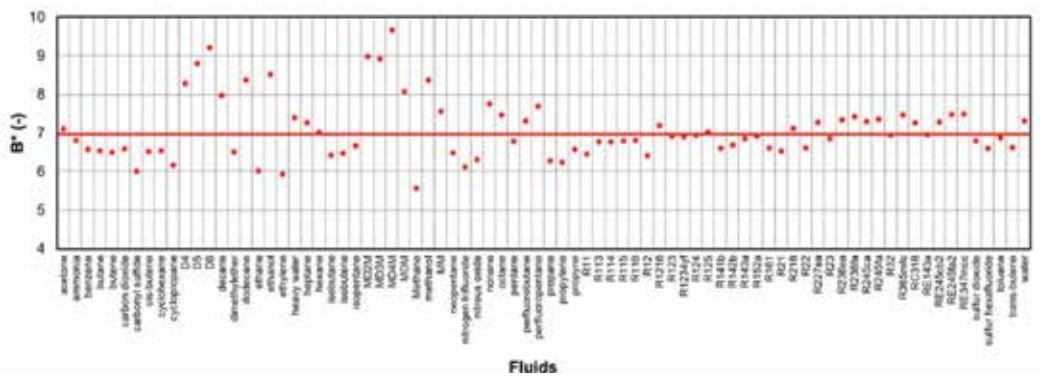

Figure 1. Parameter B* which minimises, for 90 considered fluids, the objective function $\sum_i \left(P_r^{sat}(T_i) - exp\,(B^* - B^*/T_{r,i})\right)^2$. Critical properties and saturation pressures, $P_r^{sat}(T_i)$, have been extracted from the NIST standard reference database 23, Refprop 9.1.

http://dx.doi.org/10.5772/intechopen.79290

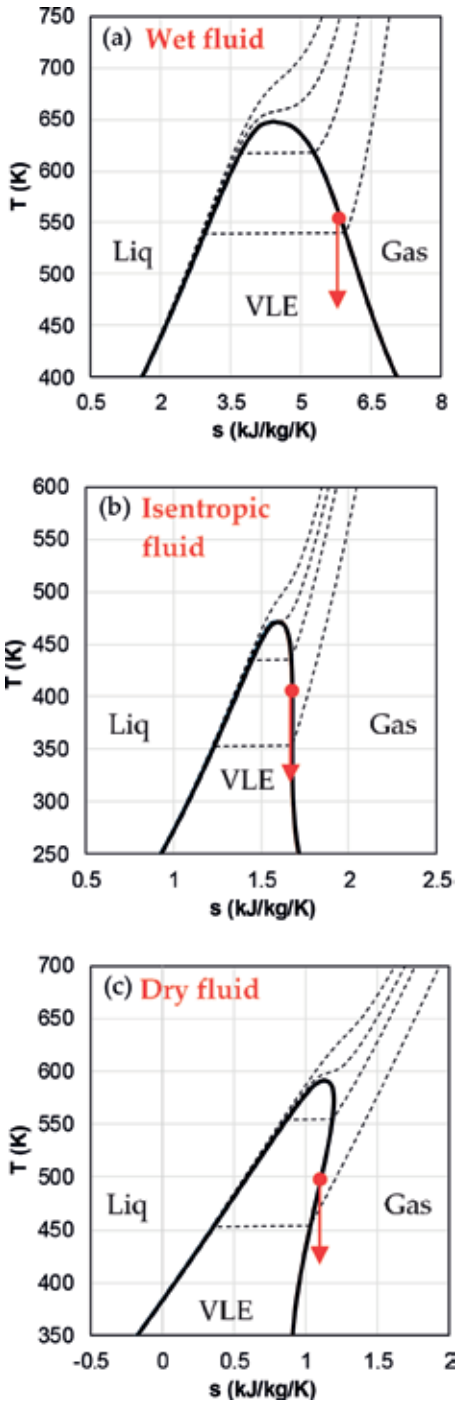

Figure 2. T-s diagrams of water (a) with isobars 5–35 MPa, R11, (b) and toluene (c) with isobars 0.5–6.5 MPa. For the sake of completeness, the red arrows indicate an isentropic expansion for the three considered fluids, from their saturated-vapour state.

Moreover, the low optimal compression ratios resulting from the use of **simple molecules** allow the reduction of the pressure levels of the fluid crossing the heat exchangers and, thus, of their sizes and investment costs.

2.1.3. Further considerations

As mentioned in Section 2.1.1, usually complex fluids are heavy fluids and, vice versa, simple fluids are light fluids. It is thus not straightforward to select an optimal fluid even considering only guidelines reported in Sections 2.1.1.

According to conclusions of Sections 2.1.1 and 2.1.2, it is always convenient to use simple molecules, from the point of view of the design and performance of both turbomachines and heat exchangers. However, the opposite effect that the molar mass of the fluid has on heat exchangers and turbomachines implies the necessity of solving a techno-economical optimisation problem.

2.2. Inert mixtures

There exist applications (an ensemble of hot and cold thermal sources and thermodynamic cycles) in which restricting the search for a working fluid in the range of available pure fluids highly limits the efficiency of the energy system. It is for this reason that, with the increasing interest to exploit a wider variety of thermal sources (other than combustion sources), in the 1990s, researchers started envisaging the possibility of using inert mixtures as working fluids, considering the selection of their composition as the most effective lever for the optimal design of closed thermodynamic cycles. The following two cases of closed power cycles represent blatant examples of the importance of utilising mixtures instead of pure working fluids to better optimise the heat exchange between working fluid and hot source and to reduce the power required for fluid compression.

2.2.1. Organic Rankine cycles

Cycles based on organic components, also called ORC (organic Rankine cycles), are mostly operated in subcritical modes (Rankine cycles). In such configurations, the isothermal evaporation and condensation of a pure fluid is the most efficient solution when the heat source and the cold sink present an isothermal profile. However, heat sources and/or sinks are usually available to these cycles with a variable temperature profile: typical heat sources are flue gases discharged by internal combustion power cycles (i.e. Brayton, Diesel and Otto engines), gaseous biomass combustion products, geothermal fluids and liquid solar fluids; variable temperature sinks are usually represented by liquid water heated for cogeneration purposes and/or cooling air used in the condenser.

In the case of variable temperature heat sources, the flexible adjustment of the composition of a zeotropic working fluid could allow the thermodynamically optimal matching between the variable temperature profile of the working fluid, characterised by a temperature glide, and the one of the thermal sources.

2.2.2. CO_2 condensation cycles

To exploit high-temperature heat sources (e.g. solar, nuclear and coal power plants) in the presence of low-temperature cooling sinks at less than 15–20 °C, carbon dioxide is usually proposed as an optimal working fluid in transcritical power cycles because of its critical properties, natural availability, corrosion-neutral properties and simpler turbomachinery design compared to helium Brayton cycles and water Rankine cycles.

However, when the available cooling source is, for example, air at ambient temperature (e.g. concentrated-solar-power technologies located in desert areas), CO_2 transcritical cycles cannot be used since the low critical temperature of pure CO_2, 31 °C, prevents CO_2 from condensation when air temperature is higher than 30 °C. To beneficiate from the use of transcritical cycles, instead of the more compression power consumer Brayton ones, it is useful to increase the critical temperature of pure CO_2 to 40–50 °C by adding a small quantity of a properly selected second component (inorganic compounds such as $TiCl_4$, $TiBr_4$, $SnCl_4$, $SnBr_4$, VCl_4, VBr_4, $GeCl_4$, fluorocarbons such as C_6F_{14}, etc.) to carbon dioxide [5–7]. In [5], it is shown how the critical temperature of the system may be increased by adding a small molar amount of C_6F_{14} or $TiCl_4$ to CO_2.

Similarly, the increase of the critical point of fluids allowed by the use of mixtures could also enable the more efficient use of condensing cycles instead of supercritical ones in very low-temperature applications. A typical example is represented by power cycles which reject their thermal heat into a stream of liquefied natural gas (cool source of the cycle), in order to convert it from liquid to vapour phase, from ambient temperature to −150 °C [8]. Currently, the use of particularly efficient pure fluids (e.g. nitrogen, argon, oxygen), which are fluids which critical temperature is lower than the minimum temperature achieved by the cycle, has been mainly proposed. Mixing one of these low critical temperature components with a small amount of a high critical temperature one (e.g. krypton) could allow the improvement of an increase of the critical temperature of the fluid and thus the lower-power consuming compression of a liquid instead of a gas.

2.2.3. Major scientific obstacles

Nowadays, the scale of the deployment of mixtures does not yet reflect the numerousness of studies undertaken to evaluate the potential of using multicomponent working fluids.

Despite the resources allocated in this research domain over the past years, this research topic still encounters some major scientific obstacles, described in the following sections 2.2.3.1–2.2.3.3, which feed the uncertainty surrounding the results of these studies and which limit the reliable use of multicomponent working fluids.

2.2.3.1. Thermodynamics of mixtures

The design of multicomponent working fluids requires mixing pure fluids characterised by some very different thermodynamic properties, which are typically critical coordinates or triple points and saturation properties.

Mixing different pure fluids (which generally involves two species) may result in a multicomponent system which thermodynamic properties highly deviate from those of each

pure component that forms the mixture. Such a deviation quantifies the level of non-ideality of the mixture (i.e. the importance of molecular interactions) and, thus, the difficulty in modelling its thermodynamic properties. An extreme typical example is represented by binary mixtures of type III (according to the classification of van Konynenburg and Scott) which present a specific composition range for which critical pressure achieves infinitely high values [5, 9].

The main issue affecting applied thermodynamics concerns the absence of a universal model (equation of state) which enables the reliable prediction of thermodynamic properties of mixtures characterised by a more or less pronounced level of non-ideality, without relying on experimental data. Still today, in fact, all the available equations of state contain parameters which need to be calibrated or, at least, validated over experimental data [10, 11].

However, the level of empiricism of thermodynamic models (mostly cubic and molecular-based equations of state) is decreasing over the years, meaning that parameters, which account for the incapability of the thermodynamic theory to model the reality, are more and more representative of physical quantities. For example, the modelisation of mixture properties by means of cubic equations of state requires the use of mixing rules to account for molecular interactions.

The application of more theoretically grounded mixing rules (e.g. the latest excess Helmholtz energy-based mixing rules instead of quadratic van der Waals mixing rules) enables the more accurate and reliable calculation of thermodynamic properties of mixtures [12, 13]. The same consideration also applies to molecular-based models [14, 15].

A typically recognised problem is the unreliable calculation of the critical region and two-phase thermodynamic properties of multicomponent working fluids intended for closed power cycles, by currently available thermodynamic models and, also, simulation tools based on inappropriate available algorithms.

Furthermore, the uncertainty of measurement of some thermodynamic properties (e.g. specific heat capacities or vapour-liquid equilibrium properties of highly non-ideal mixtures) is still too high to enable their reliable use for calibrating and validating models.

2.2.3.2. Transport properties of mixtures in two phase

The available scientific results on forced convection vaporisation or condensation of zeotropic mixtures are very limited. Many studies have analysed the performance of heat exchangers crossed by zeotropic fluids, without providing information on the local conditions in the evaporating streams [16].

The lack of information on transport properties actually feeds the overall uncertainty affecting heat exchangers sizing, on the one hand, and pressure drops evaluation, on the other.

2.2.3.3. Thermal stability of mixtures

The thermal stability of a working fluid or a mixture represents its capability to preserve all its main physical properties unchanged because of the heating. This is a key parameter for the selected working fluid in a power plant, since even a partial decomposition may cause loss of

power or, even worse, the occurrence of serious faults in fundamental components, such as turbines or heat exchangers. Moreover, as a general rule, the greater the thermal stability, the greater the maximum temperature at which the fluid can be used and the better the performance of the power plant.

Different approaches have been proposed so far to assess the thermal stability of pure fluids [17]. However, all experimental laboratories that investigate the thermal stability of fluids only focus on pure fluids, and, at present, an experimental technology being able to test the thermal stability of mixtures is still absent according to authors' knowledge.

2.3. Reactive fluids

Researches undertaken during the last years on working fluids have ignored the promising results published by a dozen scientists in the years 1960–1990 which reversibly proposed reactive working fluids for mainly military, spatial and power production applications.

Over that period, four reactive systems ($P_4 \rightleftarrows 2P_2$, $Al_2Cl_6 \rightleftarrows 2AlCl_3$, $2NOCl \rightleftarrows 2NO + Cl_2$, $N_2O_4 \rightleftarrows 2NO_2 \rightleftarrows 2NO + O_2$) and two generalised reacting schemes ($A_2 \rightleftarrows 2A$; $2A \rightleftarrows 2B + C$) have been considered. Preliminary results obtained in these studies have shown that the utilisation of certain reactive fluids (N_2O_4, NOCl) rather than pure fluids and inert mixtures can lead to the increase of the conversion efficiency of power cycles of more than 10 percentage points [18–20].

In particular, it has been observed [18, 19, 21–24] that such an improvement follows from the specific evolution of the equilibrium composition of the reactive fluid and from the involvement of the energy of reaction; more precisely, authors attested that the presence of a proper chemical reaction leads to the increase of the power output, resulting from the augmented (1) energy released by the fluid during expansion and (2) energy exchanged in heat exchangers, thanks to the increased heat capacity and coefficients of heat exchange of reactive fluids.

It can be easily shown that the adoption of reactive fluids characterised by an exothermic reaction ($\Delta_R H^\circ < 0$) along fluid expansion leads to an increased production of produced work (δw):

$$\delta w \overset{\text{Adiab.}}{\leftarrow} dh \underset{\text{gas}}{\overset{\text{Perfect}}{=}} c_p\, dT + \left(\frac{\partial h}{\partial P}\right)_{T,n} dP + \Delta_R H^\circ \frac{d\dot{\xi}}{\dot{m}} = \underbrace{c_p^*\, dT}_{<0 \text{ along fluid expansion}} + \Delta_R H^\circ \frac{d\dot{\xi}}{\dot{m}} \tag{7}$$

Despite the promising results revealed by these studies on reactive fluids, nonetheless obtained under simplification assumptions of perfect gas mixtures, researches on reactive working fluids have been abandoned at their preliminary stage of development. Many scientific obstacles, in fact, limited and still limit the applicative study of reactive working fluids.

2.3.1. Major scientific obstacles

Knowledge gaps listed in Section 2.2.3, which regard the thermodynamics, transport properties and thermal stability of mixtures, clearly represent barriers for the deployment of reversible reactive working fluids too, as they are, by definition, mixtures. Moreover, the extensive analysis of the potentiality offered by the specific use of these fluids would also require addressing the specific lacks briefly described subsequently.

2.3.1.1. Thermodynamics of adiabatic expanding and compressing fluids, which undergo reversible and instantaneous reactions

So far, thermodynamic transformations of fluids in expanders and compressors have only been studied under the assumption of inert fluid. The preliminary researches on reactive fluids do not report any indication about the thermodynamic treatment of the expansion/compression of a reactive fluid.

Different from inert (iso-composition) gaseous adiabatic expansions, which are isentropic in the case of zero thermodynamic losses, reactive expanding fluids need to be modelled as a series of infinitesimal expansions, of pressure variation dP, each one subdivided into two transformations: (1) iso-composition adiabatic expansion, from pressure P to pressure $P + dP$; and (2) adiabatic isobar reaction, at the pressure $P + dP$.

No one theoretical reference has been found in the study that analyses this thermodynamic transformation.

2.3.1.2. Theoretical comprehension of the dependence of cycle performance and design on the type of chemical reaction

There exist many types of chemical reactions which, in the direction of their spontaneous evolution, may be characterised by a fast or a slow kinetics, by an increasing or a decreasing number of moles and which may be exothermic or endothermic. The effect of the occurrence of a reaction during fluid expansion or compression, fluid heating or cooling depends on its characteristics, which can beneficiate or disadvantage the efficiency of the energy conversion process.

With the aim of expanding the research of optimal working fluids to reactive mixtures, it is necessary to preliminarily address these points.

3. Conclusion

This chapter aims to boost researches devoted to the comprehension of the impact on power cycles of the characteristics of their working fluid. To this end, the chapter presents the state of the art on pure and multicomponent inert and reactive working fluids, highlighting the major scientific obstacles that nowadays primarily need to be overcome in order to allow a thorough research of the best working fluid for each application of closed power cycles:

- definition of a predictive and universal thermodynamic model for mixtures;
- experimental and theoretical investigation of the transport properties of mixtures;
- experimental and theoretical assessment of mixture thermal stability;
- comprehension of the effects that reactive fluid characteristics have on cycle performance and design.

Acknowledgements

The authors wish to thank ASME IGTI ORC Power Systems—KCORC for funding the publication of this chapter.

Nomenclature

Symbols

T	temperature
P	pressure
h	molar enthalpy
s	molar entropy
$\Delta_R H^\circ$	enthalpy of reaction
$\dot{\xi}$	rate of extent of reaction
$\dot{m}$	mass flow rate
M	molar weight
c_p, c_v	molar heat capacity at constant pressure and constant volume
v	molar volume
A, B, A^*, B^*	parameters
w	specific work
R	universal gas constant

Subscripts

c	critical property
r	reduced property

Superscripts

•	perfect gas property
sat	saturation property

Accents

—	specific mass property

Author details

Silvia Lasala*, Romain Privat and Jean-Noël Jaubert

Address all correspondence to: silvia.lasala@univ-lorraine.fr

Ecole Nationale Supérieure des Industries Chimiques, Laboratoire Réactions et Génie des Procédés, Université de Lorraine, Nancy, France

References

[1] Astolfi M, Alfani D, Lasala S, Macchi E. Comparison between ORC and CO_2 power systems for the exploitation of low-medium temperature heat sources. Energy. 2018

[2] Macchi E. 1 – Theoretical basis of the organic Rankine cycle. In: Organic Rankine Cycle (ORC) Power Systems. 2017. pp. 3-24. Available from: https://doi.org/10.1016/B978-0-08-100510-1.00001-6

[3] Dostal V, Hejzlar P, Driscoll MJ. The supercritical carbon dioxide power cycle: Comparison to other advanced power cycles. Nuclear Technology. 2006;**154**(3):283-301. Available from: https://doi.org/10.13182/NT06-A3734

[4] El-Wakil MM. Nuclear Power Engineering. New York, USA: Mc Graw-Hill; 1962. 556 p.

[5] Lasala S, Bonalumi D, Macchi E, Privat R, Jaubert JN. The design of CO_2-based working fluids for high-temperature heat source power cycles. In: Energy Procedia. 2017. pp. 947-954. Available from: https://doi.org/10.1016/j.egypro.2017.09.125

[6] Lasala S, Invernizzi C, Iora P, Chiesa P, Macchi E. Thermal stability analysis of Perfluorohexane. Energy Procedia. 2015;**75**. Available from: https://doi.org/10.1016/j.egypro.2017.09.125

[7] Bonalumi D, Macchi E, Lasala S. Miscele a base di anidride carbonica come fluido di lavoro in cicli termodinamici. 2017

[8] Invernizzi CM, Iora P. The exploitation of the physical exergy of liquid natural gas by closed power thermodynamic cycles. An overview. Energy. 2016;**105**:2-15. Available from: https://doi.org/10.1016/j.energy.2015.09.020

[9] Privat R, Jaubert J-N. Classification of global fluid-phase equilibrium behaviors in binary systems. Chemical Engineering Research and Design. 2013;**91**(10):1807-1839. Available from: https://doi.org/10.1016/j.cherd.2013.06.026

[10] Lasala S, Chiesa P, Privat R, Jaubert J-N. Optimizing thermodynamic models: The relevance of molar fraction uncertainties. Journal of Chemical & Engineering Data. 2017 Feb 9; **62**(2):825-832. Available from: http://doi.org/10.1021/acs.jced.6b00853

[11] Lasala S, Chiesa P, Privat R, Jaubert J-N. Modeling the thermodynamics of fluids treated by CO_2 capture processes with Peng-Robinson + residual Helmholtz energy-based mixing rules. Industrial and Engineering Chemistry Research. 2017;**56**(8). Available from: http://doi.org/10.1021/acs.iecr.6b04190

[12] Lasala S, Chiesa P, Privat R, Jaubert J-N. VLE properties of CO_2–based binary systems containing N_2, O_2 and Ar: Experimental measurements and modelling results with advanced cubic equations of state. Fluid Phase Equilibria. 2016;**428**:18-31. Available from: https://doi.org/10.1016/j.fluid.2016.05.015

[13] Lasala S. Advanced Cubic Equations of State for Accurate Modelling of Fluid Mixtures. Application to CO_2 Capture Systems. Italy: Politecnico di Milano; 2016

[14] Economou IG. Statistical associating fluid theory: A successful model for the calculation of thermodynamic and phase equilibrium properties of complex fluid mixtures. Industrial and Engineering Chemistry Research. 2002;**41**(5):953-962. Available from: http://doi.org/10.1021/ie0102201

[15] Tan SP, Adidharma H, Radosz M. Recent advances and applications of statistical associating fluid theory. Industrial and Engineering Chemistry Research. 2008;**47**(21):8063-8082. Available from: http://doi.org/10.1021/ie8008764

[16] Incropera FP, DeWitt DP, Bergman TL, Lavine AS. Fundamentals of Heat and Mass Transfer. Vol. 6, Water. 2007. 997 p. ISBN: 978–0471457282

[17] Invernizzi CM, Bonalumi D. 05 – Thermal stability of organic fluids for organic Rankine cycle systems. In: Organic Rankine Cycle (ORC) Power Systems. 2017. pp. 121-151. Available from: http://doi.org/10.1016/B978-0-08-100510-1.00005-3

[18] Stochl RJ. Potential Performance Improvemet Using a Reacting Gas (Nitrogen Tetroxide) as the Working Fluid in a Closed Brayton Cycle - NASA TM-79322; 1979

[19] Angelino G. Performance of N_2O_4 gas cycles for solar power applications. Proc Inst Mech Eng 1847–1982 (vols 1–196). 1979;**193**:313-320. Available from: https://doi.org/10.1243/PIME_PROC_1979_193_033_02

[20] Huang HM, Govind R. Use of dissociating gases in Brayton cycle space power systems. Industrial and Engineering Chemistry Research. 1988;**27**:803-810. Available from: https://doi.org/10.1021/ie00077a015

[21] Huang SH, Radosz M. Equation of state for small, large, polydisperse and associating molecules. Industrial and Engineering Chemistry Research. 1990;**29**:2284-2294. Available from: http://doi.org/10.1021/ie00107a014

[22] Cheung H. Dissociating gas as a working fluid for space plant. Energy Convers. 1968;**8**: 125-128. Available from: https://doi.org/10.1016/0013-7480(68)90114-9

[23] Hasah MZ, Martin RC. Use of dissociating gases as primary coolants and working fluids in power cycles for fusion reactors. IASMiRT; 1989. Available from: https://repository.lib.ncsu.edu/bitstream/handle/1840.20/29799/DC_250636.pdf?sequence=1&isAllowed=y

[24] Jacobs TA, Lloyd JR. The influence of the equilibrium dissociation of a diatomic gas on Brayton-cycle performance. Journal of Applied Mechanics. 1963:288-290. Available from: https://doi.org/10.1115/1.3636527

Chapter 2

Effects of the Working Fluid Charge in Organic Rankine Cycle Power Systems: Numerical and Experimental Analyses

Davide Ziviani, Rémi Dickes, Vincent Lemort,
James E. Braun and Eckhard A. Groll

Additional information is available at the end of the chapter

http://dx.doi.org/10.5772/intechopen.78026

Abstract

It is well known that organic Rankine cycle (ORC) power systems often operate in conditions differing from the nominal design point due to variations of the heat source and heat sink conditions. Similar to a vapor compression cycle, the system operation (e.g., subcooling level, pump cavitation) and performance (e.g., heat exchanger effectiveness) of an ORC are affected by the working fluid charge. This chapter presents a discussion of the effects of the charge inventory in ORC systems. In particular, both numerical and experimental aspects are presented. The importance of properly predicting the total amount of working fluid charge for optimizing design and off-design conditions is highlighted. Furthermore, an overview on state-of-the-art modeling approaches is also presented.

Keywords: off-design, working fluid charge, modeling, subcooling, charge-sensitive

1. Introduction

Organic Rankine cycle (ORC) systems are widely acknowledged as one of the most suitable technologies for harvesting medium- to low-grade heat sources (i.e., below 300°C) from both renewable sources (e.g., geothermal and solar) and waste heat [1]. Nowadays, the total power capacity installed worldwide is estimated to be above 2.7 GWe, as reported by Tartière et al. in the ORC World Map [2, 3]. Furthermore, there has been a continuous increase in research activity related to ORC-based power systems over the last decades that has demonstrated the value of this technology and its potential to improve energy sustainability [4].

Generally, ORCs are designed and optimized for steady-state operating conditions, unless mobile applications are considered. However, in the vast majority of stationary applications (e.g., solar thermal power, geothermal, waste heat recovery, and combined heat and power), the heat source and heat sink conditions are subjected to fluctuations and the ORC systems often operate at part-load or off-design conditions. To this end, numerical and experimental studies on off-design ORC performance have been published in the scientific literature, as outlined by Dickes et al. [5]. Similar to vapor compression systems, ORC performance is sensitive to working fluid charge and an incorrect charge level affects the system performance, especially under part-load conditions. Yet, very limited work can be found on the impact of working fluid charge on off-design operations. In fact, besides the research conducted by the Authors [6–8], only two additional studies could be found in the literature. Liu et al. [9] discussed the effect of different working fluid charge masses on the system performance. Experimental and numerical analyses were carried out to identify the optimal working fluid charge. Pan et al. [10] analyzed the impact of the working fluid charge on the length distribution of the different zones in the heat exchangers under several operating conditions. Furthermore, different void fraction models and heat transfer correlations were compared to assess their impact on the working fluid mass estimations in the heat exchangers.

The present chapter discusses the relationship between working fluid charge and performance in ORC systems under different operating conditions. Furthermore, the fundamentals of deterministic numerical methods to account for working fluid charge in ORC simulations are also described.

2. Importance of working fluid charge in ORC systems

A general sub-critical ORC with an internal heat exchanger (or regenerator), as shown in **Figure 1**, is considered as an example to understand the effect of working fluid charge. Although this chapter focuses on sub-critical ORC systems, the principles and the methodologies discussed hereafter can be extended to transcritical cycles and other cycle configurations [11]. By referring to **Figure 1**, the system consists of three heat exchangers (e.g., brazed plate heat exchangers), a pump (either centrifugal or volumetric type), a positive displacement expander (e.g., scroll type), a liquid receiver (or buffer tank), and line sets (or pipelines) between each component. Depending on the type of expander (e.g., single- and twin-screw, swash plate, or scroll), a dedicated oil-injection loop with an additional pump may be present in the system (see **Figure 1**). An oil separator is typically installed after the expander to avoid accumulation of the lubricant oil inside the heat exchangers, where hot spots may occur.

The operation of a sub-critical ORC encompasses several aspects that are common to refrigeration systems, such as the control of the subcooling at the condenser outlet and the degree of superheating at the evaporator outlet, single- and two-phase heat transfer in the heat exchangers, as well as working fluid leaks. The amount of working fluid charged into the system has a direct effect on the performance, the flexibility, as well as on the operational costs

http://dx.doi.org/10.5772/intechopen.78026

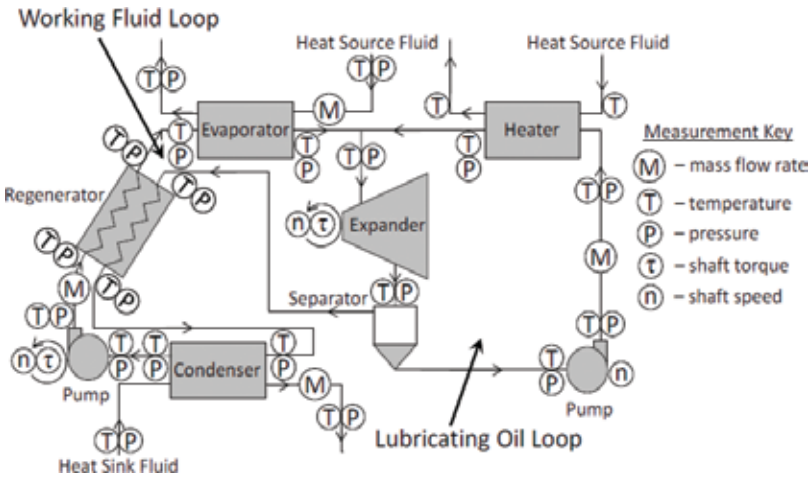

Figure 1. General schematic of a regenerative organic Rankine cycle system. An independent lubricant oil loop is also included for completeness. Typical location of the sensors is also shown.

of the unit. The costs associated with the working fluid and possible working fluid losses due to leaks can be significant, especially in large-scale systems (up to 10% of the plant cost) [12].

With respect to the system behavior, when the operating conditions shift from design to off-design, the working fluid charge migrates within the system, altering the transition between single-to two-phase heat transfer regimes inside the heat exchangers. If the system is over-charged, typically the length (or, equivalently, the spatial fraction) of the subcooled zone in the evaporator increases, reducing both the capacity and degree of superheating. However, if the system is under-charged, one of the drawbacks is the decrease of subcooling at the condenser outlet, which may cause the pump to cavitate [13]. Additionally, a liquid receiver can be installed before the pump, as shown in **Figure 1**, in order to compensate for charge migration during off-design conditions, especially in large scale ORC systems. Nevertheless, a non-proper charge level may completely empty or flood the liquid receiver.

The estimation of the optimum charge level is particularly challenging when additional aspects of the normal ORC operation are considered. In particular, lubricant oil may be pre-mixed with the working fluid to ensure the correct functioning of positive displacement expanders. In other cases, oil-separators are utilized to separate the working fluid from the lubricant oil at the expander outlet. However, oil entrainment in the vapor and oil solubility affect the distribution of charge in the system. Furthermore, non-condensable gases can also be present inside the system, which can impact the operation of the ORCs by altering the condensing pressure [14].

Based on the aforementioned reasoning, appropriate numerical methodologies are required to predict the performance of the system and to account for the total working fluid charge in a deterministic way such that the system model resembles the actual behavior of the system. Experimental results are also necessary to validate such numerical methods and to conduct additional analyses. Therefore, in the following sections, the state-of-the-art numerical methods utilized to simulate ORC systems are described and their limitations are also highlighted.

3. Charge-sensitive ORC modeling approaches

Modeling of ORC systems is typically performed for steady-state conditions using purely thermodynamic considerations. Assumptions are made regarding the minimum temperature difference (i.e., the pinch point) between the working fluid and the heat source and heat sink fluids. The degrees of subcooling at the pump inlet and superheat at the expander inlet are set, as well as the condensing and evaporating temperatures. Constant values of isentropic efficiency for the pump and expander are often assumed. Then, the cycle is solved by computing the enthalpy of the working fluid at each state point and assuming the pump and expander to be adiabatic. This type of simplified model works well as an initial working fluid screening tool and to broadly assess cycle performance trends. However, in such a model, the physical characteristics of the system components are not taken into account. It follows that a more detailed model is necessary to study the behavior of a real ORC system in off-design conditions. Such a detailed model also typically estimates the steady-state response of the system, although dynamic models have been constructed from similar considerations [15]. For the scope of this chapter, the following discussions will be limited to steady-state modeling.

3.1. Definition of a mechanistic model for ORC system

Detailed off-design models of ORC systems are built by connecting together different submodels for each component of the system and are implicitly solved by driving to zero a number of residuals to ensure that the solution is within a physical domain. Such detailed models are based upon the extensive literature available for vapor compression cooling and heat pumping systems [16, 17]. A recent overview of off-design steady-state performance studies and modeling applied to ORC systems can be found in [8].

Generally, an ORC system model can be regarded as mechanistic if the inputs and the known parameters are similar to those an ORC operator would know in practice. The model then uses physical principles and empirical or semi-empirical component models to simulate system performance given these parameters, inputs and boundary conditions. An ORC system model requires knowledge of the pump and expander displacements, the heat exchangers geometry, and the total system volume. Such a model receives as inputs the working fluid type, the inlet temperature and mass flow rate of the source and sink fluids, the rotational speeds of the pump and expander, and the condenser exit subcooling or the total working fluid charge in the system. A truly mechanistic model is charge-sensitive, meaning the total refrigerant charge is known, but the condenser exit subcooling is determined by the ORC operation [5]. In fact, if the condenser exit subcooling is fixed within the simulation, an assumption is made regarding the system state, which is not known in a real system. Outputs of the model include rotating equipment efficiency, system efficiency, heat transfer rates, condensing and evaporating temperatures, and net power production. In addition, a Second Law analysis can also be applied to estimate the system irreversibilities [18].

A detailed ORC model such as the one described above can give information about off-design performance, working fluid charge sensitivity, migration of charge between operating points, pressure drops, and the impact of working fluid transport properties on the heat transfer processes. Although, it only applies to the exact system being modeled, it provides a general framework (see for example *ORCmKit* library [19]) whereby other systems can be simulated by adjusting the geometric parameters of the model.

While constructing a charge-sensitive model, a number of challenges, both numerical and thermophysical, need to be considered:

- Since the entire ORC model is obtained by connecting several sub-models representing the system components and a number of residuals are necessary to ensure a physically-meaningful solution, a robust solution scheme is required to perform charge-sensitive simulations with reasonable computational efforts.
- Due to the presence of multiple heat transfer mechanisms, pressure drops, and flow regimes inside the heat exchangers, it is important to properly identify the convective heat transfer coefficients in multi-zone heat exchangers and understand how the working fluid charge can improve the reliability of estimating such coefficients.
- The charge estimation inside the heat exchangers relies on the proper knowledge of spatial fraction occupied by each zone (i.e., single-phase liquid or vapor, two-phase) as well as the estimation of the working fluid density. In the case of single-phase zones, such calculation is straightforward. However, in the case of two-phase zones, the density depends on the pressure, temperature, quality, and flow regime through the void fraction. Void fraction models directly impact the charge estimation.
- Presence of a liquid receiver in the system.
- Difficulties in accounting all the system volumes (e.g., valves, sight glasses, filters, sensors, and line sets).
- Estimation of working fluid dissolved in lubricant oil.
- Correctness of the model in predicting the total working fluid charge with different working fluids.
- Uncertainties associated with the exact amount of working fluid charge present in the actual system.

In order to address the majority of these modeling aspects, general guidelines for developing charge-sensitive models are discussed in the following section. Among these aspects, heat transfer correlations and the length of each zone inside the heat exchangers account for the majority of the inaccuracy in charge estimations. However, it will be shown in Section 4.3 that the solubility of working fluid in oil can also be significant. A charge tuning scheme can be applied to improve the accuracy of charge estimation, as outlined in Section 3.3. Experimental results from a test case will be used to address the last three bullet points in Section 4.

3.2. Overall charge-sensitive model description

As aforementioned, the individual components are properly arranged to form the overall cycle model. By referring to the ORC schematic of **Figure 1**, two general approaches can be identified to assemble the cycle models, which are shown as block diagrams in **Figures 2** and **3**, respectively. By looking at the two diagrams, it appears evident that the major cycle components, that is, heat exchangers, pump and expander, are arranged in the same fashion. The major difference is the approach adopted to account for the line sets connecting the active components and, therefore, the associated pressure drops and heat losses. The approach shown in **Figure 2** retains the physical description of the cycle with the line set sub-models placed between two consecutive cycle components. It follows that an accurate description of each line set, including internal and external diameters as well as equivalent length, is required. Whereas, in the block diagram of **Figure 3**, the line set losses are lumped into two single artificial components representing high- and low-pressure sides of the systems. These lumped components are placed at the outlet of the evaporator and the condenser, respectively.

Each block diagram also determines the required initial guess values and the residual to be driven to zero to solve the system. In particular, in the case of the block diagram of **Figure 2**, the five initial guesses are the pump inlet specific enthalpy ($h_{pump,suc}$), the pump inlet and outlet pressures ($p_{pump,suc}$, $p_{pump,dis}$), the expander inlet specific enthalpy ($h_{\exp,suc}$), and the expander outlet pressure ($p_{\exp,suc}$). Such guesses are chosen because of the presence of the regenerator in

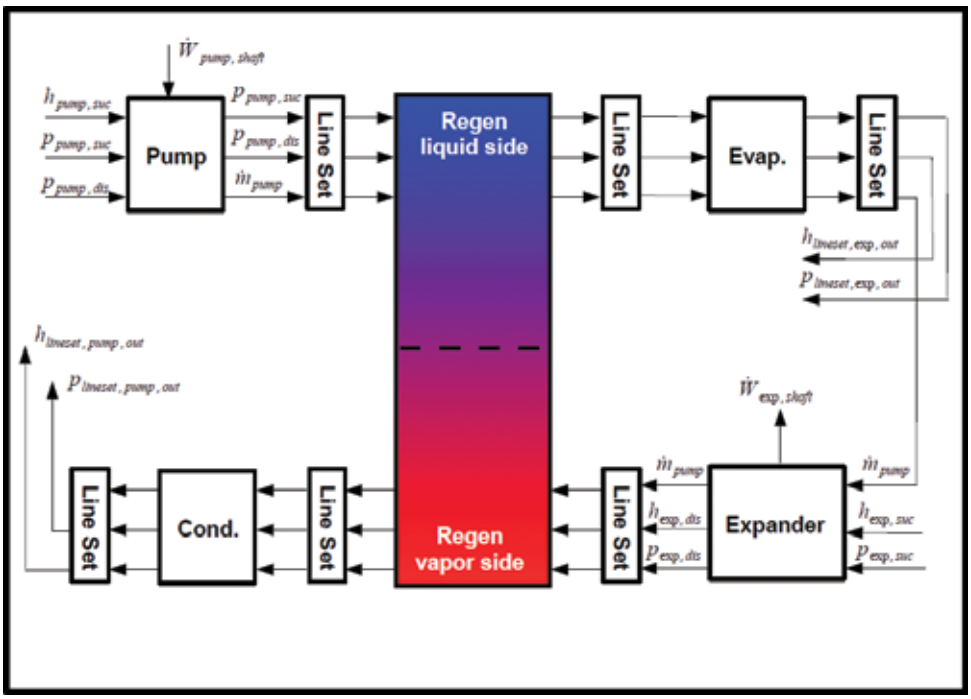

Figure 2. Block diagram showing how the individual component models are arranged to form the overall ORC model. Variables are updated as they pass through each component (adapted from [7]).

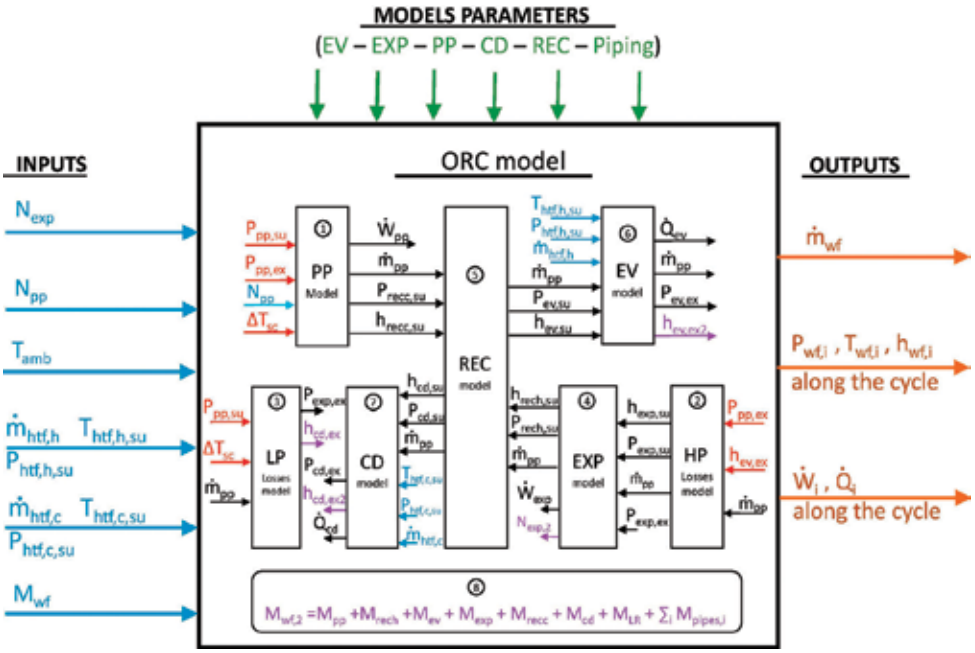

Figure 3. Block diagram showing the solver architecture of the charge-sensitive ORC model proposed by Dickes et al. [8]. The inputs are indicated in blue, the outputs in brown, the parameters in green, the iteration variables in red and the model residuals in violet.

the cycle and to ensure stability of the code. Given the set of guess values, an iteration of the cycle model consists of solving the components in the following order: pump and pump discharge line set, expander and expander discharge line set, regenerator and regenerator exit line sets for liquid and vapor sides, evaporator and expander suction line set, and condenser and pump suction line set. The solution of the cycle model is enforced by five residuals. In particular, four residuals ensure the continuity of thermodynamic states between two consecutive components. These are:

$$\begin{aligned} \Delta_1 &= h_{pump,suc} - h_{lineset,pump,out}; \quad \Delta_2 = p_{pump,suc} - p_{lineset,pump,out} \\ \Delta_3 &= h_{\exp,suc} - h_{lineset,\exp,out}; \quad \Delta_4 = p_{\exp,suc} - p_{lineset,\exp,out} \end{aligned} \tag{1}$$

The fifth residual is associated with the total system charge, which is estimated by summing all the charge contributions:

$$\Delta_{5,charge} = m_{evap} + m_{cond} + m_{regen} + m_{pump} + m_{\exp} + m_{tank} + \sum_i m_{lineset,i} - m_{wf} \tag{2}$$

where the mass of working fluid for each component is given by $m_{wf,component} = V_{component}\rho_{wf}$. Particular attention has to be given to computing the averaged density of the working fluid, ρ_{wf}, to account for single-, two-phase conditions for both pure working fluids or mixtures, as will be discussed in more detail in Section 3.3. Furthermore, it can also be mentioned that the

fifth residual associated with the total charge, $\Delta_{5,charge}$, is usually replaced by the difference between the imposed and calculated condenser exit subcooling in many off-design simulation models proposed in literature.

In the case of the block diagram of **Figure 3**, the model iterates on the evaporator outlet specific enthalpy ($h_{evap,ex}$), pump inlet and outlet pressures ($p_{pump,su}$, $p_{pump,ex}$), and condenser outlet subcooling (ΔT_{sc}). The residuals to be minimized are the condenser outlet specific enthalpy, the evaporator outlet specific enthalpy, the expander rotational speed, and the total system charge:

$$\Delta_1 = 1 - \frac{h_{cd,ex,2}}{h_{cd,ex,2}}; \quad \Delta_2 = 1 - \frac{h_{ev,ex,2}}{h_{ev,ex,2}}; \quad \Delta_3 = 1 - \frac{N_{\exp,2}}{N_{\exp}}; \quad \Delta_4 = 1 - \frac{m_{wf,2}}{m_{wf}} \tag{3}$$

where the total working fluid charge is calculated by employing an analogous expression to that one appearing in Eq. (2).

In both solution schemes, the resulting problem to be solved is multi-dimensional, leading to possible convergence issues when the charge is imposed. To increase the robustness of the model, a multi-stage solver can be employed to run the simulations. Dickes et al. [8] described these ad-hoc solvers in detail. The thermophysical properties of the working fluid can be retrieved either from CoolProp [20] or REFPROP [21].

In order to simulate the entire cycle, different sub-models are required to characterize each of the components. In the context of charge-sensitive modeling, the heat exchangers typically have the largest volumes in the system and are subjected to varying flow regimes, as outlined in Section 3.3. However, pump, expander, liquid receiver, and line sets also require proper modeling. Particular emphasis is given to estimate the working fluid charge in each of these components. For an extensive description and examples of these models, the reader is invited to referred to [5–8, 19].

As a general overview, the rotating equipment is modeled by using one or more of the following approaches: (i) a performance map based on experimental data (black box models); (ii) physics-based models with empirically determined parameters (gray box models); (iii) entirely physics-based models (white box models). Semi-empirical models are usually preferred as a compromise between physical-characteristics (e.g., under- over-expansion/compression, pressure drops, heat transfer and mechanical losses) and computational cost. Regarding the charge estimation of rotating equipment, the mass of working fluid is computed by knowing the internal volume of the machine and by computing an average density. This simplified approach is usually reasonable given the relatively small internal volumes of pumps and expanders compared to heat exchangers and other volumes of the system. However, especially in the case of oil lubricated positive displacement expanders, high pressures and temperatures may lead to dissolved refrigerant in the oil that could be accounted for using solubility data of the refrigerant-oil mixture [16, 22, 23].

A liquid receiver (or buffer tank) can be installed in an ORC system at the condenser outlet. Under normal operating conditions, the liquid receiver ensures a saturated liquid at the condenser outlet

and serves as a mass damping device during off-design conditions. In most cases, the liquid receiver is modeled by neglecting heat losses to the environment as well as potential hydrostatic effects due to the height of liquid (i.e., the pressure is considered to be uniform inside the liquid receiver). Nevertheless, it is not straightforward to predict the mass of liquid stored inside the tank at any operating condition with a steady-state model. In an experimental setup, a level sensor could be used to monitor the liquid level inside the tank. However, in commercial ORC systems, this may not be a viable option. Recently, Dickes et al. [8] proposed a liquid receiver model by introducing four hypotheses that resulted in the following constraints for calculating the mass of working fluid inside the liquid receiver:

$$m_{\text{receiver}} = \begin{cases} V_{\text{tank}}\rho_{\text{tank,su}} & \text{if } h_{\text{tank,su}} < h_{\text{sat}}(p_{\text{tank,su}}, x = 0) \\ V_{\text{tank}}\left[L_{\text{tank}}\rho_{\text{sat,l}} + (1 - L_{\text{tank}})\rho_{\text{sat,l}}\right] & \text{if } x_{\text{tank,su}} = 0 \\ V_{\text{tank}}\rho_{\text{sat,v}} & \text{if } x_{\text{tank,su}} \in [0, 1] \\ V_{\text{tank}}\rho_{\text{tank,su}} & \text{if } h_{\text{tank,su}} > h_{\text{sat}}(p_{\text{tank,su}}, x = 1) \end{cases} \tag{4}$$

where V_{tank} is the total volume of the liquid receiver, L_{tank} is the liquid level, $\rho_{sat,l}$ and $\rho_{sat,v}$ are the saturated liquid and vapor densities at the supply pressure, respectively. Under normal operating conditions and optimal charge, the receiver should be partially filled with liquid. If the charge is not proper or the ORC system is operating at strong off-design conditions, the receiver can be either full or empty of liquid. Furthermore, such mathematical formulation may result in numerical issues due to a discontinuity in the mass estimation when the fluid reaches its saturated liquid state (i.e., $x_{tank,su} = 0$) [8].

The line sets (or pipelines) connect the different system components and carry the working fluid. The line sets consist of piping, valves, fittings, sight glasses, filters and other elements and are also associated with pressure drops and heat losses. As mentioned at the beginning of this section, two different modeling approaches can be employed to estimate the working fluid charge carried by the line sets as well as the thermodynamic states at inlet and outlet of each line set. By referring to **Figure 2**, a total of six line sets is considered. In particular, each line set can carry single-phase or two-phase working fluid and they are modeled as an equivalent tube having inner and outer diameters. An equivalent length that accounts for straight sections ($L_{straight}$) and all the fittings ($L_{eq,fittings}$) is computed by using the method of loss coefficients proposed by Munson et al. [24]. Distinction is made in the calculation of pressure drops to account for single and two-phase flow conditions. In the case of single-phase flow, the pressure drop for a certain line set having a certain internal diameter is computed by introducing the Darcy friction factor:

$$\Delta p_{lineset,\,1\varphi,\,ID=const} = f\frac{\sum L_{straight} + \sum L_{eq,fittings}}{ID}\left(\frac{\rho_{lineset,su}v^2}{2}\right) \tag{5}$$

where v is the working fluid velocity. Under two-phase conditions, the Lockhart-Martinelli method for two-phase frictional pressure drop in tubes [25] is used. That is:

$$\Delta p_{lineset,\,2\varphi,\,ID=const} = -\left(\frac{dp}{dz}\right)_F \left(\sum L_{straight} + \sum L_{eq,\,fittings}\right) \tag{6}$$

The heat losses though the line sets to the surroundings can be calculated with the effectiveness-NTU method [17], as given in Eq. (7), where $NTU_{lineset}$ can be either specified or obtained by regression using experimental data.

$$T_{lineset,\,ex} = T_{amb} - e^{(-NTU_{lineset})}(T_{amb} - T_{lineset,\,su}) \tag{7}$$

A more simplified approach is proposed in **Figure 3**, where the line sets and associated losses are lumped in the high- and the low-pressure lines by using single fictitious components placed at the outlet of the evaporator and the condenser, respectively. The pressure losses are computed as a linear function of the working fluid kinetic energy with two coefficients to be calibrated using experimental data. That is:

$$\Delta p_{lineset} = K\left(\frac{m_{wf}^2}{\rho_{lineset,\,su}}\right) + B \tag{8}$$

The ambient losses are modeled by introducing an overall heat transfer coefficient of the line set ($UA_{lineset}$), which is the sum of the thermal resistance of the pipe, the thermal resistance associated with insulation and the convective UA values associated with the inside and outside of the line set:

$$Q_{lineset} = UA_{lineset}(T_{lineset,\,su} - T_{amb}) \tag{9}$$

$$UA_{lineset} = \left(\frac{1}{UA_{ID}} + \frac{1}{UA_{OD}} + R_{lineset} + R_{insulation}\right)^{-1} \tag{10}$$

The working fluid charge of each line set is calculated in a manner that is similar to the approach that will be presented for each zone of the heat exchangers (see Section 3.3). In the case of single-phase working fluid, the mass of working fluid is calculated as

$$m_{lineset} = V_{lineset}\rho_{lineset} \tag{11}$$

where $\rho_{lineset}$ is the average between inlet and outlet densities of a line set. If a line set is considered adiabatic, then $\rho_{lineset} \equiv \rho_{lineset,\,su}$. Under two-phase conditions, the average density of the working fluid is obtained by introducing an average void fraction over the length of the line set ($\alpha_{lineset}$). Mathematically, this can be expressed as:

$$\rho_{lineset} = \alpha_{lineset}\rho_{sat,\,v} + (1 - \alpha_{lineset})\rho_{sat,\,l} \tag{12}$$

3.3. Working fluid charge in heat exchangers

An ORC system operates between a heat source and heat sink by using heat exchangers (HEX) for the heat input and rejection processes, respectively. The working fluid undergoes phase

changes in both evaporator and condenser and different phases co-exist during these processes. An internal heat exchanger (or regenerator) can be present in the system to improve the cycle thermal efficiency [11]. The heat exchangers account for the majority of the volume in an ORC system and therefore, it is particularly important to have reliable models to predict the heat transfer rate, zone lengths, and working fluid charge.

To predict the different zones inside an HEX, three different numerical methods can be used: moving-boundary [7, 8], finite-volume (or discretized) [16], and hybrid approach [26]. The main advantage of moving-boundary models is their fast computation time and good accuracy. Finite-volume models provide greater spatial resolution but can be computationally expensive. Hybrid models represent a compromise between the former methods. By considering the moving-boundary model as an example, the heat exchanger can be divided in multiple zones, as shown in **Figure 4**. Each zone is characterized by a heat transfer coefficient and heat transfer area through which a certain heat transfer process occurs. By knowing the inlet conditions of both streams, the effective heat transfer rate between the hot and cold streams is calculated by enforcing that the total surface area occupied by the different zones is equal to the geometrical surface area of the heat exchanger [8]. It follows that the total working fluid mass inside the heat exchanger (m_{HEX}) can be calculated as the sum of the working fluid mass associated with each zone:

$$m_{wf,HEX} = \sum_{i=1}^{N} \rho_i (w_i V_{HEX}) \tag{13}$$

where w_i is the volume fraction occupied by the *i-th* zone in the heat exchanger, and ρ_i is the mean density of working fluid in the *i-th* zone. In order to ensure a correct estimation of the working fluid charge, the knowledge of the zone division (or in other words, correct estimation of the heat transfer rates) and the evaluation of the working fluid density under both single- and two-phase conditions are required. In particular, the latter implies the selection of the proper void fraction model that characterizes both boiling and condensing processes.

Various heat exchanger types are employed in ORC systems (e.g., brazed plate heat exchangers, fin and tubes, shell and tubes, etc.) and a number of state-of-the-art heat transfer correlations are available in the literature that are used to predict the convective heat transfer

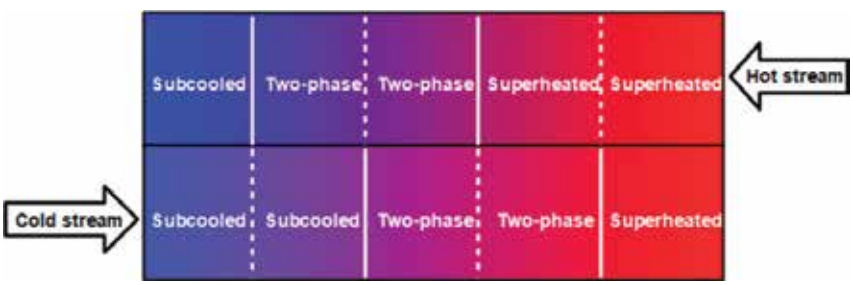

Figure 4. Schematic of counterflow HEX model simulated by moving boundary method showing phase boundaries (solid lines) and zone boundaries (dashed lines).

coefficients in each zone. However, these correlations are often purely empirical and calibrated to fit experimental data and multiple correlations may be available for the same type of heat exchanger and working fluid. Furthermore, these correlations are typically derived for refrigeration systems, which present different operating conditions than ORCs. It follows that such correlations are likely to over-predict or under-predict the actual heat transfer coefficient within a certain zone, even though the overall predictions of the heat transfer rate may be reasonable. Nevertheless, errors in predictions of heat transfer within individual zones can lead to significant errors in charge estimations [8]. To improve the accuracy in predicting the heat transfer coefficients in the different zones, empirical parameters of these correlations should be fitted with experimental results by using identification methods [8].

The accuracy of the heat transfer predictions alone does not ensure the correctness of the charge estimation. In fact, as already indicated in Eq. (14), under two-phase conditions, the density is a function of the thermodynamic conditions as well as the flow pattern characterizing each phase. The void fraction, α, is an essential parameter associated with two-phase flow and it is related to the fluid quality, x. Based on the void fraction, the working fluid mass of a two-phase zone having length L and cross section A_c is calculated as:

$$m_{wf,2\varphi} = m_{wf,v} + m_{wf,l} = A_c \left(\rho_v \int_0^L \alpha(x) dl + \rho_l \int_0^L [1 - \alpha(x)] dl \right) \tag{14}$$

To be further noted is that the void fraction $\alpha(x)$ is integrated along the length of the zone as a function of the working fluid quality. A common simplification is to assume a uniform heat flux in the two-phase zone, that is, a linear evolution of the quality along the length of the zone. However, a more appropriate approach would require evaluation of the effective spatial evolution of the quality in the heat exchanger for example by discretizing the two-phase zone into multiple sub-cells (e.g., by employing a hybrid heat exchanger model) [8]. Similar to the convective heat transfer correlations, several void fraction models can be found in the scientific literature [8, 10] that lead to different values of the mean density under two-phase conditions. An example of investigation of the combined effect of different convective heat transfer correlations and void fraction models on the total charge estimation is shown in **Figure 5** that is based on the work done by Dickes et al. [8].

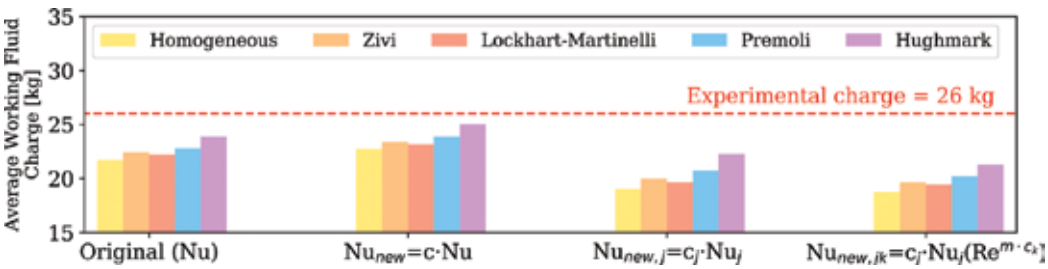

Figure 5. Working fluid charge predictions for different void fraction models as well as three adjusting methods to tune the convective heat transfer correlations [8].

The study considered a total of 360 charge-sensitive simulations including 40 experimental data points, 4 tuning methods, 5 void fraction correlations, and 72 heat exchanger models. It was concluded that the total working fluid charge estimation is mainly affected by the adjusting (or tuning) method applied to the convective heat transfer coefficient rather than the void fraction model. However, a trade-off between the two aspects exists since higher accuracy in the thermal performance predictions led to a large scatter of the charge inventory predictions.

4. Experimental considerations on working fluid charge with pure working fluids and zeotropic mixtures

In Section 3, the numerical aspects to be considered while developing a charge-sensitive ORC model have been discussed. However, in order to understand the usefulness of the model in predicting a real ORC behavior, it is necessary to consider experimental data. To this end, in the following sub-sections, several aspects related to analyzing different charge levels using both experimental and charge-sensitive model results are presented.

4.1. Data reduction and charge uncertainties

Steady-state operation of an ORC system can be detected by adopting for example the conditions proposed by Woodland et al. [15]. Alternatively, the methodology described by Dickes et al. [5] could also be employed. Due to the fact that experimental data is subject to different uncertainties, possible errors or sensor malfunction, a post-treatment data can be performed to identify possible outliers by using the open-source *GPExp* library [27]. Furthermore, a reconciliation method can also be applied to correct the measured data affected by measurement error propagation to satisfy physical system constraints (e.g., energy balances) [28].

Uncertainty propagation from the measured system properties to the calculated quantities is usually performed according to the method described by Figliola and Beasley [29]. In particular, it is important to discuss the uncertainties associated with the total system charges, which are often not thoroughly accounted for when reporting experimental results of ORC systems. In general, there are several sources of uncertainty in the measurement of the total system charge, such as inaccuracy of the scale used to weight the supply cylinder, leakage of working fluid from the system during operation, small portions of working fluid occupying charging hoses, small losses in system charge due to purging of charging hoses, stacked uncertainties due to the summing of several incremental charging steps. In experimental test rigs, the uncertainty due to purging of system charging hoses can be eliminated by leaving all charging hoses connected and full of working fluid during all tests and incremental charge conditions. Leakage of working fluid from the system during operation can be neglected after ensuring that repeated tests at the same conditions, but several days apart, yield approximately the same condenser subcooling. The main sources of uncertainty in the working fluid charge level are the inaccuracy of the scale and the stacked uncertainties due to several incremental steps in adding or subtracting charge. As an example, if a scale has a known resolution of ± 0.005 kg, and a measurement uncertainty of ten times the resolution or $\pm$ 0.045 kg is

conservatively assumed, the uncertainty of the total system charge (u_{charge}) can be estimated as a function of the number of consecutive charging steps, n_{steps}, as:

$$u_{charge} = \sqrt{(0.045)^2 \cdot n_{steps}} \tag{15}$$

As reported by Woodland [6], given a system charge of 18.1 kg, the relative uncertainty in system charge assuming a maximum of 8 charge steps is still less than 1%. Therefore, a high degree of confidence can be placed on the measured system charge level. More challenging is determining the actual charge inside the heat exchangers, which would require active measurements of their weight during operation.

In the case of a zeotropic mixture, for example, R134a-R245fa (0.625–0.375), uncertainty in the charge level of each component of the binary mixture results in some uncertainties in the concentration of the mixture, which is an important parameter in computing the thermophysical properties of the mixture. However, even with the conservative estimate on the charge uncertainty previously mentioned, the resulting relative uncertainty in the concentration is ≤0.004, which results in a relative uncertainty of 1% or less, depending on which component concentration is considered. Depending on the mixture considered, the sensitivity of the mixture thermodynamic properties to the concentration can be much smaller for single-phase states than the sensitivity to temperature. For example, in the case of R134a-R245fa, the sensitivity of enthalpy to the concentration uncertainty is two orders of magnitude less than the sensitivity to the temperature uncertainty for single-phase states [6]. As a result, the measured concentration of the working fluid is not a dominant factor in measurement uncertainty in this case.

4.2. Effect of charge variations in an ORC system

To conduct a working fluid charge study, it is desired to explore a wide range of working conditions, different working fluids, and several charge levels. In the current available literature, only the study published by Woodland [6] meets all of these criteria, and, therefore, it is used hereafter as an example. In particular, three working fluids were chosen to investigate low grade waste heat recovery by means of an ORC: R134a, R245fa, and the zeotropic mixture R134a-R245fa (0.625–0.375). In addition, two heat source temperatures, and several charge levels of the working fluids were considered. The range of conditions tested experimentally for each working fluid is summarized in **Table 1**. A complete description of the ORC system can be found in [6] and its schematic is shown in **Figure 1**. The effect of the working fluid charge on the ORC system performance is shown in **Figure 6**, where the Second Law efficiency, defined as the ratio of the system net power to the total exergy rate available, is plotted as a function of the subcooling level for different operating conditions. It can be seen that for a given working fluid and heat source inlet temperature, there exists an optimum charge level that maximizes the Second Law efficiency (i.e., power output) of the system. Furthermore, for each working fluid, the efficiency tends to be higher at lower subcooling due to lower condensing pressures dictated by lower fluid charge.

Working fluid	Charge [kg]	Source temperature [°C]	Expander speed range [rpm]	Pump speed range [rpm]
R134a	18.1	80, 100	2800–3000	1000
	20.4	80, 100	1200–3000	1000
	22.7	100	1500–2300	1000
R245fa	27.4	80, 100	1000–2000	300–500
	29.5	80, 100	1000–2000	300–500
	31.8	80, 100	1000–2000	300–500
R134a-R245fa (0.625–0.375)	24.9	80, 100	1000–1500	500–1000
	27.2	80, 100	1000–2500	500–1000
	29.5	80, 100	1000–2200	500–1000

Table 1. Summary of experimental test matrix to investigate the effect of working fluid charge [6].

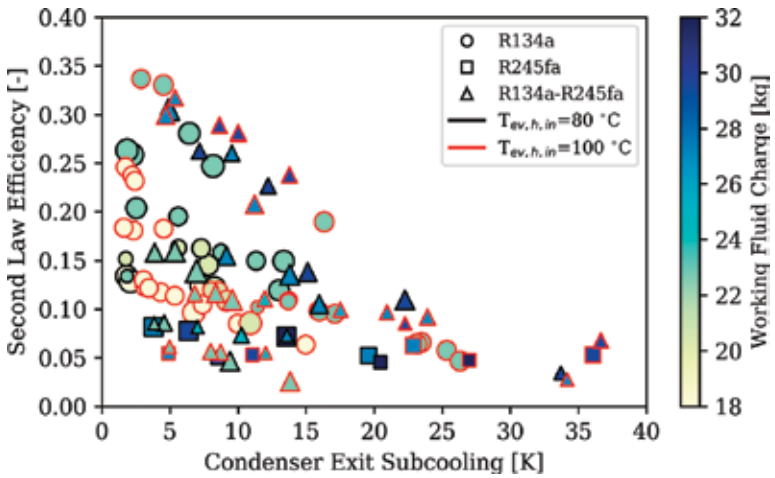

Figure 6. Measured second law efficiency versus condenser exit subcooling for each working fluid. The contour shows the working fluid charge and the size of the markers is proportional to the expander rotational speed (data from [6]).

4.3. Total working fluid charge model predictions

One of the main purposes of a charge-sensitive model is to predict the total charge of a certain ORC system for which it has been developed and its behavior (e.g., evaporating and condensing temperatures, subcooling and superheating). This needs to hold true also under the circumstances that the system is under-charged or over-charged as well as if the working fluid is changed, that is, drop-in replacement. To this end, the same ORC system considered in Section 4.2 is used as an example [6]. The charge-sensitive model is employed to simulate three different working fluids (i.e., R134a, R245fa, and R134a-R245fa (0.635–0.375)) at three different charge levels, without any tuning. The untuned model prediction of the system charge versus the measured charge for all the test points is shown in **Figure 7**. It can be seen that even without tuning, the model predictions are reasonably accurate due to the fact that the heat

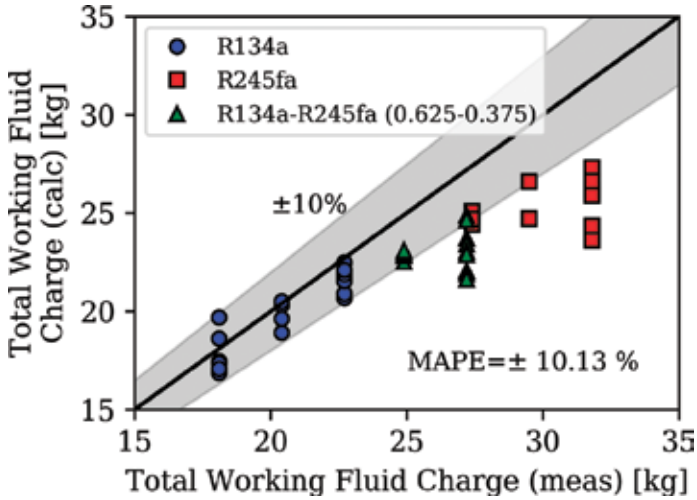

Figure 7. Parity plot showing the ability of the charge-sensitive model to predict the total working fluid charge without any charge tuning.

exchanger volumes as well as the liquid line sets have been accounted for. These liquid volumes remain constant across all experimental tests and therefore set the baseline charge level of the system. However, the model does not predict the variability in charge well for all cases. For R134a, the trend in system charge is captured well, but with increased underprediction of the charge at higher charge levels. For R245fa, the trend is not captured well. A general increase is observed, but the underprediction is significant. For the zeotropic mixture, no trend is visible at all in the charge prediction. Variability in the predicted charge is due to the changing liquid lengths in the heat exchangers, the void fraction of two-phase flow, and the solubility of the working fluid in the lubricant oil. In particular, if the boundary conditions of the ORC are fixed then an increase in the working fluid charge in the system leads to a decrease in the two-phase zone in the condenser (resp. subcooled zone), as shown in **Figure 8(a)**. If the void fraction model and the heat transfer coefficient of the two-phase zone are not estimated correctly, the charge of the subcooled region can be largely under predicted due to the rapid increase in liquid level inside the condenser, as shown in **Figure 8(b)**. Solubility of the working fluid in the oil was not considered in the model. However, it can have a significant impact on prediction of the total system charge. In fact, if an oil separator is present in the ORC system, the working fluid dissolved in the lubricant oil could be up to 10% of the total charge depending on the solubility of the working fluid-lubricant oil mixture [6].

4.4. Charge tuning schemes

As shown in **Figure 8**, the estimation of working fluid charge in system modeling is usually biased due to inaccurate estimation of system volumes, ambiguous flow patterns under two-phase flow conditions, solubility of working fluid in the lubricant oil, etc. A charge-tuning scheme can be used to eliminate the bias. Although such methods have been widely used for vapor compression heat pumping cycles [16, 17], they have not been employed in

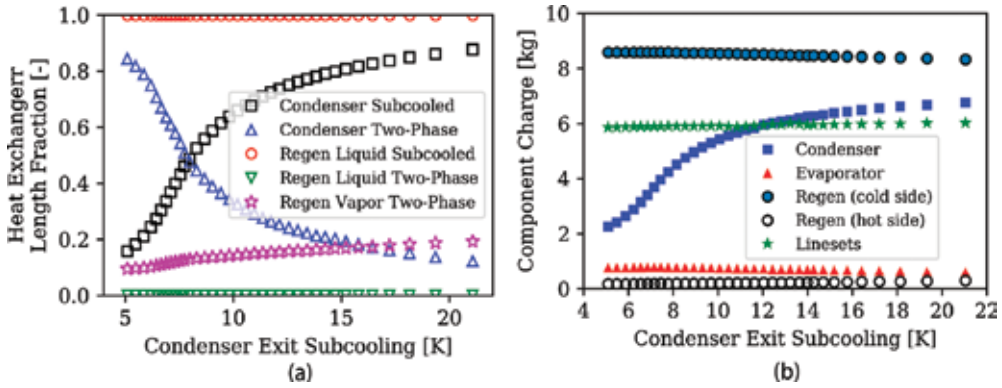

Figure 8. Heat exchanger length fraction (a) and breakdown of component charge (b) versus condenser exit subcooling when the total charge is imposed as model input. Pump speed = 1000 rpm, expander speed = 2000 rpm, source temperature = 100°C, source and sink fluid flow rates are 0.45 and 1 kg/s, respectively. The charge calculation is untuned.

charge-sensitive ORC system modeling. An empirical two-point charge tuning equation that incorporates a linear function of the length of the subcooled section in the condenser ($L_{cond,sc}$) can be employed:

$$m_{wf,meas} - m_{wf,calc} = C_{m,0} + C_{m,1} L_{cond,sc} \tag{16}$$

where $C_{m,0}$ and $C_{m,1}$ are the regression parameters to be estimated by linear regression. The estimated correction term from Eq. (16) is added to the total working fluid charge computed by the model to give an unbiased estimate [17].

5. Conclusions

In this chapter, the effects of the total working fluid charge on the performance and operation of an ORC system have been discussed. In particular, both numerical and experimental have been used to demonstrate the importance of considering the charge inventory when analyzing off-design conditions of the ORC system. Under-charging or over-charging the system has a direct effect on the spatial distribution of the different zones inside the heat exchangers. Additional aspects such as oil solubility can also have non-negligible impact on the system performance. A detailed mechanistic model of the ORC allows identification of optimal charge level. However, charge-tuning is always required to account for inaccuracies and uncertainties associated with the modeling assumptions. In fact, two-phase heat transfer correlations and void fraction models directly affect the charge inventory estimations. The analysis of the charge inventory of ORC systems is also particularly important when considering drop-in replacements such as HFOs and their blends. The size of the heat exchangers as well as the piping system require an optimal working fluid charge to ensure proper behavior of the ORC at both design and off-design conditions.

Conflict of interest

The Authors declare no conflict of interest.

Nomenclature

A	area, [m^2]
c	tuning coefficient, [−]
C	regression coefficient, [−]
h	specific enthalpy, [kJ/kg]
m	mass, [kg]
N	rotational speed, [rpm]
Nu	Nusselt number, [−]
p	pressure, [Pa]
Q	heat transfer rate, [W]
Subscripts	
calc	calculated
cond	condenser
evap	evaporator
ex	exit
exp.	expander
R	Thermal resistance, [K/W]
Re	Reynolds number, [−]
T	temperature, [K]
UA	heat conductance, [W/K]
V	volume, [m^3]
x	quality, [−]
α	void fraction, [−]
ρ	density, [kg/m^3]
meas	measured

sc	subcooled
su	supply
wf	working fluid

Author details

Davide Ziviani[1]*, Rémi Dickes[2], Vincent Lemort[2], James E. Braun[1] and Eckhard A. Groll[1]

*Address all correspondence to: dziviani@purdue.edu

1 Ray W. Herrick Laboratories, School of Mechanical Engineering, Purdue University, West Lafayette, IN, USA

2 Thermodynamics Laboratory, Aerospace and Mechanical Engineering Department, University of Liège, Liège, Belgium

References

[1] Quoilin S, van den Broek M, Declaye S, Dewallef P, Lemort V.: Techno-economic survey of organic Rankine cycle (ORC) systems. Renewable and Sustainable Energy Reviews. 2013; **22**:168-186. DOI: 10.1016/j.rser.2013.01.028

[2] Tartier T. ORC World Map [Internet]. 2016. Available from: http://www.orc-world-map.org/ [Accessed: March 17, 2018]

[3] Tartièr T, Astolfi M. A world overview of the organic Rankine cycle market. Energy Procedia. 2017;**129**:2-9. DOI: 10.1016/j.egypro.2017.09.159

[4] Imran M, Haglind F, Asim M, Alvi ZJ. Resent research trends in organic Rankine cycle technology: A bibliometric approach. Renewable and Sustainable Energy Reviews. 2018; **81**:552-562. DOI: 10.1016/j.rser.2017.08.028

[5] Dickes R, Dumont O, Daccord R, Quoilin S, Lemort V. Modelling of organic Rankine cycle power systems in off-design conditions: An experimentally-validated comparative study. Energy. 2017;**123**:710-727. DOI: 10.1016/j.energy.2017.01.130

[6] Woodland BJ. Methods of increasing net work output of organic Rankine cycles for low-grade waste heat recovery with a detailed analysis using a zeotropic working fluid mixture and scroll expander [Thesis]. Purdue University; 2015

[7] Ziviani D, Woodland BJ, Georges E, Groll EA, Braun JE, Horton WT, van den Broek M, De Paepe M. Development and a validation of a charge sensitive organic Rankine cycle (ORC) simulation tool. Energies. 2016;**9**:389. DOI: 10.3390/en9060389

[8] Dickes R, Dumont O, Guillaume L, Quoilin S, Lemort V. Charge-sensitive modelling of organic Rankine cycle power systems for off-design performance simulation. Applied Energy. 2018;**212**:1262-1281. DOI: 10.1016/j.apenergy.2018.01.004

[9] Liu L, Zhu T, Ma J. Working fluid charge oriented off-design modeling of a small scale organic Rankine cycle system. Energy Conversion and Management. 2017;**148**:944-953. DOI: 10.1016/j.enconman.2017.06.009

[10] Pan Y, Liu L, Zhu T. Simulation of working fluid mass distribution in small-scale organic Rankine cycle system under sub-critical conditions. Applied Thermal Engineering. 2018; **131**:884-896. DOI: 10.1016/j.applthermaleng.2017.16.017

[11] Lecompte S, Huisseune H, van den Broek M, Vanslambrouck B, De Paepe M. Review of organic Rankine cycle (ORC) architectures for waste heat recovery. Renewable and Sustainable Energy Reviews. 2015;**47**:448-461. DOI: 10.1016/j.rser.2015.03.089

[12] Astolfi M, Martelli E, Pierobon L. Thermodynamic and technoeconomic optimization of organic Rankine cycle systems. In: Macchi E, Astolfi M, editors. Organic Rankine Cycle (ORC) Power Systems. Technologies and Applications. 1st ed. Woodhead Publishing; 2017. pp. 173-249. DOI: 10.1016/B978-0-08-100510-1.00007-7

[13] Landelle A, Tauveron N, Revellin R, Haberschill P, Colasson S, Roussel V. Performance investigation of reciprocating pump running with organic fluid for organic Rankine cycle. Applied Thermal Engineering. 2017;**113**:982-969. DOI: 10.1016/j.applthermaleng.2016. 11.096

[14] Li J, Gao G, Li P, Pei G, Huang H, Su Y, Ji J. Experimental study of organic Rankine cycle in the presence of non-condensable gases. Energy 2018;**142**:739-753. DOI: 10.1016/j.energy. 2017.10.054

[15] Desideri A, Hernandez A, Gusev S, van den Broek M, Lemort V, Quoilin S. Steady-state and dynamic validation of a small-scale waste heat recovery system using the ThermoCycle modeling library. Energy. 2016;**115**:684-696. DOI: 10.1016/j.energy.2016.09.004

[16] Shen B, Braun JE, Groll EA. Improved methodologies for simulating unitary air conditioners at off-design conditions. International Journal of Refrigeration;**32**(209):1837-1849. DOI: 10.1016/j.ijrefrig.2009.06.009

[17] Cheung H, Braun JE. Component-based, gray-box modeling of ductless multi-split heat pump systems. International Journal of Refrigeration. 2014;**38**:30-45. DOI: 10.1016/j. ijrefrig.2013.10.007

[18] Galindo J, Ruiz S, Dolz V, Royo-Pascual L. Advanced exergy analysis for bottoming organic rankine cycle coupled to an internal combustion engine. Energy Conversion and Management. 2016;**126**:217-227. DOI: 10.1016/j.enconman.2016.07.080

[19] Dickes R, Ziviani D, De Paepe M, van den Broek M, Quoilin S, Lemort V. ORCmKit: An open-source library for organic Rankine cycle modeling and analysis. In: Proceedings of ECOS 2016, Portoroz (Slovenia), 2016. DOI: http://hdl.handle.net/2268/170508. Link: https://github.com/orcmkit

[20] Bell IH, Wronski J, Quoilin S, Lemort V. Pure and pseudo-pure fluid thermophysical property evaluation and the open-source thermophysical property library CoolProp. Industrial and Engineering Chemistry Research. 2014;**53**:2498-2508. DOI: 10.1021/ie4033999

[21] Lemmon E, Huber M, McLinden M. NIST standard reference database 23: Reference fluid thermodynamic and transport properties (REFPROP), version 9.0, National Institute of Standards and Technology

[22] Martz WL, Jacobi AM. Refrigerant-Oil Mixtures and Local Composition Modeling. Air Conditioning and Refrigeration Center. ACRC-TR-68. College of Engineering, University of Illinois at Urbana-Champaign, IL, USA; http://hdl.handle.net/2142/10986

[23] Zhelezny VP, Semenyuk YV, Ancherbak SN, Grebenkov AJ, Beliayeva OV. An experimental investigation and modelling of the solubility, density and surface tension of 1,1,1,3,3-pentafluoropropane (R-245fa)/synthetic polyolester compressor oil solutions. Journal of Fluorine Chemistry. 2007;**128**:1029-1038. DOI: 10.1016/j.jfluchem.2007.05.011

[24] Munson BR, Young DF, Okiishi TH. Fundamentals of Fluid Mechanics. New Jersey: John Wiley and Sons; 2006

[25] Lockhart RW, Martinelli RC. Proposed correlation of data for isothermal two-phase, two-component flow in pipes. Chemical Engineering Progress. 1949;**45**:39-48

[26] Lecompte S. Performance Evaluation of Organic Rankine Cycle Architectures: Application to Waste Heat Valorisation. Belgium: Ghent University; 2016. http://hdl.handle.net/1854/LU-7223134

[27] Quoilin S, Schouff J. Assessing steady-state, multi-variate thermos-fluid experimental data using Gaussian processes: The GPExp open-source library. Energies. 2016;**9**. DOI: 10.3390/en9060423

[28] Dumont O, Quoilin S, Lemort V. Importance of the reconciliation method to handle experimental data: Application to a reversible heat pump/organic Rankine cycle unit integrated in a positive energy building. International Journal of Energy and Environmental Engineering. 2016;**7**. DOI: 10.1007/s40095-016-0206-4

[29] Figliola R, Beasley D. Theory and Design for Mechanical Measurements. New Jersey: John Wiley and Sons; 2006. p. 542

Chapter 3

Expanders for Organic Rankine Cycle Technology

Fuhaid Alshammari, Muhammad Usman and
Apostolos Pesyridis

Additional information is available at the end of the chapter

http://dx.doi.org/10.5772/intechopen.78720

Abstract

The overall power conversion efficiency of organic Rankine cycle (ORC) systems is highly sensitive to the isentropic efficiency of expansion machines. No expansion machine type is universally ideal as every machine has its own advantages and disadvantages and is suitable for a comparatively narrow range of operations of the highest efficiency. Therefore, an optimum selection of an expansion machine type is important for a financially viable ORC implementation. This chapter presents the mode of operation, technical feasibility, and challenges in the application of turbo-expanders (radial inflow, radial outflow, and axial machines) and volumetric expansion machines (scroll, screw, piston, and vane) for use in ORC systems. It can be concluded that different machines are suitable for a different range of power output in commercial applications. In general, volumetric machines are suitable for 50 kWe and below but turbomachines are more suitable for power outputs higher than 50 kWe.

Keywords: turbomachines, volumetric expanders, organic Rankine cycle, expansion machines, isentropic efficiency

1. Introduction

Organic Rankine (ORC) cycle-based systems have gained popularity in the last 2 decades for heat to power conversion in various applications. In comparison with the traditional Rankine cycle, the ORC-based power systems allow the flexibility to choose working fluids and expansion machines, as an additional degree of freedom, allowing optimal configurations both from the thermodynamic as well as techno-economic aspects. ORC systems can be designed to optimally convert waste heat from internal combustion engine (ICE) exhaust, geothermal heat sources, biomass applications, solar thermal applications, and other thermal

gradient-based sources like ocean thermal energy conversion (OTEC). The maintenance-free automated operation and relatively smaller installation and operational costs compared to Rankine cycles make them ideal for commercial use specifically in <10 MW-scale applications.

ORC power systems generally comprise four major components, namely: evaporator, condenser, pump, and expander. The evaporator and condenser are primarily heat exchangers, appropriately sized for a certain duty to operate with specified fluids at specific operating conditions. The current state of the art can be considered sufficient enough to support the technological requirements to ensure the availability of heat exchangers to be used as evaporators and condensers. The pumps have also been well developed and can be bought off the shelf to fulfil the requirements of the ORC system. However, the expander can be considered as the most technically advanced component of an ORC system. The expander is the machine which extracts the energy from the expansion of high-pressure vapour resulting in low pressure while passing through its inlet to the outlet port and converts fluid energy to mechanical power (rotational or reciprocating), which is then often converted to electrical power via direct or indirect coupling to a generator. Organic Rankine cycles, in general, have low thermodynamic efficiency due to limited temperature differences between the heat source and heat sink streams. Therefore, the efficiency of the overall cycle is highly sensitive to the efficiency of the expansion machine [1]. Therefore, the selection of an appropriate expander for a certain ORC application is of great importance to avoid further efficiency reductions and for commercial viability. Depending on the application, operating conditions (temperature, pressure, and mass flow rate), working fluid, and power levels, different types of expansion machines can be used.

2. Primary classification of expanders

In general, the expansion machines are classified based on the nature of their operation. They are broadly classified as either turbo-machine or volumetric-type machines. The turbo-machines in this case refer to turbines of the dynamic or velocity type. They convert the dynamic pressure or high-velocity fluid momentum into mechanical energy while passing through a series of blades. The leaving fluid has generally low pressure and an overall enthalpy drop occurs while passing through machines. Turbomachines are more commonly used for medium to large-scale applications and are well known for their higher efficiency. For smaller power output (<50 kWe), volumetric machines are frequently the preferred choice.

The volumetric-type machines are also known as positive displacement machines. They operate on a principle of force application on a movable mechanical component to extract power. The pressurized fluid is introduced into a chamber and the chamber volume is increased as a net force is applied by a compressed fluid. When the chamber reaches its maximum expansion volume, the low-pressure fluid is released out of expander. The volumetric machines are often equipped with valves to control the inlet and outlet flow of fluid and synchronization with expanding chamber. The volumetric expanders are suitable for smaller power output and often derived from heating, ventilation, air-conditioning and cooling (HVAC) compressors modified to operate in reverse. Both turbomachines and volumetric expanders have their own advantages and disadvantages along with several types available for each main category.

2.1. Turbo-expanders

In the turbo-expander operation, a high-pressure fluid is directed from the evaporator outlet to the turbine inlet, where the high static pressure of the fluid is converted into high-flow velocity when it passes through nozzles. The high-velocity fluid then transfers its momentum to an array of moving blades, while passing through them. The moving blades are attached to a shaft which is connected to a generator to convert the mechanical energy into electrical energy.

Turbines used in ORC application are generally different from expansion machines used for air, steam, and other gases because, in steam cycles, the enthalpy drop is much higher than that in ORCs. Thus, fewer turbine stages are required in ORCs; therefore, cheaper and lighter turbines are the result. However, the dense vapour properties vary largely from ideal gas behaviour and the speed of sound is much lower than in lighter gases or steam, which influences the nozzle design [2]. The low speed of sound in dense molecule fluids often causes turbines to operate in transonic and supersonic modes. As a result, a highly dissipative system of shockwaves is common in these machines which complicate the design and sacrifice performance specifically during off-design operations [3].

Turbo-expanders have two main categories: axial turbines and radial turbines, as differentiated in **Figure 1** (adapted from [4]). The main difference between the two categories is the way the working fluid flows in relation to the shaft. In axial turbines, the flow of the working fluid is parallel to the shaft, whereas, in radial turbines, it is radial to the shaft at the inlet converting to axial at the outlet of the turbine.

Selection of the suitable turbine (axial or radial) depends mainly on the operating conditions and corresponding enthalpy drop required. At low mass flow rates, the blades of the axial turbine become very small which results in a significant efficiency drop due to the difficulty of maintaining small tip clearance between the blades and the casing. Therefore, axial turbines are always preferred in a large-scale application where the mass flow rate is high and pressure ratio is small. In contrast, radial turbines are employed with applications of low mass

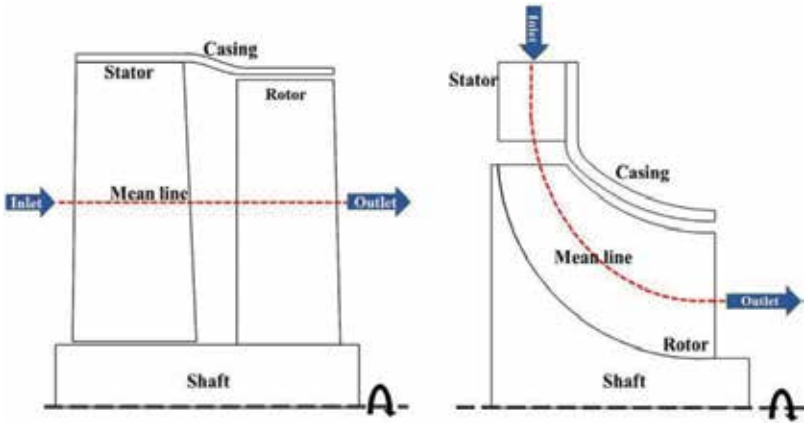

Figure 1. Schematic of axial flow (left) and radial inflow (right) turbines.

flow rate and high-pressure ratios such as turbochargers and ORC systems. For small flow rates, the radial turbines present more efficient performance due to their lower sensitivity to the blade profile than the axial ones. In addition, ORC applications employ high-density fluids which necessitate a more robust turbine due to the increased blade loading. In such conditions, radial turbines are favourable as the blades are rigidly attached to the hub. Due to the radius reduction from rotor inlet to the exit, radial turbines can handle a single-stage expansion ratio of 9:1, while axial turbines require at least two stages. Therefore, radial turbines are also favourable when the system size is taken into account.

However, generally speaking, axial turbines offer better performance at off-design conditions. Moreover, axial turbines present higher efficiency than radial turbines in large-scale applications such large gas turbines, due to the elimination of the flow turning in the meridional plane. In addition, the disc of the axial turbine is protected at high temperatures since only the blades are exposed to the heat. In radial turbines, on the other hand, both the blades and the disc are exposed to the heat since the expansion takes place at both inducer and exducer of the impeller. However, it is worth mentioning that ORC turbines operate usually at low temperatures where concerns about high temperature are significantly lower compared to other applications. The selection of the optimum configuration had been often related to two dimensionless parameters, that is, specific speed and specific diameter, which are based on the volumetric flow and enthalpy drop. **Figure 2** (adapted from [5] commonly known as Balje diagram) presents the selection map and suggests the use of axial flow machines for large specific speeds which correspond to larger flow rate. However, these diagrams should be used with caution as they were essentially developed for incompressible flow. Despite limitations, they are useful to provide initial information which can be further cross-checked by high fidelity models at later stages.

The radial turbines generally involved radial inflow configuration but recent advances in turbine development have also made the use of radial outflow turbines available in ORC technology which is discussed separately, below.

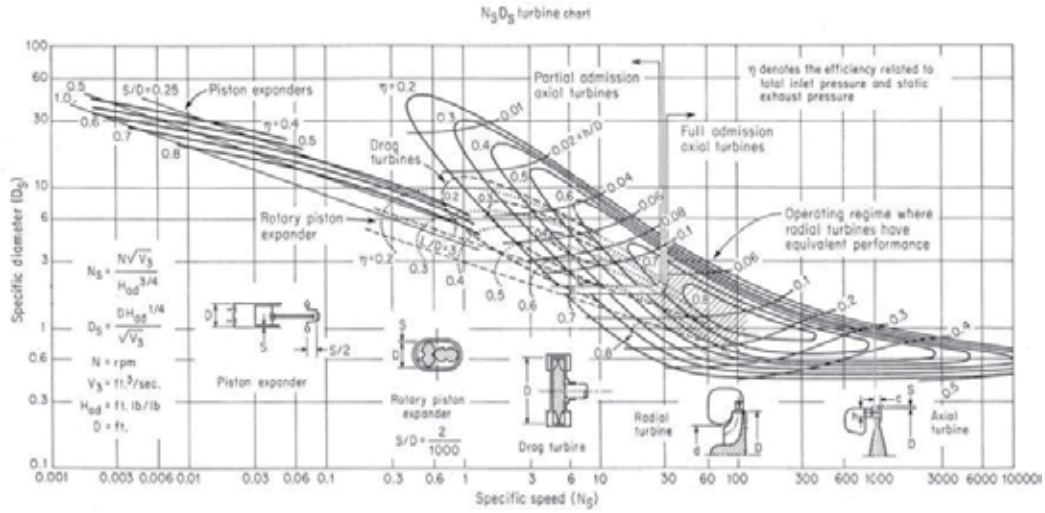

Figure 2. Turbines selection maps based on performance with respect to specific speed and specific diameter.

2.1.1. Radial inflow turbines

Figure 3 presents the meridional view and overall architecture of the turbine stage in a radial inflow turbine (RIT), which are sometimes also referred to as inward flow radial (IFR 90). As it can be observed, the high-pressure fluid enters the casing (volute) inlet and initial flow direction is primarily radial which is converted to the tangential direction circumferentially at the rotor inlet stage where it, also, contains both radial and tangential components. While passing through the rotor the flow loses its tangential component. The leaving flow must have minimum swirl flow at rotor exit. Furthermore, the direction of flow is converted from radial at the inlet to axial at rotor exit where ideally, there is no radial component. The geometric parameters mentioned in **Figure 3** are obtained from the design process and they are defined as follows: r_1 as volute inlet radius, r_2 as stator inlet radius, r_3 as stator exit radius, r_4 as rotor inlet radius, r_{5t} as rotor exit tip radius, r_{5h} as rotor exit hub radius, b_2 as nozzle inlet diameter, b_3 as nozzle exit diameter, D_4 as rotor inlet tip diameter and ξ as clearance.

The design procedure of radial inflow turbines involves, in simplified form, the steps illustrated in **Figure 4**, which presents a typical path followed. Although there is no single correct procedure, various designers use their own, bespoke techniques.

The design process of turbines (not only limited to the radial machines) often utilize the concept of mean-line flow which provides a preliminary or baseline one-dimensional design. The techniques assume the properties and parameters to be lumped and focus mainly on the inlet and outlet of cascades. The flow is assumed to be uniform and unidirectional and estimation at the centre line of flow can provide average flow characteristics of the fluid. The outcomes of a mean-line model are linked with blade design often based on experiences from NACA databases and statistical models. The overall design is transformed to a computer-aided design (CAD) model which can be used for three-dimensional computational fluid dynamic (CFD) analysis based on Reynolds average Navier-Stokes (RANS) calculations. The resulting analysis helps in the final tweaks of the fluid dynamic design and to achieve optimum performance. The detailed design and optimization techniques can be found in [6–8] for understanding the radial turbine performance. The authors in [4, 8] compiled a list of advantages of using radial turbines specifically for small-scale units over axial machines listed below:

1. Radial inflow machines are often manufactured as single piece cast or forged whereas axial machines often require separate blade and rotor manufacturing.
2. Single-piece rotors are more robust, stiff, and have enhanced rotor-dynamic stability which can help to reduce the overall cost.
3. RITs can offer better off-design performance when variable geometry nozzles are used.
4. Downsizing the axial machines for small-scale ORC applications requires blades to be very small and numerous, which increases the wetted area and frictional losses and blade blockage effects.
5. The running clearance necessary between rotor tip and casing becomes a significant fraction of the blade height which means higher proportionate leakage losses.
6. RITs support larger pressure ratios in a single stage (up to 10 is common for RIT but the axial might need three stages).

2.1.2. Radial outflow turbines

The flow direction in a radial outflow turbine (ROT) is opposite to that of the radial inflow machine. The flow enters the ROT at the centre, near the axis of rotation, axially, and then it travels outwards in the radial direction while passing through arrays of rotor and stator blades. **Figure 5**, adapted from the works of [9], presents the schematic of radial outflow turbines which are also known as centrifugal turbines.

The low speed of sound in organic fluids requires supersonic or at least transonic flows which lead to losses due to shock formation and interaction. The large volumetric expansion of organic fluids requires larger areas at the exit of turbines for the reduction in losses. The ROTs can have the inherent feature of enlargement in the area as the flow moves in a radial direction which means supersonic flows can be avoided and losses can be reduced to end up with high-efficiency turbines.

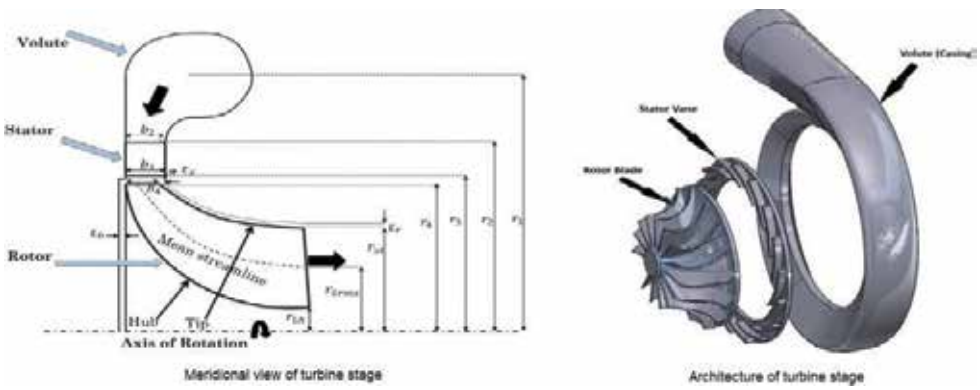

Figure 3. Meridional view (left) and architecture of turbine stage (right).

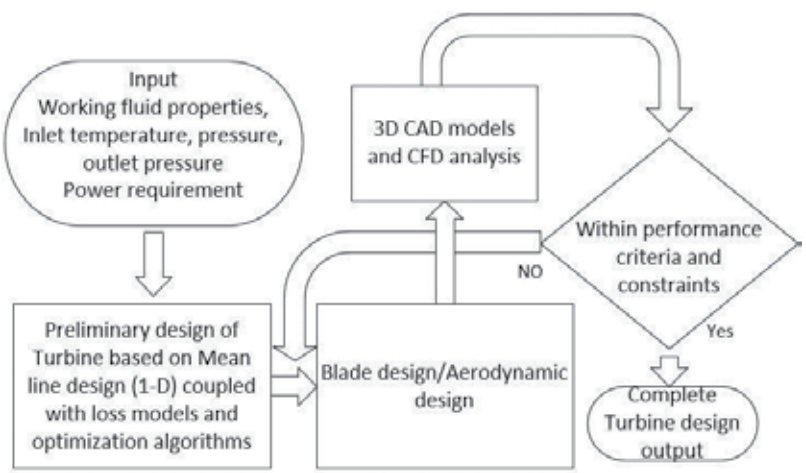

Figure 4. The fluid dynamic design process of turbine design.

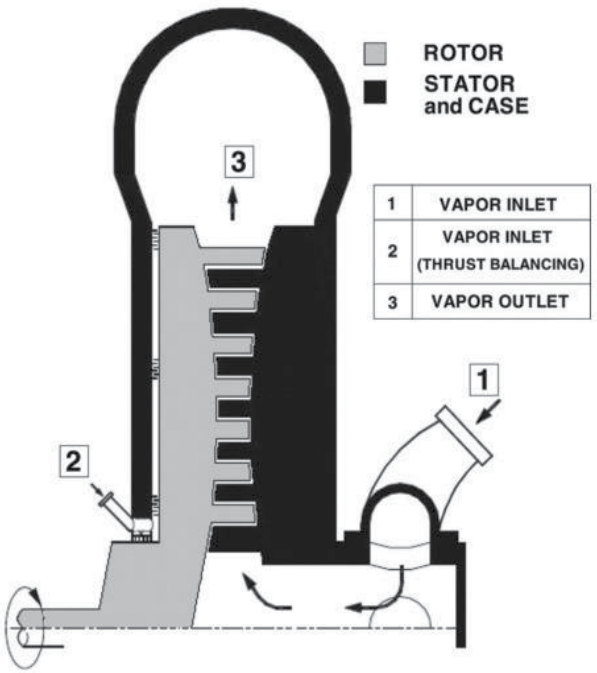

Figure 5. Schematic of radial outflow turbine.

The ROTs allow the adoption of multi-stator-rotor ring arrangements in the radial direction maintaining low peripheral speeds, resulting in low mechanical stresses, lower bearing losses, and simple connections of generator and grid. Furthermore, full-admission inlet stages can be adapted. The simplicity of multistage assembly allows tighter tolerances and thus losses can be reduced. The detailed design and analysis of ROTs are presented in [9, 10].

The disadvantages of ROTs include slightly lower efficiencies compared to RITs as large a surface area is in contact with fluid during flow. Furthermore, for heavy-/large-molecule working fluids, the first stage often has insufficient flow passage area due to the inherent square root proportionality of radius to area, therefore, limiting the turbine application for high-temperature applications. ROTs are more suitable for small-scale applications compared to micro-/mini-ORC applications.

2.1.3. Axial turbines

The axial turbines are characterized by the primary flow of the working fluid which is in axial direction and parallel to the rotational axis. Axial machines are more suitable for larger flow rates, which mean having larger specific speeds as per the Balje diagram (**Figure 2**). In ORC technology, these machines are often suitable for medium-to-large power outputs in single or multistage configurations ranging from one to five. The isentropic efficiencies of axial machines in nominal operations range from 80 to 90% [2]. The axial machines are the most commonly used turbomachine for power production, approximately 70% of power generated

is based on these machines as the preferred expander type of large power units. One of the limitations of axial machines is that considering large-stage expansion ratios, the axial channel undergoes span-wise enlargements with a negative impact on performance. Furthermore, highly supersonic conditions may be found at stator exit and converging-diverging nozzle arrangement, which may not be conducive for good off-design performance. Despite their few limitations, axial machines are adapted in large-scale applications in power plants using steam or Brayton cycles and they are also popular in nuclear power applications along with megawatt-scale power output in ORC applications.

Axial machines are adaptable and a list is populated by [11] to highlight the reasons for their flexibility.

1. Pressure can be as high as 300 bar (supercritical cycle) or too low (few hundredths of a bar, last stages of the steam cycle).
2. Overall pressure ratio could be as high as several thousand or as low as 1.0002 in wind turbines.
3. The diameters could be ranging from few centimetres to 100 m in wind turbine applications.

The design and performance evaluation of axial machines is performed in a similar manner as for radial machines and details of which can be found in works of [11]. However, the simple correlations of efficiency prediction for gas and steam turbines are not strictly valid for ORC applications.

2.2. Volumetric expanders

Volumetric expanders can be classified into four main categories: scroll, screw, piston, and rotary vane. Unlike turbo-expanders where the fluid movement is continuous, in volumetric expanders, it is cyclic. An inherent characteristic of this type of expanders is the fixed volume expansion ratio. They operate by trapping a fixed volume of the fluid and displacing this volume into the discharge of the machine, resulting in mechanical work due to the pressure drop. Therefore, they are also called displacement expanders.

Contrary to turbines, some volumetric expanders may have valves at inlet and outlet ports. The compressed fluid is fed into a chamber and inlet valves are closed, the expansion process starts, and at the end of the expansion, the outlet valve is opened to release the low-pressure fluid. These might be useful to control the timing and flow through an expander but it incurs significant losses. Piston-type expanders often have valves, scroll machines may also have these valves, but in general, screw, scroll, and vane type-expanders operate without valves.

Another peculiarity of volumetric expanders is related to their lubrication requirement. As they operate on the principle of changing volumetric capacity, there must exist some parts which are moving in contact with other surfaces to increase the volume for expansion. The contact movement adds friction which increases the wear, tear, and heat of the surfaces. Lubricant oil is often circulated especially in scroll- and screw-type expanders, which reduce the friction and also help seal the clearances and reduce leakage losses. The lubricant oils used

are often soluble in working fluid and can be circulated in the complete ORC cycle or only in the expander by means of separation mechanisms where oil is removed and re-circulated in the expander. The oil separation systems incur the cost of extra equipment and add to system complexity. The complete circulation might have detrimental effects on heat exchanger performance. In order to mitigate these issues, working fluids with good lubricant properties are preferred. Oil-free expanders have also been developed and the lubrication for their bearings is done by the application of grease [12].

Figure 6 adapted from [13] presents the under- and over-expansion losses. The volumetric machines have fixed volumetric ratio, so the thermodynamic cycle must be designed for optimum expansion ratio. It might be possible that a higher pressure ratio may theoretically lead to higher efficiency but the over-expansion losses will limit the overall performance so the close match between cycle and machine expansion ratio must exist. In recent years, volumetric expanders have received a great deal of attention in small-scale systems due to their good off-design performance.

2.2.1. Scroll expanders

Scroll expanders consist of two spirals: an orbiting scroll and fixed scroll as presented in **Figure 7** adapted from [14]. The orbiting scroll moves along with the fixed scroll within tight tolerances. The working fluid moves in from the centre and moves outwards inside the chamber between the orbiting and moving scroll. They are widely used as they can be derived from a scroll compressor, thereby, reducing the machine cost. Scroll expander can be either compliant or constrained. In the former, a lubrication system is required in order to reduce the friction between the contacting sidewalls. In the latter, lubrication is not required due to the existence of the linking mechanism between the rotating and fixed scrolls. In addition, there is no need for exhaust valves which results in noise reduction.

Scroll expanders usually operate at low power output applications (<10 kWe) due to their limited speed. In addition, they are preferred in small-scale applications due to their low parts count, which reduces the level of noise, increases the reliability, and makes them more cost

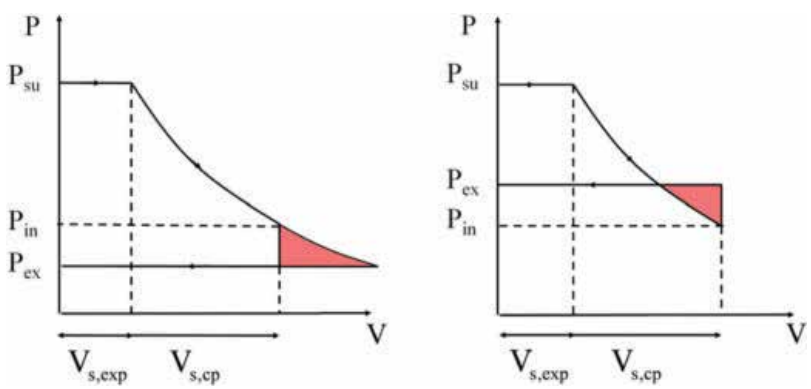

Figure 6. The under expansion (left) and over expansion (right) losses.

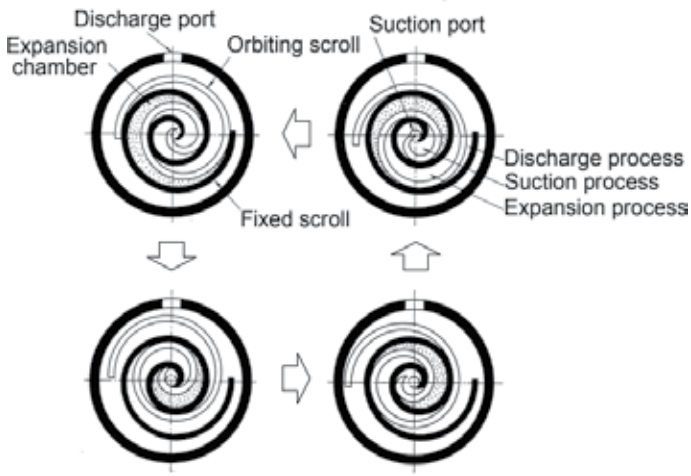

Figure 7. Operation of the scroll expander.

effective. Scroll expanders have a volumetric ratio between 1.5 and 5 and maximum power output reported of 12 kW [15]. Moreover, scroll expanders can have high efficiency as 80% at different operating conditions. Furthermore, the off-design operation of scroll machines was presented in the works of [16] and **Figure 8** adapted from [15] presents the accounting of losses of scroll machine when operated at various pressure ratios.

The results suggest that the highest efficiency is achieved when the scroll machine is operating at a built-in pressure ratio of 4–7. Furthermore, it can be inferred that decline in performance is more rapid for underexpansion when compared with overexpansion. This suggests that a slightly oversized machine will be a better choice for varying load applications. The primary operation range for scroll machines is from 0.5 kWe to 10 kWe output power range. Scroll machines are primarily derived from refrigeration and HVAC compressor units. They could be in various sealing conditions, for instance, hermetic, semi-hermetic, and open-drive configurations. Hermetic-type machines contain electric machines sealed in a single casing along with the compressor/expander. The working fluids may come in contact with electric coils and help to cool down the electrical systems. The machine is not supposed to be opened for services. The semi-hermetic configuration allows the machine to be dismantled for servicing and open-drive systems have generators/motors completely separate from the expander/compressor. The generator/motor is connected to expansion machine by a belt or magnetic coupling allowing the sealing to be limited to expansion machine components only. Technological enhancements to increase the volumetric ratio are being pursued; one of the ways to increase the built-in volume ratio is by utilizing variable thickness walls. However, no such commercial unit is available yet. The operating speeds in general for scroll machines are around 3600 RPM so the generators can be directly coupled to them.

2.2.2. Screw expanders

Screw expanders are composed of two helical rotors designed with an accurate profile to trap the required amount of the working fluid. **Figure 9** (adapted from [17]) presents a schematic

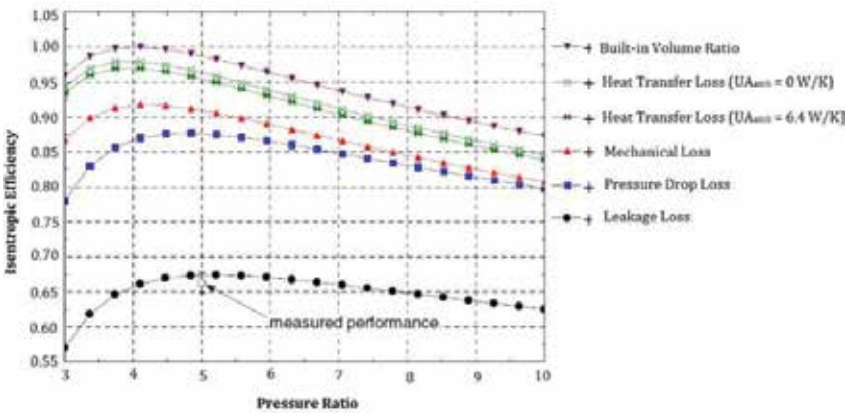

Figure 8. Variation in efficiency as a function of pressure ratio.

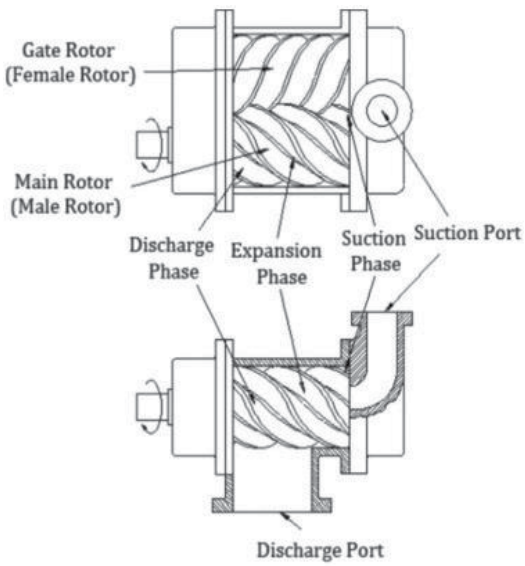

Figure 9. Schematic of a twin screw expander.

of twin screw expander. The synchronized movement of intermeshing rotors generates volume profiles that originate at one end of the rotor and terminate at another end. The working fluid is expanded in that meshed chamber. Screw expanders can be applied in systems with power outputs up to 1 MW. Lubrication is required in screw expanders due to the direct contact between the rotors. However, lubrication can be omitted if a fluid with lubrication specification is adopted. Like scroll expanders, screw expanders can operate with wet working fluids since they can accept large mass fractions.

The rotor clearance is below 50 μm so the leakage losses are comparatively small, thus reducing friction losses. Screw machines exhibit in general medium levels of noise and high costs.

The volumetric ratio can be from 2 to 8. Expander power output ranges from 1.5 kW up to 1 MW. The isentropic efficiencies have been reported to be as high as 70% [15]. They can operate at higher RPM configurations than scroll machines, and a gearbox may be required if the machine is operating above 5000 RPM, which is not uncommon for screw machines. In general screw, machines are suitable for power applications from 5 to 50 kW in ORC applications. **Figure 10** (adapted from [18]) presents the selection maps of working fluids for operation with screw machines based on evaporation and condensing temperatures.

2.2.3. Piston expanders

The working fluid enters the piston expander when the piston is around the top dead centre (TDC) and the inlet valve is then closed. The fluid expands as the piston is pushed by the internal pressure; the energy is transferred to the central crankshaft by connecting rod. The exit valve is opened up at bottom dead centre and expanded working fluid starts moving out of the chamber as the piston moves back to TDC as shown in **Figure 11**.

The piston expanders can have a single piston or multiple piston-cylinder arrangements. The designs are also not limited to the piston-connecting rod and crank-based systems. Linear piston expanders are gaining popularity where a single piston may oscillate in a cylinder and operate in two volume chambers at opposite ends. Apart from the aforementioned, axial configuration, rolling pistons, and swash plates are some of the different types of piston expanders.

Pistons expanders are known to have lower isentropic efficiencies compared to corresponding turbomachines, for example. The maximum reported efficiency is 76% and the average is reported to be around 50% [15]. Piston expanders are characterized by relatively large pressure ratios of 6–14. Due to the low power outputs, such types of volumetric expanders are preferred in small- and micro-scale applications. In general, the output of the expander around 2 kW is reported but one of the works has reported 18.6 kW with steam as the working fluid [15]. Unlike the previous categories of volumetric expanders, piston expanders are adopted with inlet and discharge valves to control the suction and discharge processes. However, for the latter process, exhaust ports can be applied instead of valves which lead to larger work and

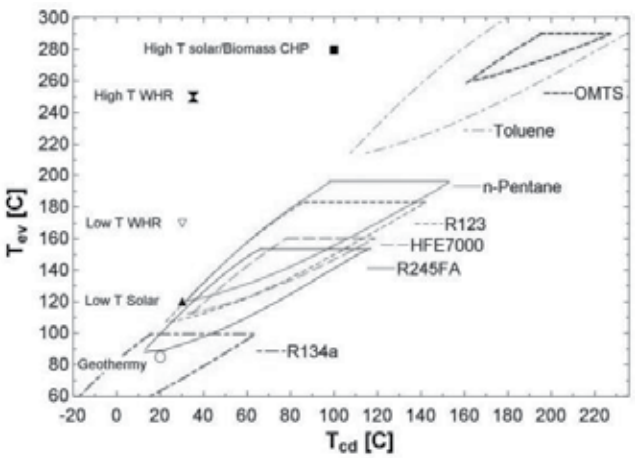

Figure 10. Selection maps for screw expander application.

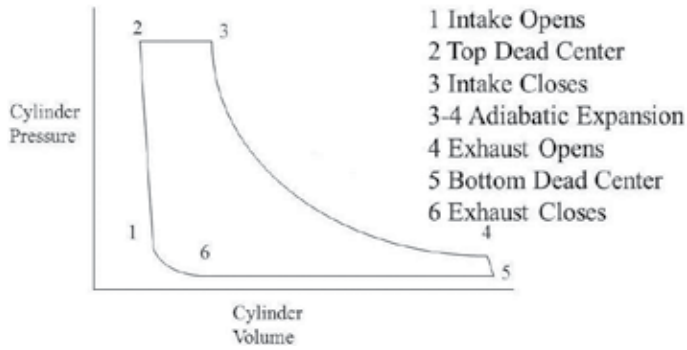

Figure 11. Pressure-volume diagram of piston expander.

lower mass flow rates. Piston expanders can operate under two-phase conditions of the working fluid. However, they are heavy and suffer from noise and vibration. However, like some volumetric expanders, lubrication is required in piston expanders but entails the difficulty of implementation because the oil should be mixed with the working fluid, which reduces the efficiency of the cycle. The piston expanders mainly suffer from the requirement for weight balancing, torque impulse, heavy weight, precise valve operation, and a large number of parts [4] but they have mature manufacturing technology available.

2.2.4. Rotary vane expanders

Rotary vane expanders are operated based on Wankel concept. **Figure 12** adapted from [19] presents the working of a vane expander. Working fluid enters the expander at the location having small clearance. A rotor with moveable vanes is attached to a rotor which is in close proximity to the casing in asymmetric orientation. The rotation of the rotor allows the vanes to move outwards while trapping working fluid, as the rotation angle increases the volume bound by consecutive vanes increases and expansion of working fluid occurs.

Their reported power output ranges from few watts to 2.2 kW. As some volumetric expanders, they can be directly attached to the generator due to their low rotational speeds. They are usually preferred to reduce the system costs because of their simple design and low manufacturing costs, higher torque, and higher volumetric efficiency. In addition, they are mechanically simple and available commercially. In addition, they are characterized by small vibration, low acoustic impact, and simple and reliable structure. However, they exhibit lower isentropic efficiencies compared to other volumetric expanders due to leakages and higher friction losses. Furthermore, the machine must be lubricated to minimize wear and enhance sealing. **Figure 13** presents a picture of actual vane expander and the size can be estimated from the figure. Despite their popularity for micro-scale applications, they have certain technical limitations. The volumetric ratio is limited with commonly reported values of 3–7. The maximum temperature at the inlet is also limited to around 140°C. To ensure the vane movement in the groove and to still minimize the leakage, a tight tolerance is maintained. If a very high-temperature working fluid is passing through it, the expansion of vanes might cause them to stick and the machine will cease its operation. This limits the use of vane expanders for high-temperature applications [12].

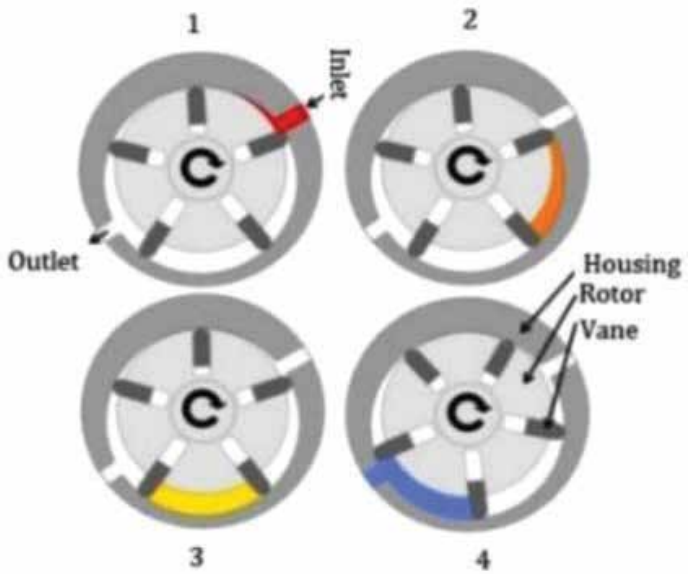

Figure 12. Operation of a rotary vane expander.

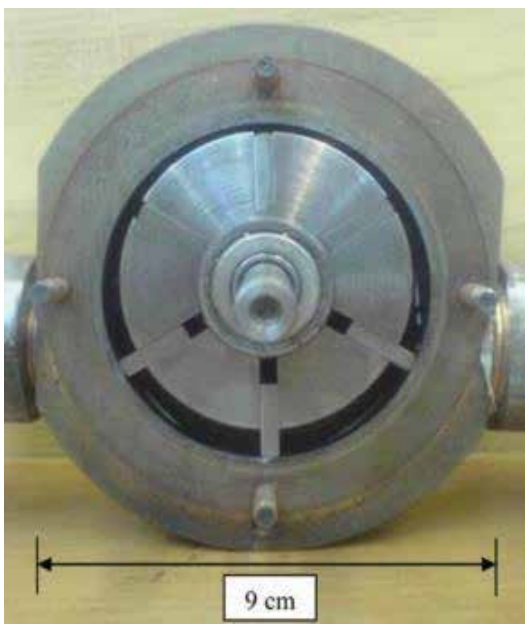

Figure 13. Photograph of the actual vane expander from the works of [20].

3. Multiphase expansion capability

Working fluids with a positive temperature-entropy slope or at least isentropic expansion capability are preferred for organic Rankine cycle applications to avoid the formation of

liquid droplets during the expansion process which can lead to erosion problems. ORC systems utilizing variable heat source conditions (flow rate or temperature) are specifically prone to two-phase fluid admittance in expansion machines. Although the degree of superheating is continuously monitored by control systems, under severe fluctuating heat source conditions, which are typical for an automobile engine operating in an urban driving cycle, the tight control of the degree of superheating becomes difficult even for state-of-the-art control schemes. The influx of the liquid phase becomes unavoidable in such cases. Furthermore, the trilateral flash cycles are considered thermodynamically beneficial [21, 22] but they need expansion machines which are capable of handling multiphase fluids.

The turbo-expanders have very limited capability to handle multiphase flows. Major erosion problems arise when liquid droplets strike the rotor blades. Thin liquid films may form on the stator and then larger droplets are shed which accelerate along the high-velocity gas molecules towards the rotor blades. The velocity of droplets is not immensely high due to their large inertia but when fast-moving rotor blades are hit the change in momentum can cause tremendous localized forces and cause the erosion of rotor blades specifically at leading edges and near the tip due to higher tangential velocities [23]. Some coatings can slow down the erosion process but increase the expander cost and complexity. Water drainage systems and blade heating systems to prevent liquid flow are very difficult to implement for small-scale systems.

Volumetric machines are generally more tolerant to admission liquid phase primarily due to lower component velocities involved. Scroll and screw machines are well known for the capability of flooded expansion. Recent research [24] compared the experimental results of a 2 kW-class scroll machine for superheated expansion and flooded expansion. The results indicate that system can run smoothly for flooded expansion and even at conditions where both inlet and outlet of the expander have two-phase conditions. The net power output was observed to be lower as the cycle work output is reduced thermodynamically. However, it was not possible to report the isentropic efficiency in the multiphase expansion regime as instrumentation capability was limited. Furthermore, a significant quantity of oil was used to test the liquid flooded expansion in the scroll machine in the works of [25] and only a modest decrease in performance was observed. It was also discovered that liquid injection can reduce the leakage losses in scroll machines and can be a promising solution for trilateral flash-cycle expanders for the smaller scale [26].

Screw expanders are particularly popular for their potential use in trilateral flash cycles. Screw machines have been tested with flooded expansion in various studies. Up to 0.1 mass fraction of liquid oil was used to test the performance of the expander in [27] and it was reported that the presence of liquid oil helps to seal the clearance volumes at lower operational speeds and as throttling losses become dominant at higher rotational speeds. The authors concluded that further work with low-viscosity working fluids and impact of gases and liquid working fluid along with lubricants needs to be pursued. The authors in [28] compared dry expansion and water-flooded expansion and concluded that water-flooded machines are preferable to dry-running machines for all circumferential speeds but oil-flooded expansion was beneficial for lower speeds. It was also proposed in the literature [29] that screw expanders can be built no larger than current gas compressors to work as two-phase expanders with far higher efficiencies than were believed to be possible for trilateral flash cycles. If the liquid-flooded working fluid can also act as the lubricant instead of oil, the expander and cycle performance

can increase substantially in organic Rankine cycle trilateral flash cycles [30]. The multiphase expansion capability of reciprocating expanders still needs to be investigated in detail with a focus on the throttling losses through the inlet valves.

4. Conclusion

It is evident that no expander technology is perfect; each type of machine has its own advantages and disadvantages. Based on the literature survey and experiences in commercial applications of ORCs, it is clear that efficiency and cost are a function of power output. In general, efficiency increases and cost reduces per kW as the power output is increased. In the context of the presented text in the chapter, it can be concluded that in general volumetric machines are suitable for smaller power output systems. Vane-type expanders are suitable for power outputs below 1.5 kWe, and scroll machines are suitable in the range of 1–5 kWe. Screw machines are suitable for the range of 5–50 kWe. Piston expanders are suitable for larger pressure ratios between 5 and 20 kWe. Turbomachines are suitable for larger-scale systems or if the cost of manufacturing is reduced then they can replace the volumetric machine with their single-stage expansion capability and high comparative efficiencies. In general, radial inflow machines are suitable from 30 to 500 kWe; recent advances in the industry have also successfully implemented radial machines in the MWe range. Axial machines are, however, the dominant type in the MW power range. Radial outflow machines appear to be competitive in the small-scale range below 50 kWe where radial inflow machines require higher rotational speeds.

Author details

Fuhaid Alshammari, Muhammad Usman and Apostolos Pesyridis*

*Address all correspondence to: a.pesyridis@brunel.ac.uk

Department of Mechanical, Aerospace and Civil Engineering, Centre for Advanced Powertrain and Fuels (CAPF), Brunel University London, Uxbridge, United Kingdom

References

[1] Ibarra M, Rovira A, Alarcón-Padilla D-C, Blanco J. Performance of a 5 kWe organic Rankine cycle at part-load operation. Applied Energy [Internet]. May 2014;**120**:147-158. Available from: http://linkinghub.elsevier.com/retrieve/pii/S0306261914000865 [Accessed: Mar 13, 2014]

[2] Colonna P, Casati E, Trapp C, Mathijssen T, Larjola J, Turunen-Saaresti T, et al. Organic Rankine cycle power systems: From the concept to current technology, applications and an outlook to the future. Journal of Engineering for Gas Turbines and Power [Internet]. 2015;**137**(October):1-19. Available from: http://gasturbinespower.asmedigitalcollection.asme.org/article.aspx?doi=10.1115/1.4029884

[3] Colonna P, Harinck J, Rebay S, Guardone A. Real-gas effects in organic Rankine cycle turbine nozzles. Journal of Propulsion and Power [Internet]. Mar 1, 2008;**24**(2):282-294. DOI: 10.2514/1.29718

[4] Rahbar K, Mahmoud S, Al-Dadah RK, Moazami N, Mirhadizadeh SA. Review of organic Rankine cycle for small-scale applications. Energy Conversion and Management [Internet]. 2017;**134**:135-155. DOI: 10.1016/j.enconman.2016.12.023

[5] Balje OE. Turbomachines: A Guide to Design, Selection, and Theory [Internet]. New York (N.Y.): Wiley; 1981 Available from: http://lib.ugent.be/catalog/rug01:000203945

[6] Persico G, Pini M. 8-Fluid dynamic design of Organic Rankine Cycle turbines. In: Organic Rankine Cycle (ORC) Power Systems. Woodhead Publishing. 2017. PP. 253-297. ISBN 9780081005101. https://doi.org/10.1016/B978-0-08-100510-1.00008-9. https://www.sciencedirect.com/science/article/pii/B9780081005101000089

[7] Pini M, De Servi C, Burigana M, Bahamonde S, Rubino A, Vitale S, et al. Fluid-dynamic design and characterization of a mini-ORC turbine for laboratory experiments. Energy Procedia [Internet]. 2017;**129**:1141-1148. DOI: 10.1016/j.egypro.2017.09.186

[8] Valdimarsson P. 10-Radial inflow turbines for Organic Rankine Cycle systems. In: Organic Rankine Cycle (ORC) Power Systems. Woodhead Publishing. 2017. PP. 321-334. ISBN 9780081005101. https://doi.org/10.1016/B978-0-08-100510-1.00010-7. https://www.sciencedirect.com/science/article/pii/B9780081005101000107

[9] Casati E, Vitale S, Pini M, Persico G, Colonna P. Centrifugal turbines for mini-ORC power systems. Journal of Engineering for Gas Turbines and Power. 2014;**136**(December):1-11

[10] Spadacini C, Rizzi D. 11-Radial outflow turbines for Organic Rankine Cycle expanders, In Organic Rankine Cycle (ORC) Power Systems, Woodhead Publishing, 2017. PP. 335-359, ISBN 9780081005101, https://doi.org/10.1016/B978-0-08-100510-1.00011-9. https://www.sciencedirect.com/science/article/pii/B9780081005101000119

[11] Macchi E, Astolfi M. 9-Axial flow turbines for Organic Rankine Cycle applications. In: Organic Rankine Cycle (ORC) Power Systems, Woodhead Publishing, 2017. PP. 299-319, ISBN 9780081005101, https://doi.org/10.1016/B978-0-08-100510-1.00009-0. (https://www.sciencedirect.com/science/article/pii/B9780081005101000090)

[12] Lemort V, Legros A. 12 - Positive displacement expanders for Organic Rankine Cycle systems. In: Organic Rankine Cycle (ORC) Power Systems. Woodhead Publishing. 2017. PP. 361-396. ISBN 9780081005101. https://doi.org/10.1016/B978-0-08-100510-1.00012-0. (https://www.sciencedirect.com/science/article/pii/B9780081005101000120)

[13] Quoilin S, Van Den BM, Declaye S, Dewallef P, Lemort V. Techno-economic survey of organic Rankine cycle (ORC) systems. Renewable and Sustainable Energy Reviews. 2013;**22**:168-186

[14] Saitoh T, Yamada N, Wakashima S. Solar Rankine cycle system using scroll expander. Journal of Environmental Engineering [Internet]. 2007;**2**(4):708-719 Available from: http://joi.jlc.jst.go.jp/JST.JSTAGE/jee/2.708?from=CrossRef

[15] Imran M, Usman M, Lee DH, Park BS. Volumetric expanders for low grade & waste heat recovery applications. Renewable and Sustainable Energy Reviews. 2016. DOI: 10.1016/j.rser.2015.12.139

[16] Lemort V, Declaye S, Quoilin S. Experimental characterization of a hermetic scroll expander for use in a micro-scale Rankine cycle. Proceedings of the Institution of Mechanical Engineers, Part A: Journal of Power and Energy. 2012;**226**(1):126-136

[17] Smith IK, Stosic N. Prospects for energy conversion effeiciency improvement by use of twin screw two phase expander. In: 2nd Int Heat Power Cycles Conf. Paris, France; 2001. DOI: 10.1.1.573.9532

[18] Quoilin S, Sart-tilman C. Expansion machine and fluid selection for the organic Rankine cycle. In: 7th International Conference on Heat Transfer, Fluid Mechanics and Thermodynamics July 19-21, 2010, Antalya, Turkey. 2010. http://hdl.handle.net/2268/62997

[19] Imran M, Usman M, Lee DH, Park BS. Volumetric expanders for low grade & waste heat recovery applications. Renewable and Sustainable Energy Reviews [Internet]. May 2016;**57**:1090-1109. Available from: http://www.sciencedirect.com/science/article/pii/S1364032115015221 [Accessed: Jan 10, 2016]

[20] Farrokhi M, Noie SH, Akbarzadeh AA. Preliminary experimental investigation of a natural gas-fired ORC-based micro-CHP system for residential buildings. Applied Thermal Engineering [Internet]. Aug 1, 2014;**69**(1-2):221-229. Available from: https://www.sciencedirect.com/science/article/pii/S1359431113008648 [Accessed: Apr 30, 2018]

[21] Astolfi M. Technical options for organic Rankine cycle systems. Organic Rankine Cycle (ORC) Power Systems: Technologies and Applications. 2016;**1**:67-89

[22] DiPippo R. Ideal thermal efficiency for geothermal binary plants. Geothermics [Internet]. Jun 2007;**36**(3):276-285. Available from: http://www.sciencedirect.com/science/article/pii/S0375650507000375 [Accessed: Oct 21, 2014]

[23] Rossi P, Raheem A, Abhari RS. Numerical model of liquid film formation and breakup in last stage of a low-pressure steam turbine. Journal of Engineering for Gas Turbines and Power [Internet]. 2017;**140**(3):32602. Available from: http://gasturbinespower.asmedigitalcollection.asme.org/article.aspx?doi=10.1115/1.4037912

[24] Sun H, Qin J, Hung TC, Lin CH, Lin YF. Performance comparison of organic Rankine cycle with expansion from superheated zone or two-phase zone based on temperature utilization rate of heat source. Energy [Internet]. 2018;**149**:566-576. DOI: 10.1016/j.energy.2018.02.047

[25] Bell IH, Lemort V, Groll EA, Braun JE, King GB, Horton WT. Liquid flooded compression and expansion in scroll machines – Part II: Experimental testing and model validation. International Journal of Refrigeration [Internet]. 2012;**35**(7):1890-1900. DOI: 10.1016/j.ijrefrig.2012.07.008

[26] Mendoza LC, Lemofouet S, Schiffmann J. Testing and modelling of a novel oil-free co-rotating scroll machine with water injection. Applied Energy [Internet]. 2017;**185**:201-213. DOI: 10.1016/j.apenergy.2016.10.089

[27] Nikolov A, Brümmer A. Investigating a small oil-flooded twin-screw expander for waste-heat utilisation in organic Rankine cycle systems. Energies. 2017;**10**(7):869. DOI:10.3390/en10070869

[28] Gräßer M, Brümmer A. Influence of liquid in clearances on the operational behaviour of twin screw expanders. IOP Conference Series Materials Science and Engineering. 2015;**90**(1):38-46

[29] Smith IK, Stošič N, Aldis CA. Development of the trilateral flash cycle system: Part 3: The design of high-efficiency two-phase screw expanders. Proceedings of the Institution of Mechanical Engineers, Part A: Journal of Power and Energy [Internet]. 1996;**210**(1):75-93 Available from: http://pia.sagepub.com/content/210/1/75%5Cnhttp://pia.sagepub.com/content/210/1/75.short

[30] Ziviani D, Groll EA, Braun JE, De Paepe M, van den Broek M. Analysis of an organic Rankine cycle with liquid-flooded expansion and internal regeneration (ORCLFE). Energy [Internet]. 2018;**144**:1092-1106. DOI: 10.1016/j.energy.2017.11.099

Section 2

Dynamic Models

Chapter 4

Modeling for Organic Rankine Cycle Waste Heat Recovery System Development

Bin Xu, Adamu Yebi and Zoran Filipi

Additional information is available at the end of the chapter

http://dx.doi.org/10.5772/intechopen.78997

Abstract

This chapter introduces the modeling of organic Rankine cycle waste heat recovery (ORC-WHR) system. The main goal of this chapter is to give an overview of ORC-WHR system modeling, especially focus on the heat exchanger models due to its key role in the ORC-WHR system development. Six heat exchanger models considered in this chapter includes static model, 0D dynamic model, 1D finite volume model, 1D moving boundary model, 2D & 3D model. Model complexity, accuracy, and computation time are analyzed for the six heat exchanger models. More importantly, the heat exchanger model selection is discussed based on different phase of ORC-WHR system development, which facilitates the development of ORC-WHR system, and reduces the system development cost. In addition, a full ORC-WHR system model is presented as a modeling example including heat exchanger model, expander model, valve model and pump model.

Keywords: modeling, overview, heat exchanger, organic Rankine cycle, waste heat recovery

1. Introduction

As the virtual representation of the ORC-WHR system, ORC-WHR model is a great tool to reduce the cost and time of system development. The ORC-WHR model can be categorized based on the heat exchanger modeling method as shown in **Figure 1**. Based on whether the model includes Ordinary Differential Equations (ODEs) or not, the heat exchanger models can be classified as dynamic model (w/ODEs) and static model (w/o ODEs). Under the dynamic category, the models are further classified based on the model dimension (0D, 1D, 2D and 3D). Under the 1D category, the models can be classified based on the concept of modeling (moving boundary model and finite volume model).

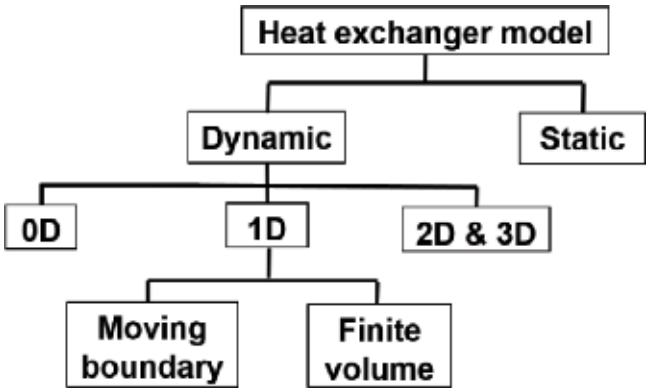

Figure 1. Heat exchanger modeling methods in ORC-WHR application.

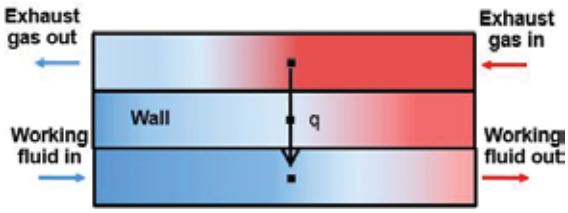

Figure 2. 0D heat exchanger dynamic model diagram.

Generally, static modeling method only considers the energy balance of heat exchanger (i.e. the heat release from the heat sources equals to the heat absorption by the working fluid) [1–3]. Due to the static models lacking ODEs, there is no time varying parameter. Thus, this method can only analyze the steady state condition.

On the contrary, dynamic modeling methods are capable of simulating the transient conditions and provide the parameter vector that changes along the time vector. 0D model [4, 5] lumps the parameter in a single point as shown in **Figure 2** and the parameter is the same in any location of heat exchanger. For example, the heat source temperature is the same between the location near the exhaust gas inlet and the location near the exhaust gas outlet of heat exchanger. 1D model considers the one dimension in the direction of flow path. Two typical 1D models are finite volume model [6–8] and moving boundary model [9–11] as shown in **Figures 3** and **4**, respectively. For instance, the heat source temperature is different at different location of the flow path. The 2D and 3D models consider not only one dimension in the flow path direction, but also the directions perpendicular to the flow path axis.

The model is critical in the ORC-WHR system development. Static modeling method is utilized to analyze the energy flow and cycle efficiency at the beginning phase of the ORC system development. With the help of static models, heat sources selection, working fluid screening, expander machine selection, and cycle efficiency calculation can be roughly conducted. Dynamic models are developed in later phase of ORC-WHR system development to help

http://dx.doi.org/10.5772/intechopen.78997

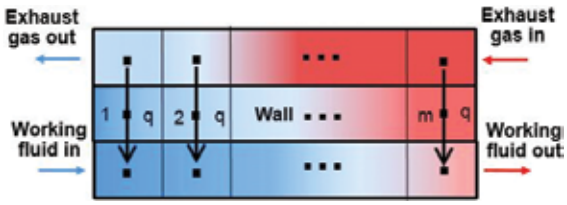

Figure 3. 1D heat exchanger finite volume model diagram.

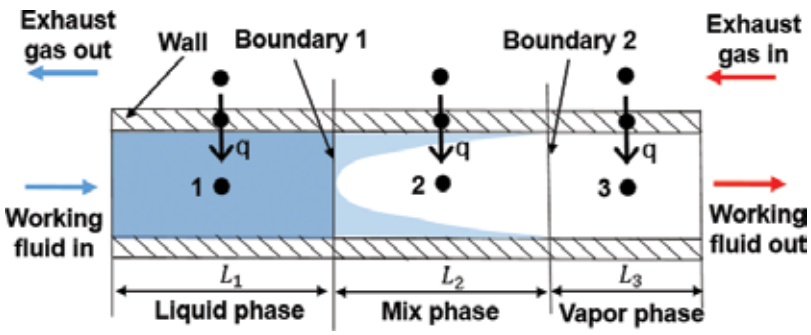

Figure 4. 1D heat exchanger moving boundary model diagram.

component development, control development and power optimization. The advantage of the dynamic model is its transient capability, which can predict the component performance over transient operating condition, evaluate the control strategies, and assist power optimization at transient conditions.

The ORC-WHR system model includes four main components and other supporting components. The four main components include evaporator, expander, condenser, and working fluid pump as shown in **Figure 5**. The other supporting components include valves, pipes, reservoir, feed pump, etc. The four main components exist in all the ORC-WHR system and the number of supporting components depend on the specific applications.

There are several challenges in the ORC-WHR system modeling:

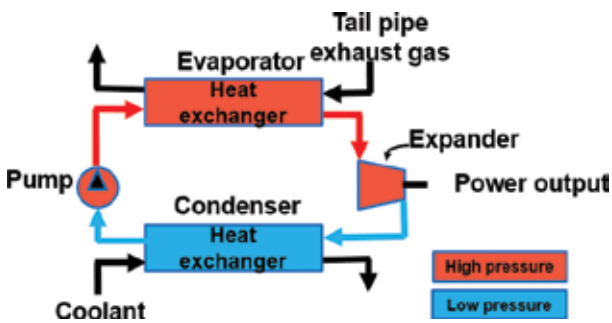

Figure 5. ORC-WHR system diagram.

The first modeling challenge is the heat exchanger modeling method selection. Heat exchanger is the key component of the system and there are several available modeling methods. The modeling process is time-consuming. Thus, it is extremely important to choose the right modeling method before diving into the modeling details.

The second challenge is the fidelity of the model or assumptions to be made. The more assumptions to be made, the less fidelity the model will be. On the other hand, the less assumptions require more modeling time and effort. Thus, there is a trade-off between the model fidelity and modeling effort. However, the smart choose of assumptions might significantly reduce the modeling time and effort depending on the purposes of the model.

The third challenge is the system model integration [7] and robustness. After the component models are finished, the component models need to be integrated together to simulate the entire ORC-WHR system. The inputs and outputs of the connected models must be compatible to each other. In addition, the robustness of the integrated model could be a problem in highly transient operating conditions such as ORC system warmup, cool down, or heat source fast step change, etc. Moreover, the coupling dynamics of working fluid temperature, pressure and phase change increases the difficulty of system model robustness improvement.

Section 2 gives an overview of the ORC-WHR system model and discusses the heat exchanger model comparison and selection at different phases of ORC-WHR system development. Section 3 presents the details of a finite volume heat exchanger model, expander model, valve model and pump model as an ORC-WHR system model example.

2. Overview of the ORC-WHR modeling

This section gives an overview of the ORC-WHR system modeling methods in terms of model complexity, accuracy, and computation time. With the modeling overview, it is easier to find the right modeling method in certain ORC-WHR system development phase. Among the four main components, pump model and expander model are generally simple compared with the heat exchanger model and there is no many choices respective to the pump and expander modeling methods. Heat exchanger model is the most challenging one in many cases. Thus, this chapter mainly focus on the heat exchanger modeling methods comparison and evaluation.

2.1. Heat exchanger model complexity

Model complexity indirectly represents the modeling time and effort required to build the model. The less complexity, the less modeling time and effort are required. In previous section, heat exchanger modeling methods are classified in **Figure 1**. In terms of model complexity, static heat exchanger model has the lowest complexity compared with dynamic model. The reason is that no ODE exists in the governing equations. All the equations are algebraic relation with energy balance. Using static method, the heat exchanger energy balance only has one equation and is given as follows:

$$\dot{m}_{hs}c_{p,hs}(T_{hs,in} - T_{hs,out}) = \dot{m}_f\left(h_{f,out} - h_{f,in}\right) \tag{1}$$

where $\dot{m}_{hs}$ is heat source mass flow rate, $c_{p,hs}$ is the heat source heat capacity, $T_{hs,in}/T_{hs,out}$ are heat source heat exchanger inlet/outlet temperature, $h_{f,in}$ and $h_{f,out}$ are the working fluid enthalpy at heat exchanger inlet and outlet. They can be calculated based on the working fluid thermodynamic table as follows:

$$h_{f,in} = map\left(p_{f,evap,}\, T_{f,in}\right) \tag{2}$$

$$h_{f,out} = map\left(p_{f,evap,}\, T_{f,out}\right) \tag{3}$$

where $T_{f,in}$, $T_{f,out}$ are working fluid heat exchanger inlet/outlet temperature, $p_{f,evap}$ is working fluid evaporation pressure. Different from static heat exchanger model, dynamic heat exchanger model considers the ODEs in the governing equations. In addition, the wall dynamics are included in the governing equations. Take 0D dynamic model as an example. Assuming there is not pressure drop across the heat exchanger, pressure dynamics are fast dynamics and can be neglected in the energy balance equation. The heat exchanger energy balance then include three equations:

Heat source energy balance:

$$m_{hs}c_{p,hs}\frac{dT_{hs}}{dt} = \dot{m}_{hs}c_{p,hs}(T_{hs,in} - T_{hs,out}) - A_{hs,w}U_{hs,w}(T_{hs} - T_w) \tag{4}$$

Working fluid energy balance:

$$m_f\frac{dh_f}{dt} = -\dot{m}_f\left(h_{f,out} - h_{f,in}\right) + A_{f,w}U_{f,w}\left(T_w - T_f\right) \tag{5}$$

Wall energy balance:

$$m_w c_{p,w}\frac{dT_w}{dt} = A_{hs,w}U_{hs,w}(T_{hs} - T_w) - A_{wf,w}U_{wf,w}\left(T_w - T_f\right) \tag{6}$$

where $A_{hs,w}$, $U_{hs,w}$ are the heat transfer area and heat transfer coefficient between heat source and wall. The wall is the medium separating the heat source and working fluid. $A_{f,w}$, $U_{f,w}$ are the heat transfer area and heat transfer coefficient between working fluid and wall.

The 0D dynamic model has three equations in energy balance, whereas static model only has one equation in energy balance. Besides more equations in 0D dynamic model, each equation has more terms than that from static model. In addition, the working fluid mass balance equation is another equation in the 0D dynamic model as presented in Eq. (7). Thus 0D dynamic model is more complex than the static model and the 0D dynamic model requires more time and effort in modeling.

$$\frac{dm_f}{dt} = \dot{m}_{f,in} - \dot{m}_{f,out} \tag{7}$$

1D dynamic models share the same four governing equations (Eqs. (4-7)) with 0D in each discretized cell. The main difference is that 0D model has only one cell and 1D models have more than one cell. 1D dynamic models include finite volume model and moving boundary model. Finite volume model includes m discretized cells, each cell has the same volume. Moving boundary model includes three cells, each cell has different volume, which are determined by the phase of working fluid. There are three phases in the working fluid inside the heat exchanger including pure liquid, mixed (liquid & vapor) and pure vapor. Each phase occupies one cell in the moving boundary model. The governing Eqs. (4-7) are applied in each cell of 1D finite volume model and moving boundary model. Therefore, the 1D heat exchanger models has more equations than the 0D heat exchanger model. In terms of model complexity, 1D heat exchanger models are more complex than the 0D model. Even though both 0D and 1D models share similar governing equations, 1D models need to consider the boundary conditions between the adjacent cells, whereas 0D model only need to consider the boundary conditions at the heat exchanger inlet and outlet. Between the two 1D models, considering finite volume model generally has more than three cells, 1D moving boundary model has less governing equations than the 1D finite volume method and the number of different equations is (m-3)*4. Even though finite volume model has more equations, different cells share equations, which means as long as Eqs. (4-7) are developed, finite volume model is almost done. However, moving boundary model three cells do not share exact Eqs. (4-7). In moving boundary model, Eqs. (4-7) are implemented into three cells. Due to the cell volume is not fixed, the equations requires further derivation and finally 12 different equations are derived. In other words, at different cell, Eqs. (4-7) have different formats. These derivation increases the model complexity of the moving boundary model and results in that moving boundary model complexity is higher than the finite volume model.

2D and 3D heat exchanger models are more complex than the 1D and 0D heat exchanger models and are generally modeled in CFD softwares (e.g. ANSYS, FLUENT, etc.).

Overall the heat exchanger model complexity rank can be given as follows: static model <0D dynamic model <1D dynamic finite volume model <1D dynamic moving boundary model <2D & 3D dynamic model.

2.2. Heat exchanger model accuracy

Accuracy is the model characteristic that everyone wants to maximize, because it determines the value of the model in some sense. Unlike model complexity, model accuracy can be easily quantified. There is a reference to compare with the model prediction and the accuracy represents the error between the model prediction and the reference.

Static heat exchanger model is utilized in the concept phase in the ORC-WHR development. In the concept phase, no components are selected and no experiments are conducted. Thus, in general, there is no reference data to evaluate the accuracy of the static model. Static model is

usually utilized to assist basic energy balance between the heat sources and working fluid. This calculation only needs to give an estimate result and does not require high accurate model. In the static modeling process, many parameters are generally not considered such as heat transfer area and heat transfer coefficient in the heat exchanger, and heat loss from the heat exchanger to the ambient. Therefore, the static heat exchanger model accuracy is not high.

0D dynamic heat exchanger model makes less assumptions than the static model, which improves the model accuracy. To be specific, 0D model considers the heat transfer area and heat transfer coefficients in the heat exchanger. In addition, 0D model is generally validated by experimental data, which also increases the model accuracy compared with static model.

1D finite volume model and moving boundary model have less assumptions than the 0D model in that they consider one more dimension than the 0D model. With 1D model, the parameters of working fluid, heat source and wall have different values at different location in the axis of flow path, whereas 0D model share the same value at different location. This one more dimension feature equips the 1D models with higher fidelity than the 0D model. Thus 1D models have higher accuracy than the 0D model. Between the two 1D models, finite volume model has finer discretization resolution than the moving boundary model (m vs. 3 in **Figures 3** and **4**). Therefore, as the number m goes larger, the 1D finite volume model could have higher accuracy than the 1D moving boundary model.

2D and 3D heat exchanger model have less assumption than the 1D or 0D heat exchanger models, which equips them with higher accuracy.

Overall, the accuracy rank of all the heat exchanger models are as follows: Static model < 0D dynamic model < 1D moving boundary model < 1D finite volume model < 2D & 3D heat exchanger model.

2.3. Heat exchanger model computation time

The computation time is very important if the model needs to run online or the model is implemented in computational costly algorithms offline like Dynamic Programming. Static model only has algebraic equations and is the fastest model among all the heat exchanger models. The computation time of 0D and 1D models can be evaluated by the number of ODEs of the corresponding model. As mentioned earlier this section, the 0D model has the least number of ODEs, followed by 1D moving boundary model and 1D finite volume model, respectively. Similarly, the 2D model has more ODEs than 1D model and less ODEs than 3D model.

Therefore, the computation time of all the heat exchanger models can be ranked as follows: static model <0D model <1D moving boundary model <1D finite volume model <2D & 3D model.

2.4. Model selection at different ORC-WHR system development phases

Selecting the right heat exchanger model at different phase of ORC-WHR system development has three benefits:

1. Meeting the certain development phase goals;
2. Reducing the time and effort of modeling;
3. Reducing the cost of modeling.

The ORC-WHR system development procedures can be explained using the diagram shown in **Figure 6**. The system development starts from concept design, in which phase the heat sources selection, working fluid selection, expander selection, expander power output form (electrical or mechanical) and system configuration are roughly evaluated and determined. It is common that some of the selection may be not finalized, which needs further investigation in the latter phases of the development. In the concept phase, some general energy balance are calculated to evaluate the power output at different operating condition and different system configuration. There is no experimental data and the calculation is not necessarily to be very accurate. Thus, the static heat exchanger model fits this development phase. The model is not very accurate, but its accuracy is enough to generate a general estimation of energy balance between heat sources and working fluid, and power output value from the expander machine.

After the concept phase, the component selection and development phase follows, during which the components hardware are selected based on the available products on the market or designed and manufactured. This is the first generation of the components selection, which may change several other generations based on the individual and integrated system experiments. Experimental data are collected from individual components. During this phase, the component models help the design of some components details such as the heat transfer area of heat exchanger, the nozzle area of turbine expander, the expansion ratio of piston expander, the size of the valve, the displacement of pump and the inner diameter of connected pipes. During this phase, the static model and 0D heat exchanger model help design the details of heat exchanger. The 0D model can be identified by the experimental data from the heat exchanger. The identified 0D model gives hints on updating the current heat exchanger generation to the next level by sweep some of key design parameters such as heat transfer area, section area of flow path, and length of flow path. The expander machine prototype can generate an efficiency or power map as a function of variables like expander speed, inlet pressure, outlet pressure, and expansion ratio. This map helps build either map-based or physics-based expander model.

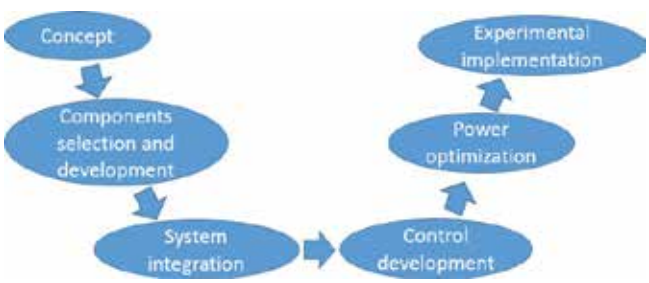

Figure 6. ORC-WHR system development procedures.

The third development phase is system integration phase, during which the ORC-WHR components hardware are connected in the test rig. During this phase, the model is not required. As the components are integrated into an entire system, the next step is to conduct the experiments. However, without control, the ORC-WHR system experiments are hard to conduct due to the coupling of working fluid temperature, evaporation pressure, and the transient heat source.

The fourth development phase is the control development. The most important control in ORC-WHR system are the working fluid temperature control and evaporation pressure control. It is possible to develop the temperature and pressure control without a model (i.e. traditional PID feedback control). However, many simulation and experiments showed that the traditional PID feedback control cannot control the ORC-WHR system very well. Feedforward plus feedback or advanced controls (e.g. model predictive control) are proposed by many researchers in the field of ORC-WHR system. Both the feedforward and advanced controls require system models, either simple models or complex models. In the feedforward control, the highly accurate model helps improve the control performance. However, due to the combination with PID feedback control, the feedforward control model does not have to be very accurate. Because the feedback control helps correct the error brought by the feedforward control. Lower accuracy requirement helps reduce the modeling effort. Thus, static model or 0D model are common in feedforward control design. In advanced controls, the model accuracy has higher requirements than the feedforward control. It is because generally there is no feedback control to correct the model error. Accuracy is one of the constraints for advanced control and computation time is the other because the advanced control needs to run online. The accuracy constraint eliminates the possibility of selecting static model or 0D model and the computation time constraint eliminates the possibility of 1D finite volume model and 2D or 3D model. Thus, most of advanced controls developed for ORC-WHR system utilized 1D moving boundary model as the heat exchanger control-oriented model even though the moving boundary model has relative high model complexity.

The fifth development phase is the power optimization phase. After the control development, the experiments can be conducted. However, there is still a gap to reach the system design goal, which is the selection of the optimal reference trajectories for working fluid temperature at the outlet of evaporator heat exchanger, evaporation pressure, condensation pressure, working fluid subcooling temperature at condenser outlet etc. The model helps identify the optimal reference trajectories corresponding to the maximum expander power or net power from the ORC-WHR system at varying heat sources operating conditions. There are three methods to achieve the power maximization goal: (1) develop a map or a correlation between the optimal reference and the inputs such as heat sources mass flow rate and temperature. The map or correlation is from the optimal results from the steady state analysis with the help of model. In this method, accuracy is the most important factor and model complexity is also important. Therefore, finite volume method fits this requirement very well. (2) Develop an optimal reference trajectory based on transient driving cycle. Compared with steady states, transient driving cycle optimization requires more computation time, especially for dynamic programming algorithm. Thus, computation time is the most important factor for the model. The model accuracy should not be too low. Therefore,

0D model meets this criteria. (3) Directly optimize the power in the advanced control developed in the control development phase. In this case, no extra effort is needed in the power optimization phase. However, due to the computation time limitation of the online advanced control, the 'optimal' power calculated by the advanced control is local optimal rather than global optimal, which is the drawback of this third method.

As long as the control development and power maximization phases are done, the experimental implementation phase does not require the model.

3. Modeling of ORC-WHR system

This section presents the details of a full ORC-WHR system model, aiming to provide an example of modeling of entire ORC-WHR system. The configuration of the example system is shown in **Figure 7**. The tail pipe (TP) exhaust gas from an internal combustion engine is considered as heat source. Electrified turbine expander is chosen as expander machine. One valve is installed upstream of turbine expander to protect turbine from liquid working fluid during the system warmup or highly transient engine conditions. Another valve is installed in the bypass of turbine to allow working fluid bypass the turbine and also controls the working fluid evaporation pressure.

3.1. Heat exchanger modeling

Two heat exchangers exist in the ORC system including evaporator and condenser. In this chapter, only TP evaporator model is presented and the condenser is modeled using the same method. Two assumptions made in the TP evaporator model: (i) axial heat conduction are not considered in all three medium (working fluid, wall and TP exhaust gas), (ii) the wall temperature gradient in the radial direction is neglected, and (iii) pressure drop across the heat exchanger is not considered.

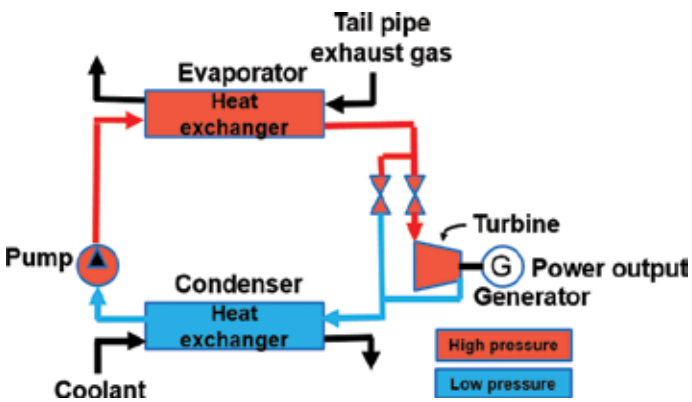

Figure 7. ORC-WHR system diagram.

The working fluid mass balance can be expressed as:

$$\frac{\partial A_{f,cross}\rho_f}{\partial t} + \frac{\partial \dot{m}_f}{\partial z} = 0 \tag{8}$$

where A_{cross} represents cross-sectional area, subscript f represents working fluid, ρ represents density, $\dot{m}$ is mass flow rate, z represents spatial position in the axial direction. Mass flow balance in the exhaust gas side is ignored due to the exhaust gas fast dynamics. The working fluid and exhaust gas energy balance are expressed in the follow form:

$$\frac{\partial (A_{cross}\rho h)}{\partial t} + \frac{\partial \dot{m} h}{\partial z} = \pi d U \Delta T \tag{9}$$

where p represent pressure, h represent enthalpy, d represents the effective flow path diameter, U represents the heat transfer coefficient, and ΔT represents temperature difference between the wall and the fluid (working fluid or exhaust gas).

The wall energy balance is shown below:

$$A_{w,cross} c_{p,w} \rho_w L_w \frac{dT_w}{dt} = A_{f,w} U_{f,w} \Delta T_{f,w} + m_\eta A_{e,w} U_{e,w} \Delta T_{e,w} \tag{10}$$

where c_p represents heat capacity, L represents the length in axial direction, $A_{f,w}$ represents the heat transfer area between working fluid and wall, $U_{f,w}$ represents the heat transfer coefficient between working fluid and wall. m_η represents the heat exchanger efficiency multiplier, which accounts for heat loss to the ambient, $A_{e,w}$ represents the heat transfer area between exhaust gas and wall, $U_{e,w}$ is the heat transfer coefficient between exhaust gas and wall, and subscript w represents wall.

Figure 3 presents the finite volume method for heat exchanger modeling. The model includes m uniform volumetric cells. In each cell, the heat q flows from the exhaust gas through the wall to working fluid and governing Eqs. (8-10) are solved in each cell. In this counterflow design, the exhaust gas flows right to left and the working fluid flows left to right.

Eqs. (8) and (9) are simplified to ODE Eqs. (4) and (7). Eq. (10), Eq. (4) and Eq. (7) are solved as follows:

$$T_{w,t(k+1)} = T_{w,t(k)} + \frac{A_{f,w} U_{f,w,t(k)} \Delta T_{f,w,t(k)} + A_{e,w} U_{e,w,t(k)} \Delta T_{e,w,t(k)}}{A_{w,cross} c_p \rho_w L_w} \Delta t \tag{11}$$

$$m_{f,t(k+1)} = m_{f,t(k)} + \left(\dot{m}_{f,in,t(k)} - \dot{m}_{f,out,t(k)}\right)\Delta t \tag{12}$$

$$(mh)_{t(k+1)} = (mh)_{t(k)} + \left(\dot{m}_{in,t(k)} h_{in,t(k)} - \dot{m}_{out} h_{out,t(k)} + A U_{t(k)} \Delta T\right)\Delta t \tag{13}$$

where k is the time step indices, Δt is length of time step. Overall, there are four equations to be solved for each cell: wall energy balance Eq. (11), working fluid mass balance Eq. (12), working fluid energy balance Eq. (13), and exhaust gas energy balance Eq. (13).

Heat transfer coefficients are calculated separately in working fluid side and exhaust gas side. In the exhaust gas side, at each time step, heat transfer coefficient is calculated once and all the m cells share the same value, which is only a function of time. Eq. (14) is the expression of friction factor for the concentric tubes [12]:

$$\xi_e = \left(1.8\,log_{10}\left(Re_e^*\right) - 1.5\right)^{-2} \tag{14}$$

$$Re_e^* = Re_e \frac{\left(1 + r_d^2\right) ln\left(r_d\right) + \left(1 - r_d\right)}{\left(1 + r_d^2\right) ln\left(r_d\right)} \tag{15}$$

$$r_d = \frac{d_{in}}{d_{out}} \tag{16}$$

where ξ is friction factor, d_{in} and d_{out} are inner and outer diameters of concentric tube, respectively. The thermal conductivity of the exhaust gas is shown as follows:

$$k_{1,e} = 1.07 + \frac{900}{Re_e} - \frac{0.63}{\left(1 + 10Pr_e\right)} \tag{17}$$

$$Re_e = \frac{\dot{m}_e d_e}{A_{e,cross} v_d} \tag{18}$$

$$Pr_e = \frac{v_{d,e} c_{p,e}}{k_e} \tag{19}$$

where d is hydraulic diameter, v_d is dynamic viscosity, Pr is Prandtl number. Nusselt number expression, Eq. (20), of a concentric tube with insulated outer pipe wall is selected based on the heat exchanger structure [13].

$$Nu_e = \frac{\left(\frac{\xi_e}{8}\right) Re_e Pr_e}{k_{1,e} + 12.7\sqrt{\frac{\xi_e}{8}}\left(Pr_e^{0.667} - 1\right)} \left[1 + \left(\frac{d_e}{l}\right)^{0.667}\right] \tag{20}$$

where l is length of the pipe in the heat exchanger. The heat transfer coefficient between exhaust gas and wall are calculated with Eq. (21) [14]. The experimental evaporator construction differs slightly from concentric tubes, so a heat transfer coefficient multiplier (m_U) is applied.

$$U_{e,w} = m_U \frac{Nu_e k_e}{d_e} \tag{21}$$

For the working fluid side heat transfer coefficients, they are not only time dependent, but also space dependent due to the phase change of working fluid along the heat exchanger. The single phase heat transfer coefficients are calculated in Eq. (22). The expression is chosen based on geometry structure of the heat exchanger [13].

$$U_{f,w,i} = \frac{\left(\frac{\xi_{f,i}}{8}\right) Re_{f,i} Pr_{f,i}}{1 + 12.7\sqrt{\frac{\xi_{f,i}}{8}}\left(Pr_{f,i}^{0.667} - 1\right)} \frac{k_{f,i}}{d_{f,i}} \tag{22}$$

$$\xi_{f,i} = 0.0075\left(\frac{d_f}{D_f}\right)^{0.5} + \frac{0.079}{Re_{f,i}^{0.25}} \tag{23}$$

During the evaporation process, both liquid and vapor phase exist. The heat transfer coefficient for this situation is calculated using a vertical tube two-phase heat transfer coefficient expression as shown in Eq. (24) [13]. $U_{f,w,sat}$ and $U_{f,w,vap}$ are calculated from Eq. (22).

$$U_{f,tp} = \left\{ (1-x)^{0.01} \left[(1-x) + 1.9x^{0.4} \left(\frac{\rho_{f,sat}}{\rho_{f,vap}}\right)^{0.35} \right]^{-2.2} + x^{0.01} \left[\frac{U_{f,vap}}{U_{f,sat}} \left(1 + 8(1-x)^{0.7} \left(\frac{\rho_{f,sat}}{\rho_{f,vap}}\right)^{0.67} \right) \right]^{-2} \right\}^{-0.5} \tag{24}$$

3.2. Expander modeling

The turbine is integrated with an electric generator in this work. However, it can also be mechanically connected to engine crank shaft through a gearbox. Turbine expander mass flow rate has a linear relationship to turbine inlet pressure, Eq. (25), due to the choked flow status at high expansion ratios (10–30).

$$\dot{m}_{in} = a_{turb} p_{in} + b_{turb} \tag{25}$$

The outlet enthalpy is calculated by isentropic efficiency as follows:

$$h_{out} = h_{in} - \eta_{is}(h_{in} - h_{out,is}) \tag{26}$$

$$\eta_{is} = map\left(N_{turb}, p_{in}/p_{out}, T_{in}\right) \tag{27}$$

$$h_{out,is} = map\left(s_{out}, p_{out}\right) \tag{28}$$

$$s_{out} = s_{in} \tag{29}$$

$$s_{in} = map\left(h_{in}, p_{in}\right) \tag{30}$$

Outlet temperature, T_{out}, is calculated from outlet enthalpy and outlet pressure using a thermodynamic table of the working fluid.

$$T_{out} = map\left(h_{out}, p_{out}\right) \tag{31}$$

The turbine power is given as follows

$$P_{Turb} = \eta_{conv}\eta_{em}\eta_{is}\dot{m}_{in}(h_{in} - h_{out,is}) \tag{32}$$

where turbine power electronics efficiency $\eta_{conv} = 0.99$ and turbine electric motor efficiency $\eta_{em} = 0.95$.

3.3. Valve modeling

The turbine inlet valve and turbine bypass valve both experience vapor phase flow. They are modeled based on the compressible flow status: subsonic flow or supersonic flow [15]:

$$\begin{cases} If\left(\frac{2}{\gamma+1}\right)^{\frac{\gamma}{\gamma-1}} \le \frac{p_{out}}{p_{in}} \le 1 (subsonic): & \dot{m} = OC_dA_0\sqrt{\frac{2\gamma}{\gamma-1}p_{in}\rho_{in}\left[\left(\frac{p_{out}}{p_{in}}\right)^{\frac{2}{\gamma}} - \left(\frac{p_{out}}{p_{in}}\right)^{\frac{\gamma+1}{\gamma}}\right]} \\ If 0 \le \frac{p_{out}}{p_{in}} \le \left(\frac{2}{\gamma+1}\right)^{\frac{\gamma}{\gamma-1}} (supersonic): & \dot{m} = OC_dA_0\left(\frac{2}{\gamma+1}\right)^{\frac{\gamma+1}{2(\gamma-1)}}\sqrt{\gamma p_{in}\rho_{in}} \end{cases} \tag{33}$$

where $\gamma = \frac{c_p}{c_v}$ is heat capacity ratio. Assuming the working fluid experiences an isentropic process across the valve ($h_{out} = h_{in}$), the outlet temperature is calculated:

$$T_{out} = f(p_{out}, h_{out}) \tag{34}$$

3.4. Pump modeling

The ORC-WHR system pumps maintain both working fluid mass flow and pressure. The pump is a positive displacement type, whereas the feed pump is an inline roller cell pump. The mass flow rate of the pump is interpolated from a 2-D map as shown in Eq. (35). Pump power consumption and outlet temperature are calculated from physics expressions via Eqs. (36, 37).

$$\dot{m}_{pump} = map(N_{pump}) \tag{35}$$

$$P_{pump} = \frac{\dot{m}_{pump}}{\rho}\frac{\left(p_{out,pump} - p_{in,pump}\right)}{\eta_{is,pump}} \tag{36}$$

$$T_{out,pump} = T_{in,pump} + \frac{\left(1 - \eta_{is,pump}\right)P_{pump}}{\dot{m}_{pump}c_{p,pump}} \tag{37}$$

where ρ is the pump upstream working fluid density, $p_{in,pump}$, $p_{out,pump}$ are upstream and downstream pressure respectively, $c_{p,pump}$ is the upstream specific heat capacity of the working fluid, $\eta_{is,pump}$ is isentropic efficiency and is expressed as a function of pump mass flow rate. The empirical expression and coefficients are found in [8, 16].

$$\eta_{is,pump} = 0.93 - 0.11\ log\left(\frac{\dot{m}_{pump}}{\dot{m}_{pump,max}}\right) - 0.2\ log\left(\frac{\dot{m}_{pump}}{\dot{m}_{pump,max}}\right)^2 - 0.06\ log\left(\frac{\dot{m}_{pump}}{\dot{m}_{pump,max}}\right)^3 \tag{38}$$

4. Conclusion

This chapter mainly focuses on the modeling of ORC-WHR system including the overview of model complexity, accuracy, computation time of different heat exchanger models such as static model, 0D model, 1D finite volume model, 1D moving boundary model etc. static heat exchanger model ends up popular in calculating the energy balance at the concept phase of the ORC-WHR system development. 0D model is suitable for the computational costly optimization algorithm like Dynamic Programming due to its less computation time compared with higher dimensional models like moving boundary model and finite volume model. Moving boundary model ends up with the best choice as a control model in advanced controls due to its low computation cost than finite volume model and higher accuracy than the 0D model, even though it has higher model complexity than 0D model and finite volume model. Finite volume model is the best choice to work as offline plant model due to its high accuracy and stability compared with moving boundary model and 0D model. 2D and 3D model is suitable for the heat exchanger component development due to their capability of revealing detailed information inside different locations of the heat exchanger. The ORC-WHR system model example presented in Section 3 shows the complete system model. After reading this chapter, the readers will be equipped with the basic understanding of ORC-WHR system model and how to start modeling in the ORC-WHR system development.

Author details

Bin Xu*, Adamu Yebi and Zoran Filipi

*Address all correspondence to: xbin@clemson.edu

Department of Automotive Engineering, Clemson University, Greenville, SC, USA

References

[1] Wei MS, Fang JL, Ma CC, Danish SN. Waste heat recovery from heavy-duty diesel engine exhaust gases by medium temperature ORC system. Science China-Technological Sciences. 2011;**54**:2746-2753

[2] Arunachalam PN, Shen MQ, Tuner M, Tunestal P, Thern M. Waste heat recovery from multiple heat sources in a HD truck diesel engine using a Rankine cycle—A theoretical evaluation. SAE International 2012-01-1602; 2012

[3] Grelet V, Reiche T, Lemort V, Nadri M, Dufour P. Transient performance evaluation of waste heat recovery Rankine cycle based system for heavy duty trucks. Applied Energy. 2016;**165**:878-892

[4] Horst TA, Tegethoff W, Eilts P, Koehler J. Prediction of dynamic Rankine cycle waste heat recovery performance and fuel saving potential in passenger car applications considering

interactions with vehicles' energy management. Energy Conversion and Management. 2014;**78**:438-451

[5] Peralez J, Tona P, Sciarretta A, Dufour P, Nadri M. Optimal control of a vehicular organic Rankine cycle via dynamic programming with adaptive discretization grid. IFAC Proceedings Volumes. 2014;**47**:5671-5678

[6] Xie H, Yang C. Dynamic behavior of Rankine cycle system for waste heat recovery of heavy duty diesel engines under driving cycle. Applied Energy. 2013;**112**:130-141

[7] Xu B, Rathod D, Kulkarni S, Yebi A, Filipi Z, Onori S, et al. Transient dynamic modeling and validation of an organic Rankine cycle waste heat recovery system for heavy duty diesel engine applications. Applied Energy. 2017;**205**:260-279

[8] Quoilin S, Aumann R, Grill A, Schuster A, Lemort V, Spliethoff H. Dynamic modeling and optimal control strategy of waste heat recovery organic Rankine cycles. Applied Energy. 2011;**88**:2183-2190

[9] Peralez J, Tona P, Lepreux O, Sciarretta A, Voise L, Dufour P, et al. Improving the control performance of an organic Rankine cycle system for waste heat recovery from a heavy-duty diesel engine using a model-based approach. In: 2013 IEEE 52nd Annual Conference on Decision and Control (Cdc); 2013. pp. 6830-6836

[10] Luong D, Tsao TC. Linear quadratic integral control of an organic Rankine cycle for waste heat recovery in heavy-duty diesel Powertrain. In: 2014 American Control Conference (Acc); 2014. pp. 3147-3152

[11] Yebi A, Xu B, Liu X, Shutty J, Anschel P, Filipi Z, et al. Estimation and predictive control of a parallel evaporator diesel engine waste heat recovery system. IEEE Transactions on Control Systems Technology. 2017;**PP**:1-14

[12] Gnielinski V. Berechnung des Druckverlustes in glatten konzentrischen Ringspalten bei ausgebildeter laminarer und turbulenter isothermer Strömung. Chemie Ingenieur Technik. 2007;**79**:91-95

[13] Blaß E, Chemieingenieurwesen GVu. VDI-Gesellschaft Verfahrenstechnik und Chemieingenieurwesen GVC: gestern, heute, morgen; eine Jubiläumsschrift anläßlich des Jahrestreffens der Verfahrensingenieure 1984 in München zum 50-jährigen Bestehen der GVC: Saur; 1984

[14] Bergman TL, Incropera FP, Lavine AS. Fundamentals of Heat and Mass Transfer. Hoboken, New Jersey, USA: John Wiley & Sons; 2011

[15] Weiss HH, Boshwirth L. A simple but efficient equipment for experimental determination of valve loss coefficient under compressible and steady flow conditions. In: International Compressor Engineering Conference; 1982. pp. 69-76

[16] Vetter G. Rotierende Verdrängerpumpen für die Prozesstechnik. Vulkan-Verlag GmbH; 2006

Chapter 5

Optimal Sizing of Waste Heat Recovery Systems for Dynamic Engine Conditions

Emanuel Feru, Srajan Goyal and Frank Willems

Additional information is available at the end of the chapter

http://dx.doi.org/10.5772/intechopen.78590

Abstract

In this study, a methodology for optimal sizing of waste heat recovery (WHR) systems is presented. It deals with dynamic engine conditions. This study focuses on Euro-VI truck applications with a mechanically coupled Organic Rankine Cycle-based WHR system. An alternating optimization architecture is developed for optimal system sizing and control of the WHR system. The sizing problem is formulated as a fuel consumption and system cost optimization problem using a newly developed, scalable WHR system model. Constraints related to safe WHR operation and system mass are included in this methodology. The components scaled in this study are the expander and the EGR and exhaust gas evaporators. The WHR system size is optimized over a hot World Harmonized Transient Cycle (WHTC), which consists of urban, rural and highway driving conditions. The optimal component sizes are found to vary for these different driving conditions. By implementing a switching model predictive control (MPC) strategy on the optimally sized WHR system, its performance is validated. The net fuel consumption is found to be reduced by 1.1% as compared to the originally sized WHR system over the total WHTC.

Keywords: scalable models, component sizing, control, heavy-duty diesel engine

1. Introduction

Heavy-duty (HD) engines are the workhorse in the transport sector. Driven by societal concerns about global warming and energy security, this sector faces enormous challenges to dramatically reduce green house gas emissions and fuel consumption over the upcoming decades. In the EU, CO_2 legislation for HD vehicles is in preparation. For 2050, a 60% CO_2 reduction sectorial target is set.

To meet these challenging targets for trucks, besides vehicle and logistic measures, increase of the powertrain efficiency is an important research area. In modern diesel engines, around 25% of the fuel energy is converted into heat and is wasted with the exhaust gases into the environment. Extracting this energy and converting it into useful propulsion energy will potentially lead to significant reductions in fuel consumption.

The Organic Rankine Cycle (ORC) seems a promising waste heat recovery (WHR) technology for heavy-duty applications [1, 2]. For future implementation, further optimization of the cost-benefit ratio is crucial. More precisely, optimal sizing of the WHR system is necessary to maximize the WHR power output and fuel economy of the vehicle. However, this is challenging, since there are many factors that affect the optimality of WHR system size, including: driving conditions, system constraints, and the control strategy. In [3], it is shown that dynamic operating conditions play an important role for optimization of WHR systems, especially in truck applications. A huge gap was observed between predictions based on steady-state and dynamic conditions. Similar results are found in [4]: performance evaluation in steady-state operating points derived by driving cycle reduction tends to overestimate the fuel gain induced by the WHR system. In addition, the coupling between system and control design has to be dealt with.

In the literature, publications dedicated to topology design and architecture, control and integration with the powertrain system can be found for ORC-based WHR systems in automotive applications. The studied physics-based models [5–9] are based on stock component models, which are already available commercially. The size of the components is chosen based on the packaging requirements and cost. In summary, models with scalable components and component sizing approaches are lacking.

In this study, a new methodology is presented for optimal component sizing of WHR systems in the presence of highly dynamic engine conditions. The main goal is to minimize overall powertrain fuel consumption, while meeting safety constraints. This study is an extension of the work done in [10], where models and control techniques are developed to enable waste heat recovery for a Euro VI heavy duty diesel engine. By following an alternating optimization approach, system and control design is separated. A general optimization framework is defined that deals with the impact of component size on overall fuel consumption, system costs and system mass. A new, scalable WHR system model is proposed to support this optimization methodology. It is noted that the optimization is performed using a stand-alone WHR system, since it is seen from our research that this does not affect the optimality of the results, compared to using the complete powertrain model.

This work is organized as follows. The studied engine with WHR system and the general WHR optimization problem are introduced in Sections 2 and 3, respectively. Section 4 presents the scalable WHR system model. In the proposed alternating optimization approach, optimal component sizing and control design are split. Section 5 introduces the sizing optimization problem, which is followed to determine optimal scaling factors for evaporators and expander using the developed, scalable WHR model. For a switching MPC controller, the optimally sized WHR system performance is validated over the hot start World Harmonized Transient Cycle (WHTC) in Section 6. Finally, the main conclusions are summarized in Section 7.

http://dx.doi.org/10.5772/intechopen.78590

2. System description

Figure 1 shows the studied system, which is based on a 13 liter, 6 cylinder Euro-VI heavy-duty diesel engine. This engine is equipped with common rail fuel injection, a high-pressure exhaust gas recirculation (EGR) system, variable turbocharger geometry (VTG) and an aftertreatment system. This aftertreatment system consists of a diesel oxidation catalyst (DOC), a diesel particulate filter (DPF) and a selective catalytic reduction (SCR) system with ammonia oxidation catalyst (AMOX).

A waste heat recovery system is installed that recovers heat from the EGR line as well as the line downstream of the aftertreatment system using an EGR and Exhaust Gas (EXH) evaporator, respectively. The working principle of this WHR system is based on an Organic Rankine Cycle (ORC). The working fluid is ethanol. It is pumped from the open reservoir, which is at ambient pressure, through the evaporators by two electrically driven pumps. In the evaporators, heat is extracted from the exhaust gases and is used to vaporize the ethanol. This vapor expands in the two-piston expander and generates mechanical power. Note that the expander is mechanically coupled to the engine crankshaft. The expander is said to operate safely if vapor state is maintained before the expander, that is, the working fluid must be in superheated state. The presence of droplets can damage the expander. After expansion, the working fluid is cooled in the condenser. The resulting liquid working fluid flows back to the reservoir, where it is stored at atmospheric pressure. For WHR system control, both pumps are used. A throttle valve u_t at the expander inlet is also available to accommodate gear shifting. When the driver's requested power is less than the net power delivered by the WHR system, $P_{req} \leq P_{whr}$,

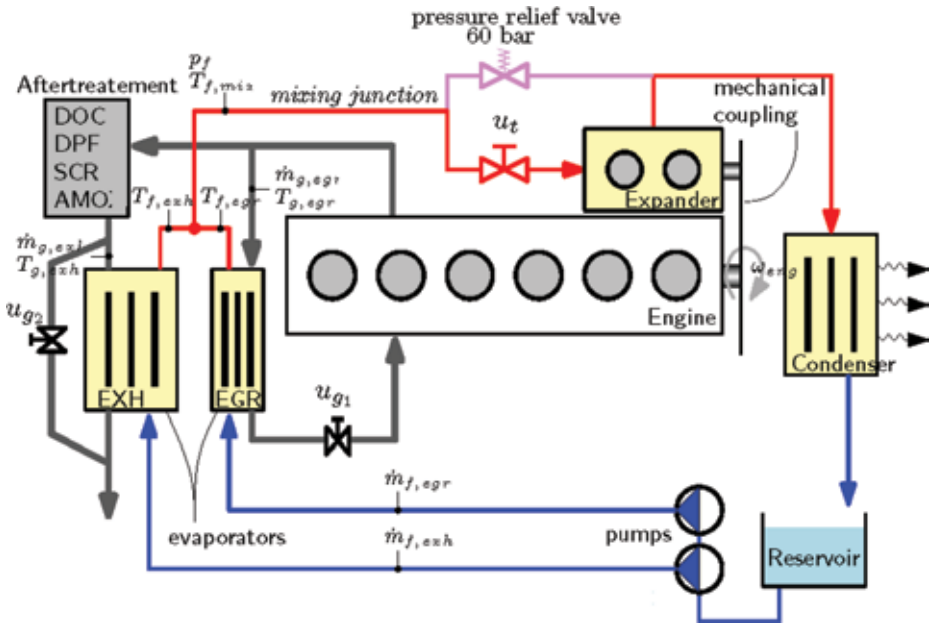

Figure 1. Scheme of the complete powertrain with WHR system [11].

this valve is closed to avoid unwanted torque responses. In this study, this valve is maintained at fully opened position, since we focus on realizing maximum power output. The system pressure is limited to 60 bar by a pressure relief valve. The EGR valve u_{g1} is controlled by the engine control unit (ECU), whereas the exhaust gas bypass valve u_{g2} is controlled, such that the condenser cooling capacity is not exceeded.

In previous work [10], an electrified WHR system is also studied. This WHR system is equipped with a battery for energy storage, and the expander is coupled to a generator instead of the engine crankshaft. However, to demonstrate the potential of the WHR component sizing methodology, the configuration shown in **Figure 1** is chosen. This configuration is more attractive for short-term application due to its relatively low system costs and complexity.

3. Optimization problem

3.1. General problem definition

The high-level objective of this study is to minimize fuel consumption of the overall powertrain by optimal sizing and control of WHR system components over a transient drive cycle, while guaranteeing safe operation. In other words, optimal component scaling factors (λ_i) in combination with optimal speed settings for both pumps (ω_{p1} and ω_{p2}) have to be determined:

$$\underset{\omega_{p1},\,\omega_{p2},\,\lambda_i}{\text{minimize}} \quad \int_0^{t_f} \dot{m}_{fuel}(t)dt \tag{1}$$

where t_f is the duration of drive cycle. The fuel mass flow is a function of engine torque τ_e, engine speed N_e and EGR valve and VTG positions:

$$\dot{m}_{fuel} = f(\tau_e, \mathrm{N_e}, \mathrm{EGR\%}, \mathrm{VTG\%}) \tag{2}$$

The dynamic model of the engine with WHR system is shown in **Figure 2**. This scheme illustrates the components and their interaction. Ambient temperature and pressure (T_{amb} and p_{atm}), the requested engine speed N_d and the torque τ_d associated with the drive cycle are the external model inputs (in green). The variables to be optimized, that is, control inputs $\omega_{p1,2}$ and scaling parameters λ_i, are indicated in blue.

To meet the torque request τ_d, the required engine torque is given by:

$$\tau_e = \tau_d - \tau_{whr} \tag{3}$$

with the torque τ_whr provided by the WHR system:

$$\tau_{whr} = \frac{P_{whr}}{\omega_e} = \frac{P_{exp} - P_{p1} - P_{p2}}{\omega_e} \tag{4}$$

http://dx.doi.org/10.5772/intechopen.78590

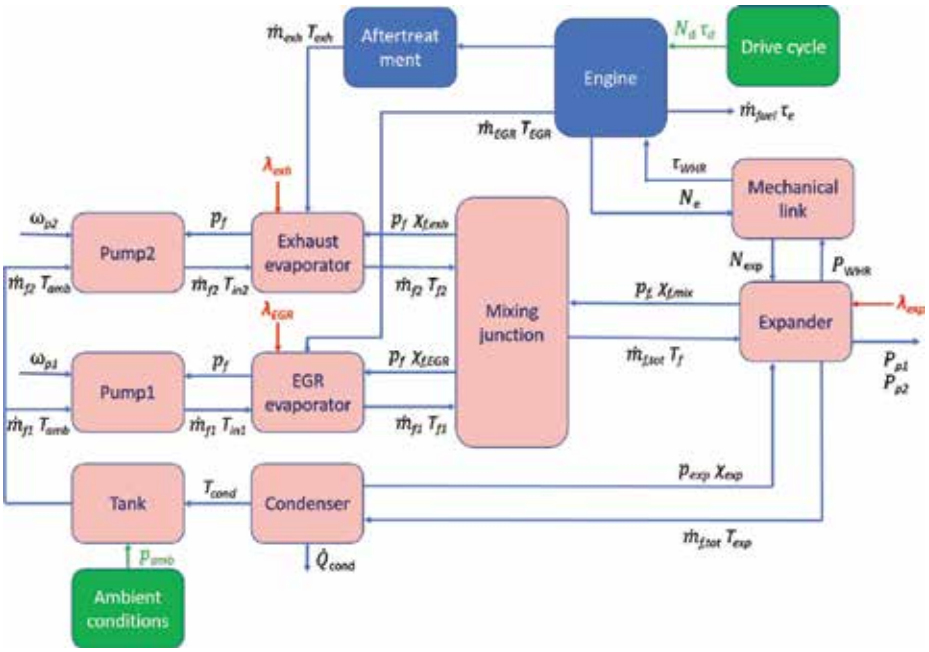

Figure 2. Scheme of the dynamic model for the studied engine-WHR system. WHR-related components are indicated by red blocks.

As this study focuses on maximizing the WHR system performance, the fuel consumption in Eq. (2) can be reduced by lowering the engine torque τ_e. This is done by maximizing the net WHR power output P_{whr}, Eq. (3)–(4). The external inputs to the WHR system are the EGR and exhaust gas flows from the engine and aftertreatment system, which are also a function of τ_e, N_e, EGR and VTG positions.

In conclusion, a combined design and control optimization problem is formulated:

Problem 1

$$
\begin{aligned}
&\textit{minimize}_{\,\omega_{p1},\,\omega_{p2},\,\lambda_i} \int_0^{t_f} \mathrm{P_{whr}(t)dt} \\
&\textit{subject to}: \quad \omega_p^{min} \le \omega_{p1,p2}(t) \le \omega_p^{max} \\
&\qquad\qquad \lambda_i^{min} \le \lambda_i \le \lambda_i^{max} \;\; ; \;\; \{\mathrm{i} = 1 \ldots \mathrm{n}\} \\
&\qquad\qquad T_{egr}^{out}(t) \ge 120^\circ C \\
&\qquad\qquad T_{f1,2}(t) \le 270^\circ C \\
&\qquad\qquad \chi_f(t) \ge 1
\end{aligned}
\tag{5}
$$

with optimization variables:

- **Pump speeds** $\omega_{p1}(t)$ and $\omega_{p2}(t)$, which control the mass flow rate of the working fluid required to extract heat energy from both the evaporators;
- **Design variables** λ_i: these time-independent scaling factors are applied to vary the size of different components of WHR system, where n is the number of components to be scaled.

This optimization problem is subject to the following constraints:

- ω_p^{min} and ω_p^{max} are the minimum and maximum pump speeds to limit the mass flow rate of working fluid in the WHR system;
- Exhaust gas temperature $T_{egr}^{out}(t)$ at the EGR evaporator outlet should be more than 120°C to prevent condensation;
- Ethanol temperature should always be less than 270°C to avoid degradation;
- $\chi_f(t)$ is the vapor fraction of the working fluid, which is given by:

$$\chi_f = \frac{h_f - h_l\left(p_f\right)}{h_v\left(p_f\right) - h_l\left(p_f\right)} \tag{6}$$

where $h_l\left(p_f\right)$ and $h_v\left(p_f\right)$ denote the specific saturated liquid and vapor enthalpy, respectively, as a function of system pressure p_f. To avoid damage by droplets, this fraction should be larger than 1 at the expander inlet.

Note that maximizing the WHR system power output by optimizing component sizes can lead to an increase in the needed cooling power in the condenser. However, in this work, we assume that this cooling capacity is always available (ideal condenser).

3.2. Optimization methodologies

The problem stated above is nonconvex and highly nonlinear where both control and design parameters are optimization variables. For combined plant and control design problems, three approaches can be distinguished [12]:

- **Alternating plant and control design**: the plant is optimized first, which is then followed by an optimal control design. Subsequently, this process is repeated until the coupled variables converge;
- **Nested optimization**: the control design is nested within the plant design, that is, for each evaluation of the plant, the controller design is optimized. Often, nested optimization architectures are also called bi-level, referring to the two design layers;
- **Simultaneous optimization**: optimization of plant and controller design is done simultaneously, that is, solving Eq. (5) all-in-one.

The WHR system shown in **Figure 1** is controlled by a switching model predictive control (MPC) strategy. With an alternating optimization architecture, an MPC tuned for one system

size might not be functional for a different size, due to the changing heat exchanger system dynamics. When using a nested framework, for every evaluation of plant design, multiple MPCs must be obtained covering the WHR operating area. Moreover, high tuning effort is required to implement a switching MPC strategy to obtain good disturbance rejection.

Due to the high complexity of the optimization problem, the alternating optimization method is selected in this study. The main reasons are as follows: applicability to other WHR systems topologies and possibility to sequentially run the controller and plant optimization, which reduces the instantaneous computational burden.

Remark 1.

The sizing optimization requires significant controller tuning effort for different plant sizes. Therefore, a size independent feed forward controller is necessary to significantly reduce the tuning effort and thus the computational complexity of the optimization problem. Even though a feed forward controller does not give the full performance, it is still representative for solving sizing problems. Moreover, in Section 6, we will show that using such a controller produces results with acceptable validation properties.

3.3. Feedforward pump control

The low-level pump controllers have to guarantee that the working fluid at the expander inlet is at superheated state: $\chi_f \geq 1$. Both pumps control the mass flow of the working flow through the evaporators and by that the heat transfer between the exhaust gas and the working fluid. The discussed MPC strategy needs relatively high tuning effort when the WHR system has to be simulated on a grid of design points.

Considering these issues, a feed forward (FF) pump controller is introduced, which is independent of the plant size. It is based on the measured EGR and exhaust gas heat flows from the engine, measured temperature of the working fluid at the evaporator inlet, and the working fluid system pressure. For stationary conditions, the amount of heat that needs to be transferred from the exhaust gas to the working fluid is determined from the energy balance:

$$\dot{Q}_g - \dot{Q}_{g,loss} = \dot{Q}_f \tag{7}$$

where $\dot{Q}_g$ is the heat flow from the exhaust gas, $\dot{Q}_{g,loss}$ are the heat transfer losses and $\dot{Q}_f$ is the heat flow toward the working fluid. From this equation, the required working fluid mass flow can be determined, using:

$$\dot{m}_f = \frac{\dot{Q}_g - \dot{Q}_{g,loss}}{h_{f_{out}}^{ref} - h_{f_{in}}} \tag{8}$$

where $h_{f_{in}}$ is the actual enthalpy of the working fluid at the evaporator inlet and $h_{f_{out}}^{ref}$ is the estimated enthalpy of the working fluid corresponding to a post-evaporator temperature of 10˚C above the saturation temperature. The feed forward pump controller realizes this required working fluid flow.

4. Scalable WHR system model

In this section, the Waste Heat Recovery model from [13] is made scalable for component size. For each component, the physical parameters that have the biggest impact on the WHR power output are identified to scale the overall size of these components. The WHR system model is described using a component-based approach. The pumps and expander are map-based components. The remaining components, that is, evaporators, condenser, valves, and pressure volumes, are based on conservation of mass and energy principles.

The following assumptions are made in the model:

- Transport delays and pressure drops along the pipes are neglected;
- Change in exhaust gas density as a function of temperature and pressure is neglected;
- Pressure dynamics in the heat exchangers are not considered because of small time scales compared to temperature phenomena;
- Temperature along the transverse direction is considered to be uniform for both exhaust gas and working fluid;
- Condenser model is ideal, such that the reservoir provides the working fluid at an ambient pressure of 1 bar and temperature of 65˚C. Hence, condenser sizing is not considered in this study.

4.1. Pumps

There are two identical pumps in the WHR system to pump the working fluid from the reservoir to the EGR and exhaust gas evaporators. Pumping power $P_{p1,2}$ is directly proportional to the displacement volume and rotational speed of the pump. Thus, it can be inferred that a smaller pump can rotate at higher rotational speeds to meet the demands of mass flow rates of working fluid, while maintaining the same pressure difference without necessarily affecting the power output. Therefore, any variation in their displacement volume would not affect the required working fluid mass flow rate for the same operation cycle. Hence, sizing of the pumps is not considered here.

4.2. Expander

The expansion process in the two-piston expander is illustrated in **Figure 3**. This cycle consists of two isobaric strokes (1→2 and 4→5), two isentropic stokes (2→3 and 5→6) and two isenthalpic mass transfers at the end of the strokes (3→4 and 6→1).

The expander power is ideally calculated by multiplying net work done in the cycle with the expander speed, given by

$$P_{exp,\,ideal} = W_{net,\,ideal} \cdot \frac{N_{exp}}{60} \tag{9}$$

where

http://dx.doi.org/10.5772/intechopen.78590

$$W_{net,\,ideal} = W_{12} + W_{23} + W_{45} + W_{56} \tag{10}$$

Using the ideal gas law, work delivered for different sub processes in the cycle are given by [14]:

$$\begin{aligned} W_{12} &= p \cdot (V_2 - V_{head}) \\ W_{23} &= \frac{pV_2^{\kappa}}{(1-\kappa)} \cdot \left(\frac{1}{(V_{head} + V_d)^{\kappa-1}} - \frac{1}{V_2^{\kappa-1}} \right) \\ W_{45} &= p_{atm} \cdot (V_5 - V_{head} - V_d) \\ W_{56} &= \frac{p_{atm} V_5^{\kappa}}{(1-\kappa)} \cdot \left(\frac{1}{(V_{head})^{\kappa-1}} - \frac{1}{V_5^{\kappa-1}} \right) \end{aligned} \tag{11}$$

where κ is the adiabatic index, and p_{atm} is the atmospheric pressure.

The physical parameter that is affecting the power output of the expander is its volume, as indicated by Eq. (11). Thus, applying the same scaling factor to V_{head} and V_d, will change the overall dimensions of the expander. By applying the scaling factor to these volumes, it is assumed that the bore-to-stroke ratio of the cylinder is not changed. Hence, new volumes are defined:

$$\begin{aligned} V_{head}^{*} &= \lambda_{exp} \cdot V_{head} \\ V_{d}^{*} &= \lambda_{exp} \cdot V_{d} \end{aligned} \tag{12}$$

To keep the valve timings of the expander same as the original system, the same scaling factor, λ_{exp} is applied to V_2 and V_5.

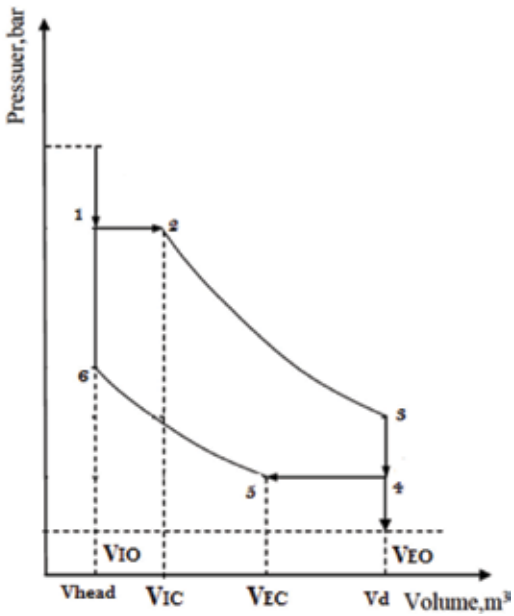

Figure 3. p-V diagram of the expansion process ($V_2 = V_{IC}$: intake valve closing volume; $V_5 = V_{EC}$: exhaust valve closing volume; V_{head}: clearance volume; V_d: displacement volume).

$$V_2^* = \lambda_{exp} \cdot V_2$$
$$V_5^* = \lambda_{exp} \cdot V_5 \tag{13}$$

The ideal physics-based model of the expander deviates from the measurements because the model simulates an ideal cycle, and a number of adverse effects are not taken into account, for example, drag in the outlet, formation of droplets, Van der Waals interactions and volumetric efficiency. Hence, a steady state physics-based model of the expander was estimated in [14] based on the measurement data. This data were obtained during steady-state dynamometer testing for different values of expander speed N_{exp} and system pressure p_f [10]. Results for different expander sizes are provided by the expander manufacturer. It suggests that the nominal power output increases linearly with increase in displacement volume. This is due to the modular design of the expanders. Therefore, for this study, the losses P_{loss} are considered equal for different expander sizes ($\lambda_{\exp}$), so **Figure 4** is used:

$$P_{whr} = P_{whr,ideal} \cdot \left[1 - P_{loss}\left(N_{exp}, p_f\right)\right] \tag{14}$$

4.3. Evaporators

The evaporator model [15] is based on the conservation principles of mass and energy. To scale the evaporators size, the scaling factor needs to be applied on the volume of the evaporator. And the volume of evaporator can be varied by changing either length or width or height of the evaporator. The general structure of the studied evaporator is shown in **Figure 5**.

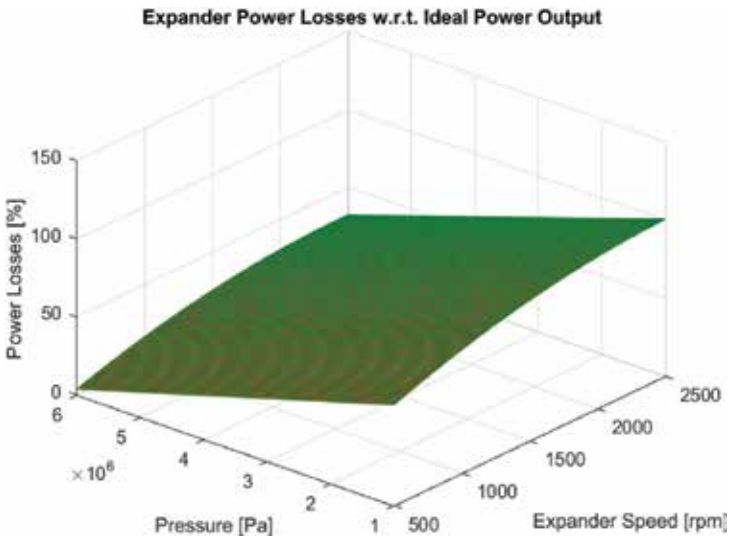

Figure 4. Expander power losses.

http://dx.doi.org/10.5772/intechopen.78590

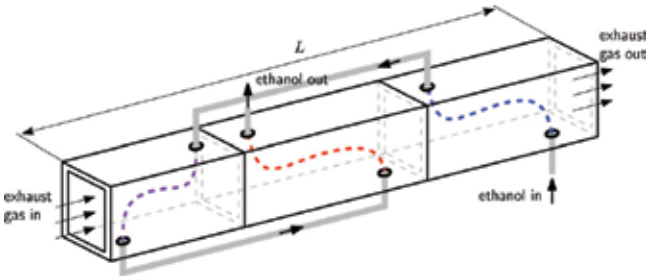

Figure 5. Exhaust gas recirculation heat exchanger modular design.

Scaling factors λ_l, λ_w and λ_h are applied to length l, width w and height h of the evaporators:

$$\begin{aligned} l_{new} &= \lambda_l \cdot l \\ w_{new} &= \lambda_w \cdot w \\ h_{new} &= \lambda_h \cdot h \end{aligned} \tag{15}$$

Consequently, the following model parameters are affected. The number of plates inside the evaporator will vary, when its height is changed,

$$n_{p,\,new} = \lambda_h \cdot n_p \tag{16}$$

Note that number of plates should be a discrete number, that is, $n_{p,\,new} \in \mathbf{N}$. But in this study, it is varied continuously with the scaling factors, as it does not affect the end results.

In addition, the surface area available for the working fluid to extract the heat energy from exhaust gases through the wall or plates is affected:

$$S_f = 2 \cdot n_{p,\,new} \cdot w_{new} \cdot l_{new} \tag{17}$$

This also impacts the surface area available for the exhaust gas to transmit its heat to the working fluid through wall or plates, which is given by:

$$S_g = S_f + S_{g,fins} \tag{18}$$

where $S_{g,fins}$ is the surface area of fins at exhaust gas side. The surface area of the wall is linear dependent on evaporator length and width:

$$S_w = l_{new} \cdot w_{new} \tag{19}$$

Finally, the flow cross-sectional area, A_i is given by,

$$A_{i,\,new} = w_{new} \cdot h_{new} \qquad \{\mathrm{i} = \mathrm{fluid},\ \ \mathrm{gas}\} \tag{20}$$

Accordingly, the Reynolds number for the working fluid and gas side is affected:

$$Re_i = \frac{\dot{m}_i \cdot dh_i}{A_{i,new} \cdot \eta_i} \tag{21}$$

where η_i is the viscosity, dh_i is the hydraulic diameter, that is, outer gap height of one plate and $\dot{m}_i$ is the mass flow rate of the working fluid and gas. The heat transfer coefficient α_i for the working fluid and exhaust gas also depends on $A_{i,new}$:

$$\alpha_i = \frac{Nu_i \cdot \Lambda_i}{dh_i} = \frac{Nu_i}{Re_i} \cdot \frac{\dot{m}_i \Lambda_i}{A_{i,new} \cdot \eta_i} \tag{22}$$

where Λ_i is the thermal conductivity of the working fluid and exhaust gas.

For varying evaporator length, there will be no change in the flow cross sectional area as well as in the exhaust gas side cross sectional area. As a result, there will be no effect on Reynolds number, *Re*, and the Nusselt number, *Nu*, which is directly proportional to *Re*. The surface areas available for exhaust gas and working fluid increase with increasing *l* and vice versa (see Eqs. (17)–(19)). These areas directly affect the working fluid temperature at the evaporator's outlet.

The cross-sectional areas $A_{i,new}$ varies with width as well as with height and is inversely proportional to the heat transfer coefficients α_{fluid} and α_{gas}. The surface areas S_f and S_g increase with *w* and *h* and, hence, the working fluid temperature at the evaporator's outlet will behave in the same direction through equations for conservation of energy. However, S_w will stay the same with change in height, because the number of plates will change with this dimension.

With the introduced scaling factors, the evaporator size can be changed by varying its length, width or height depending on the requirements from the system, input heat flows, and type of working fluid. These three parameters have different impact on the evaporator's performance. Therefore, a sensitivity analysis has to be done to select the parameter that has the most positive impact on WHR system power output.

5. WHR system size optimization

This section presents a methodology to optimize component size for WHR systems under transient driving conditions. **Figure 6** gives an outline of the approach that is followed in this study. The scalable WHR system model developed in the previous section is crucial input for this approach. From a sensitivity analysis for the exhaust evaporator, scaling of the evaporator length is identified as the most promising route to maximize WHR power output. Details can be found in [16]. As a result, evaporator width and height will be set to their original system values in the sequel of this study. In summary, the following parameters are considered for optimal component sizing in order to maximize WHR power output:

- Expander scaling λ_{exp};
- Exhaust gas evaporator length scaling λ_{exh};
- EGR evaporator length scaling λ_{EGR}.

http://dx.doi.org/10.5772/intechopen.78590

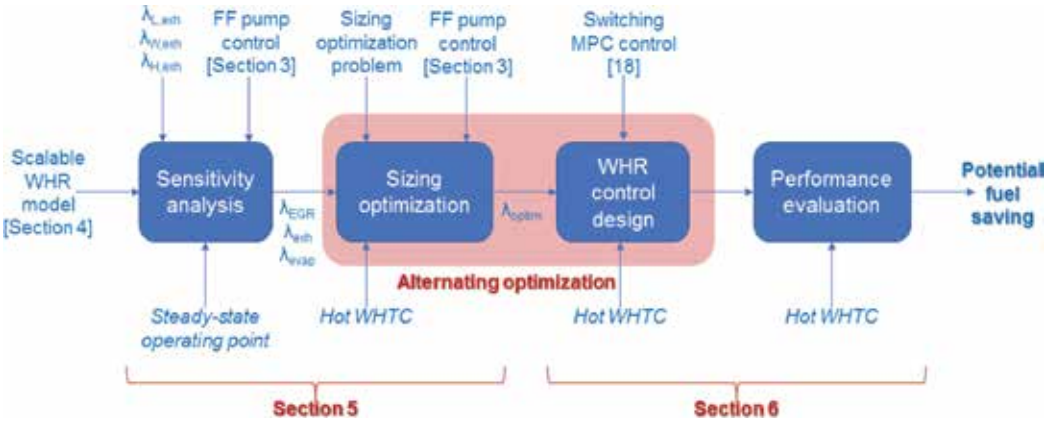

Figure 6. Approach for optimal sizing and control of WHR systems.

The component sizes are optimized based on fuel consumption and investment cost criteria. In the next section, the alternating optimization method is described in detail. The optimal sizes λ_{opt} that are finally determined are input for the overall performance analysis with switching Model Predictive Control (MPC) strategy in Section 6.

5.1. Alternating system optimization

Optimizing the controller and plant iteratively to converge the coupled variables can be computationally too expensive. Therefore, an alternating architecture is followed for only one complete loop, see **Figure 7**. The controller designed for a specific WHR system will give different performance for a resized WHR system. Consequently, the feed forward controller from Section 3.3 is applied, which calculates the pumps speeds, such that $\chi_f \geq 1$ at the outlet of both the evaporators for given engine exhaust heat flows. Although with lower performance

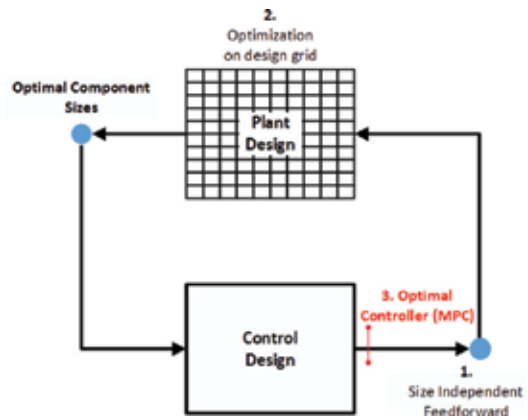

Figure 7. Optimization architecture.

compared to PI control or MPC, it is seen to maintain the same trend for fuel consumption with different components sizes, without affecting the optimality of WHR system components sizes.

The standalone WHR system with feed forward controller is simulated on a 3D design grid of different sizes of EGR evaporator, exhaust evaporator and expander for a hot-start WHTC. WHR system performance is strongly affected by operating conditions. Therefore, besides overall (complete cycle) performance, also optimization is performed on urban, rural and highway driving parts, which are illustrated in **Figure 8**. The design grid is chosen such that: (1) it captures the main trend in outputs due to component sizing and (2) costs and total system mass remain acceptable. For the scaling factors, the following grid is chosen: $\lambda_{EGR} = \lambda_{exh} = [0.4 : 0.1 : 1.5]$ and $\lambda_{exp} = [0.4 : 0.1 : 2.5]$.

5.1.1. Objective functions

Using exhaustive search, also referred to as brute force search, the WHR system performance is determined for each point on the grid. To obtain the optimal size of the plant, the following objective functions are defined:

- **Fuel consumption** (FC), which is determined from Eqs. (2)–(3). For the specified design space, WHTC results are summarized in **Figure 9**. Note that the net fuel consumption is normalized by using engine-only (without WHR system) results. Minimal fuel consumption is found at maximum evaporator size, although the reduction in fuel consumption decreases with increasing size. For highway conditions, where engine exhaust heat flows are relatively high, fuel economy increases for increasing expander sizes. The exhaust evaporator's size has a significant impact on fuel consumption, especially in the urban

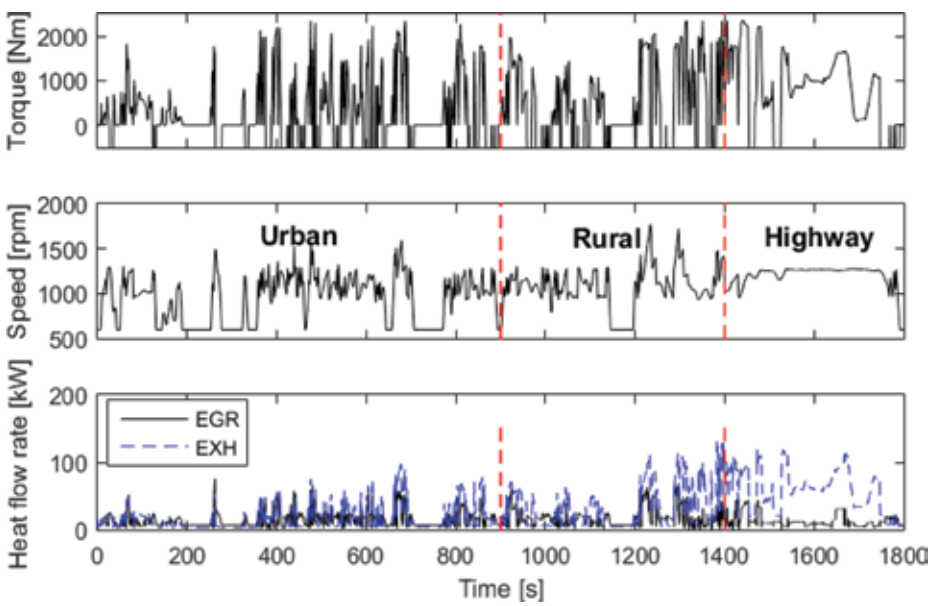

Figure 8. Engine torque, engine speed and heat flows for hot start WHTC.

http://dx.doi.org/10.5772/intechopen.78590

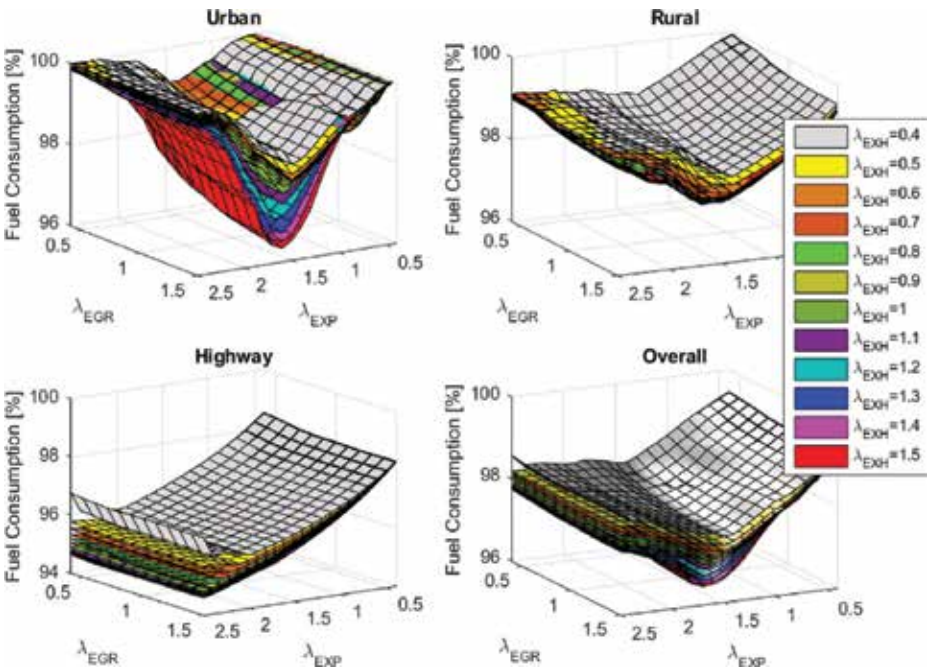

Figure 9. Normalized fuel consumption for different sizes of WHR system components on different driving conditions from hot-start WHTC.

region. Due to low exhaust gas heat flows in this region, the time for the working fluid to extract heat increases with increase in length (or surface area) of evaporator.

- **Specific investment cost** (SIC, in €/kJ): in this study, we focus on installation ($Cost_{labor}$) and material and production cost of the components ($Cost_{comp}$) corresponding a specific WHR energy output:

$$SIC = \frac{Cost_{labor} + Cost_{comp}}{\int_0^{t_v} P_{whr}(t)dt} \tag{23}$$

where $P_{whr}(t)$ is the instantaneous net WHR power output and t_v is cumulative time in vapor. For the evaporators and expander, cost correlations are taken from [17]:

$$\begin{aligned} Cost_{evap} &= 190 + 310 \cdot A_{evap} \cdot \lambda_{evap} \\ Cost_{exp} &= 1.5 \cdot \left(225 + 170 \cdot V_{exp} \cdot \lambda_{exp}\right) \end{aligned} \tag{24}$$

These equations clearly show that the component costs are proportional to the scaling factors to be applied. The cost of other components, such as pumps, piping, condenser and valves, are not included in the SIC. Their sizes are assumed to be fixed in this study, which will not affect the objective function. For SIC, similar graphs are generated as for FC. From these results, it is concluded that λ_{EGR} has negligible effect on SIC, whereas λ_{exp} has the biggest impact, because of its dominant share in the total system cost. Details can be found in [16].

5.1.2. Sizing optimization problem

Having defined the objective functions for FC and SIC, the optimization problem boils down to:

$$\min_{\lambda_{exh},\, \lambda_{EGR},\, \lambda_{exp}} J \tag{25}$$

subject to,

$$m_{egr}(\lambda_{EGR}) + m_{exh}(\lambda_{exh}) + m_{exp}\left(\lambda_{exp}\right) \leq M_{tot}^{max} \tag{26}$$

where the multi-objective function J is given by:

$$J = \begin{cases} \int_0^{t_f} \dot{m}_{fuel} dt \\ \\ \text{SIC} \end{cases} \tag{27}$$

Note that mass of the WHR system is directly proportional to the components sizes and directly affects the overall load carrying capacity of a truck. Therefore, a limit, M_{tot}^{max}, is defined on the component mass associated with sizing.

5.1.3. Sizing optimization for different system mass

As a next step to solve Eqs. (25)–(27), optimal λ setting is determined for different mass constraints M_{tot}^{max}. This is done using the lambda sweep plots for FC as well as SIC, similar to **Figure 9**. For each objective function, the best λ_{EGR}, λ_{exh} and λ_{exp} combination is determined, which gives lowest FC or SIC while meeting a varying M_{tot}^{max}. **Figure 10** shows an example of results for using the FC objective function. The resulting scaling parameters are given for four different operating conditions associated with the hot WHTC. For the overall WHTC, the corresponding fuel consumption is shown in the lower plot. Similar plots are made for SIC.

5.1.4. Best WHR sizing per objective function

Final step in the optimization approach is to select M_{tot}^{max}. For the purpose of benchmarking, the optimal component sizes associates with the two different optimization criteria are compared for a mass constraint equal to the original mass of the system: M_{tot}^{max} = 210 kg, which is indicated in the plots of **Figure 10** by the blue vertical lines. The results of this final step are summarized in **Figure 11**.

The results clearly indicate that different operating conditions and different optimization criteria lead to different component sizing. However, optimal exhaust evaporator size is smaller (i.e., $\lambda_{exh} < 1$) than its original size for all the driving conditions and both FC and SIC optimization. The exhaust evaporator has the biggest mass of the three scaled components. Although longer exhaust evaporator have better performance, the increment reduces with

http://dx.doi.org/10.5772/intechopen.78590

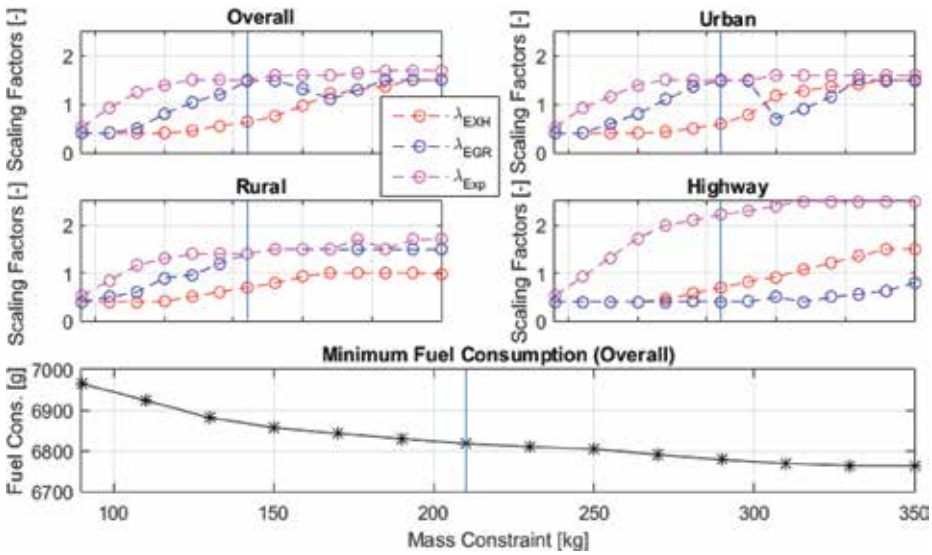

Figure 10. Optimal component sizes to realize minimal fuel consumption for different mass constraints.

increasing λ_{exh}. Hence, M_{tot}^{max} plays a bigger role in sizing because increasing the size of other components is much more beneficial in terms of energy recovery.

Apart from highway driving conditions, the optimal scaling of EGR evaporator is found to be bigger than the original one. During highway driving, the amount of heat that needs to be extracted from the exhaust gases is high, which leads to higher ethanol flows. The results

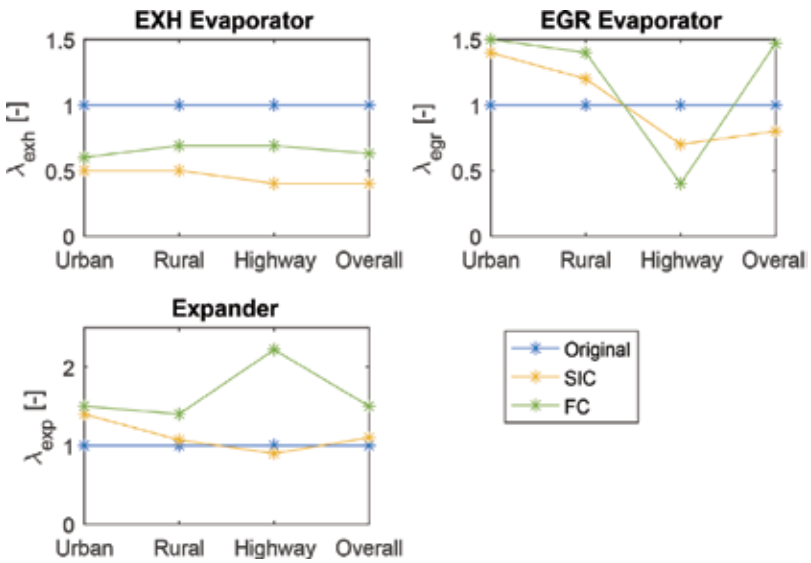

Figure 11. Optimal components sizes for $M_{tot}^{max} = 210$kg and for different objective functions.

indicate that the original evaporator is over dimensioned for this condition. For urban and rural conditions, where exhaust heat flows are low, the ethanol flow needs to be low to extract the maximum amount of heat. However, when mass flows reach the lower boundary condition and no vapor is generated, increased evaporator length would provide more surface area and hence more time for the working fluid to extract heat. This effect is confirmed for the EGR evaporator with bigger optimal sizes for urban and rural regions. As these regions play an important role in the overall cycle result, it is expected that similar λ_{EGR} is found for the overall cycle.

The optimal expander scaling is found to be bigger than the original one for all driving conditions. This especially holds for FC optimization. For highway conditions, λ_{exp} is twice the original one due, in order to exploit the high heat flows. The expander has the biggest impact on WHR system performance. With mass comparable to other components, this leaves room for increasing λ_{exp}.

Finally, these results also indicate that optimal sizing of a single component strongly depends on the performance of all components. Interaction between evaporators and expander as well as the total mass constraint play an important role.

5.2. Selected optimal scaling of WHR components

In order to make a final decision on optimal component scaling, a trade off has to be made between the optimization criteria. Therefore, the impact on FC and SIC are analyzed for both criteria. Focus is on the overall cycle result, since this is assumed to be representative for real-world performance. As expected, fuel consumption can be reduced by 0.85% compared to the originally sized system (and 2.78% compared to engine-only mode) in case of FC minimization. In case of SIC minimization, compared to the original system, there is no FC reduction, but system costs are reduced by 25%. The SIC of the FC optimal system is 60 €/kJ higher than that for the SIC minimal case.

Comparison of both cases learns that the additional system costs associated with the FC minimum case, requires an additional 1 month truck operation for return on investment. Therefore, the final optimal components scaling for the WHR system are based on the values for FC minimization:

$$\lambda_{exh,\,opt} = 0.63 \qquad \lambda_{EGR,\,opt} = 1.47 \qquad \lambda_{exp\,,\,opt} = 1.50 \tag{28}$$

These values will be used in the sequel of this study.

6. Simulation results

In this section, the switching MPC strategy from [18] is applied to the standalone WHR system with optimal component sizes. A comparison is made with the original WHR system. The MPC strategy is first evaluated on a simple stepwise cycle data from a real Euro VI heavy-duty diesel engine and then on a hot-start World Harmonized Transient Cycle (WHTC) [16].

Considering the real time system dynamics of WHR system, the controller sampling time is chosen to be $T_s = 0.4$ seconds. The prediction and control horizon are $N_y = 50$ and $N_u = 4$ time steps, respectively, for all the three linear models.

6.1. Controller performance validation

The proposed switching MPC strategy is validated on the highly dynamic, hot start WHTC. Disturbances from the engine, that is, engine speed and EGR and exhaust gas heat flows, are inputs for the simulation. The objective of the controller is to maintain vapor state. However, due to the highly dynamic disturbances and limitations of the control input, it is challenging to achieve this target for all the time. To avoid damage, the expander is bypassed using the bypass valve, such that net power output: $P_{whr} = 0$.

Figure 12 shows the vapor fraction after EGR and EXH evaporators, and the mixing junction for the original and optimized system. Vapor fraction is not meeting the reference (indicated by dashed line) between 200 and 400 s, due to the low heat flows in the urban region. However, the controller shows improved overall performance in terms of disturbance rejection, where the controller specifications, $\chi_{f,mix} \geq 1$, are met with short periods of time reaching at 0.9 (around 800 and 1200 s).

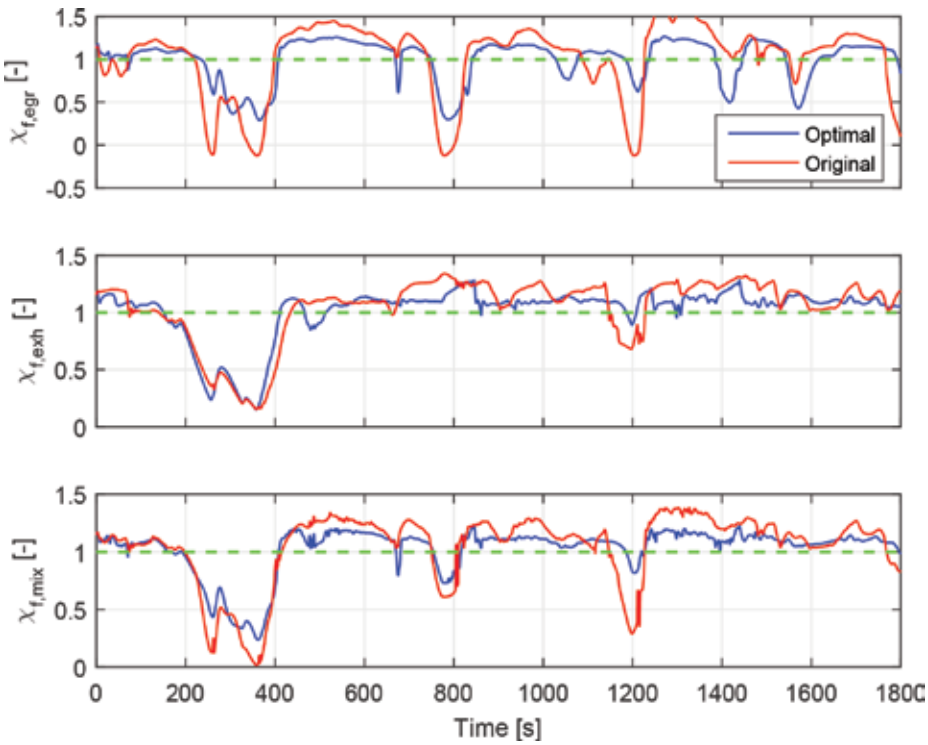

Figure 12. Comparison of vapor fraction after the EGR and EXH evaporators, mixing junction for MPC strategy between original and optimally sized system (with vapor fraction according to Eq. (6)).

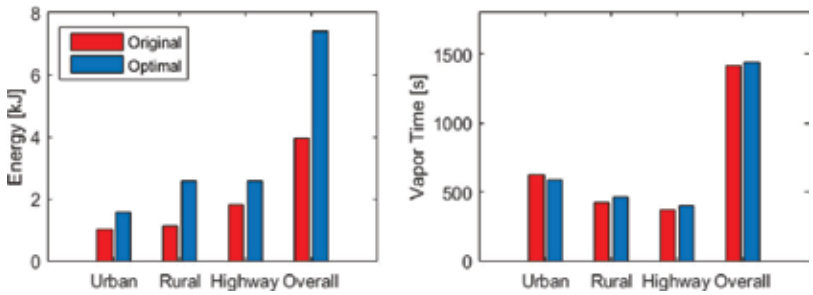

Figure 13. Performance indices in terms of recovered thermal energy (left) and time in vapor (right) compared with original system.

The main objective of MPC tuning is to keep the vapor fraction of working fluid after both the evaporators' outlets close to reference data with good disturbance rejection properties. Due to different system dynamics, the values of the weighting matrices $W_{\Delta u}$ and W_y vary from the original to the optimally sized system. Hence, the performance of the two controllers, that is, MPC for original system and optimally sized system, is quantified in terms of net thermal energy recovered and total time in vapor state, t_v for different parts of the WHTC. **Figure 13** illustrates that the optimally sized system outperforms the original system in terms of recovered thermal energy for all the driving conditions. Note that the recovered energy is almost doubled when complete cycle is considered. This is due to the increased expander size leading to more power output. In terms of time in vapor, both systems behave similarly, with slightly increased t_v for the optimal system over the full WHTC.

6.2. Powertrain performance validation

The net fuel consumption results for the studied cases are compared with the engine only mode in **Figure 14**. The original sized WHR system gives a 1.94% reduction in fuel consumption using the feed forward controller ($\lambda_i = 1$(FF)). An additional 0.8% reduction is found in

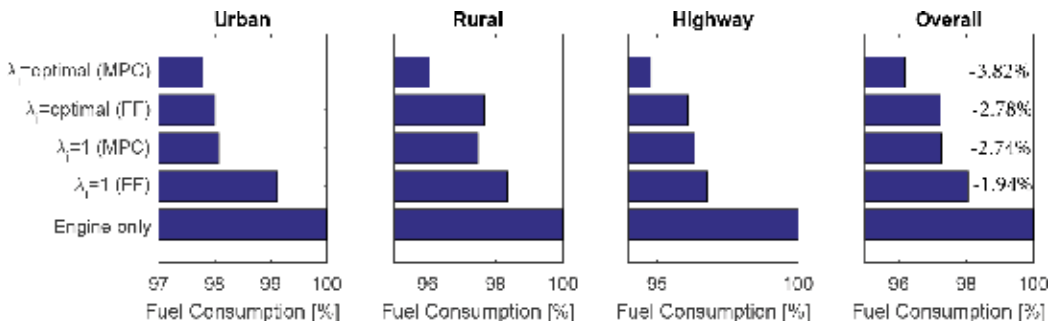

Figure 14. Fuel consumption for different driving conditions from hot-start WHTC.

case a switching MPC strategy ($\lambda_i = 1(\text{MPC})$) is applied. The optimally sized WHR system with feed forward control strategy ($\lambda_i = \text{optimal}(\text{FF})$) reduces fuel consumption by 2.78%. Using a switching MPC strategy ($\lambda_i = \text{optimal}(\text{MPC})$) gives a fuel consumption reduction of 3.82% as compared to the engine only mode. In summary, by optimizing the size of WHR system components, an additional 1.08% reduction in fuel consumption can be achieved compared to the original WHR system using the methodology given in this study.

7. Conclusions

A methodology for optimal components sizing is presented for waste heat recovery systems operated during dynamic engine conditions. Optimality was defined in terms of minimizing the fuel consumption of the overall powertrain system. The main challenge in developing this methodology is the coupling between system design and control parameters. Focus is on Euro-VI heavy-duty engines with a mechanically coupled WHR system. Based on this work, the following conclusions are drawn:

- An existing WHR system model [13] is extended with a detailed expander model and is made scalable for component size. Expander volume as well as evaporator length, width and height can be varied;
- Sensitivity analysis shows that length is the most promising route to optimize power output for evaporators;
- An alternating optimization architecture is presented, which uses the standalone, scalable WHR system model. This methodology combines an constrained optimization problem based on fuel consumption, system costs and system mass considerations with a feed forward pump controller in order to isolate system design from control design;
- This methodology is successfully followed for optimal design and control of WHR system for transient driving conditions while satisfying safe operation. The components scaled in this study are EGR and exhaust gas evaporator, and expander. Different optimal component sizes are found for city, urban, rural and overall hot-start WHTC driving conditions;
- By implementing a switching model predictive control (MPC) strategy on the optimally sized WHR system, time in vapor state is identical, while the net fuel consumption, as compared to the originally sized WHR system, is reduced by:
    - **Overall hot-start WHTC:** 1.08%.
    - **Urban:** 0.30%.
    - **Rural:** 1.46%.
    - **Highway:** 1.61%.

Author details

Emanuel Feru[1,2], Srajan Goyal[2,3] and Frank Willems[1,2]*

*Address all correspondence to: frank.willems@tno.nl

1 TNO Automotive, Helmond, The Netherlands

2 Eindhoven University of Technology, Eindhoven, The Netherlands

3 FlandersMake, Lommel, Belgium

References

[1] Park T, Teng H, Hunter GL, van der Velde B, Klaver J. A rankine cycle system for recovering waste heat from hd diesel engines-experimental results, Technical report. SAE Technical Paper. 2011-01-1337. 2011

[2] Bredel DE, Nickl IJ, Bartosch D-IS. Waste heat recovery in drive systems of today and tomorrow. MTZ Worldwide eMagazine. 2011;**72**(4):52-56

[3] Grelet V. Rankine cycle based waste heat recovery system applied to heavy duty vehicles: Topological optimization and model based control. Ph.D. thesis, Université de Liège, Liège, Belgique; 2016

[4] Goyal S. Optimal sizing of waste heat recovery system for HD truck: Steady state analysis, Technical report. Eindhoven University of Technology; 2016

[5] Horst TA, Rottengruber H-S, Seifert M, Ringler J. Dynamic heat exchanger model for performance prediction and control system design of automotive waste heat recovery systems. Applied Energy. 2013;**105**:293-303

[6] Horst TA, Tegethoff W, Eilts P, Koehler J. Prediction of dynamic rankine cycle waste heat recovery performance and fuel saving potential in passenger car applications considering interactions with vehicles energy management. Energy Conversion and Management. 2014;**78**:438-451

[7] Lecompte S, Huisseune H, van den Broek M, De Schampheleire S, De Paepe M. Part load based thermo-economic optimization of the organic rankine cycle (orc) applied to a combined heat and power (chp) system. Applied Energy. 2013;**111**:871-881

[8] Seher D, Lengenfelder T, Gerhardt J, Eisenmenger N, Hackner M, Krinn I. Waste heat recovery for commercial vehicles with a rankine process. In: 21st Aachen Colloquium on Automobile and Engine Technology, Aachen, Germany. Oct, 2012. pp. 7-9

[9] Quoilin S, Aumann R, Grill A, Schuster A, Lemort V, Spliethoff H. Dynamic modeling and optimal control strategy of waste heat recovery organic rankine cycles. Applied Energy. 2011;**88**(6):2183-2190

[10] Feru EE. Auto-calibration for efficient diesel engines with a waste heat recovery system. Ph.D. thesis, Eindhoven University of Technology; 2015

[11] Feru E, Willems F, de Jager B, Steinxbuch M. Modeling and control of a parallel waste heat recovery system for Euro-VI heavy-duty diesel engines. Energies. 2014;**7**(10):6571-6592

[12] Silvas E, Hofman T, Murgovski N, Etman LFP., Steinbuch M. Review of optimization strategies for system-level design in hybrid electric vehicles. In: IEEE Transactions on Vehicular Technology. Jan 2017;**66**(1):57-70. DOI: 10.1109/TVT.2016.2547897

[13] Feru E, Kupper F, Rojer C, Seykens X, Scappin F, Willems F, Smits J, De Jager B, Steinbuch M. Experimental validation of a dynamic waste heat recovery system model for control purposes, Technical report. SAE Technical Paper; 2013-01-1647. 2013

[14] Oom M. Identification and validation of an expander model for automotive waste heat recovery systems, Technical report. Eindhoven University of Technology; 2014

[15] Feru E, de Jager B, Willems F, Steinbuch M. Two-phase plate-fin heat exchanger modeling for waste heat recovery systems in diesel engines. Applied Energy. 2014;**133**:183-196

[16] Goyal S. Optimal sizing of waste heat recovery system for dynamic engine conditions, Master thesis CST 2016.137. Eindhoven University of Technology; 2016

[17] Quoilin S, Declaye S, Tchanche BF, Lemort V. Thermo-economic optimization of waste heat recovery organic rankine cycles. Applied Thermal Engineering. 2011;**31**(14):2885-2893

[18] Feru E, Willems F, de Jager B, Steinbuch M. Model predictive control of a waste heat recovery system for automotive diesel engines. In: System Theory, Control and Computing (ICSTCC), 2014 18th International Conference. IEEE; 2014. pp. 658-663

Chapter 6

Dynamic Modeling of ORC Power Plants

Mohsen Assadi and Yaser Mollaei Barzi

Additional information is available at the end of the chapter

http://dx.doi.org/10.5772/intechopen.78390

Abstract

This chapter presents dynamic modeling approaches suitable for organic Rankine cycle (ORC) power plants. Dynamic models are necessary for the better understanding of the plants' behavior during transient operation, such as start-up, shutdown, and during rapid load changes. The estimation of plant operating parameters during transient operation is crucial for monitoring and control of the plant so that the system state variables do not exceed the pre-defined operating range. One example is the proportion of liquid and vapor phase in the condenser and evaporator that must be kept within acceptable ranges to avoid stalling or temperature shocks during transient conditions. Using dynamic models enables plant operators to predict changes in power output as a function of the plant's boundary conditions such as temperature of the heat source and ambient conditions, so that they can respond to the expected heat and power demand accordingly. The aim of the chapter is to investigate and review the methodologies applicable for dynamic simulation of ORC power plants.

Keywords: dynamic modeling, transient conditions, simulation, time constants, ORC, thermal power plant

1. Introduction

1.1. Basics of dynamic modeling

The mathematical modeling of the dynamic systems and analysis of their dynamic characteristics is essential for developing the control and monitoring systems. A dynamic model is able to trace the variation of the system operating parameters in all operating conditions and consequently detect the critical points and outranges. Generally, the dynamic behavior of a system including mechanical, electrical, fluid, thermal, and so on can be described by a set of

transient differential equations (ODE or PDE) which originates from the governing physical principals and inherent physical characteristics.

The basic concepts that have to be known in dynamic modeling include system inertia, initial condition, input stimulus variable, and time constant.

The *inertia of a system* is defined by its tendency to remain unchanged or its resistivity against the variation. Obviously, the system's dynamic response depends on its inherent inertia and also the input stimulus which causes the system to break through its initial steady-state condition. To simulate and predict a system's dynamic response, all parameters and properties of the system which affect system inertia have to be known and considered. In mathematics and particularly in dynamic systems, an *initial condition* is the value of an evolving variable at some specific point in time (typically denoted as t = 0). Generally, initial conditions are needed in order to be able to trace the changes in the system's variables in time. Initial conditions affect the value of dynamic variables (state variables) at any time in the future [1].

In dynamic modeling, it is assumed that the system's initial state is disturbed due to an external excitation or load change which forces the system to respond dynamically. This input excitation pulse is called *input stimulus variable*. The input stimulus can be an impulse function, a step function, a linear function, a sinusoidal function or any other type of time-dependent function.

Moreover, *time constant* is defined as a time which represents the speed with which a particular system can respond to change, typically equal to the time taken for a specified parameter to vary conventionally by a factor of 1–1/*e* (approximately 0.6321). Actually, it is a criterion that enables us to evaluate the response speed and inertia of the system and also to compare the response time of different systems to each other. Physically, a smaller time constant means a quicker system response. For example, time constants are a feature of the lumped system analysis (lumped capacity analysis method) for thermal systems, used when objects cool or warm uniformly under the influence of convective cooling or heating [2]. This concept is also used in other dynamic systems including mechanical vibration and damping, electrical circuits, electronic systems, fluid and hydraulic systems, thermodynamic systems, chemical and electrochemical processes, and so on [3].

In this chapter, we are going to focus on thermal power plants' dynamic behavior modeling and specialize it for ORC power plants.

1.2. Theory of thermal power systems and organic Rankine cycles' dynamic operation

In the development of thermal power plants, a good estimation/prediction of the plant behavior under design and/or during operation is highly desired [4]. Thermal power systems and especially organic Rankine cycles (ORCs) have complex starting and shut-down mechanisms and normally undergo fluctuations in operating conditions during their service period. Therefore, their dynamic behavior has to be identified to ensure the secure and continuous operation of the system when facing fluctuations and perturbations. The dynamic plant

performance is also the foundation for developing control systems during the early design stage of an ORC power plant. In an ORC dynamic operation analysis, the following factors are of interest to be investigated and identified [5].

- the time response of the ORC components (including turbine, pump, heat exchangers, etc.) and identification of the slowest responding component to an input parameter change;
- the total system response time, overshoots, and identification of limitations and outranges;
- recognition of the start-up and shut-down operation mode;
- an unexpected slow or sharp transient in response to change in one or multiple physical variables like thermal input, power output, and so on;
- the part-load capability of the system.

1.3. State of the art (literature review)

Much of the recent research on ORC systems focused on finding the ideal working fluids and developing turbines and heat exchangers that can provide the highest efficiency for the given power plant layout and the nominal steady-state operational conditions. A wide range of literature is available dealing with the steady-state operation of ORC systems for geothermal power plants, while dynamic models and studies are not so common [6].

A thorough exposition on the dynamic modeling of ORCs is given in a two-part series by Paliano and Putten [7] and [8]. They give insight into the requirements for dynamic model development and validation of Rankine cycle systems and present a simulation of a 600 kWe biomass-fired steam power plant. They use a self-developed dynamic cycle analysis library using an object-oriented, general simulation software (http://www.mathworks.com). The developed models are designed for observing transients around the steady state and do not cope well with unusual circumstances, such as sudden large drops in the temperature of the heating fluid or start-up and shutdown.

The dynamic modeling of the organic Rankine cycle (ORC) was also carried out by Wei et al. [9] targeting ORC system control and diagnostic. They tested two different modeling approaches for this purpose, focusing on computational time, simulation accuracy, and complexity. The first approach was based on the moving boundary numerical method and the second one was performed using the general discretization technique. The code was developed in Modelica and simulated by the Dymola module. After comparison and evaluation of the two approaches, they suggested the moving boundary approach as the most suitable ones for control design applications.

Sohel et al. [6] published their study on the dynamic modeling of a 5.4 MW binary cycle unit of a geothermal power plant. Pentane was used as the ORC motive fluid and it is powered by separated brine from the geothermal fluid. The results of simulation were compared to the plant performance data and the prediction capability of the model at steady and transient operational conditions was proved with reasonably good accuracy.

An ORC dynamic modeling package was presented by Casella et al. [10] for the system design and prediction of the off-design conditions. They validated their results with Triogen ORC system data [11]. The system standard module included Triogen turbo-generator, turbo pump, condenser, and recuperator, while the evaporator could be designed and customized for available energy sources. For evaporator heat exchanger modeling purpose, they used one-dimensional heat transfer equations and considered a standard geometry with some simplifying correlations.

Desideri et al. [12] developed a dynamic model of the ORC system, validated both in steady-state and transient conditions via experimental data using a 10 kWe waste heat recovery (WHR) ORC system with a screw expander. They used an open-source Modelica library, ThermoCycle, developed by the Energy Systems Research Unit at the University of Liege. The commercial program Dymola (Dynamic Modeling Laboratory) was used to perform all the simulations. They implemented a liquid receiver model after the condenser to incorporate the accumulated liquid in the tank based on the phase equilibrium assumption. Moreover, effects of the non-condensable gases were incorporated in their model using the gas mixture theory.

Eventually, they demonstrated that the ThermoCycle library can reliably be used for the modeling of such thermodynamic systems, allowing, for instance, the implementation and simulation of various control strategies.

Ziviani et al. [13] discussed the challenges involved in ORC modeling for low-grade thermal energy recovery. They studied and reviewed various software packages, to identify the most applicable and suitable ones for ORC system modeling. Their recommended package list included Matlab/Simulink, EES, Phyton, Modelica, AMESim, and Cycle-Tempo.

In another relevant study, Grelet et al. [14] presented a method to model heat exchangers used in waste heat recovery Rankine-based systems in heavy-duty trucks using the water ethanol mixture and recovering heat from the exhaust gas recirculation (EGR) system. The model predicted both the heat transfer and physical properties of the working fluid such as temperature and density after the heat exchange process. The authors claim that the model presents an advantage of being low in terms of computational needs and is suitable for control software integration. Grelet et al. [15] published also another paper investigating the transient performance of a waste heat recovery Rankine cycle-based system for a heavy-duty truck and compared it to the steady-state study. Simple thermodynamic simulations are carried out assuming certain conditions for the comparison of several working fluids. Fluid choice and concept optimization are conducted, taking into account integration constraints (heat rejection, packaging, etc.). The study exposes the importance of the modeling phase when designing Rankine cycle-based heat recovery systems (HRSs) and yields a better understanding when it comes to the integration of a Rankine cycle in a truck.

Marchionni et al. [16] presented a modeling approach to analyze and design waste heat to power conversion units based on an ORC. They implemented the model in the commercial software platform GT-SUITE. Sub-models were developed and calibrated for the components like plate heat exchangers and multistage centrifugal pumps using performance data of industrial map data at design and off-design conditions. The pump and turbine speed were optimized at different operating conditions of the evaporator to maximize the net power output. Furthermore, the effects of thermal inertial of the evaporator, in response to transient

input heat load, were assessed using the dynamic model with reference to a sample heat load profile of the hot water source and at different timescales.

Furthermore, Xu et al. [17] developed a dynamic organic Rankine cycle waste heat recovery model (ORC-WHR) using Simulink and an engine model for heavy-duty diesel applications. Their physics-based ORC-WHR system model, constructed in GT-POWER software platform, included parallel evaporators, flow control valves, a turbine expander, a reservoir, pumps, compressible volumes, and junctions. Experimental data for the ORC-WHR component models were identified and collected over a wide range of steady-state and transient operational conditions. The data were collected from an ORC-WHR system on a 13 L heavy-duty diesel engine. The model was supposed to serve as a virtual plant for offline simulations to explore the potential of fuel savings and emission reduction for different driving cycles of the heavy-duty trucks and provide guidelines for the experimental studies.

The reviewed papers presented here illuminate different modeling methodologies and strategies with various levels of accuracy and computational time/cost (based on the system application and modeling purpose). In addition, it is expected that a comprehensive dynamic model enables a full-range analysis of a system's transient response to variation of input parameters, that is, minimum (near-zero) to maximum possible input thermal load. The function, representing the input variations, should be flexible enough to enable the users to study the effects on the power output as the function of time.

It is also advantageous to be able to switch these inputs and outputs around for improved flexibility. In addition, adaptation of the model to closed loop control systems should be considered too.

In this chapter, a general framework is devised to provide a flexible dynamic modeling approach adaptable to different ORC system applications and different dynamic modeling purposes based on the reviewed modeling attempts and reported results. The modeling framework incorporates step-by-step dynamic modeling methodology for both component and system levels. Technical aspects as well as assumptions and required considerations for ORC dynamic modeling are described. Besides, component assembling approaches to build dynamic models of the whole ORC system are discussed and key aspects and related noticeable remarks are highlighted. Moreover, the potential applicable software tools as well as developed computer codes and data libraries customized for transient modeling of ORC power plants are reviewed, evaluated, and described.

2. Dynamic modeling of ORC at the component level

To build a comprehensive and meanwhile enough fast dynamic model of an ORC power system, the intelligent selection of component models with proper input/output parameters as well as appropriate simplifying assumptions is crucial. The ORC systems are generally utilized for the very vast range of heat recovery applications for each of which the specific type of components might be used with different operating characteristics and conditions. For example, various types and sizes of heat exchangers, expanders, pumps, valves, and so on are used for the ORCs depending on the scale of thermal power input, working fluid, secondary

transfer fluid, and the specific operating conditions. Based on the ORC system application and its specific operating conditions, a proper model with reasonable simplifying assumptions has to be considered for component modeling. In this section, we will discuss modeling methodology and analogy of the ORC components, trying to clarify general aspects of the mathematic formulation and simulation details. In some cases, we need to specialize the models for a particular component or specific assumptions requiring further modeling details.

2.1. Heat exchanger (evaporator, condenser, etc.)

In the ORC waste heat recovery systems, the heat exchangers are generally used either as evaporators or as condensers. Evaporators absorb heat from the heat source and release it to the working fluid while the condensers reject heat from the working fluid to cooling water. Since the evaporators and condensers are crucial components when determining the overall dynamic behavior of the ORCs, the heat exchanger model should be characterized by sufficient flexibility to allow simple generalization of the design.

Different types of heat exchangers might be used in the ORC systems including plate/compact heat exchangers, tubular co-flow/counter-flow heat exchangers, shell and tube heat exchangers, and so on. The detailed heat and mass transfer equations are slightly different for different types of heat exchangers due to their configuration and geometry, but the principles are the same for all these heat exchanger types. Here, we will present the modeling methodology and general equations used.

For the modeling purpose, the heat exchangers are normally represented as a straight pipe, despite the fact that different and more complex designs are usually adopted in order to enhance the heat exchanged and to reduce the overall dimensions of the system (see a schematic sample configuration in **Figure 1**) [18]. The assumption of a straight pipe, however, simplifies the resulting dynamic problem to a great extent and is commonly adopted when the heat exchanger dynamic modeling is considered [9, 19].

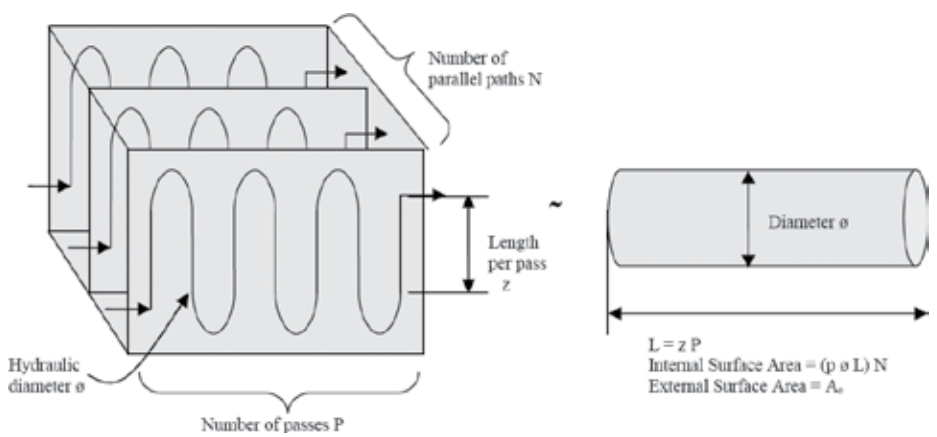

Figure 1. An example of a compact heat exchanger development into a unidirectional pipe [18].

Generally, the heat exchanger as a power plant component is simulated using one-dimensional heat and mass transfer equations because of the acceptable accuracy of one-dimensional models and limitation in computational time especially for the dynamic models and control applications. One-dimensional consideration leads to the following assumptions which normally are applied:

- The pressure drop is considered in some models but omitted in others. It depends on the importance of the pressure loss in a specific modeling strategy.
- Energy accumulation is considered in both metal pipe and the two working fluids.
- Mass accumulation is considered for the fluids (even though it is neglected in some developed models for simplicity).
- The heat exchanger could be assumed either with or without phase change depending on the actual case under study.
- One-dimensional mass and energy equations are considered and the equations are solved numerically along the heat exchanger. For more simple modeling, lumped thermal capacitance can also be assumed for both the metal pipe and the fluids; hence, just one thermal node needs to be defined with such assumptions.
- The external pipe is assumed to be ideally insulated from the environment; hence, heat losses are neglected.
- The wall and fluid temperature in the radial direction is internally uniform.
- Axial heat conduction in working fluid, wall, and exhaust gas is not considered (even though in some modeling attempts, it is taken into account).

Heat exchanger modeling tools are generally based on the finite difference method, applying the energy conservation and mass conservation equations in a differential form. The straight pipe in a typical heat exchanger design is split into n_x longitudinal lumped volumes, each of length Δx, that are the places where the conservation equations are applied. For each discrete volume three nodes can be defined in the radial direction: one referring to the state of the transfer fluid in the annulus (indexed by tf), one to the state of the metal constituting the metal pipe (indexed by p), and one referring to the organic fluid within the internal pipe (indexed by f), according to the scheme of **Figure 2**.

The system inputs are characterized by the parameters representing the two fluids at the heat exchanger inlet. Particularly their temperature, pressure, and mass flow rate must be known, and the fluid pressures are introduced since many properties depend also upon pressure. The output generated by the system can be any of the state variables but of particular interest; in the view of linking the heat exchanger to other components in a complex network, the state of the fluids leaving the exchanger must be provided, as the temperature of the two fluids. Due to the counter-flow design this temperature will be the one calculated at the node with index 1 for the fluid flowing in the annulus, as shown in **Figure 3** [18].

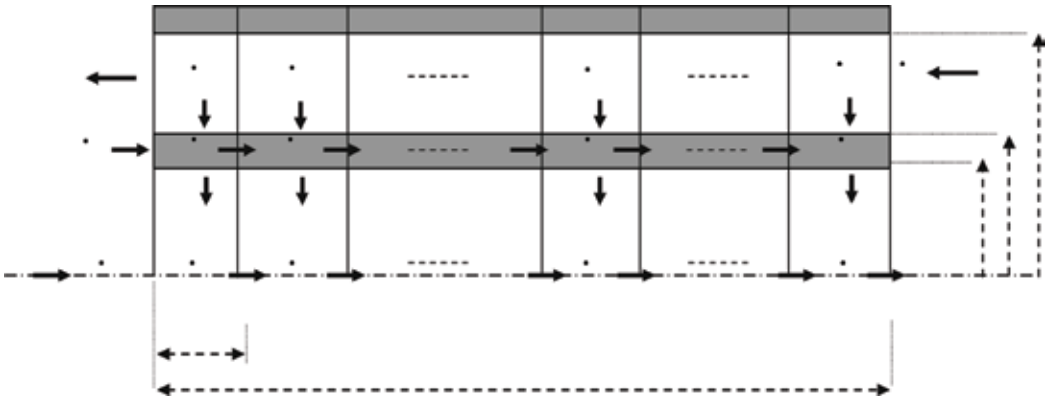

Figure 2. Discretization assumed for typical tubular counter-flow heat exchanger with phase change and main heat fluxes involved [18].

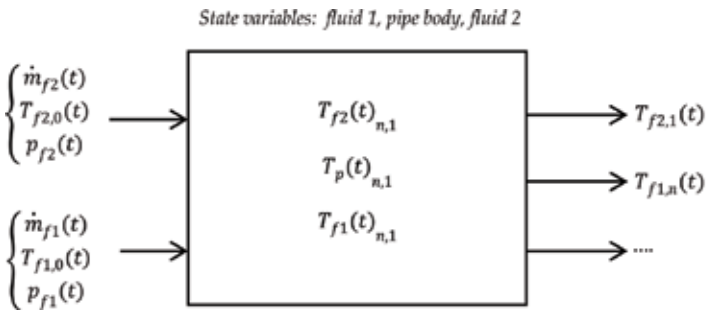

Figure 3. The heat exchanger block.

Subscribes f_1 and f_2 refer to fluid 1 (in the inner pipe) and fluid 2 (in the annulus), respectively, and subscribe p relates to the pipe body. Once the system has been fully defined, the heat and mass transfer coefficients and correlations must be introduced to calculate the actual thermal fluxes.

An interesting study conducted on this topic is by García-Vallardes et al. [20], in which the thermal and fluid dynamic behavior of a tubular heat exchanger (could be applied as evaporator or condenser) are simulated numerically. Continuity, momentum and energy conservation equations were applied for the internal and annulus tubes to accurately predict the heat and mass transfer inside the heat exchanger. Energy conservation equations have in fact been applied to the external tube and insulation, hence dropping the hypothesis of the ideally insulated system. However, such detailed simulation of the heat exchanger is not useful for the modeling of dynamic ORC systems, since one needs to compromise between expected accuracy and computational time and cost.

2.2. Expander

The expander turbine is simulated generally as a component based upon steady-state characteristic curves. Inputs/outputs of the system are shown in **Figure 4**.

Here, the rotational speed and the pressure ratio are input variables, while mass flow rate and efficiency (from which power and torque can be derived) are outputs; however, the input/output variables could be changed or replaced depending on specific application requirements or design/optimization strategies [17]. The turbine can be integrated with an electric generator or it can also be mechanically connected to an engine crank shaft through a transmission, as in [21]. Due to the choked flow status at high expansion ratios 10–30, turbine expander mass flow rate can be written as a linear function of turbine inlet pressure as shown in Eq. (1) [17].

$$\dot{m}_{turb} = a_{turb}\, p_{in,turb} + b_{turb} \tag{1}$$

The outlet enthalpy is calculated by isentropic efficiency as follows:

$$h_{out,turb} = h_{in,turb} - \eta_{is,turb}\left(h_{in,turb} - h_{out,is,turb}\right) \tag{2}$$

$$\eta_{is,turb} = map\left(N_{turb}, p_{in,turb}/p_{out,turb}, T_{in,turb}\right) \tag{3}$$

$$h_{out,is,turb} = map\left(S_{out,turb}, p_{out,turb}\right) \tag{4}$$

$$S_{out,turb} = S_{in,turb} \tag{5}$$

$$S_{is,turb} = map\left(h_{in,turb}, p_{in,turb}\right) \tag{6}$$

The turbine efficiency map has to be provided by the turbine manufacturer. Outlet temperature, $T_{out,tur}$, is calculated from outlet enthalpy and outlet pressure using a thermodynamic table of the working fluid.

$$T_{out,turb} = map\left(h_{out,turb}, p_{out,turb}\right) \tag{7}$$

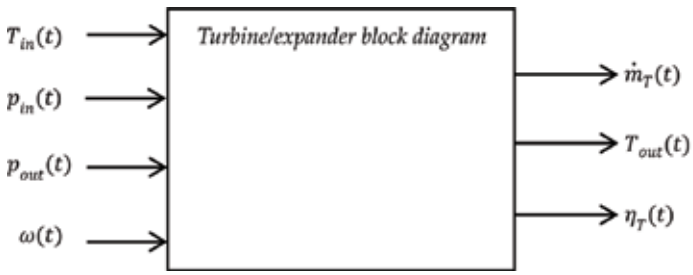

Figure 4. Block diagram of the turbine/expander model.

Turbine boundary conditions are pressure and enthalpy at the inlet and pressure at outlet. In addition, the inlet and outlet are adiabatic. The heat transfer between turbine outer surface and ambient is considered based on the turbine isentropic efficiency map.

2.3. Pump

The pumps of the ORC system have to maintain both pressure and working fluid mass flow. The HP pump is considered here to be a positive displacement type, whereas the feed pump is an inline roller cell pump. Due to the dominance of the HP pump, only the HP pump model is formulated here. The pump mass flow rate is interpolated using the map (Eq. (8)) provided by the ORC system manufacturer [22]. Pump power consumption and outlet temperature are calculated by Eq. (9) and (10).

$$\dot{m}_{pump} = map\left(N_{pump} \right) \tag{8}$$

$$P_{pump} = \frac{\dot{m}_{pump}}{\rho} \frac{\left(p_{out,pump} - p_{in,pump} \right)}{\eta_{is,pump}} \tag{9}$$

$$T_{out,pump} = T_{in,pump} + \frac{\left(1 - \eta_{is,pump} \right) P_{pump}}{\dot{m}_{pump} C_{p,pump}} \tag{10}$$

where ρ is the working fluid density upstream of the pump, $p_{in,pump}$, $p_{out,pump}$ are upstream and downstream pressures, respectively, $c_{p,pump}$ is the upstream specific heat capacity of the working fluid, and $\eta_{is,pump}$ is isentropic efficiency and is expressed as a function of pump mass flow rate and the rotational speed, which can be drawn from the pump map data [22].

2.4. Reservoir

The reservoir in an ORC system works as a buffer storage for the working fluid in order to supply fluid or accumulate it as the ORC system experiences transients. When the ORC system starts, the working fluid level is low in the reservoir because the entire circuit is full of liquid. When the system warms up, part of the ORC system is occupied by vaporized working fluid and the working fluid level in the reservoir increases compared to the cold condition. To calculate the working fluid level as well as the mean temperature, both mass balance and energy balance are applied in the reservoir. The mass balance can be described by Eq. (11) and the energy balance is given typically by Eq. (12). The reservoir working fluid level can be obtained by Eq. (13) [17].

$$\frac{d\, m_f}{dt} = \dot{m}_{f,in} - \dot{m}_{f,out} \tag{11}$$

$$\frac{d(mh)}{dt} = \dot{m}_{in} h_{in} - \dot{m}_{out} h_{out} \tag{12}$$

$$H_{res} = \frac{V}{V_0} \tag{13}$$

Here, V_0 is the entire reservoir volume and V is instant volume of the working fluid. Then, H_{res} represents the ratio of the reservoir's fluid level to the reservoir's total height. Reservoir boundary conditions are mass flow rate and enthalpy at the inlet and mass flow rate at the outlet. The reservoir is assumed to be adiabatic, that is, no heat loss to the environment.

2.5. Valve

The proportional valves or distribution/control valves are commonly used in ORC heat recovery units to enhance the flexibility and controllability of the system. Depending on the fluid state when flowing over the valve, the flow might be either incompressible or compressible. The valve located after the pump operates normally with incompressible fluid flow, while the working fluid passes through a valve before the expander, is usually super-heated vapor and shows compressible behavior. Hence, the mathematical model defined for the valves is different based on the thermodynamic state of the fluid.

When the working fluid is in liquid state and thus incompressible, the outlet temperature is assumed to be equal to the inlet temperature due to the small temperature change across the incompressible valves. The necessary boundary condition for the incompressible flow valve is mass flow rate from the pump at the inlet. The valves are assumed adiabatic, that is, no heat loss to the environment. Therefore, a simple mass conservation equation, describing the relation between the valve opening ratio and the mass flow passing through the valve, can be used. Then the valve opening ratio has to be given as an input parameter. Besides, the valve's pressure loss (if found to be considerable) can be calculated by the formulation provided by the manufacturer as a function of mass flow rate. The turbine inlet valve and turbine bypass valve both experience vapor phase flow. They can be modeled based on the compressible flow status: subsonic flow or supersonic flow depending on inlet/outlet pressure ratio [23]:

$$\dot{m} = O\,C_d\,A_0\sqrt{\frac{2\gamma}{\gamma-1}\,p_{in}\,\rho_{in}\left[\left(\frac{p_{out}}{p_{in}}\right)^{\frac{2}{\gamma}}-\left(\frac{p_{out}}{p_{in}}\right)^{\frac{\gamma+1}{\gamma}}\right]} \quad if\ \left(\frac{2}{\gamma+1}\right)^{\frac{\gamma}{(\gamma-1)}} \le \frac{p_{out}}{p_{in}} \le 1\ (Subsonic)$$

$$\dot{m} = O\,C_d\,A_0\left(\frac{2}{\gamma+1}\right)^{\frac{\gamma+1}{2(\gamma-1)}}\sqrt{\gamma\,p_{in}\,\rho_{in}}\ if\ 0 \le \frac{p_{out}}{p_{in}} \le \left(\frac{2}{\gamma+1}\right)^{\frac{\gamma}{(\gamma-1)}}(Supersonic) \tag{14}$$

Here, $\gamma = \frac{C_p}{C_v}$ is heat capacity ratio. With the isentropic assumption of the process across the valve and no heat loss consideration ($h_{in} = h_{out}$), the outlet temperature is calculated as [8]:

$$T_{out} = f(p_{out}, h_{out}) \tag{15}$$

The boundary conditions necessary for these valves are pressure and enthalpy at the inlet and pressure at the outlet.

2.6. Pipes and junctions

2.6.1. Pipes

The pressure and heat loss through the pipes containing the liquid state are normally negligible compared with other components. If in a certain case their contribution is found to be considerable, they could be mathematically modeled using the general fluid mechanics principles using pipe-flow pressure loss and heat transfer equations. However, the pipe flow after the evaporators and upstream of the turbine valves are considered as compressible volumes, which has to be taken into account, especially for their dynamic inertia applied to the system [24]. Three equations are utilized in this volume: mass balance, energy balance, and the ideal gas law [25]. Three parameters can be calculated by solving these three equations: working fluid's mass inside the volume, working fluid's mean temperature, and mean pressure inside the volume [8].

$$u\frac{dm}{dt} + m\,C_v\frac{dT}{dt} = \dot{H}_{in} - \dot{H}_{out} \tag{16}$$

$$\frac{RT}{V}\frac{dm}{dt} + \frac{p}{T}\frac{dT}{dt} - \frac{dp}{dt} = 0 \tag{17}$$

where u represents specific internal energy, c_v represents specific heat capacity, $\dot{H}_{in}$ and $\dot{H}_{out}$ represent inlet and outlet enthalpy flow rate, R represents ideal gas constant, and V represents vapor volume. Boundary conditions of the compressible vapor volume are mass flow rate and enthalpy at the inlet and mass flow rate at the outlet. Meanwhile, the inlet, outlet, and outer surfaces are all assumed to be adiabatic.

2.6.2. Junctions

Pressure loss in the pipe junctions is negligible. Besides, the junctions are assumed to be adiabatic with no heat loss to the environment. Similar to the reservoir, junctions are modeled by mass balance and energy balance via Eq. (18) and (19), respectively [8].

$$\dot{m}_{mix} = \dot{m}_1 + \dot{m}_2 \tag{18}$$

$$\dot{m}_{mix}\,h_{mix} = \dot{m}_1\,h_1 + \dot{m}_2\,h_2 \tag{19}$$

The junction boundary conditions are mass flow rate and enthalpy at the inlet and the outlet which are considered to be adiabatic.

http://dx.doi.org/10.5772/intechopen.78390

3. System-level dynamic modeling

3.1. Integration of the component dynamic models

Once dynamic models of every individual component are ready and evaluated with known input state variables and calculated outputs, the components are interconnected to build a thermodynamic model of the whole thermal power system. Before interconnecting the individual component models to each other, the following important issues have to be reviewed:

- ensuring the validity and accuracy of the component models for both steady-state and transient conditions;
- creating and fully parameterizing the ORC components, the boundary sources, and sinks. Besides, the operating range and limitations for all components have to specified and inserted in the simulation models;
- defining appropriate known and unknown variables for the system, based on the design or optimization requirements and strategy. More detailed aspects of the system variable definition that need to be considered are presented in Section 3.3.
- omitting the unnecessary fixed common variables of the individual component models or adding new fixed common state variables.

After above-listed considerations and the preparation of required data, the ORC components will be connected properly to establish the system model. Connecting the component models means uniting the common variables of a specific component to its neighboring components so that the set of components create a closed loop by linking them to each other.

3.2. Initialization of the system simulation model

Apparently, the initialization of closed-loop dynamic models is a difficult task which should be carefully approached and planned. To initialize the dynamic model, the initial conditions have to be defined appropriately. At some point during the initialization process, one must thoroughly plan the thermodynamic cycle as a steady-state problem to find appropriate states for the initialization of the problem [5]. Initial state points can be set as parameters calculated by a steady-state model in which the analysis is expected to begin in a time domain. Initialization problems require starting arrays for all components, which can also be stored as parameters in the test bench level. Diagnostic and summary variables should also be included in the initial condition list definition [9].

3.3. Input and output parameters and identification of the constraints

The ORC dynamic model developers must prepare an input/output variable list considering the aspects mentioned in Section 3.1, where all fixed model inputs based on the real-test

condition are presented. The model outputs which are to be calculated as a result of the simulation need to be fixed too. Then the variation of the outputs as a function of the time step can be studied and investigated. Besides, different post-processing activities can be considered, using the simulation results.

It has to be kept in mind that the number of unknown variables of the whole system has to be equal to the number of equations so that the differential sets of equations are closed. Otherwise, the equations are not solved or won't have unique results. When the component models are integrated to build the thermal power system, the number of unknown variables for each component will be different from the case when the component models were simulated individually. It is usually helpful if components are connected one by one and simulated step by step to ensure the correct connectivity and the number of input/output variables.

Moreover, the output variable trends are strongly dependent on the constraints forced to the simulation model. Obviously, the output trends will follow the real plant's output when the system constraints imposed during simulation are the same as for the real plant [26].

3.4. Key aspects of ORC power systems to be considered for the analysis

3.4.1. Working fluid

There are several aspects to be taken into account when using a working fluid for a specific application. The aspects that have to be considered include fluid deterioration, environmental aspects, as well as boiling, condensation, and freezing temperatures that decide the operating ranges. The above limitations have to be incorporated in the simulation tool.

3.4.2. Heat sources

The heat sources have different grades of quality (temperature levels) and quantity (amount of thermal energy). The dynamic model has to take into account the possible range of operating temperatures and the amount of thermal energy of the heat sources. If the number of heat sources is larger than one, additional complexity and more challenges for the design of the system (fluid, expansion machine, control, etc.) will arise. Generally, variation in heat source parameters is a common input to the stimulation of the ORC systems, which leads to a dynamic response.

3.4.3. Heat sink

For a specific ORC application, the heat sink available is usually an independent or commonly used cooling package including radiators containing a coolant, which is cooled by means of cooling fans or an air-cooling module. The integration of a heat recovery system model into the cooling module results in more conclusive and realistic results, which eventually limit the amount of heat that can be converted into useful work. In addition, thermal and mass inertia of the heat sink (cooling module) may affect dynamic behavior and time response of the whole system. Therefore, a complete system analysis including the cooling package is necessary to find the optimal way of recovering the heat from a heat source and to design a reliable control and monitoring system.

3.4.4. Subsystem interaction

In ORC-based heat recovery systems, the operation of the plant that generates heat might be influenced by the integration of the ORC. For such systems, the impact on lateral subsystems has to be considered and incorporated in the simulation.

For example, in an ORC heat recovery system for a heavy-duty truck (experimented and simulated by Grelet et al. [15] and also Xu et al. [17]), the ORC system shares the cooling system of the vehicle and therefore the charge air cooling capacity can be lower, which has a negative impact on the engine performance. Another example is the use of exhaust gas recirculation (EGR) as the heat source in a heat recovery system designed for heavy-duty trucks. This leads to a trade-off between EGR cooling and ORC performance, which could impact negatively the engine emissions. Several other interactions such as the exhaust back pressure or the weight penalty could also be cited. In such heat recovery systems (HRSs), the performance, and thereby the fuel economy, will be dependent on all the aspects mentioned above. It is therefore critical to model the complete system and its surrounding environment in order to optimize the whole integrated setup. It helps to select the best design using simulation and thereby reduce the number of experimental tests needed to be carried out [15].

3.5. Survey of available codes for modeling power plant systems

After reviewing the modeling methodologies of ORC systems, an analysis has been conducted in this section, in order to determine available commercial software that might have been employed as tools for implementing the modeling processes. Other computer-based models within the field of the energy conversion system, available in the open literature, have also been surveyed. The analysis has brought to identify some software that may appear to be proper for the scope. Software that have been used for power cycle modeling purposes are Matlab/Simulink, AMESim, Trnsys, Modelica (OpenModelica, Dymola, Wolfram System Modeler, and MapleSim are all based on Modelica), GateCycle, EES, Phyton, Cycle-Tempo, and GT-SUITE. It should be noted that the analysis of commercial software reported here is neither complete nor exhaustive but is limited to those packages that have been found by the authors to be applicable for dynamic, thermodynamic, and energy modeling purposes. These software have been utilized in order to provide a deeper understanding of their characteristics and a brief description is presented here. Some of these software like GateCycle and Trnsys, while appropriate for some applications, turned out to be improper for the scope of the ORC dynamic analysis, and therefore will not be discussed here. Matlab/Simulink, AMESim, and Modelica feature some common characteristics that make them more suitable for the development of customized dynamic component models of energy systems, for both control purposes and optimization. Therefore, they will be further discussed briefly here [18].

3.5.1. Matlab/Simulink

Matlab is a high-performance language for technical modeling and computation; the name Matlab stands for matrix laboratory. The Matlab language is a high-level matrix/array language with controls flow statements, functions, data structures, input/output, and object-oriented programming features. Matlab/Simulink is a general purpose software package

suitable for dynamic systems, which is well known among the control community as it offers excellent performance qualities for designing regulation algorithms. It makes the tool an ideal candidate for process and control engineers, working with the same software package. The environment provided by Matlab software facilitates a general overview of all computations step by step, that can be used for a wide range of applications including simulation, data acquisition, data analysis, and visualization as well as scientific and engineering graphics.

For the dynamic modeling purpose, Simulink provides a graphical user interface (GUI) for building models as block diagrams, using click-and-drag mouse operations. Because Matlab and Simulink are integrated, one can simulate, analyze, and revise models in either environment at any point. Application of Matlab language code and its integration with the Simulink environment, in order to create the desired models of components considered in the analysis of energy systems, depend on the equations used, the methodology applied, and the input/output parameters, which will be discussed in the next sections [18].

3.5.2. AMESim

AMESim is an advanced modeling environment for performing simulations of engineering systems. The main features and applications of this tool are:

- performance evaluation of intelligent systems from the early stage of development until on-site application of the system;
- the optimization of interactions between subsystems of a multi-mechanism system like electric/electronic, mechanical, hydraulic, pneumatic, and thermal systems;
- overall product quality and performance improvement through exploration of critical functions and design update;
- enhancing the product development process using novel design features and applying proper algorithms.

The software has the typical feature of an icon-based program and engineering systems can be built by adding symbols or icons to a drawing area. AMESim therefore enables the users to build complex multi-domain system models through an interactive graphical interface. The resulting sketch is easy to understand and offers a logical representation of the system model under investigation. When the sketch is complete, simulation of the system proceeds in the following stages:

- Graphical representation of the components is associated with the mathematical models.
- The component parameters are defined.
- The system is simulated.
- Graphical representation of the results is prepared and post-processing is performed to customize the results' visualization.

The system modeling is carried out in four steps [18]:

- Sketch mode: The stage in which different components are linked.
- Sub-model mode: The stage in which the physical sub-model associated with each component is chosen.
- Parameter mode: The stage in which the parameters for each sub-model are chosen.
- Run mode: The stage in which the simulation is executed.

3.5.3. Modelica

Modelica language is designed basically for the modeling of multi-component systems to provide an environment in which a virtual system can be built, similar to what is implemented by engineers in real system development. As an example, standard components like compressor, turbine, and heat exchanger can be selected based on the manufacturers' catalogs with related technical interfaces and specifications [27]. For this purpose, some manufacturer's catalogs are proposed to be used with Modelica standard libraries. If a particular subsystem or component doesn't exist in the software library, it can be built by the user based on software standardized interfaces.

Mathematical component models are generally described by differential, algebraic, and discrete equations in Modelica. Hence, the solution method of the describing equations doesn't need to be specified by the users. The software decides the algorithm, the computational methodology, or strategy to be used to solve the equations of a particular system and its components.

In [28], the results of development of a Modelica library for CO_2 refrigeration systems based on the free Modelica library ThermoFluid are presented. The library development is carried out in an Airbus Deutschland research project and is focused on obtaining a library for detailed numerical investigation of refrigeration systems with carbon dioxide (CO_2) as the refrigerant. Using the developed component library a CO_2 refrigeration cycle has been analyzed (**Figure 5**). The developed model can be used for optimization of specific heat exchangers and evaluation of optimum system configuration as well as for optimization of system control layout.

3.5.4. Customized tools for simulation of energy systems

The literature survey concerning non-commercial models of inter-connectable components of energy system networks resulted in very few examples, which has led to the conclusion that this field still lacks a complete and exhaustive review work. The models proposed are mainly developed for specific applications and often are limited concerning scalability, flexibility, or generality. Examples of custom libraries of components for dynamic modeling and analysis of complex energy systems can be found in [29–31].

In [29, 30] a modular code for dynamic simulation of a single-shaft gas turbine is presented. The code, called CAMEL, is a modular object-oriented process simulator, for energy

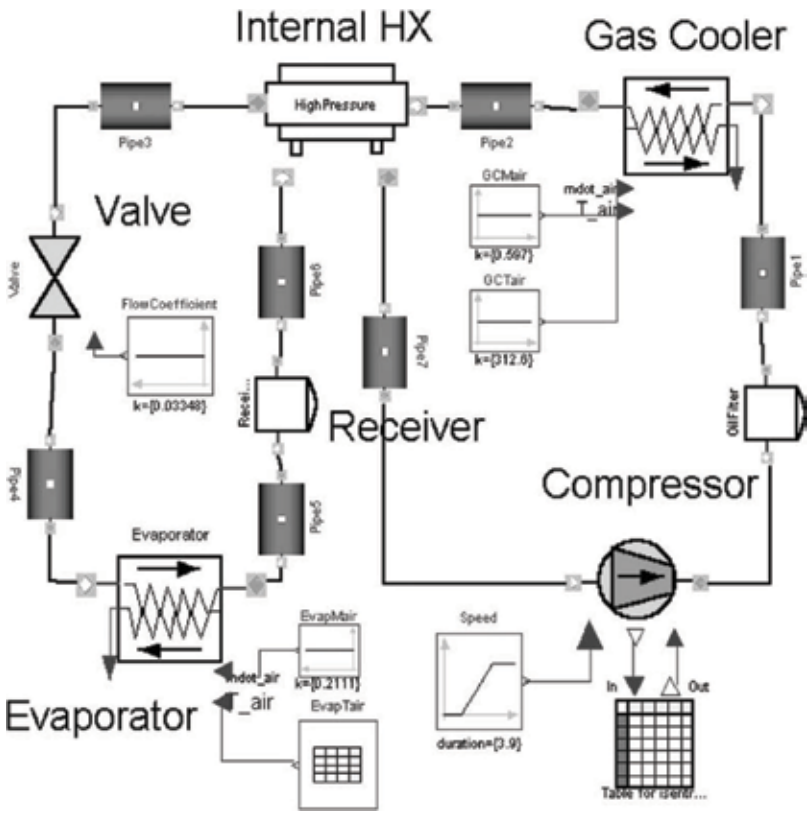

Figure 5. Modelica object diagram of a CO_2 cooling cycle [28].

conversion system (with specific reference to micro-turbines), and the modeling method is a black-box approach. Each component of the system under analysis can be assembled in an engineering process scheme where the connections between two elements represent either mechanical power coupling or a working fluid stream. The code is devoted to energy system design and is based on C++. For each separate component, a proper set of first-order (linear/non-linear) algebraic or differential equations are cast and all the block equations pertaining to the different blocks are assembled together and solved in matrix form, once assigned proper boundary conditions and parameters. Equations are integrated in time according to a fourth-order Runge-Kutta method. The code is used for both steady-state off-design and dynamic operating conditions.

In another original code [31] called TRANSEO, transient and dynamic simulation of micro-gas turbine-based systems is presented. The code is a model-based software developed in the Simulink platform The library features some advanced components such as heat exchangers, which are modeled according to finite volume approach. Many of the blocks have been validated with reference to a commercial recuperated micro-turbine. From the models realized, some advance-cycle configurations have been proposed and analyzed: for example, externally fired micro-turbine cycles, closed Brayton cycles for space applications, and hybrid micro-turbine fuel cell systems. The library indeed provides some advanced components, and

significant modeling techniques are applied in order to generate components applicable to any kind of micro-turbine-based energy conversion system.

4. Conclusion

Dynamic models are necessary for the better understanding of the ORC plants' behavior during transient operation, such as start-up, shutdown, and during rapid load changes. The estimation of plant operating parameters during transient operation is crucial for monitoring and control of the plant so that the system state variables do not exceed the pre-defined operating ranges. Using dynamic models enables plant operators to predict changes in power output as a function of the plant's boundary conditions such as temperature of the heat source and ambient conditions, so that they can respond to the expected heat and power demand accordingly.

Key elements of an ORC dynamic model are firstly the proper transient configuration of the component's sub-models and secondly the assembly of individual sub-models to build the whole system model. Thermal and mass inertia of the components (component body and containing fluid) are two decisive factors for the system's response time.

Arrangement of the input/output variables and the system constraints play an important role in receiving reliable results. The fixed input state variables and constraints of the model have to be coincident with the real plant fixed and controlled variables.

For the dynamic modeling of an ORC system the initial conditions have to be defined and applied appropriately to the model for simulation initialization. All system variables have to be pre-defined as an array at the starting time based on the assumed initial state conditions. Obviously, the initial conditions have to be set up based on the purpose of the dynamic analysis: start-up, shut-down, system response to an input, or any other operating modes. For many cases, the initial conditions can be generated as a result of a steady-state simulation with the initial operating condition setup of the system.

For transient modeling of ORC plants, one can either use suitable commercial software or open source codes for formulation and parameter selection flexibility. Some ready-made data libraries for system components as well as material properties have been developed and customized for the transient modeling of thermal power systems.

In sum, the following general steps are defined and proposed based on ORC power plants' dynamic modeling framework:

1. specifying the modeling assumptions for every single component as well as the whole system according to the purpose of the analysis and application;
2. validation of the component models, to guarantee validity and accuracy for both steady-state and transient conditions;
3. parameterizing the ORC components and the boundary sources and sinks;

4. defining the operating ranges and limitations for all components and introducing them to individual component models;
5. defining appropriate known and unknown (input/output) variables for the system, based on the design and analysis requirements and strategies. This may lead to omitting unnecessary fixed variables of the individual component models or adding new fixed common state variables;
6. interconnecting the ORC components properly to build the whole system model;
7. compiling, executing and diagnosis of the system model, first for steady-state conditions;
8. initial condition definition and data preparation;
9. running the transient model, diagnosis and validation;
10. customizing the dynamic model for a particular purpose or application.

Author details

Mohsen Assadi[1]* and Yaser Mollaei Barzi[2]

*Address all correspondence to: mohsen.assadi@uis.no

1 Department of Energy and Petroleum Engineering, University of Stavanger, Stavanger, Norway

2 Department of Mechanical Engineering, Islamic Azad University, Kaeshan Branch, Kashan, Iran

References

[1] William J. Baumol, Economic Dynamics: An Introduction, 3rd edition, London: Collier-Macmillan. pp. 160, 1970. ISBN: 0-02-306660-1

[2] North GR. Lessons from energy balance models, In: Schlesinger ME. (Eds.), Physically-Based Modeling and Simulation of Climate and Climatic Change, NATO ASI Series (Series C: Mathematical and Physical Sciences), Vol. 243. Springer, Dordrecht, pp. 627-651, 1988. ISBN 90-277-2789-9

[3] Mollayi Barzi Y, Ghassemi M, Hamedi MH. A 2D transient numerical model combining heat/mass transport effects in a tubular solid oxide fuel cell. Journal of Power Sources. 2009;**192**:200-207

[4] Franco A, Villani M. Optimal design of binary cycle power plants for water-dominated, medium-temperature geothermal fields. Geothermics. 2009;**38**(4):379-391

[5] Twomey BL. Dynamic simulation and experimental validation of an organic Rankine cycle model [PhD thesis]. University of Queensland, School of Mechanical and Mining Engineering; 2015

[6] Sohel MI, Krumdieck S, Sellier M, Brackney LJ. Dynamic modeling and simulation of an organic Rankine cycle unit of a geothermal power plant. In: Proceedings World Geothermal Congress 2010; Bali, Indonesia; April 25-29, 2010

[7] Colonna Paliano P, van Putten H. Dynamic modeling of steam power cycles. Part I—Modeling paradigm and validation. Applied Thermal Engineering. 2007;**27**(2-3):467-480

[8] van Putten H, Colonna Paliano P. Dynamic modeling of steam power cycles: Part II—Simulation of a small simple Rankine cycle system. Applied Thermal Engineering. 2007;**27**(14-15):2566-2582

[9] Wei D, Lu X, Lu Z, Gu J. Dynamic modeling and simulation of an organic Rankine cycle (ORC) system for waste heat recovery. Applied Thermal Engineering. 2008;**28**:1216-1224

[10] Casella F, Mathijssen T, Colonna di Paliano P, Buijtenen J. Dynamic modeling of organic Rankine cycle power systems. Journal of Engineering for Gas Turbines and Power. 2013;**135**:042310-1-12

[11] Triogen. Triogen High-speed Turbo Generator [Online]. 2013. Available from: http://www.triogen.nl/technology/triogen-high-speed-turbo-generator [Accessed: July 24, 2013]

[12] Desideri A, Gusev MV, Lecompte S, Lemort V, Quoilin S. Experimental study and dynamic modeling of a WHR ORC power system with screw expander. In: 2nd International Seminar on ORC Power Systems; Rotterdam, Netherlands; October 2013

[13] Ziviani D, Beyene A, Venturini M. Advances and challenges in ORC systems modeling for low grade thermal energy recovery. Applied Energy. 2014;**121**:79-95

[14] Grelet V, Lemort V, Nadri M, Dufour P, Reiche T. Waste heat recovery Rankine cycle based system modeling for heavy duty trucks fuel saving assessment. In: 3rd International Seminar on ORC Power Systems; Brussels, Belgium; October 12-14, 2015

[15] Grelet V, Reiche T, Lemort V, Nadri M, Dufour P. Transient performance evaluation of waste heat recovery Rankine cycle based system for heavy duty trucks. Applied Energy Journal. 2016;**165**:878-892

[16] Marchionni M, Bianchi G, Kontakiotis AK, Pesiridis A, Tassou SA. Dynamic modeling and optimization of an ORC unit equipped with plate heat exchangers and turbomachines. Journal of Energy Procedia. 2017;**129**:224-231

[17] Xu B, Rathod D, Kulkarni S, Yebi A, Filipi Z, Onori S, Hoffman M. Transient dynamic modeling and validation of an organic Rankine cycle waste heat recovery system for heavy duty diesel engine applications. Applied Energy Journal. 2017;**205**:260-279

[18] Vaja I. Definition of an object oriented library for the dynamic simulation of advanced energy systems [PhD thesis]. Department of Industrial Engineering, University of Parma Studies; 2009

[19] Bestrin R, Vermeulen AG. Mathematical modeling and analysis of vapour compression system. International Report. Eindhoven, Netherlands: University of Technology; August 2003

[20] García-Vallardes O, Pérez-Segarra CD, Rigola J. Numerical simulation of double-pipe condensers and evaporators. International Journal of Refrigeration. 2004;**27**:656-670

[21] Xu B, Yebi A, Onori S, Filipi Z, Liu X, Shutty J. Power maximization of a heavy duty diesel organic Rankine cycle waste heat recovery system utilizing mechanically coupled and fully electrified turbine expanders. In: Proceedings of the ASME 2016 Internal Combustion Fall Technical Conference; Greenville, SC, USA; 2016. p. 11

[22] Invernizzi C, Iora P, Silva P. Bottoming micro-Rankine cycles for micro-gas turbines. Applied Thermal Energy. 2007;**27**:100-110

[23] Weiss HH, Boshwirth L. A simple but efficient equipment for experimental determination of valve loss coefficient under compressible and steady flow conditions. In: International Compressor Engineering Conference; 1982. pp. 69-76

[24] Feru E, Willems F, de Jager B, Steinbuch M. Modeling and control of a parallel waste heat recovery system for Euro-VI heavy-duty diesel engines. Energies, vol. 7, pp. 6571-6592, 2014

[25] Moran MJ, Shapiro HN. Fundamentals of Engineering Thermodynamics. 5th ed., Chichester, England: John Wiley & Sons, Inc; 2006

[26] Mollaei Barzi Y, Assadi M, Parham K. A waste heat recovery system development and analysis using ORC for the energy efficiency improvement in aluminum electrolysis cells. International Journal of Energy Research. 2017:1-13

[27] Elmqvist H, Mattsson SE. An introduction to the physical modeling language Modelica. In: Proceedings of the 9th European Simulation Symposium, ESS'97; October 19-23, 1997; Passau, Germany; 1997

[28] Pfafferott T, Schmitz G. Modeling and transient simulation of CO_2-refrigeration systems with Modelica. International Journal of Refrigeration. 2004;**27**:42-52

[29] Cennerilli S, Sciubba E. Application of the CAMEL process simulator to the dynamic simulation of gas turbines. Energy Conversion and Management. 2007;**48**:2792-2801

[30] Cennerilli S, Fiorini P, Sciubba E. Application of the Camel process simulator to the dynamic simulation of gas turbines. In: ECOS 2006 Proceedings; Vol. 1; 2006. pp. 355-363

[31] Traverso A. TRANSEO: A new simulation tool for transient analysis of innovative energy systems [PhD thesis]. Italy: TPG-DiMSET, University of Genova; 2004

Applications

Chapter 7

The Development and Application of Organic Rankine Cycle for Vehicle Waste Heat Recovery

Yiji Lu, Anthony Paul Roskilly and Xiaoli Yu

Additional information is available at the end of the chapter

http://dx.doi.org/10.5772/intechopen.78401

Abstract

The development of engine waste heat recovery (WHR) technologies attracts ever increasing interests due to the rising strict policy requirements and environmental concerns. Organic Rankine Cycle (ORC) can convert low medium grade heat into electrical or mechanical power and has been widely recognized as the most promising heat-driven technologies. A typical internal combustion engine (ICE) converts around 30% of the overall fuel energy into effective mechanical power and the rest of fuel energy is dumped through the engine exhaust system and cooling system. Integrating a well-designed ORC system to ICE can effectively improve the overall energy efficiency and reduce emissions with around 2–5 years payback period through fuel saving. This book chapter is meant to provide an overview of the technical development and application of ORC technology to recover wasted thermal energy from the ICE with a particular focus on vehicle applications.

Keywords: internal combustion engine, vehicle application, organic Rankine cycle, engine waste heat recovery

1. Introduction

Over the last century, the internal combustion engine (ICE) as one of the main power sources has been widely adopted in the vehicle and marine propulsion systems such as automobiles, trains, trucks, boats, and ships. The increasing concerns on the environmental problems caused by burning fossil fuels promote the technology development of more efficient, more compact, and more cost-effective ICE, which can potentially improve the overall energy efficiency, reduce the emissions and generate more effective engine shaft power by burning fossil

fuels [1]. Moreover, the increasingly strict emission legislations are focusing on the nitrogen oxides (NOx), particulate matter (PM), carbon monoxide (CO), and hydrocarbon (HC).

Engine manufacturers have developed and adopted the technologies such as turbocharging, variable valve timing [2], Miller timing strategies [3], advanced injection strategies, and engine friction reduction technologies in order to improve the system thermal efficiency. However, adopting the stated technologies the ICE is still difficult to convert more than 40% of the fuel energy into effective mechanical power [4, 5]. And there is around 60–70% of fuel energy is wasted from the exhaust system and cooling system of ICE [4, 5]. Other approaches such as burning alternative fuels [6] and the development of hybrid pneumatic system [7] to recover the engine kinetic energy were also considered. Recent research attentions are focusing on the development of engine bottoming technologies such as advanced after treatment systems or engine waste heat recovery (WHR) technologies [8]. The Organic Rankine Cycle (ORC) is one of the most promising heat-driven technologies converting heat into mechanical power or electricity [9, 10]. ORC system can recover various heat sources such as biomass combustion heat, solar energy, geothermal heat, and industry wasted heat and heat from Internal Combustion Engine (ICE) [9]. Adopting ORC technology for engine waste heat recovery can effectively improve the overall system efficiency and reduce the emissions. A well-designed ORC system can potentially achieve around 2–5 years payback period through fuel saving [4, 5, 10]. However, Velez et al. [10] pointed out the market available ORC system with the power ranges of 0.2–2 MWe under the cost around 1and 4 × 103 € /kWe, and lower powers are in pre-commercial status because of the relatively long payback period using small-scale ORC system. The technical development, main research barriers, and potential solutions of the technology are summarized in this chapter, which aims to have an overview of the ORC technology and promote its applications.

1.1. Emerging applications of the technology for vehicles

The applications and extensively research interests of waste heat recovery technologies started in the 1970s during the oil crisis [11]. The first application of ORC for engine waste heat recovery was reported by Patel and Dovle in 1976 [12]. The research project conducted by Mack Trucks and the Thermo Electron Corporation was sponsored by US Department of Energy (DOE). The first prototype ORC machine was installed on a Mack 676 diesel engine to recover the exhaust waste heat. The system adopted Fluorinol-50 as the ORC working fluid and a three-stage axial flow turbine expander. The mechanical power of the expander was transferred to the power take-off device coupled with a speed reduction gearbox. They demonstrated the technical feasibility of the system and its economic interests. The optimal performance of the system could achieve a 13% increase in maximum power with around 15% reduction of fuel consumption. Follow on progress reported by Pate et al. [13] announced a 1 year test program of an ORC bottoming system coupled on a Mack diesel engine in 1979 and they declared a plan of expanding the ORC system on 10 trucks in 1981–1982. In 1983, the research group reported the testing results of the program [14], which demonstrated 12.5% improvement of the average fuel consumption on high-way vehicle fuel economy tests. However, no follow on progress for the expanding plan can be found from the literature. The ORC systems developed nowadays can achieve much higher efficiency because of the broad choice of advanced working fluids and the development of system components, such as expansion devices and heat exchangers. However,

the commercial ORC system for vehicle application is still not available from the market. One of the possible reasons is the concern on the substantial capital cost due to the complexity of the system and complicated control strategies required for vehicle application.

1.2. Representative prototypes developed by vehicle manufactures

The application of steam Rankine cycle for vehicle waste hear recovery has been reported by BMW in 2005 [15], who later announced the proposed system can achieve 15% improvement for engine performance [16, 17]. **Figure 1** is the schematic diagram of the BMW turbosteamer concept, who converts both engine coolant and exhaust energy into engine mechanical power. The system adopts two-stage turbine machines, which is similar as large-scale stationary power generation system.

In 2008, Honda has reported the project exploring the application of steam Rankine cycle for engine exhaust heat recovery as illustrated in **Figure 2** [18]. The system adopts an axial piston swash plate type expander as the expansion machine under the controlled steam operational conditions ranging from 400 to 500°C at the pressure ranging from 7 to 9 MPa in order to optimize the Rankine cycle performance in engine transient driving conditions. The expander was directly connected to an electric generator producing electricity to recharge the battery pack. The maximum thermal efficiency of the system is 13% at 23 kW and the maximum power from the expander is 32 kW. Results are shown in 62 miles/h constant speed driving tests; the overall thermal efficiency can be improved by 3.8%. However, Honda announced the system will not be considered for production unless higher efficiencies can be achieved [18].

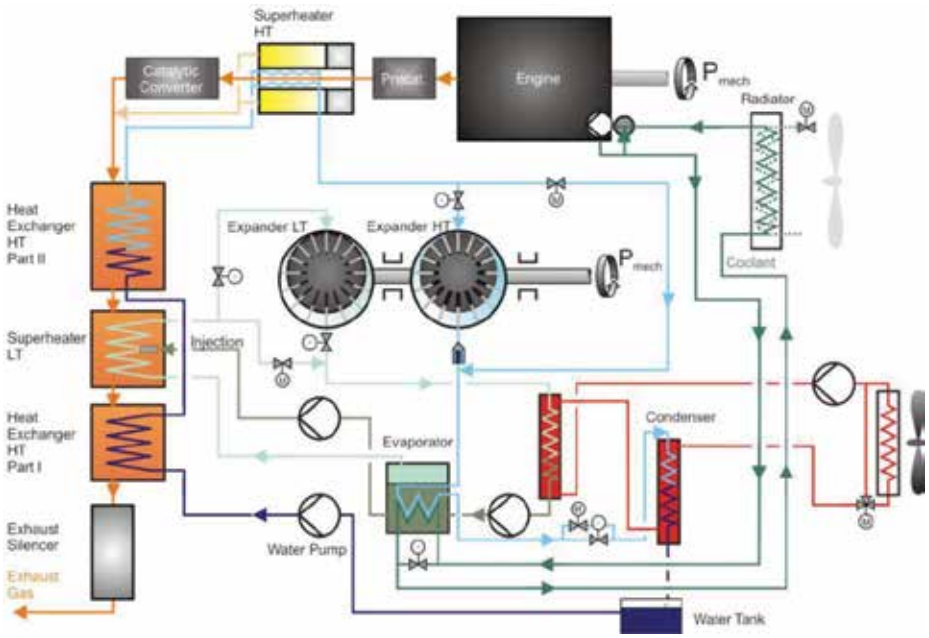

Figure 1. Schematic diagram of BMW-Turbosteamer concept [16].

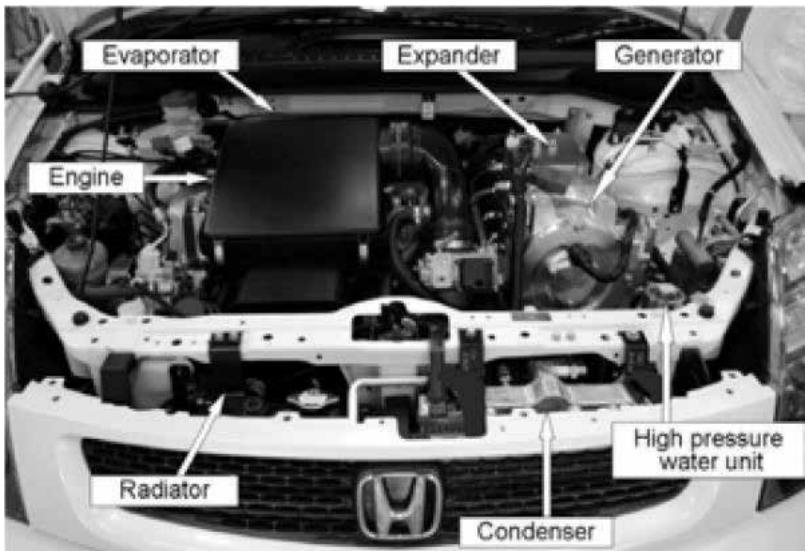

Figure 2. Layout of the Honda Rankine cycle prototype [18].

Cummins has conducted a project funded by U.S. Department of Energy to study an advanced engine waste heat recovery system using ORC technology since 2005 [19]. Cummins announced the developed ORC system can potentially improve the engine total efficiency by 5–8% [19]. The company further developed the waste heat recovery system and integrated with other advanced engine technologies aiming to boost the heavy-duty diesel engine to as high as 55% efficiency as reported in 2013 [20].

2. Organic Rankine cycle (OCR) for vehicle waste heat recovery (WHR)

2.1. Heat sources from ICEs

The designed temperature difference between evaporation and condensation temperature determines the overall efficiency of a typical ORC. For on-road vehicle application, the condensation temperature is controlled by the radiator and the capability of engine radiator determines the lowest condensation temperature. Therefore, the majority studies of Waste Heat Recovery (WHR) from ICE focus on the engine exhaust energy [21], because the exhaust temperature of ICE is various from 200 to 700°C, which is much higher than the coolant temperature ranging from 80 to 100°C [4, 5]. The other two heat sources are the charge air (50–70°C) and engine oil (80–120°C) [22]. The maximum ratio of utilization the fuel energy converting into engine brake power for propulsion is about 40–45%. The rest of fuel energy is dumped through engine exhaust, wasted because of friction losses and heat transfer loses. It is, therefore, necessary to study the heat sources from ICE to design and evaluate an ORC system for engine waste heat recovery.

The heat sources from the engine are usually calculated under engine steady state points from either experimental tests or simulation results. Although it is theoretically feasible and potentially worthwhile to recover the heat from charger air cooler and engine lube oil as reported in the literature [23], the practical applications of ORC system for engine waste heat recovery are mainly focusing on the exhaust energy and engine coolant energy. These two heat sources contain the majority of wasted heat energy from the engine. The maximizing utilization of these two heat sources can benefit for the overall vehicle thermal management and improve the cooling circuit impact.

Rather than the engine used in stationary power generation system, who usually operated under fixed rotational speed for an electrical generation [24], the engine used for vehicle application operates under variable speed and torque conditions. Therefore, the full engine operational map analysis method is popularly used to evaluate the heat sources from the engine for vehicle application. For example, Zhang et al. [25] used similar analysis methods and conducted the analysis of a 105 kW light-duty diesel engine. In order to conduct the parametric performance study of engine waste heat recovery system, the following four parameters are critical to being identified: the temperature and mass flow rate of exhaust and coolant energy under variable engine operational conditions. Another alternative method to evaluate the recoverable waste heat from the engine coolant and exhaust energy was introduced by Ringler et al. [17], who pointed out that the ratio of the recoverable heat from the coolant and exhaust energy of ICE ranges from 1.5 to 0.5. The results from the reported work also supported the conclusion [26–28]. Similar analysis method to evaluate the recoverable coolant and exhaust energy from a single cylinder engine was used and reported by Lu et al. as illustrated in **Figure 3** [30].

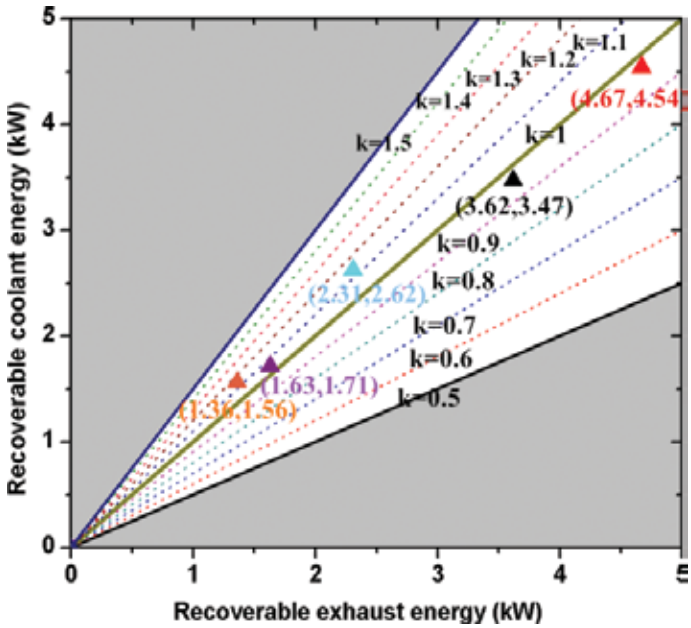

Figure 3. Recoverable coolant and exhaust energy from a single cylinder ICE [29].

2.2. Working principle of Rankine-based power generation systems

2.2.1. Rankine cycle

Steam Rankine cycle has been widely employed in large-scale power plants in the industry. This technology has been recognized as the most popular energy conversion systems, which mainly consists of four components, a pump, an evaporator, a turbine, and a condenser shown in **Figure 4**. The working principle of steam Rankine cycle can be described as follows. The liquid-phase water is first compressed to high-pressure state and flows into the evaporator, where the heat is provided from the heat sources to change the water from the liquid phase into the gas phase. The high-temperature and high-pressure steam then flow through an expansion machine where the power can be retrieved or converted into electricity. In the final step, the condenser rejects the heat from the expander steam and condenses the steam into the liquid phase.

Rankine cycle applies water as the working fluid, which has the advantages of high specific heat capacity, broad ranges of working conditions, non-toxic, and safe to use and environmentally friendly. However, steam Rankine system requires very high driven temperature in order to keep the steam in the gas phase at the exit of the expander. Because the exiting of liquid phase of fluid requires being prevented otherwise the blades of the turbine will be gradually damaged resulting in the reduction of lifetime and decrease of the expander efficiency [31].

2.2.2. Organic Rankine cycle (OCR)

As mentioned before, steam Rankine cycle requires very high heat source temperature. The Organic Rankine Cycles have been widely investigated since the 1880s. Instead of using water in Rankine cycle, the Organic Rankine Cycles employ organic working fluids such as refrigerants and hydrocarbons to recover the low-grade heat from biomass power plant, geothermal power and solar ponds [32]. The selection of working fluid plays a key role in ORC performance [33–36].

The working fluids used in Organic Rankine Cycle can be classified as wet, dry and isentropic types, who have different slopes of the vapor saturation curves in the *T-s* diagram as shown

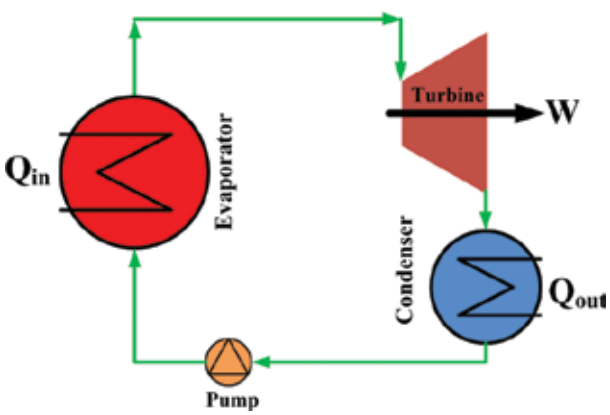

Figure 4. Schematic diagram of steam Rankine cycle.

http://dx.doi.org/10.5772/intechopen.78401

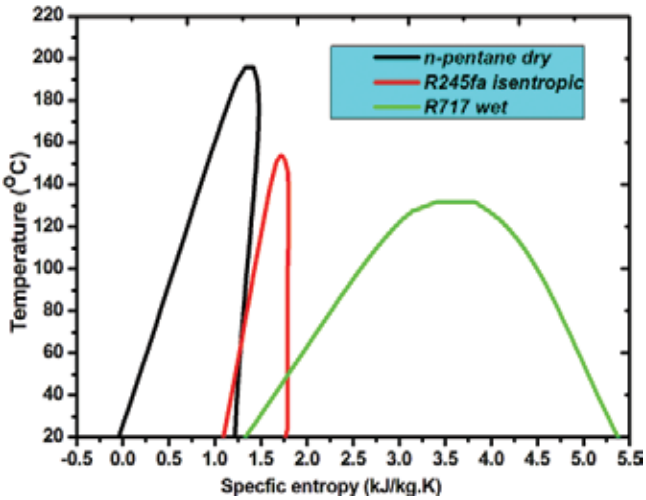

Figure 5. Three types of ORC working fluids: dry, isentropic, and wet.

in **Figure 5**. The wet fluids such as R717 have a negative slope of the vapor saturation curve. On the other hand, the dry fluids have a positive slope. The isentropic fluids have a vertical slope of the vapor saturation curve such as R134a.

A wrong choice of working fluid could lead to a low-efficient and expensive plant of ORC system. Tchanche et al. [37] assessed the thermodynamic and environmental properties of 20 different fluids for solar Organic Rankine Cycle by comparing the system efficiency, irreversibility, flow rate, pressure ratio, toxicity, flammability, ozone depletion potential (ODP), and global warming potential (GWP). The influence of fluid properties on an ORC and a supercritical Rankine cycle with 35 different working fluids was assessed by Chen et al. [36] considering the latent heat, density, specific heat, and the effectiveness of superheating. An exergy-based study of fluid selection for geothermal generated ORC system was conducted by Heberle et al. [38]. The exergy analysis indicated in a series circuit, working fluids with high critical temperatures such as isopentane are more favorable to be used. The working fluids with low critical temperatures, such as R227ea, are favored in parallel circuits and power generation under the heat source temperature below 450 K. The author investigated a small-scale solar-powered regenerative ORC system using six different refrigerants. The first and second law analysis suggested that R600 and R600a have the best performance under the temperature ranges from 70to 120°C [31]. Wang et al. [33] report a study to compare the performance of 10 kW net power output ORC system using different working fluids for engine exhaust heat recovery. Results indicate R11, R141b, R113, and R123 manifest slightly higher thermodynamic performances than other working fluids [33]. The system performance study of a geothermal ORC system using 31 pure working fluids has been conducted by Saleh et al. [34]. The maximum thermal efficiency is 0.13 with n-butane as working fluid under 120°C heat source temperature [34]. There is no working fluid can be recognized as the best to be used in any ORC systems. The section of optimal working fluid needs to consider the system thermodynamic performance, the economics of the system, designed system parameters such as maximum and minimum temperature and pressure conditions, environmental, and safety aspects.

2.3. Expander candidates

The expansion machines can be divided into two types: turbine machine using the kinetic energy of the working fluid to drive the expander and positive displace expander producing power by changing the volume of working chamber.

2.3.1. Turbines

Turbines have been widely applied as the expansion machine to replace the piston type of expander in steam Rankine cycle since the nineteenth century and have been acknowledged as the optimal expander for large-scale power plants. It consumes the internal energy of vapor into kinetic energy, which results the velocity of the flow are relatively high but the pressure and forces between the supply and exhaust point are rather small [39]. The mechanical power is then been obtained from the shaft of the turbine by turning the rotor blades when the high-velocity fluid passes through the turbine. There are mainly two types of turbines: axial flow turbines and radial flow turbines [40]. The axial flow turbines are driven by the flow in the parallel direction to the shaft, while the radial flow turbines are rotated by the flow traveling through the hub to the tipoff the turbine as indicated in **Figure 6**. However, the application of turbines for small-scale power generation system has not been widely accepted as the best expansion machine, especially in the power plants lower than 100 kW. Radial flow turbines are one of the exceptions, which have been recently used for small-scale application in Organic Rankine Cycle (ORC) [42–47]. Kang reports the design and experimental investigation of an ORC using R245fa as the working fluid and radial flow turbine as the expansion machine [42]. The radial turbine

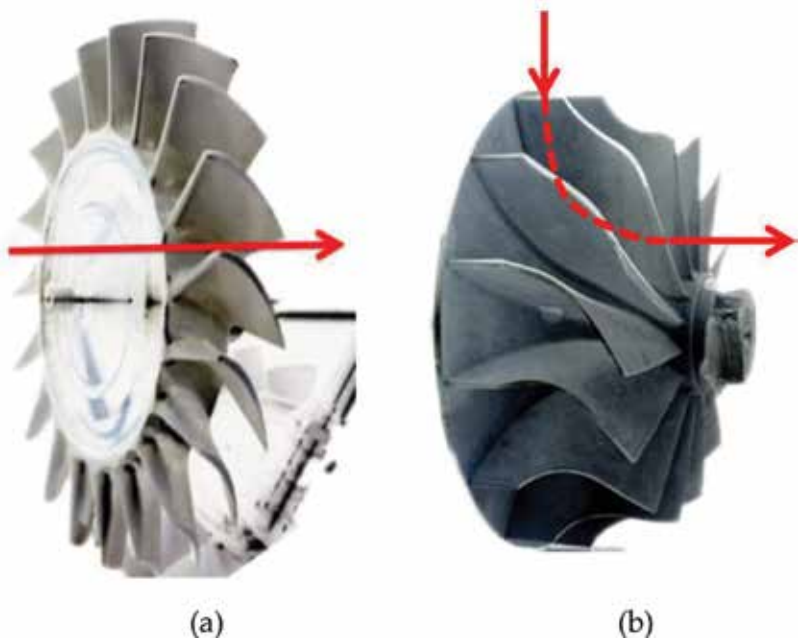

Figure 6. Working principle of turbine machines. (a) Axial flow turbine and (b) radial flow turbine [41].

was directly connected to a high-speed generator to produce electricity and results indicated the maximum cycle efficiency, the isentropic turbine efficiency, and electricity power obtained from the testing rig is 5.22%, 78.7%, and 32.7 kW, respectively [42]. Pei et al. [47, 48] carried out an experimental investigation on a 1–2 kW ORC system using a special designed and constructed radial flow turbine. The reported study achieves the isentropic efficiency of the radial flow turbine at 65–68% with the rotational speed around 20,000–40,000 using R123 as the organic working fluid in the ORC system [46, 47]. Compared with positive displacement expander, turbines are easier to be designed with relatively less required parts. A single stage turbine only requires two bearings to be mounted to the generator on the shaft. Furthermore, there is no contact seal existing in the turbines, which means no lubrication oil is necessary to be adapted to the system. The application of turbine for small-scale application is still not successful because the turbine is designed under rather low-expansion ratios and high-volume flows. The rotational speed of conventional turbines ranges from 10,000 to 100, 000 rpm because of the physical design of this type of expansion machine, which results to a limited or hard sourcing of proper generator for electricity production. One of the solutions to adapt the turbine machine directly with the generator is to use a high-speed generator, which will lead to high initial cost and increase the overall cost of electricity generation system. The other method to obtain the mechanical work from the turbine and convert it into electricity is by using gear. This method can effectively solve the high initial cost of the system but will require larger space for the turbine unit and reduce the efficiency of the turbine machine due to mechanical losses in the gear. Furthermore, the availability of small-scale turbine machine is still limited. The currently used radial flow turbines in small-scale power generation system are either from specially designed by the researcher or modified from a conventional turbine from an automotive turbocharger.

2.3.2. Positive displacement expanders

Different from the working principle turbine machines, positive displacement expanders use the expansion power by changing the volume inside the expansion chambers, which can also be named volumetric expanders. The most commonly used positive displacement expanders include piston type expander, screw expander, and scroll expander and vane expander. The positive displacement expanders can be classified into two types reciprocating piston expanders and rotary expanders. Screw expander, scroll expander, and vane expander are three main types of rotary expanders.

The piston type of machines attracts extensive intentions since it was invented and has been widely applied in different areas to meet various requirements such as the most commonly used as an Internal Combustion Engine. In the past 30 years, piston expander has been adopted and developed as the expander into steam Rankine system integrating with the internal combustion engine to recover the exhaust energy [4]. The piston type of expander can be designed and constructed with one valve version and two valve version in order to allow the expansion process starting and ending inside the piston volume chamber. The working principle of these two types of reciprocating piston expanders is illustrated in **Figure 7**. Piston type of expansion machine requires precisely controlled methods for the intake and exhaust valves, which will result to the requirement of a complex control system although this type of expander can potentially reach very high-expansion efficiency [50]. Moreover, piston

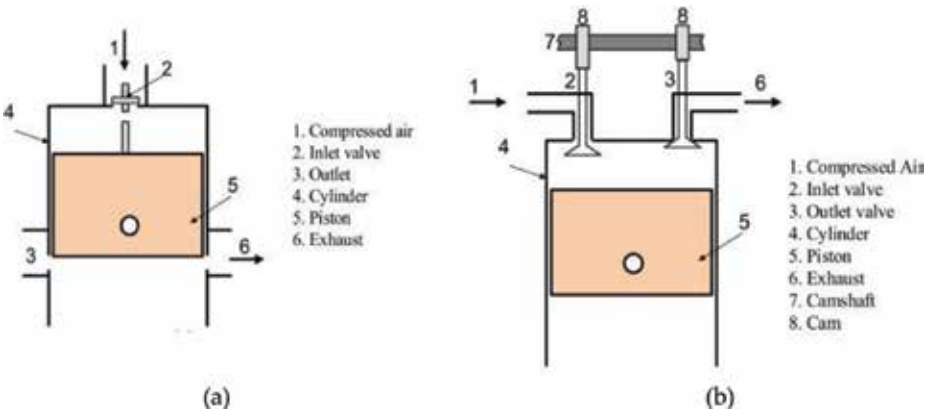

Figure 7. Working principle of reciprocating piston expander. (a) Single valve piston expander and (b) two valve piston expander [49].

expander requires a lot of bearings, a great number of moving parts, and balancing setting up, which results in a relatively complex and costly system.

Screw expander is composed of two meshing helical rotors a male and a female rotor, which requires at least four bearings for the two rotors as shown in **Figure 8**. This type of expansion machine has been widely applied in steam Rankine cycle plants for geothermal waste heat recovery system [52]. Lubrication oil is commonly used in the screw machine to seal the expanded working fluid inside the expansion chamber, which can effectively reduce the internal leakage losses during the expansion process. Screw expander has a relatively high rotational speed in positive displacement expanders and the rotation speed of this machine can reach as high as 6000 rpm [52]. The electricity production from screw expander, therefore, requires a specially designed high-speed generator or adding a gearbox to convert the mechanical power from the screw machine into electricity. This type of expansion devices has the advantages such as medium internal frictions, medium leakage losses, low vibration noise, wide ranges of power output, and long lifetime. The power produced from this expansion machine as reported by previous researchers ranging from 1.5 kW to 1 MW with the expansion ratio of 2–8 [53]. Leibowitz et al. developed an ORC power generation system using screw expander in a demonstration unit to cost-effectively recover the waste heat into power. Results indicated that screw expander is a good candidate expansion machine for the ORC system with the power output at 20 kW with installation cost in the range of $1500 –$2000/kWe [54]. However, there is

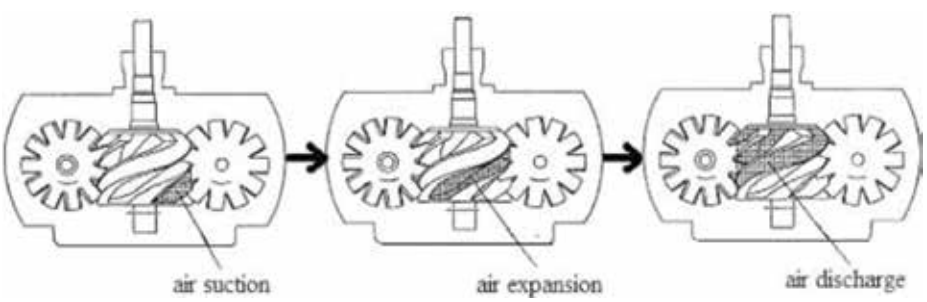

Figure 8. Working principle of screw expander [51].

no commercially available product under the power output lower than 10 kW from the market as reported by Ian et al. [55]. Because small size of screw expander needs extremely precise machining requirements to make the rotors and internal leakages of small size screw expander are relatively higher than that of the large-scale device [51, 56].

Scroll type of machine was first developed by a French inventor in 1905 and then the scroll machine starts to attract attention to be applied in Air condition system as a compressor to produce refrigeration since the mid of 1980s [57]. The most of the available scroll expanders from the market are modified from scroll compressor by swapping the inlet and outlet ports to change the device working mode from compressor to the expander. Scroll device is relatively simple equipment, which mainly includes two scrolls. The scroll expander has the advantages of little vibration, low-noise, a limited number of moving parts, broad availability, high-reliability and low initial cost [58, 59]. Scroll device has two scrolls and one of the scrolls is fixed on the shell, which is called situational scroll, while the other scroll orbiting eccentrically without rotating is named orbiting scroll. During the expansion process, high-pressure vapor enters and expands centrally of two scrolls pushing the orbiting scroll to start orbit as illustrated in **Figure 9**. The mechanical work can be continually obtained from the orbiting scroll through the shaft. Likewise the other positive displacement expanders, scroll expander has a fixed built-in expansion ratio. The optimal performance of scroll expander can be obtained when the specific volume ratio of the designed system equal to the built-in expansion ratio. Quoilin et al. pointed out the losses appearing when scroll type of expansion machine is working under and over expansion processes [9]. For example, 1 kW

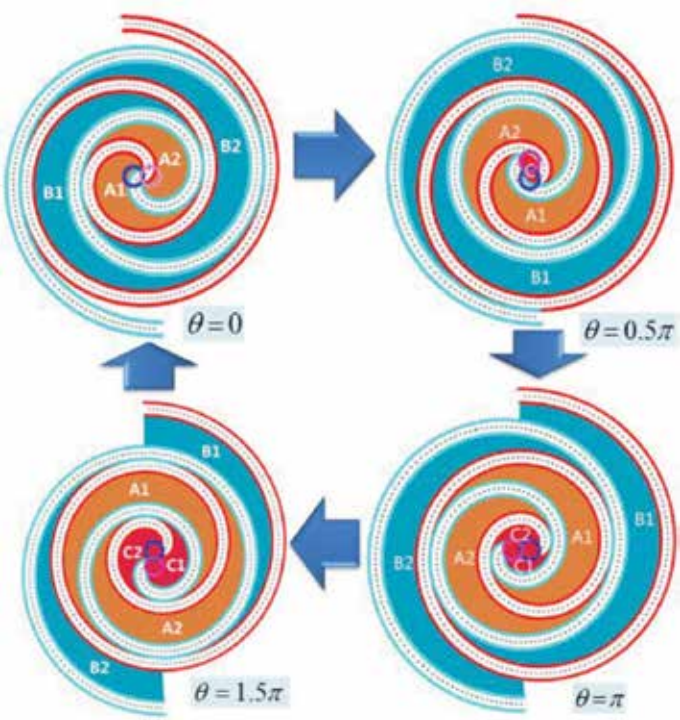

Figure 9. Expansion process of the scroll device under different crank angles [60].

oil-free scroll expander was used in an ORC system to recover the exhaust gas heat from a 30 kW gas turbine as reported by June et al. [61]. The ORC system used a zeotropic mixture with 48.5% R245fa and 51.5% R365mfc as the working fluid and the experimental results indicated the overall efficiency of the ORC system was about 3.9% [61]. The scroll expander was operated in the over-expansion region, which can therefore only achieve the efficiency of 28.4% under the tested condition. The overall ORC efficiency can be much higher than 3.9% if the expansion machine has been operated within the optimal conditions [61]. A prototype of ORC system using an open-drive oil-free scroll expander with R123 as the working fluid was experimentally investigated by Lemort et al. [62]. Results indicated the maximum isentropic efficiency of the scroll expander could be as high as 68% [62]. Muhammad et al. [63] reported the experimental study of a small-scale ORC system recovering the heat from hot steam. An oil-free scroll expander was used in the system to produce electrical power. Results show the maximum electrical power from the system was 1.016 kW when the system thermal efficiency was 5.64% and the isentropic efficiency of the expander was 58.3% [63]. During the experiment, the maximum ORC thermal efficiency was achieved at 5.75% and the scroll expander achieved the maximum isentropic efficiency as high as 77.74% [63]. A hermetic type refrigerant scroll compressor with built-in volume ratio at 3.24 was modified as an expander and used in an ORC system as reported by Yang et al. [64]. The experimental results indicated the maximum shaft power was 2.64 kW when the ORC thermal efficiency was 5.92% [64]. The majority of scroll expanders available from the market are modified from scroll compressors, which are not designed to be used for expansion applications. A separate lubrication system is normally required to lubricate the contact seals of two scrolls and reduce the radial leakage. The other function of the oil is to seal the working fluid inside the expansion chambers during the expansion process to prevent and reduce the flank leakage of the scroll type machine.

Vane expanders have the advantages of simple construction, easy manufacture, low-cost, self-start under load and smooth torque production [35, 65]. The expansion process happens between the cylinder wall and the sliding vanes. When the high-pressure working fluid flows into the inlet port and fills chamber A, the spinning power from the rotor can be gathered as illustrated in **Figure 10**. The pressure differences among the chambers resulted by expansion process driver the rotor. Qiu et al. [56, 66] investigated a vane expander in a biomass fire CHP system with ORC and achieved the isentropic efficiency of 54.5% at the speed of 824 RPM (mechanical work of 1.552 kW). The electricity generated by the vane expander was 792 W, which lighted seventeen 50 W bulbs. The efficiencies of several vane expanders using different working fluids at different working temperatures and pressures were summarized by Aoun [67]. Results showed that the maximum efficiency of 80% was achieved by a vane expander using R-11 at 800 RPM. The rotational speed of vane type of expanders is relatively lower than other expansion machines with commonly from 1500 to 3000 rpm, which can be directly installed to the generator without requiring of gear box [35]. However, the average isentropic efficiency of vane expanders is with the range of 15–55%, which is not that competitive compared with other volumetric expansion machines, as reported by Muhammad et al. [53]. Moreover, this type of expander requires a lubrication system to lubricate the contact surface of the rotor and vane. The existing of lubricate oil will contaminate the working fluid and flow back to the system.

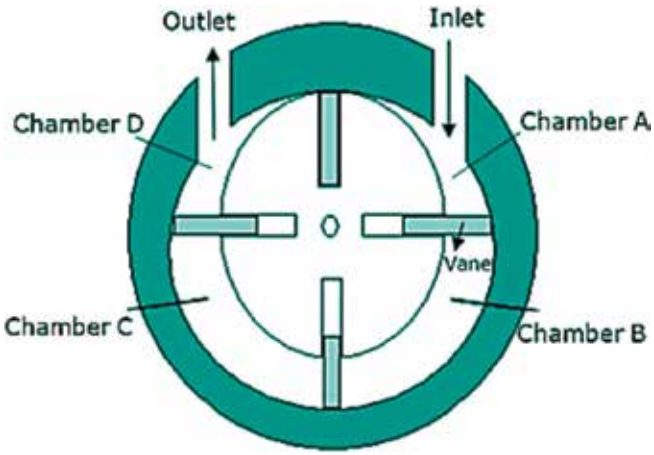

Figure 10. Working principle of vane-type expander [56].

2.4. Cycle investigations

Due to the limited space, the demand of high-power to weight ratio for ORC system and complicated control strategies for vehicle application, the ORC systems are still under technical development and testing stages. The current commercialization status of ORC technology for engine waste heat recovery is mainly for stationary power generation applications because of their desirable stable operating profiles [11]. A representative study on ORC system recovering exhaust energy from a stationary compressed natural gas (CNG) engine was reported by Song et al. [24]. The results showed the electric efficiency of the CNG engine could be potentially improved by a maximum 6.0% and the overall engine brake specific fuel consumption (BSFC) can be reduced by a maximum of 5.0% [24].

The two primary heat sources from ICE systems are engine cooling system and exhaust gases, which almost contain 60–70% of the fuel energy. Engine coolant energy is normally recognized as a heat source that is not worth to recover because the coolant temperature is about 80–100°C. However, the coolant energy contains about 30% of the fuel energy. The effective utilization of engine coolant energy for ORC waste heat recovery of the ICE could potentially improve the overall system efficiency and reduce the pay-back period of the overall cost with a properly designed system [9, 10]. A typical single-loop ORC system recovering both engine coolant and exhaust energy can be shown in **Figure 11**. A recuperator can be used to recover unused heat at the exit of expansion machine to preheat the working. The coolant energy can either be used as preheating source or main heat source for ORC systems. Only part of the coolant energy can be recovered if it was used as preheating source. For example, a study conducted by Yu et al. [69] investigated the potential of using engine coolant energy as ORC preheating source. The simulation results indicated there is around 75% exhaust heat and 9.5% coolant energy can be recovered from a diesel engine [69]. Tian et al. [70] deeply investigated the effects of fluids and parameters of the ORC system for engine exhaust heat recovery. The performance ORC system using 20 working fluids (boiling point range from −51.6 to 32.05°C) was studied to evaluate the

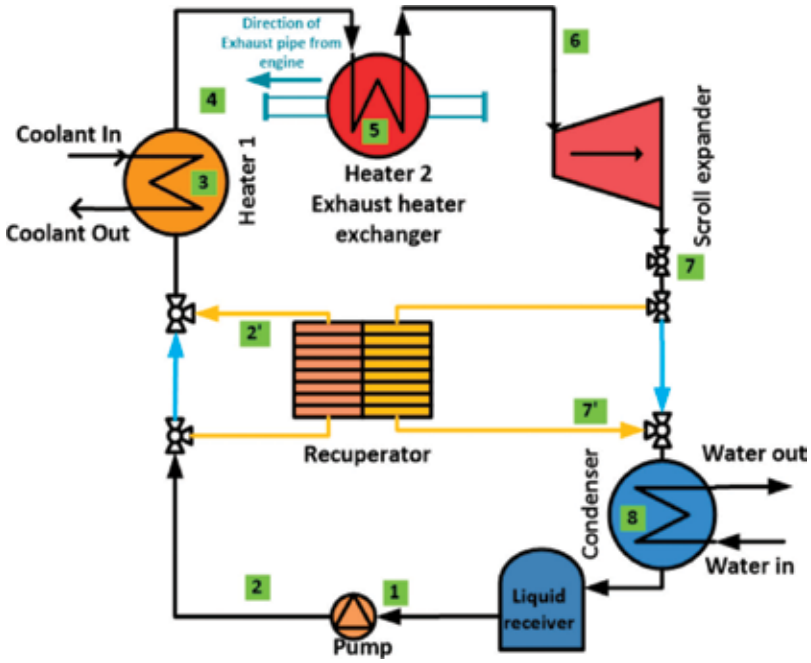

Figure 11. Single-loop ORC for engine coolant and exhaust recovery [68].

cycle parameters such as the overall thermal efficiency, expansion ratio, effective power output and electricity production cost [70]. R141b, R123, and R245fa were identified as the optimal working fluids. The highest thermal efficiency of these three working fluids ranges from 16.6% to 13.3% with the electricity production cost various from 0.30 to 0.35 €/kWh [70]. A simulation study of an ORC system for diesel engine exhaust heat recovery was reported by Zhao et al. [71]. Results indicated the BSFC reduction and the overall thermal efficiency of the engine integrated with ORC unit is 3.61 g/(kWh)–0.66% [71]. Shu et al. [72] recommended to use alkane-based working fluids for diesel engine exhaust heat recovery from the technical and economic point of view [72].

Another potential approach for engine coolant and exhaust recovery is using dual-loop ORC, which adopts two separately ORC systems to regenerate multi-heat sources from ICE [28, 73, 74]. The schematic system diagram and *T-s* diagram of dual loop ORC system can be found in **Figure 12**. Wang et al. [28, 73] conducted the study on a dual loop ORC to evaluate the performance of a gasoline engine and a light-duty diesel engine. The dual loop ORC system contains a high-temperature loop recovering engine exhaust heat and a low-temperature loop for coolant heat recovery. The proposed concept has the potential to comprehensively reuse all the recoverable heat from engine coolant and exhaust sources [73]. The investigations of using dual loop ORC system were also conducted on a selected gasoline engine and a diesel engine. For the selected gasoline engine, the results showed the dual loop ORC system can effectively improve the overall system efficiency by 3–6% throughout the engine operating region [73]. When the system was used on a light-duty diesel engine, the evaluation results indicated the thermal efficiency can be improved by 8% compared to that of the original engine [28]. At the engine rated power condition, the power output of the combined system can be improved by 26.63% [28]. Further study of the dual-loop ORC for engine coolant and exhaust recovery

http://dx.doi.org/10.5772/intechopen.78401

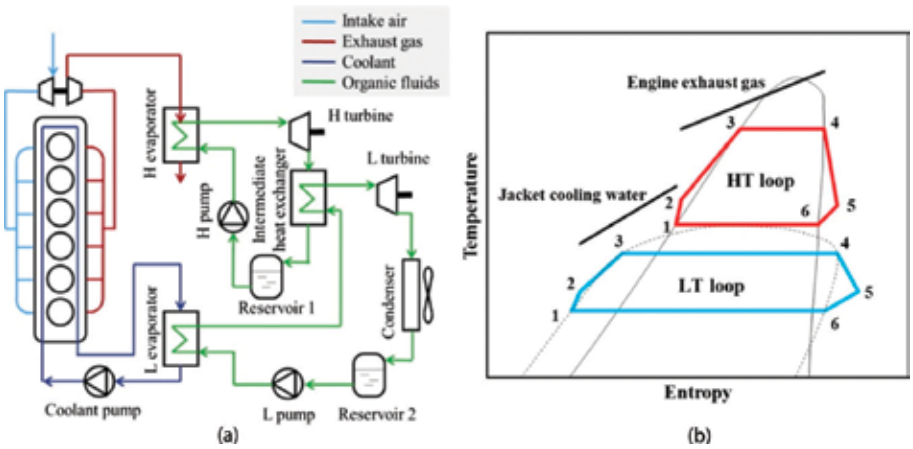

Figure 12. Dual-loop ORC system (a) schematic diagram and (b) *T-s* diagram [26, 75].

was reported by Shu et al. [74], who investigated the influence of using different working fluids. The high-temperature loop adopted water to recovery the exhaust energy and six working fluids have been selected for the low-temperature [74]. The dual-loop ORC system can achieve the maximum overall exergy efficiency as high as 55.05% using R1234yf as working fluid [74]. The dual-loop ORC requires two sets of ORC system components and advanced controlling strategies to balance the different heat sources, which will increase the capital cost of the system and result in high payback period.

2.5. Technical barriers

The power output from the ORC system can be either mechanical or electrical. As introduced in the previous section, the expansion machines can be divided into two types turbine machine using the kinetic energy of the working fluid to drive the expander and positively displace expander producing power by changing the volume of working chamber. When the mechanical configuration is used, the expander shaft is connected to the engine drive belt or a gear. Alternatively, an alternator is used to convert the mechanical work from the ORC expander to electricity. The generated electricity can be used to power the vehicle battery or supply auxiliary utilities. One of the main drawbacks of the solution is the efficiency of available vehicle alternators, which is around 50–60% [5, 9].

The designed evaporation and condensation temperature determines the overall efficiency of ORC system. A higher temperature difference between evaporation and condensation can result in a higher overall ORC efficiency. The engine front radiator is therefore required to reject high-load of heat in order to maintain the low condensation temperature. The limited space for vehicle application restricts the size of engine cooling system. An electrically driven cooling fan is generally not recommended to achieve low condensation temperature because it would sharply reduce the overall system performance.

Another main technical constraint is the dynamic/transient heat sources. In order to maintain the ORC system within the optimal operating region, the control of pump speed, and expander speed are required. Therefore, the complex control strategies are critical to being

developed or advanced ORC systems should be investigated. Using variable speed pump, adding control valves and integrating thermal energy storage system to manage fluctuation waste heat are some common strategies as reported by Manuel et al. [76].

3. Conclusions

Vehicle waste heat recovery technologies are currently under enormous interests for the purpose of reducing emissions and improving overall efficiency. Organic Rankine Cycle is one of the best solutions to recover engine waste heat into mechanical or electrical power. Key conclusions of this chapter can be summarized as follows.

It is critical to characterize the recoverable heat from the engine before designing the ORC system. A broad range of working fluids are available to be selected but there is no working fluid can be recognized as the best to be used in any ORC systems. A high-efficiency alternator to be coupled with ORC expander is in high-demand in order to promote the application of electrical version engine waste heat recovery system. For vehicle application, a compact system is desirable because of the limitation of space. A well-designed engine thermal management system should be considered. The transient heat source performance is the major technical obstacle to use ORC system for engine waste heat recovery and it can be expected either advanced control strategies or thermal energy storage technology should be used to solve the problem and promote the practical application of the ORC system for the vehicle.

Acknowledgements

The authors would like to thank the supports from EPSRC through (EP/P001173/1)-Centre for Energy Systems Integration, (EP/K503885/1) toward the project- Study of engine waste heat technologies, from NSFC-RS Joint Project under the grant number No. 5151101443 and IE/151256. The support from Cao Guang Biao High Tech Talent Fund, Zhejiang University is also highly acknowledged.

Author details

Yiji Lu[1,2]*, Anthony Paul Roskilly[1,2] and Xiaoli Yu[1]

*Address all correspondence to: luyiji0620@gmail.com

1 Department of Energy Engineering, Zhejiang University, Hangzhou, China

2 Sir Joseph Swan Centre for Energy Research, Newcastle University, Newcastle, United Kingdom

References

[1] Lu Y, Roskilly AP, Yu X, Jiang L, Chen L. Technical feasibility study of scroll-type rotary gasoline engine: A compact and efficient small-scale Humphrey cycle engine. Applied Energy. 2018;**221**:67-74

[2] Li Q, Liu J, Fu J, Zhou X, Liao C. Comparative study on the pumping losses between continuous variable valve lift (CVVL) engine and variable valve timing (VVT) engine. Applied Thermal Engineering. 2018;**137**:710-720

[3] Zhao J. Research and application of over-expansion cycle (Atkinson and Miller) engines—A review. Applied Energy. 2017;**185**:300-319

[4] Wang T, Zhang Y, Peng Z, Shu G. A review of researches on thermal exhaust heat recovery with Rankine cycle. Renewable and Sustainable Energy Reviews. 2011;**15**:2862-2871

[5] Sprouse C III, Depcik C. Review of organic Rankine cycles for internal combustion engine exhaust waste heat recovery. Applied Thermal Engineering. 2013;**51**:711-722

[6] Chen L, Zhang Z, Lu Y, Zhang C, Zhang X, Zhang C, et al. Experimental study of the gaseous and particulate matter emissions from a gas turbine combustor burning butyl butyrate and ethanol blends. Applied Energy. 2017;**195**:693-701

[7] Fang Y, Lu Y, Yu X, Roskilly AP. Experimental study of a pneumatic engine with heat supply to improve the overall performance. Applied Thermal Engineering. 2018;**134**:78-85

[8] Johnson TV. Reviewof vehicular emissions trends. SAE International Journal of Engines. 2015;**8**:1152-1167

[9] Quoilin S, Broek MVD, Declaye S, Dewallef P, Lemort V. Techno-economic survey of organic Rankine cycle (ORC) systems. Renewable and Sustainable Energy Reviews. 2013;**22**:168-186

[10] Vélez F, Segovia JJ, Martín MC, Antolín G, Chejne F, Quijano A. A technical, economical and market review of organic Rankine cycles for the conversion of low-grade heat for power generation. Renewable and Sustainable Energy Reviews. 2012;**16**:4175-4189

[11] Tchanche BF, Lambrinos G, Frangoudakis A, Papadakis G. Low-grade heat conversion into power using organic Rankine cycles—A review of various applications. Renewable and Sustainable Energy Reviews. 2011;**15**:3963-3979

[12] Patel PS, Doyle EF. Compounding the Truck Diesel Engine with an Organic Rankine-Cycle System: SAE Technical Paper; 1976

[13] Doyle E, DiNanno L, Kramer S. Installation of a diesel-organic Rankine compound engine in a class 8 truck for a single-vehicle test. SAE Technical Paper. 1979

[14] DiBella FA, DiNanno LR, Koplow MD. Laboratory and on-highway testing of diesel organic Rankine compound long-haul vehicle engine. SAE International. 1983

[15] Hanlon M. BMW unveils the turbosteamer concept. 2005

[16] Obieglo A, Ringler J, Seifert M, Hall W. Future efficient dynamics with heat recovery. In: Presentation at US Department of Energy Directions in Engine Efficiency and Emissions Research (DEER) Conference; Dearborn, Michigan. 2009

[17] Ringler J, Seifert M, Guyotot V, Hübner W. Rankine cycle for waste heat recovery of IC engines. SAE International Journal of Engines. 2009;**2**(1):67-76

[18] Rosebro J. Honda Researching Advanced Hybrid Drive with Rankine Cycle Co-Generation. GreenCar Congress. 2008

[19] Nelson C. Exhaust energy recovery. In: Diesel Engine-Efficiency and Emissions Research (DEER) Conference. Dearborn, MI. August 2008

[20] Koeberlein D. Cummins SuperTruck Program Technology and System Level Demonstration of Highly Efficient and Clean, Diesel Powered Class 8 Trucks. presentation at US Department of Energy Merit Review. 2013

[21] Liu JP, Fu JQ, Ren CQ, Wang LJ, Xu ZX, Deng BL. Comparison and analysis of engine exhaust gas energy recovery potential through various bottom cycles. Applied Thermal Engineering. 2013;**50**:1219-1234

[22] Lion S, Michos CN, Vlaskos I, Rouaud C, Taccani R. A review of waste heat recovery and organic Rankine cycles (ORC) in on-off highway vehicle heavy duty diesel engine applications. Renewable and Sustainable Energy Reviews. 2017;**79**:691-708

[23] Hountalas DT, Mavropoulos GC, Katsanos C, Knecht W. Improvement of bottoming cycle efficiency and heat rejection for HD truck applications by utilization of EGR and CAC heat. Energy Conversion and Management. 2012;**53**:19-32

[24] Song S, Zhang H, Lou Z, Yang F, Yang K, Wang H, et al. Performance analysis of exhaust waste heat recovery system for stationary CNG engine based on organic Rankine cycle. Applied Thermal Engineering. 2015;**76**:301-309

[25] Zhang HG, Wang EH, Fan BY. A performance analysis of a novel system of a dual loop bottoming organic Rankine cycle (ORC) with a light-duty diesel engine. Applied Energy. 2013;**102**:1504-1513

[26] Song J, C-w G. Parametric analysis of a dual loop organic Rankine cycle (ORC) system for engine waste heat recovery. Energy Conversion and Management. 2015;**105**: 995-1005

[27] Lu Y, Wang Y, Dong C, Wang L, Roskilly AP. Design and assessment on a novel integrated system for power and refrigeration using waste heat from diesel engine. Applied Thermal Engineering. 2015;**91**:591-599

[28] Wang EH, Zhang HG, Fan BY, Ouyang MG, Yang FY, Yang K, et al. Parametric analysis of a dual-loop ORC system for waste heat recovery of a diesel engine. Applied Thermal Engineering. 2014;**67**:168-178

[29] Lu Y, Roskilly AP, Smallbone A, Yu X, Wang Y. Design and parametric study of an organic Rankine cycle using a scroll expander for engine waste heat recovery. Energy Procedia. 2017;**105C**:1421-1426

[30] Lu Y, Roskilly AP, Yu X, Tang K, Jiang L, Smallbone A, et al. Parametric study for small scale engine coolant and exhaust heat recovery system using different organic Rankine cycle layouts. Applied Thermal Engineering. 2017;**127**:1252-1266

[31] Lu Y, Wang L, Tian G, Roskilly AP. Study on a Small Scale Solar Powered Organic Rankine Cycle Utilizing Scroll Expander. In: International Conference on Applied Energy; July 5-8, 2012; Suzhou, China

[32] Hung TC, Shai TY, Wang SK. A review of organic rankine cycles (ORCs) for the recovery of low-grade waste heat. Energy. 1997;**22**:661-667

[33] Wang EH, Zhang HG, Fan BY, Ouyang MG, Zhao Y, Mu QH. Study of working fluid selection of organic Rankine cycle (ORC) for engine waste heat recovery. Energy. 2011;**36**:3406-3418

[34] Saleh B, Koglbauer G, Wendland M, Fischer J. Working fluids for low-temperature organic Rankine cycles. Energy. 2007;**32**:1210-1221

[35] Bao J, Zhao L. A review of working fluid and expander selections for organic Rankine cycle. Renewable and Sustainable Energy Reviews. 2013;**24**:325-342

[36] Chen H, Goswami DY, Stefanakos EK. A review of thermodynamic cycles and working fluids for the conversion of low-grade heat. Renewable and Sustainable Energy Reviews. 2010;**14**:3059-3067

[37] Tchanche BF, Papadakis G, Lambrinos G, Frangoudakis A. Fluid selection for a low-temperature solar organic Rankine cycle. Applied Thermal Engineering. 2009;**29**:2468-2476

[38] Heberle F, Brüggemann D. Exergy based fluid selection for a geothermal organic Rankine cycle for combined heat and power generation. Applied Thermal Engineering. 2010;**30**:1326-1332

[39] Weiß AP. Volumetric expander versus turbine-which is the better choice for small ORC plants? In: 3rd International Seminar on ORC Power Systems; Brussels, Belgium. 2015

[40] Barber-nichols. Turbines. Available from: http://www.barber-nichols.com/products/turbines [Accessed: 26-08-2012]

[41] Technology B. Microturbines and Micro Gas Turbines. Available from: http://wwwgas-turbineworldcouk/microturbineguidehtml [Accessed: 02-05-2018]

[42] Kang SH. Design and experimental study of ORC (organic Rankine cycle) and radial turbine using R245fa working fluid. Energy. 2012;**41**:514-524

[43] Yamamoto T, Furuhata T, Arai N, Mori K. Design and testing of the organic Rankine cycle. Energy. 2001;**26**:239-251

[44] Nguyen VM, Doherty PS, Riffat SB. Development of a prototype low-temperature Rankine cycle electricity generation system. Applied Thermal Engineering. 2001;**21**:169-181

[45] Yagoub W, Doherty P, Riffat SB. Solar energy-gas driven micro-CHP system for an office building. Applied Thermal Engineering. 2006;**26**:1604-1610

[46] Pei G, Li J, Li Y, Wang D, Ji J. Construction and dynamic test of a small-scale organic rankine cycle. Energy. 2011;**36**:3215-3223

[47] Li J, Pei G, Li Y, Wang D, Ji J. Energetic and exergetic investigation of an organic Rankine cycle at different heat source temperatures. Energy. 2012;**38**:85-95

[48] Pei G, Li YZ, Li j, Ji J. A High-Speed Micro Turbine for Organic Rankine Cycle. World Society of Sustainable Energy Technologies (WSSET)-Newsletter. 2009

[49] Zhang X, Xu Y, Xu J, Xue H, Chen H. Study of a single-valve reciprocating expander. Journal of the Energy Institute. 2016;**89**(3):400-413

[50] Zhang B, Peng X, He Z, Xing Z, Shu P. Development of a double acting free piston expander for power recovery in transcritical CO2 cycle. Applied Thermal Engineering. 2007;**27**:1629-1636

[51] Xia G-D, Zhang Y-Q, Wu Y-T, Ma C-F, Ji W-N, Liu S-W, et al. Experimental study on the performance of single-screw expander with different inlet vapor dryness. Applied Thermal Engineering. 2015;**87**:34-40

[52] Tang H, Wu H, Wang X, Xing Z. Performance study of a twin-screw expander used in a geothermal organic Rankine cycle power generator. Energy. 2015;**90**(Part 1):631-642

[53] Imran M, Usman M, Park B-S, Lee D-H. Volumetric expanders for low grade heat and waste heat recovery applications. Renewable and Sustainable Energy Reviews. 2016;**57**:1090-1109

[54] Leibowitz H, Smith K, Stosic N. Cost effective small scale ORC systems for power recovery from low grade heat sources. In: ASME 2006 International Mechanical Engineering Congress and Exposition. American Society of Mechanical Engineer. Chicago, Illinois, USA. 2006:521-527

[55] Smith IK, Stosic N, Kovacevic A. Screw expanders increase output and decrease the cost of geothermal binary power plant systems. In: Transactions of Geothermal Resource Council. Reno, NV; 2005

[56] Qiu G, Liu H, Riffat S. Expanders for micro-CHP systems with organic Rankine cycle. Applied Thermal Engineering. 2011;**31**:3301-3307

[57] Carrier Corporation Syracuse NY. Scroll compressor, High efficiency compression for commercial and industrial applications. October 2004

[58] Scroll-compressor. Available from: http://en.wikipedia.org/wiki/Scroll_compressor [Accessed: 20-11-2011]

[59] Guangbin L, Yuanyang Z, Liansheng L, Pengcheng S. Simulation and experiment research on wide ranging working process of scroll expander driven by compressed air. Applied Thermal Engineering. 2010;**30**:2073-2079

[60] Lu Y, Roskilly AP, Tang K, Wang Y, Jiang L, Yuan Y, et al. Investigation and performance study of a dual-source chemisorption power generation cycle using scroll expander. Applied Energy. 2017;**204**:979-993

[61] Jung H-C, Taylor L, Krumdieck S. An experimental and modelling study of a 1kW organic Rankine cycle unit with mixture working fluid. Energy. 2015;**81**:601-614

[62] Lemort V, Quoilin S, Cuevas C, Lebrun J. Testing and modeling a scroll expander integrated into an organic Rankine cycle. Applied Thermal Engineering. 2009;**29**:3094-3102

[63] Muhammad U, Imran M, Lee DH, PBS. Design and experimental investigation of a 1 kW organic Rankine cycle system using R245fa as working fluid for low-grade waste heat recovery from steam. Energy Conversion and Management. 2015;**103**:1089-1100

[64] Yang S-C, Hung T-C, Feng Y-Q, Wu C-J, Wong K-W, Huang K-C. Experimental investigation on a 3 kW organic Rankine cycle for low-grade waste heat under different operation parameters. Applied Thermal Engineering. 2017;**113**:756-764

[65] Yang B, Peng X, He Z, Guo B, Xing Z. Experimental investigation on the internal working process of a CO2 rotary vane expander. Applied Thermal Engineering. 2009;**29**:2289-2296

[66] Qiu G, Shao Y, Li J, Liu H, Riffat SB. Experimental investigation of a biomass-fired ORC-based micro-CHP for domestic applications. Fuel. 2012;**96**:374-382

[67] Aoun B. Micro combined heat and power operating on renewable energy for residential building, [PhD thesis], https://pastel.archives-ouvertes.fr/pastel-00005092. École Nationale Supérieure des Mines de Paris. 2008

[68] Lu Y, Roskilly AP, Jiang L, Chen L, Yu X. Analysis of a 1 kW organic Rankine cycle using a scroll expander for engine coolant and exhaust heat recovery. Frontiers in Energy. 2017;**11**:527-534

[69] Yu G, Shu G, Tian H, Wei H, Liu L. Simulation and thermodynamic analysis of a bottoming organic Rankine cycle(ORC) of diesel engine (DE). Energy. 2013;**51**:281-290

[70] Tian H, Shu G, Wei H, Liang X, Liu L. Fluids and parameters optimization for the organic Rankine cycles (ORCs) used inexhaust heat recovery of internal combustion engine (ICE). Energy. 2012;**47**:125-136

[71] Zhao M, Wei M, Song P, Liu Z, Tian G. Performance evaluation of a diesel engine integrated with ORC system. Applied Thermal Engineering. 2017;**115**:221-228

[72] Shu G, Li X, Tian H, Liang X, Wei H, Wang X. Alkanes as working fluids for high-temperature exhaust heat recovery of diesel engine using organic Rankine cycle. Applied Energy. 2014;**119**:204-217

[73] Wang EH, Zhang HG, Zhao Y, Fan BY, Wu YT, Mu QH. Performance analysis of a novel system combining a dual loop organic Rankine cycle (ORC) with a gasoline engine. Energy. 2012;**43**:385-395

[74] Shu G, Liu L, Tian H, Wei H, Yu G. Parametric and working fluid analysis of a dual-loop organic Rankine cycle (DORC) used in engine waste heat recovery. Applied Energy. 2014;**113**:1188-1198

[75] Chen T, Zhuge W, Zhang Y, Zhang L. A novel cascade organic Rankine cycle (ORC) system for waste heat recovery of truck diesel engines. Energy Conversion and Management. 2017;**138**:210-223

[76] Jiménez-Arreola M, Pili R, Dal Magro F, Wieland C, Rajoo S, Romagnoli A. Thermal power fluctuations in waste heat to power systems: An overview on the challenges and current solutions. Applied Thermal Engineering. 2018;**134**:576-584

Chapter 8

Organic Rankine Cycle for Recovery of Liquefied Natural Gas (LNG) Cold Energy

Junjiang Bao

Additional information is available at the end of the chapter

http://dx.doi.org/10.5772/intechopen.77990

Abstract

Natural gas (NG) is an environment-friendly energy source. NG is of gas state in the environmental condition and it is liquefied to LNG at temperature of about −162°C for transportation and storage. Electric energy of 292–958 kWh is consumed when one ton of LNG is produced. Before being used, LNG must be regasified to NG again at the receiving site, and this process will release a great deal of energy, which is called cold energy. It's very important to recovery LNG cold energy, which is clean and of high quality. Power generation is a conventional and effective way to utilize LNG cold energy. For the low efficiency of the traditional power generation system with liquefied natural gas (LNG) cold energy utilization, by improving the heat transfer characteristic between the working fluid and LNG, this chapter has proposed a conception of multi-stage condensation Rankine cycle system. Furthermore, the performance of power generation systems will be enhanced with two aspects: improvement of system configuration and optimization of working fluids.

Keywords: organic Rankine cycle, LNG cold energy, two-stage condensation Rankine cycle, zeotropic mixture, system configuration

1. Introduction

Energy shortage and environmental pollution are two major themes in today's world [1]. More and more attentions are paid to Natural gas (NG) because it is clean and has high calorific value [2, 3], and it is widely consumed all over the world [4]. NG is of gas state in the environmental condition and it is liquefied to LNG at temperature of about −162°C for transportation and storage [5]. Electric energy of 292–958 kWh is consumed when one ton of LNG

is produced [6]. Before being used, LNG must be regasified to NG again at the receiving site, and this process will release a great deal of energy, which is called cold energy [7]. It is very important to recovery LNG cold energy which is clean and of high quality. Usually LNG is heated by sea water or air, so that LNG cold energy is wasted and the sea near the regasification site also is affected [8]. Therefore, the recovery of the LNG cold energy a dual purpose [8].

One of effective ways to utilize LNG cold energy is power generation [9]. The traditional cycles include direct expansion cycle (DE), organic Rankine cycle (ORC) and combined cycle (CC) [10]. Although the simplicity for direct expansion cycle, it has limited applications with low efficiency and high operation pressure. Organic Rankine cycle and combined cycle are more popular and relatively mature. Osaka Gas Company in Japan built ORC and CC system using propane in 1979 and 1982, and the power output reached 1450 and 6000 kW, respectively [11]. Due to the importance of system parameters on the performance of power generation system, many researches are carried out. With seawater as heat source and LNG as heat sink, Kim et al. [12] found that there is an optimum condenser outlet temperature for ORC system. Heat source inlet temperature, evaporation pressure and condensation temperature are studied by Wang et al. [13] to achieve high exergy efficiency of ORC recovering LNG cold energy. With the heat integration of LNG at vaporization pressure of 70 bar, Koku et al. [14] obtained a thermal efficiency of 6% for the combined cycle with propane as working fluid.

Improvement of system structure and proper working fluid selection are two effective way to enhance the system performance. For system structure, the combinations of simple Rankine cycle in series or parallel is often considered by Zhang et al. [7] and García et al. [15] and they found that they were indeed more efficient. Cascaded Rankine cycles are also common improvement and are proved to be superior to simple Rankine cycles by Li et al. [16], Choi et al. [17], Cao et al. [18], and Wang et al. [19]. By combining the Rankine cycle and refrigeration cycle, the study of Zhang et al. [20] showed that both electricity and refrigeration can be produced simultaneously. Mosaffa et al. [21] compared four different cycles, and pointed out that different system structure is best when the objective function changes.

Selection of working fluids is also critical for the performance and economy of system except for cycle structure. By using eight kinds of working fluids, Zhang et al. [7] found n-pentane has the best system performance. A comparative study by Sung et al. [22] showed that R123 were the optimal working fluids for a dual-loop cycle with LNG cold energy as heat sink. Considering ethane, ethene, carbon dioxide, R134a, R143a and propene, Ferreira et al. [23] concluded that ethene and ethane had higher system efficiency. Zeotropic mixtures are also considered in power generation system for recovery of LNG cold energy. Ammonia-water mixture is used by Wang et al. [24], and they found there was an optimal mass fraction at which work output was largest. With R601-R23-R14 ternary mixture as the working fluid, Lee et al. [25] found that the exergy loss of ORC using mixture is lower than that of pure fluids. Kim et al. [26] selected R14-propane mixture as the working fluids for the first stage of a cascaded system and ethane-n-pentane mixture for the other two stages. Modi and Haglind [27] thought that zeotropic mixture is the development direction of working fluids with its higher thermodynamic performance.

In this chapter, the performance of power generation systems by LNG cold energy will be enhanced with two aspects: improvement of system configuration and optimization of working fluids. Firstly, the two-stage condensation Rankine cycle is introduced. Based on this, the effect of stage number of condensation process is discussed. Then, the influence of the arrangements for compression process and expansion process is studied. Regarding to the optimization of working fluids, pure working fluids are firstly compared, and then zeotropic mixtures are optimized. Finally, a simultaneous approach to optimize the component and composition of zeotropic mixture is put forward.

2. Improvement of system configuration

2.1. Two-stage condensation Rankine cycle (TCRC)

As shown in **Figure 1**, the TCRC system consists of an evaporator, two turbines, two condensers, a mixer, a splitter and two feed pumps. After heated in the evaporator by sea water, working fluid is evaporated to vapor and is divided into two streams in the splitter. The two streams flow into different turbines respectively and are expanded to two different condensation pressures. These two streams transferred heat energy to LNG in two different condensers and cooled to liquid. The two streams are pressurized by two different pumps and mixed in the mixer. The converged stream enters the evaporator again and the new cycle recommences. Except for absorbing the condensation heat from working fluids in two condensers, LNG is further heated to the scheduled temperature in the reheater with sea water. T-s diagram of the TCRC system is plotted in **Figure 2**, and the labeled state points in **Figure 2** is the same as that in **Figure 1**.

In order to determine whether the new proposed cycle has a better performance, the novel system is compared with the conventional methods under the same conditions.

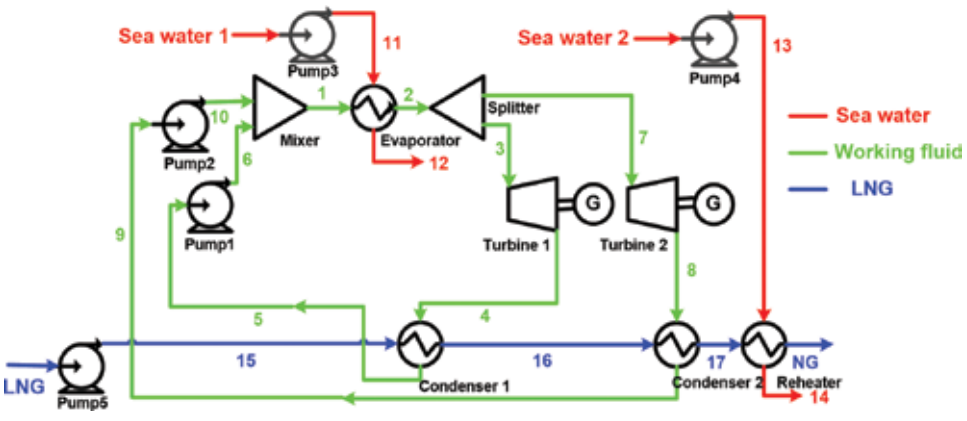

Figure 1. Schematic diagram of the TCRC system.

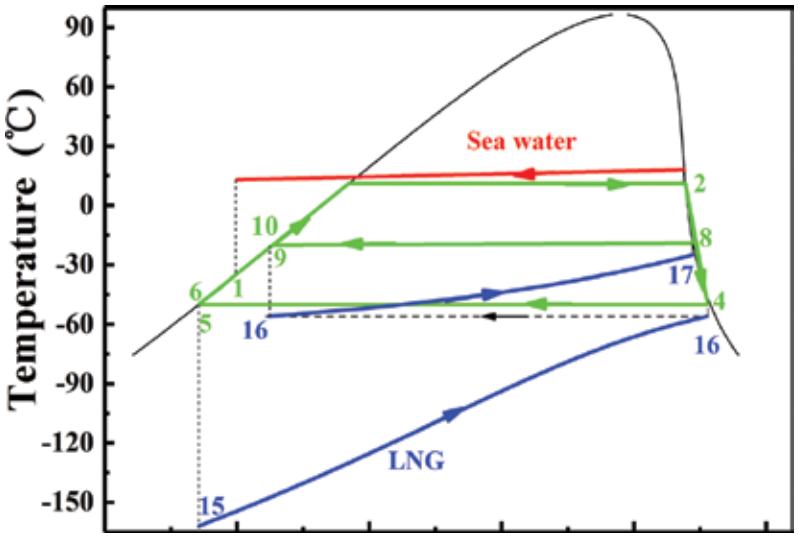

Figure 2. T-s diagram of the TCRC system.

Net power output, thermal efficiency and exergy efficiency of TCRC system is compared with the traditional cycles (DEC, ORC and CC), as shown in **Figure 3**. It should be pointed out that four systems all used propane as working fluid. From **Figure 3**, it can be found that the performance of proposed system is remarkably superior to the traditional power generation cycles. Combined cycle has the highest net power output, thermal efficiency and exergy efficiency among the traditional systems. However, compared with CC system, TCRC system has a 45.27%, 42.91% and 52.31% increase respectively, in term of net power output, thermal efficiency and exergy efficiency.

In order to explain the reason why TCRC system could have a better performance than the traditional cycle, the heat transfer curves between working fluid and LNG of ORC and TCRC systems are plotted in **Figure 4**. It can be seen from **Figure 4** that heat transfer irreversibility of ORC system is larger than that of TCRC system. The main reason is that compared with ORC system, the condensation process of TCRC system is two-stage, which could lower the heat transfer irreversibility of the condenser.

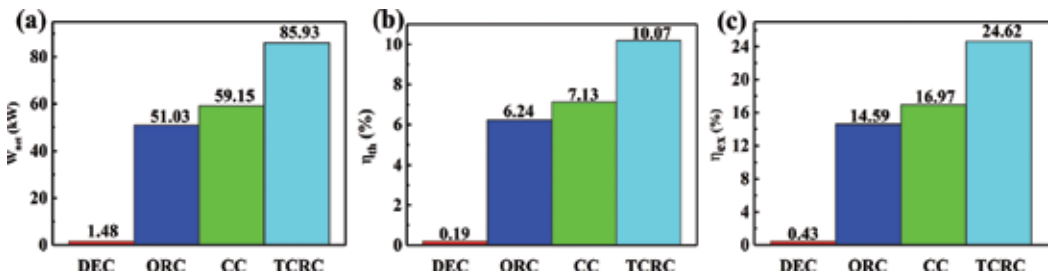

Figure 3. System performance of the four power generation methods: (a) net power output, (b) thermal efficiency, and (c) exergy efficiency.

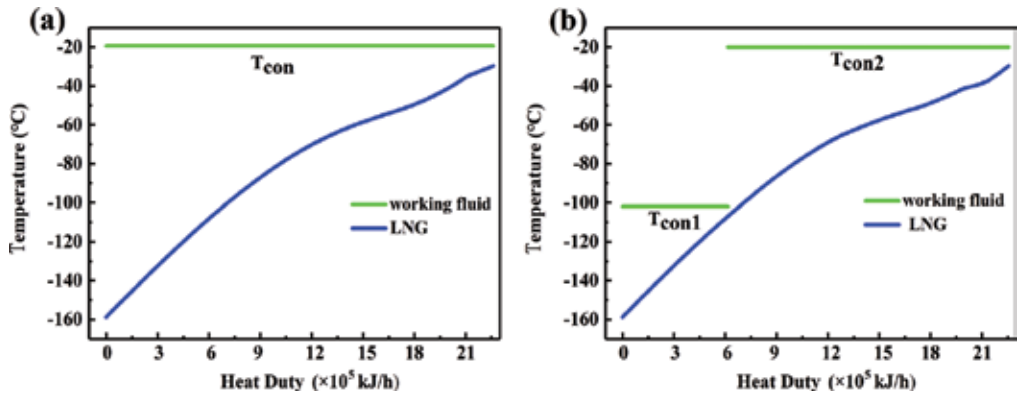

Figure 4. Heat transfer characteristics between working fluid and LNG: (a) ORC and (b) TCRC.

2.2. Effects of stage number of condensation process

In the previous section, it has been proved that two-stage condensation process has the potential to improve the performance of power generation systems by LNG cold energy. If the number of condensation stage is increased, the performance of power generation systems should be better at the cost of greater initial investment with more equipment. How many stages of condensation process should be chosen?

Figure 5 shows the schematic of six different cycles from single-stage to three-stage condensation Rankine cycle with or without direction expansion. To take a comparison object, direction expansion cycle (DC) is also considered.

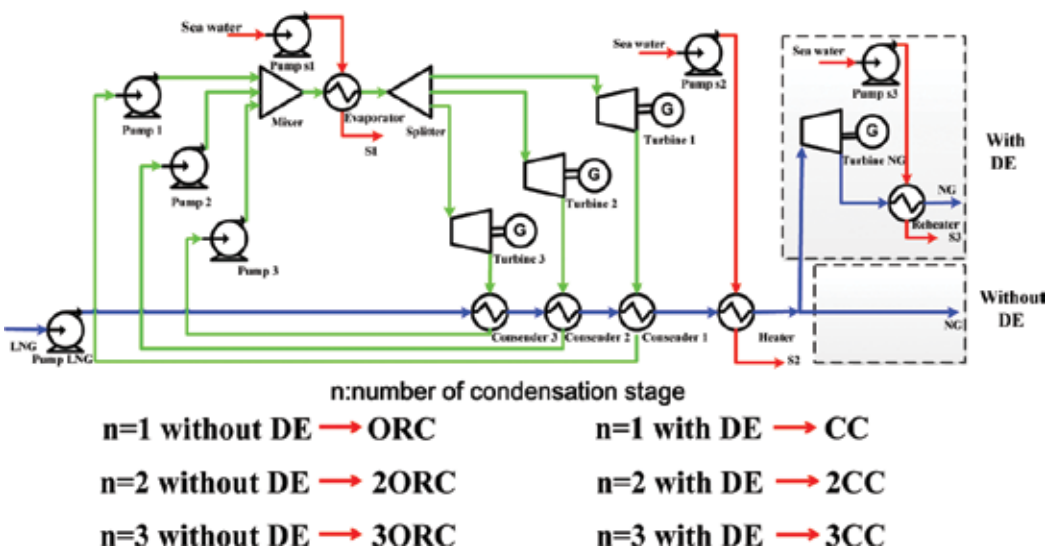

Figure 5. Schematic of single-stage, two-stage and three-stage condensation Rankine cycles with or without direction expansion.

Net power output of system:

$$W_{net} = \sum W_{tur,j} - \sum W_{p,l} \tag{1}$$

The electricity production cost (EPC) can be expressed as:

$$EPC = \frac{3600\, C_{total}}{W_{net}} \tag{2}$$

The annual total net income (ATNI) of the system can be defined as:

$$ATNI = 7300(EP - EPC)\, W_{net} \tag{3}$$

where EP is electricity price.

From **Figure 6** it can be seen that the net power output of the 3CC is the largest and the DE is the least at any LNG vaporization pressure. When stage number of condensation process increases, the net power output of Rankine cycles and combined cycles both increases. The performance of combined cycles is better than that of Rankine cycles at the same stage number of condensation process.

Figure 7 shows the minimum EPC of seven different cycles at different LNG vaporization pressures. The EPC of the Rankine cycle is larger than that of the combined system at the same stage number of condensation process. The EPC of combined cycle is the least at the LNG vaporization pressure less than 30 bar. With the increase of the stage number of condensation process, EPC of combined cycles and Rankine cycles augments, but its increase rate decreases. When the LNG vaporization pressure increases, the difference of EPC between combined cycles and Rankine cycles at the same stage number of condensation process tends to zero.

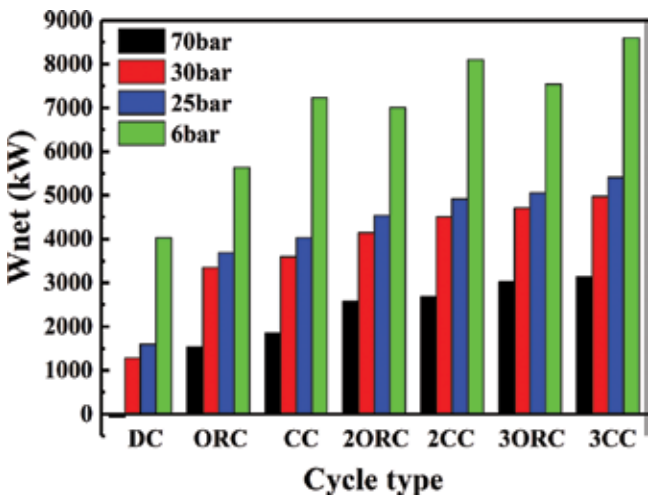

Figure 6. The maximum net power output at different LNG vaporization pressures.

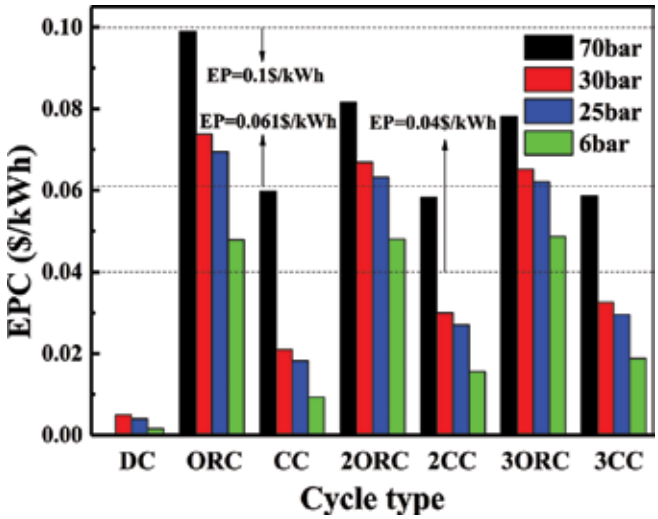

Figure 7. The minimum EPC of seven systems at different LNG vapor pressures.

The electricity prices of literatures are different, such as 0.04, 0.061, 0.1, 0.123 and 0.18$/kWh [28]. DC and CC systems should be selected at the LNG vaporization pressure less than 30 bar if the electricity price is 0.04$/kWh. No system is profitable at the LNG vaporization pressure of 70 bar. The CC systems are suitable at all the LNG vaporization pressure when the electricity price is 0.061$/kWh. At the LNG vaporization pressure less than 30 bar, it should be considered DE system. Seven cycles could be profitable if electricity price is larger than 0.1$/kWh.

The capacity of power generation can be weight by net power output, and whether cycle is profitable could evaluated by EPC. But the maximum profitability of the system is determined by both the net power output and EPC, which be reflected by annual net income. The electricity price of 0.123 $/kWh is taken as the referenced electricity price. It can be seen from **Figure 8** that the annual net income of the 3CC system is largest, while the least is the DC cycle. The annual net income of the Rankine cycles is lower than that of the combined cycles at the same stage number of the condensation process. When the stage number of the condensation process increases, both the annual net income of the Rankine cycle and the combined cycle systems goes up, but their increase rates decrease.

2.3. Influence of the arrangements for compression process and expansion process

In the field of utilizing LNG cold energy by ORC (organic Rankine cycle), most studies focus on how to reduce the irreversible loss of the heat exchange process but pay little attention to the arrangements for compression and expansion process. The compression and expansion process, as the parts of the cycle that consumes and products energy, affect the cycle performance as well due to that their different arrangements make the efficiency of the component different.

The structures of four different two-stage condensation Rankine cycles are shown in **Figure 9**. There are two types of arrangements for the pumps in the compression process.

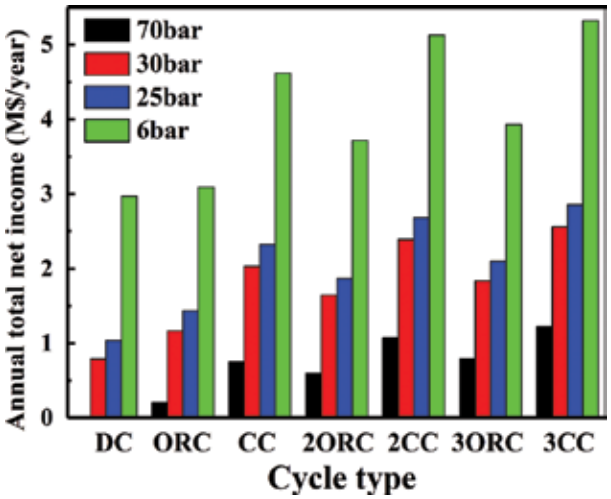

Figure 8. The maximized annual net income of seven cycles at different LNG vapor pressures.

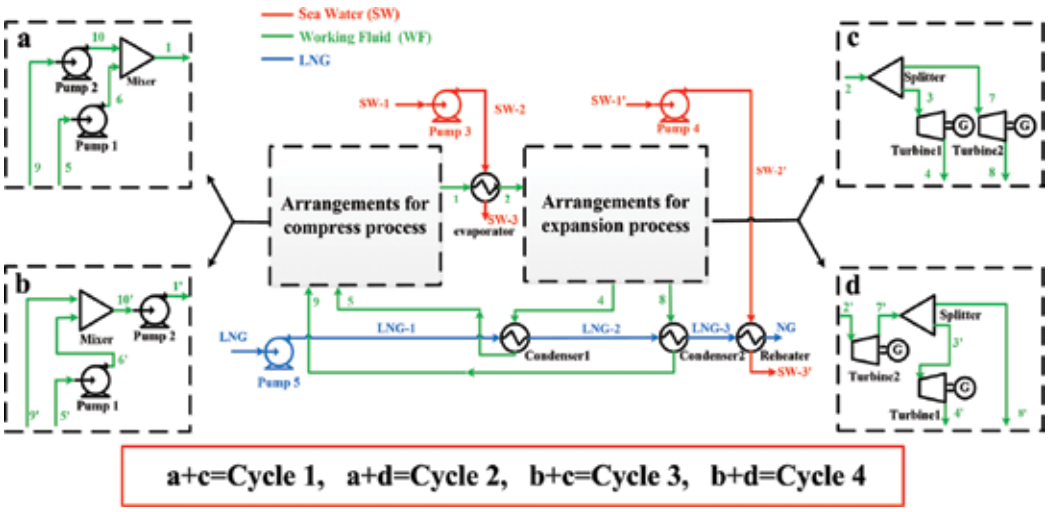

Figure 9. The configurations of four different two-stage condensation Rankine cycles.

The arrangement a shown in **Figure 9** is called parallel compression arrangement. The other arrangement b shown in **Figure 9** is called series compression arrangement. Similarly, there are also two types of arrangements for the turbines in the expansion process. The arrangement c shown in **Figure 9** is called parallel expansion arrangement. The arrangement d shown in **Figure 9** is called series expansion arrangement.

This paper takes 80% as the reference efficiency when the turbine efficiency is constant. When the turbine efficiency is non-constant, this paper adopted the turbine efficiency prediction model with the turbine size parameter (SP) and the specific volume (Vr) as the input parameters, as is shown in Eq. (4).

$$\eta_{turb,is} = \sum_{n=0}^{15} F_n A_n \quad (4)$$

where F_n is input parameter SP and Vr, and A_n is the regression coefficients, which could be found in Ref. [29].

In order to study the arrangements of the pumps, cycle 1 is compared with cycle 3 with constant turbine efficiency and same arrangements of the turbines, as shown in **Figure 10a**. Although the condensation temperatures vary within a range, cycle 1 performs almost the same as Cycle 3, which indicating that the impact of the arrangements of the pumps on the system performance is little. The reason is that the consumed power of WF-pump 1 and WF-pump 2 is small (< 0.05 kW), which has a very little effect on the net power output.

To investigate the arrangements of the turbines, Cycle 1 is compared with Cycle 2, as shown in in **Figure 10b**. It can be seen that the net output power of Cycle 2 is always a little higher than that of Cycle 1 at different condensation temperatures, which suggests that the series compress arrangement performs better than the parallel.

Net power output of cycle 1 is compared with cycle 2 and cycle 3 with non-constant turbine efficiency, as shown in **Figure 11**. It could be found that the impact of the arrangements for

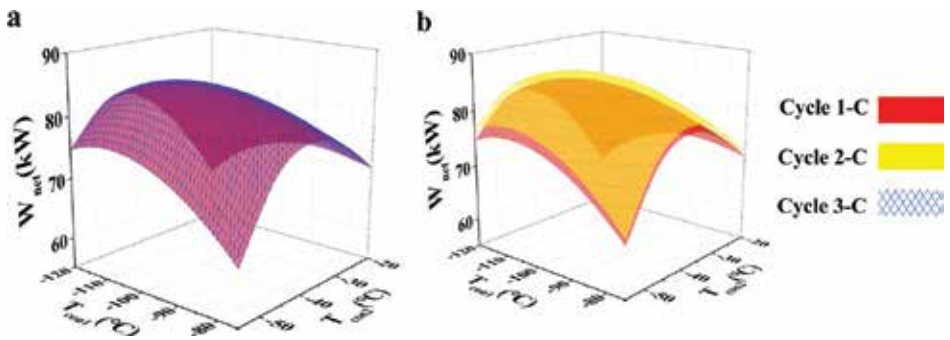

Figure 10. The comparison of the net power output between (a) cycle 1 and cycle 3, (b) cycle 1 and cycle 2 under the constant turbine efficiency.

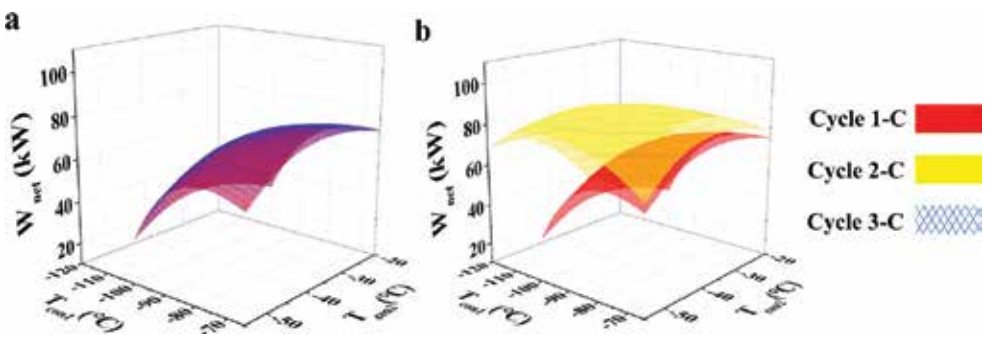

Figure 11. The comparison of the net power output between (a) cycle 1 and cycle 3, (b) cycle 1 and cycle 2 under non-constant efficiency.

pumps on the system performance is little but the influence of the arrangements for turbine is great. The series arrangement for turbines has a greater impact on the system performance than the parallel arrangement. Meanwhile, this impact for non-constant turbine efficiency is much more pronounced than that for constant turbine efficiency, with comparing **Figures 10** and **11**.

3. Optimization of working fluids

3.1. Pure working fluids

For power generation systems using LNG cold energy, the choice of working fluid has a great influence on the performance of the system. Due to the low temperature of the LNG, it is necessary to consider several aspects when selecting working fluid. Based on the previous study, this paper selects 11 kinds of working fluids, including hydrocarbons (HCs) and hydrofluorocarbons (HFCs), and the physical properties of them are shown in **Table 1**.

The evaporation temperature, the condensation temperatures and the inlet pressure of NG turbine of the two-stage condensation combined cycle are optimized with the net power output as objective function. T The maximum net power output and the critical temperatures of the 11 different pure working fluids are shown in **Figure 12**.

It can be seen from **Figure 12** that the net power output of the two-stage condensation combined cycle is the largest when n-C_5H_{12} is chosen as working fluid, and the net power output of C_2F_6 is the least. From the trend lines of the net power output and the critical temperature for 11 kinds of working fluids, it can be found that the variation trend of the net power

Working fluids	Chemical formula	Critical temperature (°C)	Critical pressure (bar)	Normal boiling point (°C)
R170	C_2H_6	32.17	48.72	−88.82
R1270	C_3H_6	91.06	45.55	−47.62
R290	C_3H_8	96.74	42.51	−42.11
—	i-C_4H_8	144.94	40.09	−7.00
R600	n-C_4H_{10}	151.98	37.96	−0.49
R601	n-C_5H_{12}	196.55	33.70	36.06
R23	CHF_3	26.14	48.32	−82.09
R134a	$C_2H_2F_4$	101.06	40.59	−26.07
R125	C_2HF_5	66.02	36.18	−48.09
R116	C_2F_6	19.88	30.48	−78.09
R218	C_3F_8	71.87	26.40	−36.79

Table 1. Physical properties of selected pure working fluids.

output is approximately the same as that of the critical temperature of working fluids. With the increase of the critical temperature, the net power output of the system increases roughly.

3.2. Mixed working fluids

In this section, 11 pure working fluids are combined to binary mixtures. With the net power output as the objective function, evaporation temperature, condensation temperatures, the inlet pressure of the NG turbine and the molar fraction of binary working fluids are optimized. When the net power output of the system is maximum, the optimized results of different binary mixtures are shown in **Figure 13**.

The gray dotted line in **Figure 13b** represents the trend line of net power output of 11 pure working fluids, and the black dotted line represents the trend line of maximum net power output in each column. From Figure b, it can be found that the optimal net power output for pure fluids changes from 2158.49 to 2712.41 kW. While the optimal net power output for mixtures distributes between 2894.47 and 3107.91 kW, which has an obvious increase than that for pure fluids and the variation range for mixtures is much smaller than that of pure fluids.

Figure 14 shows the maximum net power output of the two-stage condensation combined cycle when the component numbers of working fluids change from one to five. When the component number of mixed working fluid is five, it is actually quaternary mixture due to the results of optimization. As shown in **Figure 14**, with the increase of the component number of mixed working fluid, the net power output of the two-stage condensation combined cycle is increased, but the increase rate is gradually reduced. When the component numbers of the mixed working fluid are three and four, the net power output of the system is almost the

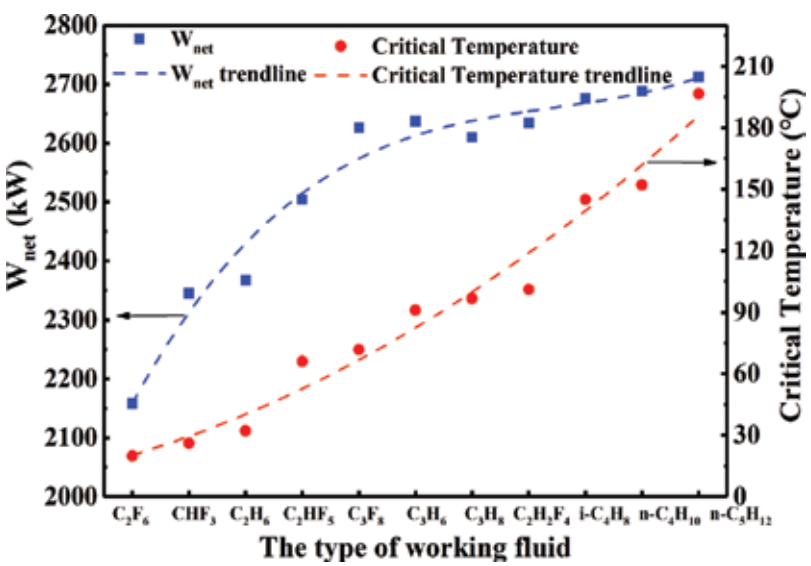

Figure 12. The maximum net power output and the critical temperature for different working fluids.

same. With the increase of the component number of mixture, the difficulty of charging working fluids into system becomes significant. Therefore, considering the increase rate of the net power output and the difficulty of charging working fluids, the optimum component number of hydrocarbon mixtures is three for the two-stage condensation combined cycle.

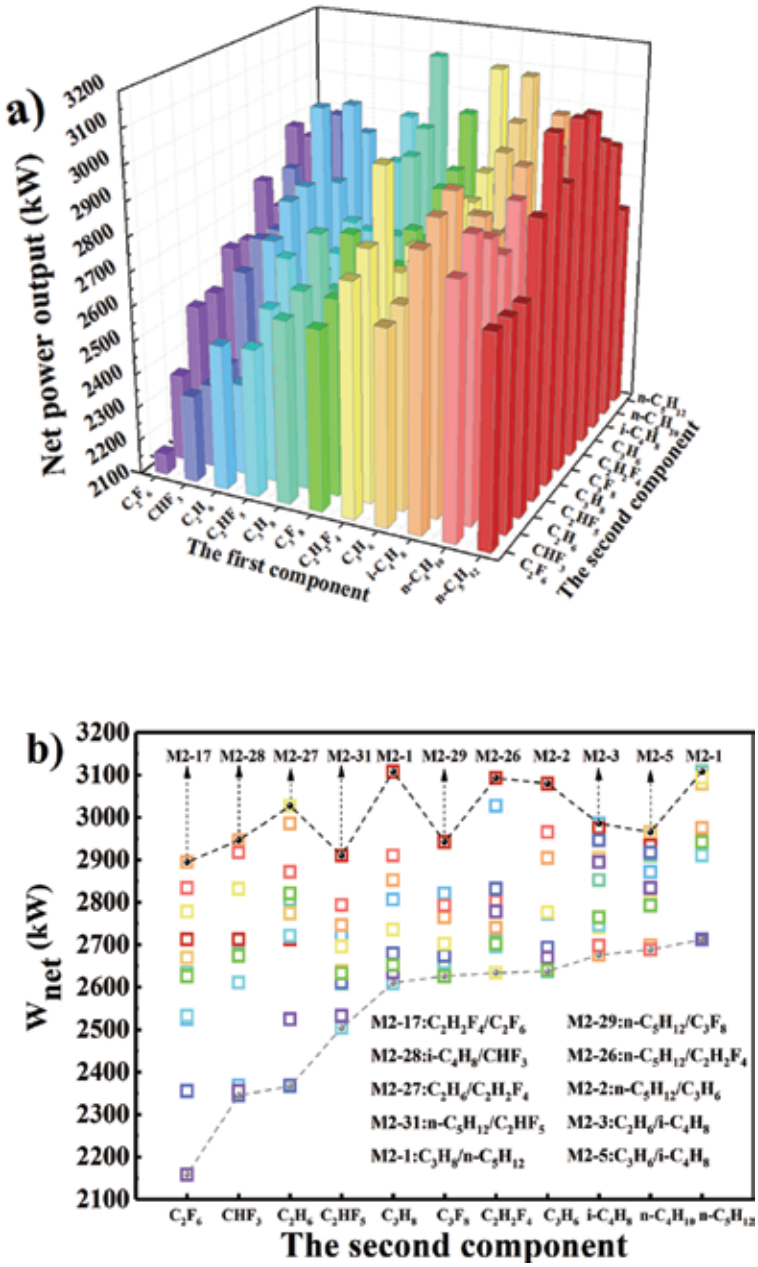

Figure 13. The maximum net power output of different pure working fluids and binary mixtures: (a) 3-D histogram and (b) 2-D diagram.

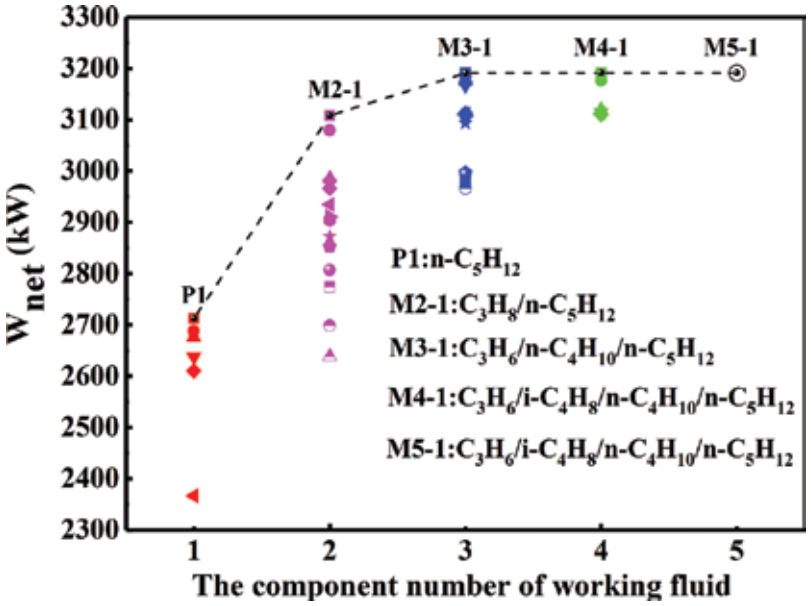

Figure 14. The net power output of the system corresponding to the mixtures with different component numbers.

3.3. A simultaneous approach to optimize the component and composition of zeotropic mixture

The traditional method of determining the components and compositions of mixtures is firstly to predefine some fluids, and then, according to the number of components, these fluids are chosen and combined as the component of mixed working fluids one by one. At last, the compositions of the formed mixtures and the corresponding system parameters are optimized at the specified system structure respectively. It is difficult to optimize the components of a

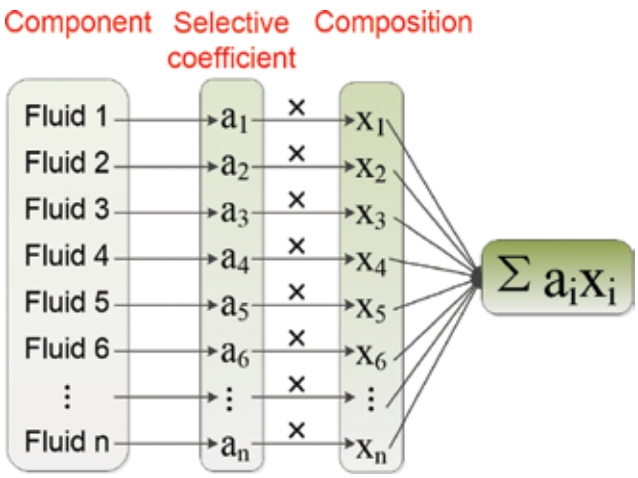

Figure 15. Basic idea for simultaneous approach to optimize component and composition of zeotropic mixture.

mixture, because the components of the mixed working fluids are independent of each other and discrete, and meanwhile it is difficult to describe them with mathematical variables. In order to reduce the intensity of calculation for components and compositions of zeotropic mixtures and achieve the simultaneous optimization of components and compositions for zeotropic mixtures, a selective coefficient a_i is introduced, as shown in **Figure 15**. Because the components of mixture are discrete, only discrete variables can be used to describe them. Each component of mixture is expressed by a selective coefficient. The selective coefficient a_i is a binary variable, and it has two values 0 or 1. When the value of selective coefficient a_i is 1, the component expressed by this selective coefficient is selected. While the value of selective

Control variables	Range	Results of pure fluid	Optimal results of binary mixture	Optimal results of ternary mixture
Ethane selective coefficient a_1	{0,1}	0	0	0
Ethylene selective coefficient a_2	{0,1}	0	0	0
Propylene selective coefficient a_3	{0,1}	0	0	1
Propane selective coefficient a_4	{0,1}	0	0	0
Butane selective coefficient a_5	{0,1}	0	0	0
Isobutane selective coefficient a_6	{0,1}	0	1	1
Pentane selective coefficient a_7	{0,1}	1	1	1
R23 selective coefficient a_8	{0,1}	0	0	0
R32 selective coefficient a_9	{0,1}	0	0	0
R41 selective coefficient a_{10}	{0,1}	0	0	0
R116 selective coefficient a_{11}	{0,1}	0	0	0
Ethane mole fraction x_1	[0,1]	0.441	0.485	0.598
Ethylene mole fraction x_2	[0,1]	0.162	0.488	0.254
Propylene mole fraction x_3	[0,1]	0.399	0.527	0.492
Propane mole fraction x_4	[0,1]	0.211	0.410	0.852
Butane mole fraction x_5	[0,1]	0.752	0.539	0.570
Isobutane mole fraction x_6	[0,1]	0.825	0.836	0.319
Pentane mole fraction x_7	[0,1]	1	0.164	0.189
R23 mole fraction x_8	[0,1]	0.622	0.734	0.494
R32 mole fraction x_9	[0,1]	0.300	0.390	0.351
R41 mole fraction x_{10}	[0,1]	0.705	0.503	0.188
R116 mole fraction x_{11}	[0,1]	0.583	0.304	0.452
Evaporation temperature x_{12} (°C)	[5,10]	6.3	10.0	10.0
First-stage condensation temperature x_{13} (°C)	[−140, −90]	−100.0	−113.9	−129.7
Second-stage condensation temperature x_{14} (°C)	[−80, −40]	−42.9	−56.2	−71.2

Table 2. The range of control variables and their optimal results in case 2.

coefficient a_i is 0, it means this component is not selected. The sum of the selective coefficient a_i is used to control the number of component for mixture. For example, binary mixture can be optimized by $\Sigma a_i = 2$. While the composition x_i of each component is the continuous variable and its value is between 0 and 1. There are no constraint conditions for composition x_i, but the total sum of compositions for all the selected components should be 1, i.e., $\Sigma a_i x_i = 1$.

Net power output is selected as the objective function, and the optimization variables include the selective coefficients of components, operation parameters of system and compositions of components. For the two-stage condensation Rankine cycle shown in **Figure 1**, the main operation parameters are evaporation temperature, the first-stage condensation temperature and the second-stage condensation temperature. The range of control variables and their optimal results are shown in **Table 2**.

Table 2 shows that the best ternary mixture is propylene/isobutane/pentane (0.492/0.319/0.189, by mole fraction), and the optimum binary mixture isobutane/pentane (0.836/0.164, by mole fraction). Pure fluid pentane is best among pure fluids.

4. Conclusions

This chapter has proposed a conception of multi-stage condensation Rankine cycle (TCRC) system. The performance of the power generation systems is enhanced by two aspects: improvement of system configuration and optimization of working fluids. Compared with the combined cycle, the net work output, thermal efficiency and exergy efficiency of the TCRC system are respectively increased by 45.27, 42.91 and 52.31%. The two-stage condensation Rankine cycle is more suitable from the viewpoint of economy. For the arrangements for compression process and expansion process of TCRC, the arrangements for pumps have little impact on the net output power and the series arrangement for turbines performs better than the parallel arrangement. With the increase of the critical temperature for pure fluids, the net power output of the system increases roughly. Zeotropic mixture can improve the performance, and the optimum component number of hydrocarbon mixtures is three for the two-stage condensation combined cycle. A simultaneous approach to optimize the component and composition of zeotropic mixture is put forward which can reduce the consumed calculation time greatly.

Acknowledgements

This research was financially supported by the National Natural Science Foundation of China (No. 51606025).

Conflict of interest

The author declared that there is no conflict of interest.

Author details

Junjiang Bao

Address all correspondence to: baojj@dlut.edu.cn

School of Petroleum and Chemical Engineering, Dalian University of Technology, Panjin, China

References

[1] Neseli MA, Ozgener O, Ozgener L. Energy and exergy analysis of electricity generation from natural gas pressure reducing stations. Energy Conversion and Management. 2015;**93**:109-120. DOI: 10.1016/j.enconman.2015.01.011

[2] Liu H, You L. Characteristics and applications of the cold heat exergy of liquefied natural gas. Energy Conversion and Management. 1999;**40**:1515-1525. DOI: 10.1016/S0196-8904(99)00046-1

[3] Fahmy M, Nabih H. Impact of ambient air temperature and heat load variation on the performance of air-cooled heat exchangers in propane cycles in LNG plants—Analytical approach. Energy Conversion and Management. 2016;**121**:22-35. DOI: 10.1016/j.enconman.2016.05.013

[4] Safaei A, Freire F, Henggeler Antunes C. Life-cycle greenhouse gas assessment of Nigerian liquefied natural gas addressing uncertainty. Environmental Science & Technology. 2015;**49**:3949-3957. DOI: 10.1021/es505435j

[5] Liu M, Lior N, Zhang N, Han W. Thermoeconomic analysis of a novel zero-CO_2-emission high-efficiency power cycle using LNG coldness. Energy Conversion and Management. 2009;**50**:2768-2781. DOI: 10.1016/j.enconman.2009.06.033

[6] Song R, Cui M, Liu J. Single and multiple objective optimization of a natural gas liquefaction process. Energy. 2017;**124**:19-28. DOI: 10.1016/j.energy.2017.02.073

[7] Zhang M-G, Zhao L-J, Liu C, Cai Y-L, Xie X-M. A combined system utilizing LNG and low-temperature waste heat energy. Applied Thermal Engineering. 2016;**101**:525-536. DOI: 10.1016/j.applthermaleng.2015.09.066

[8] Dispenza C, Dispenza G, La Rocca V, Panno G. Exergy recovery in regasification facilities–cold utilization: A modular unit. Applied Thermal Engineering. 2009;**29**:3595-3608. DOI: 10.1016/j.applthermaleng.2009.06.016

[9] Liu C, Zhang J, Xu Q, Gossage JL. Thermodynamic-analysis-based design and operation for boil-off gas flare minimization at LNG receiving terminals. Industrial & Engineering Chemistry Research. 2010;**49**:7412-7420. DOI: 10.1021/ie1008426

[10] Gómez MR, Garcia RF, Gómez JR, Carril JC. Review of thermal cycles exploiting the exergy of liquefied natural gas in the regasification process. Renewable and Sustainable Energy Reviews. 2014;**38**:781-795. DOI: 10.1016/j.rser.2014.07.029

[11] Hisazumi Y, Yamasaki Y, Sugiyama S. Proposal for a high efficiency LNG power-generation system utilizing waste heat from the combined cycle1. Applied Energy. 1998;**60**:169-182. DOI: 10.1016/S0306-2619(98)00034-8

[12] Kim C, Chang S, Ro S. Analysis of the power cycle utilizing the cold energy of LNG. International Journal of Energy Research. 1995;**19**:741-749. DOI: 10.1002/er.4440-190902

[13] Qiang W, Yanzhong L, Jiang W. Analysis of power cycle based on cold energy of liquefied natural gas and low-grade heat source. Applied thermal engineering. 2004;**24**:539-548. DOI: 10.1016/j.applthermaleng.2003.09.010

[14] Koku O, Perry S, Kim J-K. Techno-economic evaluation for the heat integration of vaporisation cold energy in natural gas processing. Applied Energy. 2014;**114**:250-261. DOI: 10.1016/j.apenergy.2013.09.066

[15] García RF, Carril JC, Gomez JR, Gomez MR. Power plant based on three series Rankine cycles combined with a direct expander using LNG cold as heat sink. Energy Conversion and Management. 2015;**101**:285-294. DOI: 10.1016/j.enconman.2015.05.051

[16] Li P, Li J, Pei G, Munir A, Ji J. A cascade organic Rankine cycle power generation system using hybrid solar energy and liquefied natural gas. Solar Energy. 2016;**127**:136-146. DOI: 10.1016/j.solener.2016.01.029

[17] Choi I-H, Lee S, Seo Y, Chang D. Analysis and optimization of cascade Rankine cycle for liquefied natural gas cold energy recovery. Energy. 2013;**61**:179-195. DOI: 10.1016/j.energy.2013.08.047

[18] Cao Y, Ren J, Sang Y, Dai Y. Thermodynamic analysis and optimization of a gas turbine and cascade CO_2 combined cycle. Energy Conversion and Management. 2017;**144**:193-204. DOI: 10.1016/j.applthermaleng.2017.07.144

[19] Wang G-B, Zhang X-R. Thermodynamic analysis of a novel pumped thermal energy storage system utilizing ambient thermal energy and LNG cold energy. Energy Conversion and Management. 2017;**148**:1248-1264. DOI: 10.1016/j.enconman.2017.06.044

[20] Zhang G, Zheng J, Yang Y, Liu W. A novel LNG cryogenic energy utilization method for inlet air cooling to improve the performance of combined cycle. Applied Energy. 2016;**179**:638-649. DOI: 10.1016/j.apenergy.2016.07.035

[21] Mosaffa A, Mokarram NH, Farshi LG. Thermo-economic analysis of combined different ORCs geothermal power plants and LNG cold energy. Geothermics. 2017;**65**:113-125. DOI: 10.1016/j.geothermics.2016.09.004

[22] Sung T, Kim KC. Thermodynamic analysis of a novel dual-loop organic Rankine cycle for engine waste heat and LNG cold. Applied Thermal Engineering. 2016;**100**:1031-1041. DOI: 10.1016/j.applthermaleng.2016.02.102

[23] Ferreira P, Catarino I, Vaz D. Thermodynamic analysis for working fluids comparison in Rankine-type cycles exploiting the cryogenic exergy in liquefied natural gas (LNG) regasification. Applied Thermal Engineering. 2017;**121**:887-896. DOI: 10.1016/j.enconman.2016.05.013

[24] Wang J, Yan Z, Wang M, Dai Y. Thermodynamic analysis and optimization of an ammonia-water power system with LNG (liquefied natural gas) as its heat sink. Energy. 2013;**50**:513-522. DOI: 10.1016/j.energy.2012.11.034

[25] Lee U, Kim K, Han C. Design and optimization of multi-component organic rankine cycle using liquefied natural gas cryogenic exergy. Energy. 2014;**77**:520-532. DOI: 10.1016/j.energy.2014.09.036

[26] Kim K, Lee U, Kim C, Han C. Design and optimization of cascade organic Rankine cycle for recovering cryogenic energy from liquefied natural gas using binary working fluid. Energy. 2015;**88**:304-313. DOI: 10.1016/j.energy.2015.05.047

[27] Modi A, Haglind F. A review of recent research on the use of zeotropic mixtures in power generation systems. Energy Conversión and Management. 2017;**138**:603-626. DOI: 10.1016/j.enconman.2017.02.032

[28] Bao J, Lin Y, Zhang R, Zhang N, He G. Effects of stage number of condensing process on the power generation systems for LNG cold energy recovery. Applied Thermal Engineering. 2017;**126**:566-582. DOI: 10.1016/j.applthermaleng.2017.07.144

[29] Macchi E, Astolfi M. Organic Rankine Cycle (ORC) Power Systems: Technologies and Applications. Woodhead Publishing, Elsevier; 2016. 313 p. DOI: 10.1016/B978-0-08-100510-1.00009-0

Chapter 9

Power Generation with Thermolytic Reverse Electrodialysis for Low-Grade Waste Heat Recovery

Deok Han Kim, Byung Ho Park, Kilsung Kwon, Longnan Li and Daejoong Kim

Additional information is available at the end of the chapter

http://dx.doi.org/10.5772/intechopen.81006

Abstract

Closed-loop reverse electrodialysis (RED) systems that use a thermolytic solution for low-grade waste heat recovery have attracted significant attention. They have several cost benefits, e.g., the absence of repetitive pretreatment and removal of locational constraints, when compared with open-loop RED systems using seawater and river water. This study presents a model of RED that uses ammonium bicarbonate, and this is a promising solution for closed-loop systems. The modified Planck-Henderson equation is used to calculate the ion exchange membrane potential. The calculation is based on the conductivity measurements as ionization carbonate electrochemical information has not been reported before this study. The solution resistance is experimentally determined. The experimentally obtained permselectivity is implemented into the model to predict the membrane potential more accurately. The results of the improved model are well matched with experimental results under results under various operating conditions of the RED system. In addition, in the model of this study, the net power density was characterized with the consideration of the pumping loss. The improved model predicts a maximum net power density of 0.84 W/m^2 with an intermembrane distance of 0.1 mm, a flow rate of 3 mL/min, and a concentration ratio of 200 as optimum conditions. The results of the study are expected to improve our understanding of the ammonium bicarbonate-RED system and contribute to modeling studies using ammonium bicarbonate or certain other compounds for novel technologies of waste heat recovery.

Keywords: reverse electrodialysis (RED), closed-loop, waste heat, ammonium bicarbonate, thermolytic solution

1. Introduction

The increase in world energy consumption has led to a significant increase in the demand for fossil fuels. The increase in fossil fuel consumption causes various problems, including global warming and climate change. The Paris climate conference underscores the collective, world-wide attention on preventing bigger disasters. Several studies have focused on lessening and replacing the consumption of fossil fuels. An emerging source is waste heat, which is not only a cause of heat pollution but also a source for generating electricity in a different way [1, 2]. There are several techniques to harness waste heat, e.g., the organic Rankine cycle (ORC) and thermoelectric power. However, there are several disadvantages for the recovery of energy by using these techniques, such as environmentally harmful refrigerants, downsizing in ORC systems, low efficiency, and poor form factor in thermoelectric elements [3–9].

The reverse electrodialysis (RED) system combined with thermal separation components could form a closed loop that harnesses the waste heat by utilizing the salinity gradient energy (SGE) [10]. RED is a power generation technique based on SGE. RED mixes of two different salinity solutions with ion exchange membranes (IEM). It includes advantage of not emitting environmentally harmful gases. It also obtains unlimited, free fuel supply in the vicinity of places where seawater and river water meet. Conversely, the accessibility to these natural resources limits its locational options. Furthermore, the high cost of maintenance of the RD stack is a challenging problem for actual implementation. Especially, the IEMs, a core component, are still exposed to fouling problems, and the fouled IEMs should be either replaced with new ones or recovered [11, 12]. These problems of RED can be overcome by combining a RED system with a thermal separation component because of its closed-loop characteristics [13–16]. The difference of salinity solution concentrations retains the electromotive force by separating the increased solute from the diluted side and recapturing it in the concentrated solution without any fresh solution supply, and thus the process is operated as a closed-loop system. The closed-loop system mitigates the geographical limitations as a continuous supply of fresh seawater (high concentration solution) and river water (low concentration solution) is not necessary, thereby preventing the possible risks of membrane fouling as well as saving pretreatment costs.

A thermolytic solution that is easily separated at a relatively low temperature is necessary for the process. Traditionally, organic and ammonia solutions are used as thermolytic solutions in waste heat recovery systems. Organic solutions, such as R-21 and R-123, have a low boiling point; however, they do not solve in water and show low osmotic efficiency [4]. Ammonia water (ammonium hydroxide) is another widely used ORC solution; however, it is corrosive, which means the damage of the materials of RED such as membranes and spacers. An ammonium bicarbonate is a promising thermolytic solution owing to its high solubility in water, large osmotic efficiency, circulation capacity, and relatively low molecular weight [17, 18]. More importantly, ammonium bicarbonate can be recovered with moderate heat, which suggests significant energy advantages compared with the regeneration of other draw solutes. Ammonium bicarbonate has low decomposition temperature, of approximately 60°C at 1 atm, and it decomposes at 120°C. Luo et al. conducted RED experiments by using an ammonium bicarbonate solution under different inlet conditions. They set different feed

solution flow rate and feed solution concentration combinations [10]. They achieved a maximum power density of 0.89 W/m^2 with an intermembrane distance of 0.3 mm and with concentrated and diluted solutions of 2 and 0.02 M, respectively [19]. Kwon and his coworkers quantitatively tested parameters such as intermembrane distances and IEM types [20]. They obtained a power density of 0.77 W/m^2 with an intermembrane distance of 0.2 mm and with concentrated and diluted solutions of 1.5 and 0.01 M, respectively. Geise et al. provided deep insights into the transport phenomena of ammonium bicarbonate through IEMs [21–24]. They analyzed the relationship between the permselectivity, membrane resistance, membrane structure, and functional groups fixed on several types of IEMs and individual ion species of the ammonium bicarbonate electrolyte.

Since 2011, the studies have focused on RED numerical simulations. Veerman et al. developed a one-dimensional numerical model for a unit cell [25]. Tedesco et al. improved the model of Veerman with respect to the previously neglected nonideal phenomena, such as concentration polarization (CP) and temperature variation, and validated a wider concentration range [26]. Kwon and his coworkers further developed the model. They applied some updated thermodynamic properties in the model, such as dielectric constant and viscosity. CP phenomena were considered in their model through the implementation with empirical equations. This upgraded model can predict the actual physics more accurately, and it enabled the calculation of higher concentration combinations. However, the calculation with bicarbonate is yet to be improved because of its complexity. Compared to a binary electrolyte (e.g., sodium chloride), it is hard to of extensively expressing the electrochemical information.

The key issue in this calculation is to predict the internal resistance and membrane potential in the system. Compared with NaCl, which is the conventional electrolyte for the RED process, the electrochemical information of ammonium bicarbonate requires the estimation of the membrane potential and internal resistance, including activity and transport number. The transportation properties of ammonium bicarbonate remain unclarified and unexplored by extant studies. A recent study estimated the membrane potential based on electrical conductivity measurements [27]. The solution resistance was computed in the range of concentration of our interest based on the definition of molar conductivity.

In this study, we performed a numerical simulation of RED power generation. The simulation was based on ammonium bicarbonate and validated through our experimental results. The permselectivity of the IEM was assumed as in previous studies [25, 26, 28]. Moreover, we measured all the properties by an experiment to predict the RED performance more precisely. Following the model validation, the optimum operating conditions of RED systems were characterized with different settings in terms of flow rate, intermembrane distance, and concentration ratio.

2. Modeling approach

A thermal-driven electrochemical generator (TDEG) is illustrated in **Figure 1**. The TDEG consists of a RED system and a separator based on thermal energy [10]. The mixed diluted

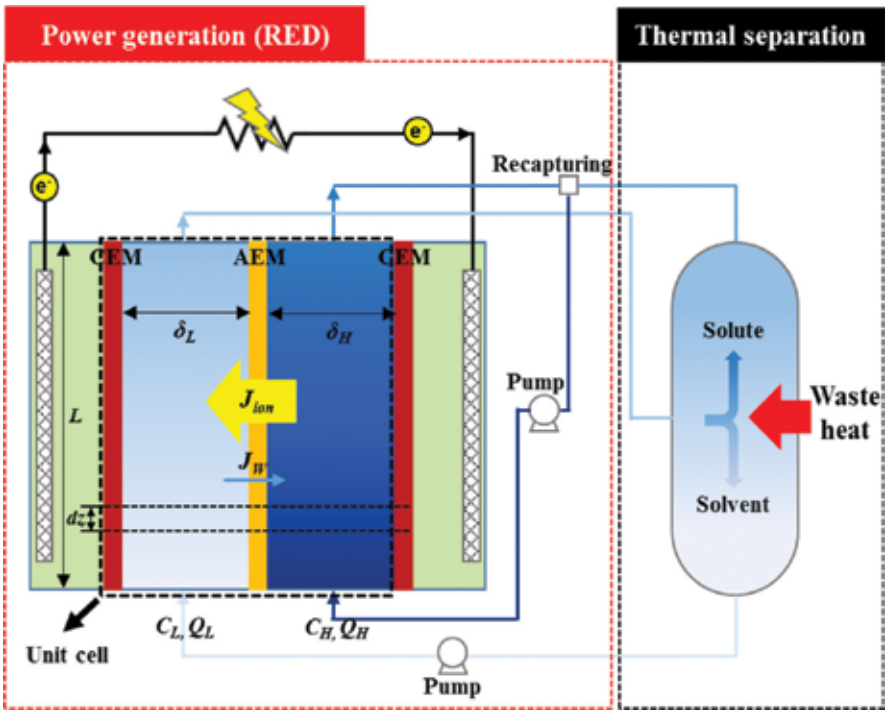

Figure 1. Schematic illustration of a TDEG. The figure on the left-hand side shows an RED single-cell model, and it has a flow length of *L*. The solution flows through the channel (thickness δ) with a flow rate of Q.

solution can be separated by applying waste heat in the separator. Then, it will be recaptured in the concentrated solution. Specifically, electricity would be generated when the high concentration and low concentration ammonium bicarbonate solutions flow through each side of the IEM. Meanwhile, ions would pass though the membrane, and the two solutions with different concentrations are mixed. Then, the flow stream would flow into a thermal separator (e.g., a distillation column). Waste heat is utilized in the thermal separator to separate the solute (NH_3 and CO_2) from the concentration flow stream. The solute from the thermal separator would be recaptured by the high concentration flow stream to form a renewed high concentration flow stream, which is supplied to the RED again. Thus, the renewed high and low concentration streams flow back to the RED stack. The concentration gradient between the different sides of the IEM is maintained. A unit cell pair in RED is composed of a concentrated solution channel, a diluted solution channel, a cation exchange membrane (CEM), and an anion exchange membrane (AEM). The solution concentrations are estimated along the channel with length *L* and width *W* in this study.

The present model was developed based on the following four assumptions [25]: (1) the resistance of the IEMs is held at a constant value; (2) the electrode potential of a stack is linearly proportional to the number of cells; (3) the effect of the electrodes at both ends of the stack is neglected; and (4) the inlet flow is uniformly distributed into each channel.

The input parameters used in the model are listed in **Table 1**.

When we consider the RED system as an electric circuit, the RED stack exhibits potential difference and internal resistance. Equation (1) shows the potential difference across an IEM between two solutions of different concentration, which is described for all ionic species present in the solution [31]:

$$V(z) = \frac{R_g T}{F} \sum_i \frac{t_i}{z_i} \ln\left(\frac{\gamma_i^H C_i^H(z)}{\gamma_i^L C_i^L(z)}\right) \quad (1)$$

Here, T denotes the temperature, R_g denotes the universal gas constant (8.314 J/mol·K), F denotes the Faraday constant (96485 C/mol), C denotes the concentration of solution, z_i denotes the valence number of ion species i, and γ denotes the activity coefficient.

The definition of ionic transport number for species i (t_i) is the ionic flux of that species divided by the overall ionic current across the IEM membrane. The electrochemical information of ammonium bicarbonate is needed when calculating equating membrane potential. This is because the equilibrium and ionization constant of ammonium bicarbonate were not clear [27]. Given that Eq. (1) is not intuitive to determine transport number and activity of

Spacer properties		
Open ratio (—)		0.56
Porosity (—)		0.74
Solution properties		
Diffusivity of ammonium bicarbonate (m^2/s) [a]		1×10^{-12}
Diffusivity of water (m^2/s)		1.2×10^{-9}[29]
IEMs' properties		
CEM	Resistance ($\Omega \cdot cm^2$) [b]	2 [23]
	Permselectivity (—)	Experiment
	Thickness (m)	120 [29]
AEM	Resistance ($\Omega \cdot cm^2$) [b]	12 [23]
	Permselectivity (—)	Experiment
	Thickness (m)	120 [29]

[a]From extant studies [26], the stack performance is not significantly affected by the diffusivity of NaCl for a wide range (two order magnitude). We verified the same tendency on an ammonium bicarbonate electrolyte for a wider range (three order magnitude), between 1×10^{-11} and 1×10^{-14} m^2/s, because of the heavier molecular weight of ammonium bicarbonate than that of NaCl [30]. Thus, the value of 1×10^{-12} m^2/s is considered as a reliable assumption.
[b]The membrane resistance was measured through the direct current (DC) method at 0.5 M ammonium bicarbonate on both sides [23].

Table 1. Input parameters used in the RED model.

ammonium bicarbonate compared with NaCl [25, 26, 30, 32], Huang et al. adopted the Planck-Henderson equation to compute the membrane potential as below [27, 31]:

$$V(z) \approx \frac{R_g T}{F} \frac{\sum \frac{|z_i| u_i}{z_i} \left[C_i^L(z) - C_i^H(z) \right]}{\sum |z_i| u_i \left[C_i^L(z) - C_i^H(z) \right]} \ln \left(\frac{\sum |z_i| u_i C_i^H(z)}{\sum |z_i| u_i C_i^L(z)} \right) \tag{2}$$

In this equation, we assume that the activity of each species is proportional to the ionic mobility (u_i) and the molar concentration (C_i). Here, we assume that the valence number of all electrolytes in the ammonium bicarbonate solution is dominantly monovalent (+1 or −1) which can be measured by the pH of the solution [27].

For the binary electrolyte, Eq. (2) is transformed into Eq. (3) by imposing the electrical conductivity described in Eq. (4) and the permselectivity of the IEM [33–39]:

$$V \approx \alpha_{IEM} \frac{R_g T}{F} \ln \left(\frac{\kappa^H}{\kappa^L} \right) \tag{3}$$

$$\kappa = F \sum |z_i| u_i C_i \tag{4}$$

The total internal resistance in the system is computed by the following Eq. (5):

$$\boldsymbol{R_{ohmic}(z) = \frac{1}{\beta} \left(R_{CEM} + R_{AEM} + \frac{\delta_H}{\Lambda_H(z) C_H(\mathbf{z})} + \frac{\delta_L}{\Lambda_L(z) C_L(\mathbf{z})} \right)} \tag{5}$$

Here, δ denotes the thickness of the channels, β denotes an open ratio of the spacer, and Λ denotes the molar conductivity of the solutions. The third and fourth terms in the right-hand side denote the resistance of the solution bodies. R_{CEM} and R_{AEM} denote the resistances of the IEMs measured by the direct current method under standard conditions [23, 39].

The previous Falkenhagen-Leist-Kelbg (FLK) equation describes the molar conductivity generally based on an NaCl solution, and here, we modified it for the case of ammonium bicarbonate [26, 32]. We utilized empirical values by using the definition of electrical conductivity of ammonium bicarbonate ($\Lambda = \kappa/C$) obtained by conductivity measurements as shown in **Figure 2**. The Arrhenius law [40] shows that if a temperature variation exists, then a new electrical conductivity profile must be established such that the electrical conductivity increases with the increase in temperature based on the Arrhenius law [40].

The current value is calculated by Ohm's law, which is based on the system voltage and resistance, as follows:

$$I(z) = \frac{V_{OC}(z)}{R_{\text{int}}(z) + R_{load}} \tag{6}$$

Here, the subscripts *int* and *load* mean the internal resistance of the cell and external resistance, respectively. The current density i is obtained by integrating $I(z)$ along the channel. Then, the

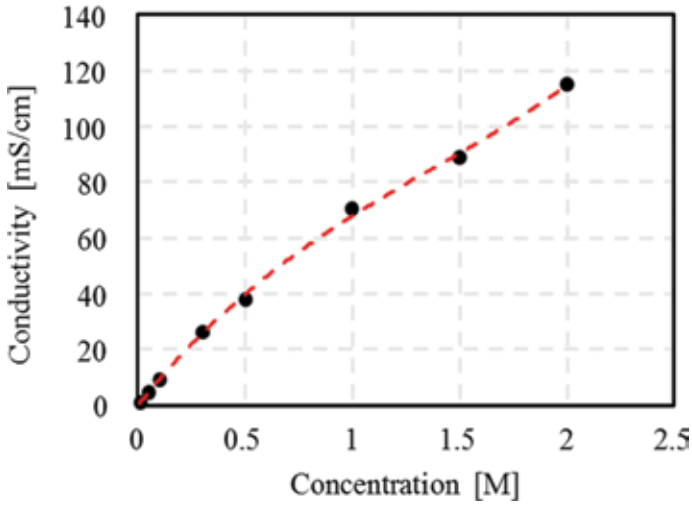

Figure 2. Electrical conductivity of ammonium bicarbonate solution for various concentrations. The red dashed line denotes a third order regression line and $R^2 = 0.99$.

current value is divided by the projecting membrane area. The factor 1/2 is related to the pair membrane area (CEM and AEM) in a cell as follows:

$$i = \frac{\sum_{z=0}^{L} I(z)dz}{2LW} \tag{7}$$

Finally, the power output and power density of the system can be calculated as Eq. (8):

$$\boldsymbol{P}(z) = \boldsymbol{I}(z)^2 \boldsymbol{R}_{load} \tag{8}$$

$$p = \frac{\sum_{z=0}^{L} P(z)dz}{2LW} \tag{9}$$

Equation (10) shows the total solute transportation (flux) in the system. The total solute flux (J_s) can be divided into two different parts. The first term of the right-hand side of the equation indicates the counter-ion transport through the membrane, and it is the coulombic part. The other term in the right-hand side shows the co-ion transport. The co-ion transport can be expressed by the diffusivity (D_{AmBi}) of ammonium bicarbonate and the ion exchange membrane thickness (h) [25]:

$$J_s(z) = \frac{i(z)}{F} + \left(\frac{D_{AmBi}}{h_{CEM}} + \frac{D_{AmBi}}{h_{AEM}} \right) \left(C_H(z) - C_L(z) \right) \tag{10}$$

Another mass transport phenomenon that happens in the system is water flux across the membrane, which is in the opposite direction owing to the osmosis [29] caused by the concentration difference across the IEM;

$$J_w(z) = -\left(\frac{D_w}{h_{CEM}} + \frac{D_w}{h_{AEM}}\right)\left(C_H(z) - C_L(z)\right) \tag{11}$$

Here, D_w denotes the water diffusivity.

The concentration profile along the flow channel is calculated by mass conservation equations for an infinitesimal control volume as follows [25]:

$$\frac{dC_H}{dz}(z) = -\frac{W}{Q_H}J_s(z) + C_H(z)\frac{W}{Q_H}J_w(z)V_w \tag{12}$$

$$\frac{dC_L}{dz}(z) = \frac{W}{Q_L}J_s(z) - C_L(z)\frac{W}{Q_L}J_w(z)V_w \tag{13}$$

Here, V_w denotes the water molar density.

First, the feed solution concentration and solution flow rate are assigned to the model as the input conditions. Second, the local electric variables are calculated. Finally, the next node concentration is obtained through Eqs. (12) and (13) with the solute and water transport. The backward finite difference approximation with a node size of $dz = L/3000$ is applied.

3. Experimental approach

3.1. Experimental setup for RED

In the experiment, instead of NaCl, ammonium bicarbonate (11213, Sigma-Aldrich) was used. **Figure 3(a)** illustrates the RED stack, which includes two electrodes combined with endplates, CEMs and AEMs, silicon gaskets, and polymer spacers. The endplates were fabricated with polymethyl methacrylate (PMMA). The electrodes combined with the endplates were fabricated by titanium and coated with iridium and ruthenium. The calibration of the membranes (CMV/AMV, Asahi glass) was performed in a 0.6 M NH_4HCO solution for more than 24 h after washed by deionized water. The RED stack consists of five cells, and the effective membrane area was 49 cm^2. The polymer spacers (PETEX 06–745/56, Sefar) were used as the channel supporter, and the vertical material exchange is precipitated in the channel to prevent forming the boundary layer. The gaskets were composed of silicone rubber sheets with a thickness of 0.3 mm. The gaskets and spacers were cut in the desired 5 M $K_4Fe(CN)_6$ (31254, Sigma-Aldrich), 0.05 M $K_3Fe(CN)_6$ (31253, Sigma-Aldrich), 0.05 $K_4Fe(CN)_6$ (31254, Sigma-Aldrich), and 0.3 M NH_4HCO_3. Those experiments were carried out at the room temperature of 25 ± 0.3°C.

Figure 3(b) shows the RED experimental setup. All the solutions were fed by peristaltic pumps (EMP-2000 W, EMS Tech). A four-wire mode cable was connected to the electrodes, and a source meter (2410, Keithley) was employed to measure the RED performance. We used polarization and power density curves to characterize the RED system electrochemical performance. We measured the terminal voltage over the stack by the galvanostat method with the

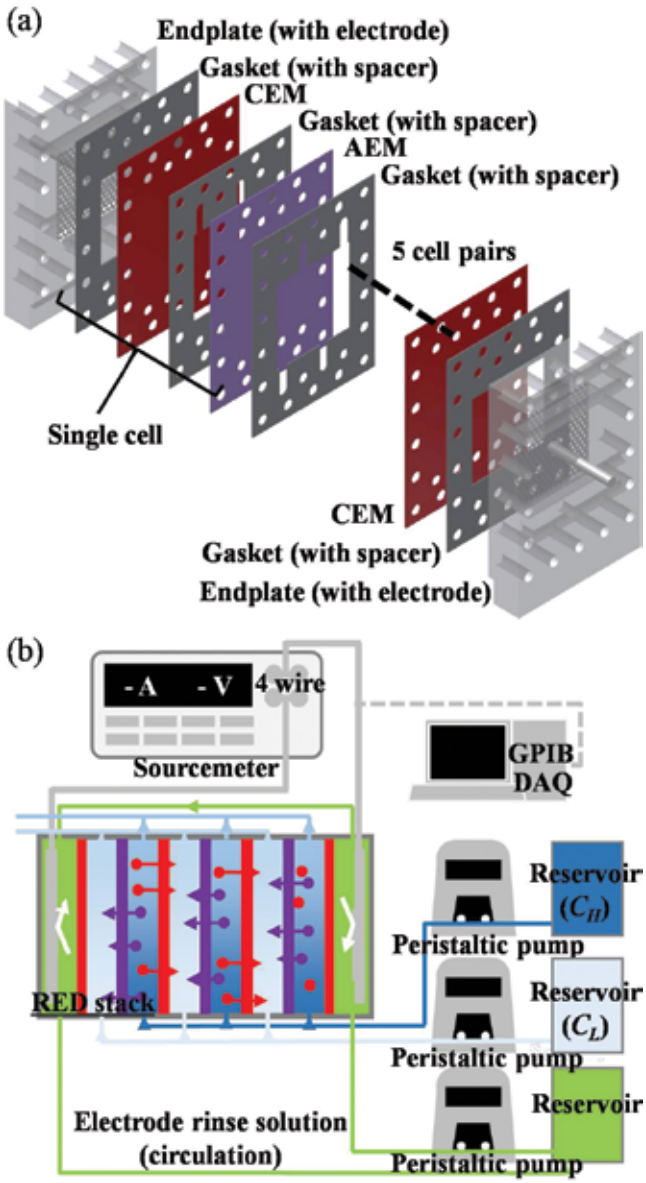

Figure 3. Schematic illustration of (a) the RED stack and (b) the RED experimental setup. The red and purple colors in the schematic indicate the cation and anion, respectively (e.g., cation or cation exchange membrane).

current variation in a step-like way of 10 mA. The power density curve is determined according to the voltage and the current density.

3.2. Membrane potential measurement

In previous studies related to the RED numerical model, permselectivity was assumed as either unity or a constant value. However, it was reported that the permselectivity of an IEM

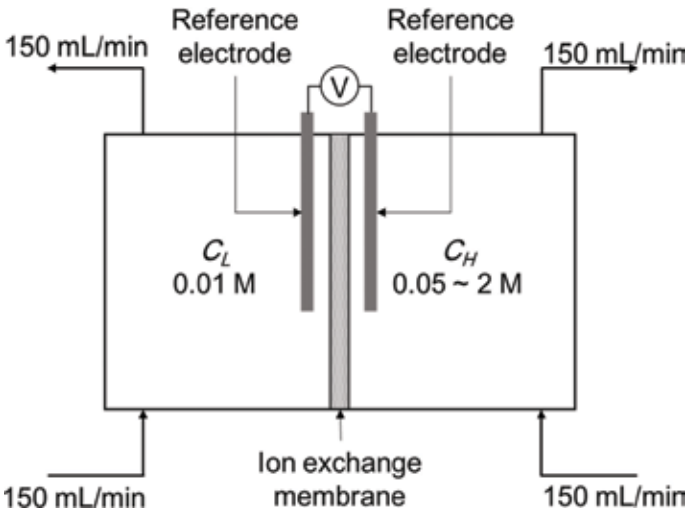

Figure 4. Schematic illustration of the experimental setup to determine the permselectivity of the IEM.

varies with different combinations of the concentrated and diluted solutions [22, 27, 36, 41]. Therefore, to predict the RED performance more precisely, we applied the actual permselectivity of the IEMs as follows.

The permselectivity is calculated by the following equation [39]:

$$\alpha = \frac{\Delta V_{actual}}{\Delta V_{theoretical}} \tag{14}$$

To calculate permselectivity, a simple experiment was needed to measure the IEM potential. **Figure 4** shows the method we used to measure permselectivity. Two reservoirs contain solutions with different concentration combinations. Two reference electrodes and an IEM are inserted between the reservoirs [42, 43]. Ag/AgCl is used as reference electrode, as it has a very low potential. The total area of the IEM was 0.785 cm^2, and the solution contained in each reservoir was 100 mL. In order to reduce the CP effect, the solutions were circulated, and the membrane potential was measured by the Ag/AgCl electrodes after 15–30 min when the system reached a steady state [39].

4. Results and discussion

4.1. Application of actual permselectivity

In **Figure 5**, the conductivity-based estimation of the membrane potential is presented with a blue line, which is calculated by Eq. (4). Here, α is set to unity. The experimental membrane potentials across each IEM are denoted as circular and triangular symbols. For each case, the

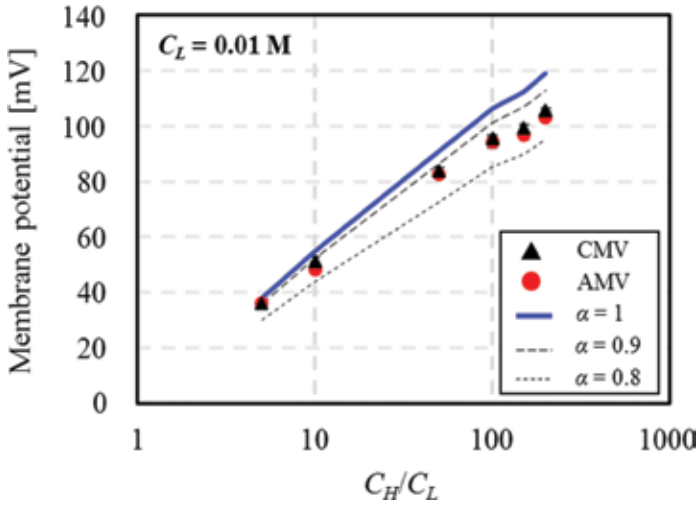

Figure 5. Comparison of the experimental membrane potential data (circular and triangular symbols) and the solution conductivity-based estimation by using Eq. (4).

concentration of the diluted solution was kept constant at 0.01 M. The concentration of the concentrated solution changed with concentration ratios of 5, 10, 50, 100, 150, and 200. The measured membrane potentials of CMV are greater than those of AMV for most cases caused by the higher constant charge density of CMV [44–46]. Calculated by Eq. (14), the permselectivity of the CMV drops from 0.952 to 0.888. Moreover, the membrane potential of AMV also monotonously decreased from 0.959 to 0.866 with an increase in concentration ratio. This tendency can be explained by two reasons. First, the concentration difference induces osmotic dwelling, which is when strong osmotic cling occurs because of high osmotic pressure between the membrane's internal solution and the bulk solution [22, 41, 47, 48]. Next, the possibility of co-ions percolation rises to a higher degree with a higher concentration ratio gradient due to an increase of the CP phenomena, and this leads to an increase at a higher concentration difference ratio [30, 41, 43]. A new data set of the permselectivity is acquired when the operating temperature varies. For the electrical conductivity, a similar way should be followed. Because the mechanism of an interaction between ions and membranes is too complexed, the effects of the temperature on the permselectivity is partly studied based on the temperature dependence of the diffusivity of each ion [49, 50].

We calculated the open circuit voltage (OCV) obtained at zero current by applying the actual permselectivity of the IEMs obtained from **Figure 5**. We compared it with the experimental data. A comparison of the OCVs between the calculation and the experiment is displayed in **Figure 6**. The red and black bars represent the simulated and measured values of the OCV, respectively. The flow rate was fixed at 10 mL/min for each cell. The tendency of the simulation results shows in good agreement with the tendency of the experimental results, although the simulation values are slightly higher in all cases. This is due to two main reasons: (1) the uniform flow distribution for the experimental case was not the same completely because of the flow stream variation due to the effect of flow inlet and outlet branches, leading to the

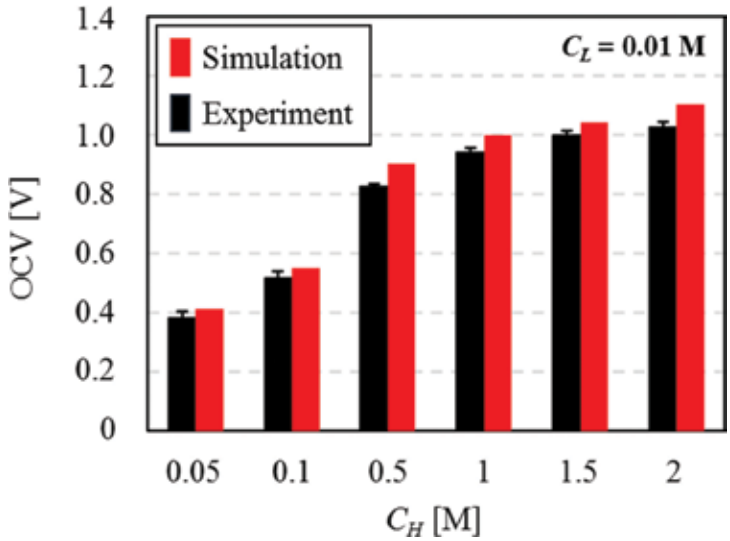

Figure 6. Comparison of the OCV obtained from the simulation and experiment.

production of additional shadow areas [32]. (2) The gaseous bubble (CO_2, NH_3) which is promoted under the room temperature degraded the system performance, while it was not considered in this study [17, 51].

Figure 7 shows the effect of actual permselectivity on RED performance when the concentrated and diluted solutions were fixed as 1 and 0.01 mol, respectively. **Figure 7(a)** and **(b)** show the polarization curves when applying actual permselectivity, and **Figure 7(c)** and **(d)** present the power density curves, calculated with $\alpha = 1$ and the experimentally obtained value $\alpha = 0.891$, respectively. The experimental result is the average of the actual permselectivity of CEM and AEM. The maximum difference of the power density between the calculated and experimental results was 0.2 W/m^2. When we considered the actual permselectivity (in the experiments), however, the gap was reduced to 0.04 W/m^2 (0.5%). Therefore, the consideration of the actual permselectivity plays a critical role in modeling the RED process with ammonium bicarbonate.

4.2. Model validation with experiments

We numerically and experimentally evaluated the power density based on the variation of concentration ratio. The evaluation results are shown in **Figure 8**. In the six cases evaluated, the concentrated solution varied, while the diluted solution was fixed as constant at 0.01 M. The intermembrane distance was 0.3 mm, and the feed flow rate was fixed as 10 mL/min for each cell. The dashed lines represent the simulation results, and the symbols represent the experimental results. When the concentrated solution was equal to or exceeded 1 M, then all the simulation results of the power density curve fall in the error bar area. However, the simulation results deviated from the error bars when the concentrated solution was 0.5 M or less. This phenomenon could be caused by the lower concentration of the concentrated solution which induces an increase of the membrane resistance [24, 52].

http://dx.doi.org/10.5772/intechopen.81006

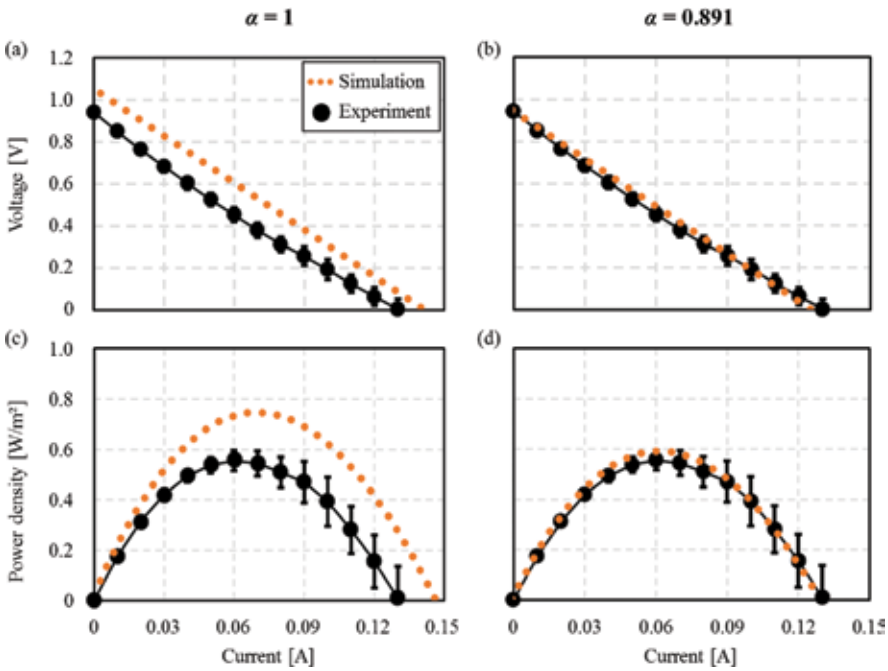

Figure 7. Polarization curves (a) and (b) and power density curves (c) and (d), with actual and ideal permselectivity of the IEM.

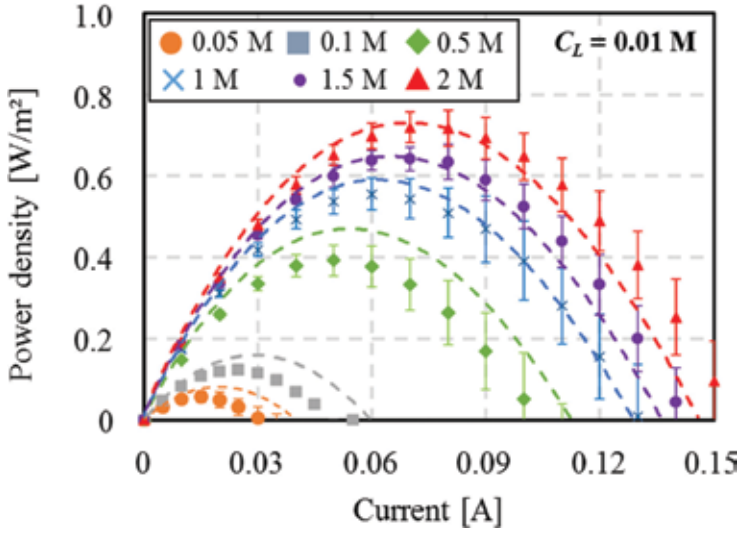

Figure 8. Power density curves with varying concentration ratios. The dashed lines denote the simulation results, and the symbols denote the experimental results.

The change time of the solution in the flow channel depends on the solution feed flow rate. This results in the change of OCV difference between the concentrated and diluted solutions. The influence of the flow rate on the RED system power density and the OCV were estimated.

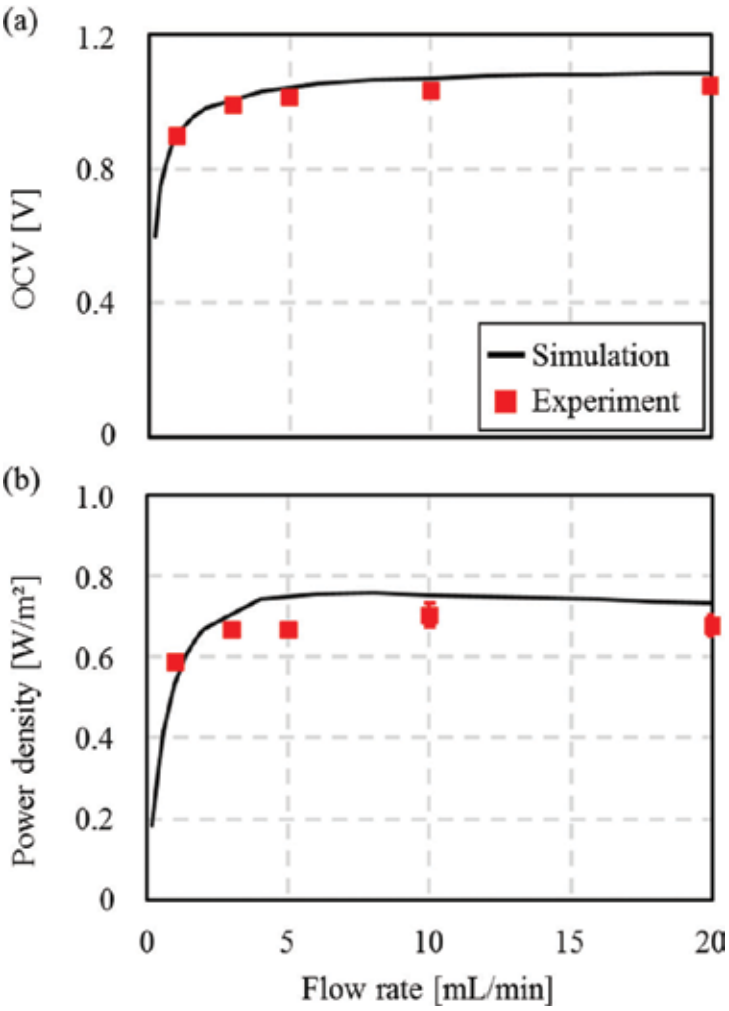

Figure 9. (a) OCV and (b) power density with varying flow rates.

The power density is given in **Figure 9(a)** where the OCV was varied with the solution flow rate simulated from 0.1 mL to 20 mL/min. The diluted and concentrated solutions were kept constant at 2 and 0.01 M, respectively. The intermembrane distance was configured at 0.3 mm. The OCV was increased rapidly below 2 mL/min. Then, it was almost saturated when the flow rate was over 5 mL/min. It shows that the calculated results quite match with the experimental ones.

Figure 9(b) shows the effect of flow rate on power density of the system. The simulation results of power density also showed a slightly different trend from that of OCV. It firstly showed a steep increase below 2 mL/min and then showed a maximum value at a flow rate value of 8 mL/min. After the power density reached a maximum value, it decreased gradually. Overall, the simulation can predict the power density trend very well.

http://dx.doi.org/10.5772/intechopen.81006

4.3. RED system performance prediction and optimization

The flow rate and the intermembrane distance terms in Eqs. (5), (12), and (13) are vital parameters of the RED system. These two parameters influence the residence time in such a way that they control the mixing rate and the internal resistance of the system. In the part, the RED performance in terms of the flow rate and the intermembrane distance was validated by using the aforementioned model. **Figure 10(a)** shows the power density relative to the intermembrane distance. The feed solution flow rate in the channel was set at a constant value of 10 mL/min. Both intermembrane distances for the two compartments were varied from 0.02 to 1 mm. The rich and lean solutions were configured at 2 and 0.01 M, respectively. When the

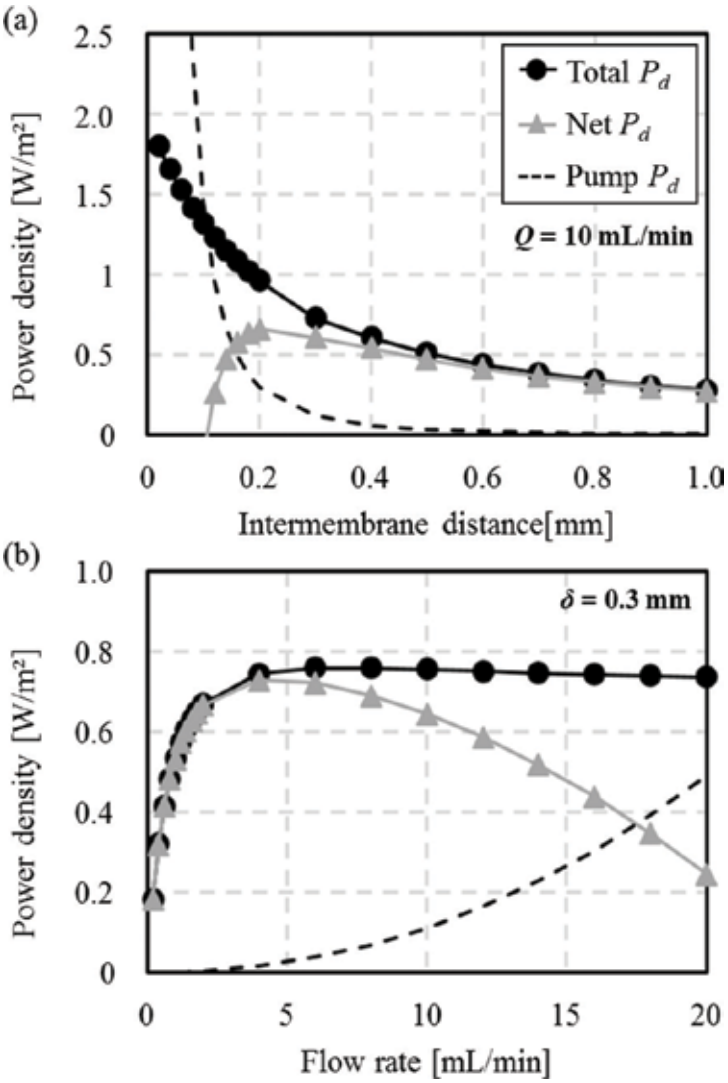

Figure 10. Three different power densities (P_d) of RED relative to (a) intermembrane distance and (b) flow rate.

intermembrane distance was less than 0.5 mm, the power density is increased evidently and arrived at 1.8 W/m^2 at an intermembrane distance of 0.02 mm.

Here, we also considered the pumping loss in the RED system. This can help us to develop the actual RED system in practice [53, 54]. The pumping loss is proportional to the pressure drop, Δp, between the inlet and outlet of the channel, while the flow rate Q is inversely proportional to the pump efficiency, η_{pump}, as listed in Eq. (15):

$$P_{pump}^{RED} = \frac{\Delta p_H Q_H^{RED} + \Delta p_L Q_L^{RED}}{\eta_{pump}} \tag{15}$$

The pumping loss can be normalized to the effective ion exchange area as Eq. (16):

$$p_{pump}^{RED} = \frac{P_{pump}^{RED}}{2LW} \tag{16}$$

The pressure drop was modeled as the well-known Darcy-Weisbach equation, which considers the effect of the spacer [54], as follows:

$$\Delta p = \frac{12\mu L^2}{0.25 d_h^2 t} \tag{17}$$

$$d_h = \frac{4n}{\left(\frac{2}{\delta}\right) + (1-n)\left(\frac{8}{\delta}\right)} \tag{18}$$

Here, μ denotes the viscosity (25°C), and d_h denotes the hydraulic diameter considering the effect of the spacer porosity n.

Figure 10(a) shows the effect of intermembrane distance on power density including the pumping loss. The pumping loss increases greatly when the intermembrane distance is smaller than 0.3 mm. We calculated the power density by subtracting the pumping loss from the total power. The net power density reached a maximum value at the intermembrane distance of 0.2 mm, and then, it was reduced to below zero at 0.1 mm. This is due to the high pumping loss. **Figure 10(b)** shows the relation between the power density and the flow rate when the intermembrane distance was specified at 0.3 mm, and the rich and lean solutions were 2 and 0.01 M, respectively. The highest power density value was 0.76 W/m^2 at a flow rate of 6 mL/min. The optimal value of 0.73 W/m^2 for the net power density was obtained at a flow rate of 4 mL/min. Afterwards, the power density decreased gradually.

Figure 11 shows the effects of the intermembrane distance (δ), the flow rate (Q), and the concentration ratio on the net power density. In this figure, the net power densities arrived their maximum values of 0.85 W/m^2 at δ = 0.1 mm and Q = 3 mL/min, 0.82 W/m^2 at δ = 0.2 mm and Q = 4 mL/min, and 0.73 W/m^2 at δ = 0.3 mm and Q = 5 mL/min.

The highest net power density is obtained when δ = 0.1 mm. The flow rate has a very important impact on the system performance due to the high pumping loss. However, it is less sensitive

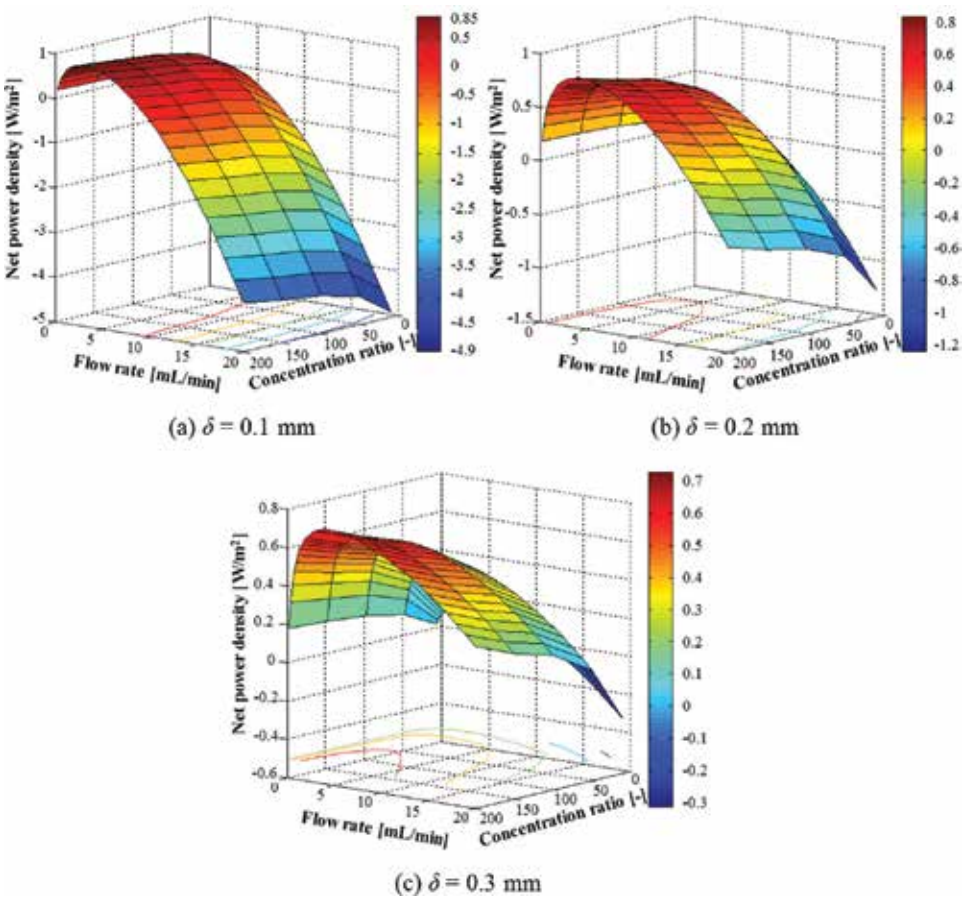

Figure 11. Optimization of net power density with changes in flow rate and concentration ratio. The intermembrane distances (δ) are (a) 0.1, (b) 0.2, and (c) 0.3 mm, and the diluted solution was fixed at 0.01 M.

to the concentration ratio. For the case of δ = 0.3 mm, the performance was less sensitive to the flow rate, whereas it was more sensitive to the concentration ratio.

5. Conclusion

An ammonium bicarbonate-based RED system operating as a closed-loop system was designed to convert low-grade waste heat into electricity. It is possible to harness a variety of waste heat such as released from industrial plants and vehicles or generated by geothermal and solar heat. In this chapter, a mathematical model for the power generation from a RED system used NH_4HCO_3 instead of NaCl. The properties of NH_4HCO_3 were used, and the activity of NH_4HCO_3 in the Nernst equation was substituted by the electrical conductivity via the Planck-Henderson equation. The molar conductivity of NH_4HCO_3 was also replaced by a calculated value. To predict the performance of the RED system, it is very important to measure the membrane potential precisely so as to obtain the actual permselectivity.

The model simulation showed an accurate estimation of the OCV within a wide range of flow rates and concentration ratios. The simulation results also fit well for power density with the experimental results relative to the various flow rates and concentration ratios. Especially, when the concentrated solution is equal to or exceeds 1 M, which is a preferable operating condition for high power generation. The difference between the simulation and experiment for the solution with lower concentration could be potentially attributed to the concentration of electrolytes, which affects the membrane resistance. The improvement in the membrane resistance model with the concentration variation is an interesting topic in order to obtain a better estimation.

We evaluated the net power density through the validated model including the pumping loss as a function of the flow rate, intermembrane distance, and concentration ratio. Consequently, the best performance for the working parameters was obtained. When we fixed the intermembrane distance at 0.1 mm and the flow rate was 3 mL/min, we obtained the highest net power density of 0.84 W/m^2 with the feed solution concentration ratio was 200 (2 M/0.01 M).

The results of this study can help to improve our understanding of the RED system with ammonium bicarbonate. This study also provides a good reference for the RED system modeling to get a higher energy density by using NH_4HCO_3 or other compounds.

Acknowledgements

The study was supported by a National Research Foundation of Korea (NRF) grant funded by the Korean government (MEST) (No. NRF-2014R1A2A2A01003618).

Nomenclature

C	solution concentration [M]
D	diffusion coefficient [m^2/s]
F	Faraday constant [96485 C/mol]
I	electric current [A]
J	molar flux [mol/m^2s]
L	length [m]
P	power [W]
Q	volumetric flow rate [mL/min]
R	resistance [Ω]
R_g	universal gas constant [8.314 J/mol·K]
T	ambient temperature [K]

V	electric voltage [V]
V_w	molar volume of water [mol/m^3]
W	width [m]
d_h	hydraulic diameter [m]
h	membrane thickness [m]
t_i	transport number of ion species i [-]
i	current density [A/m^2]
n	porosity [-]
p	power density [W/m^2]
t	residence time [s]
z_i	valence number of ion species i [-]

Greek symbols

Δp	pressure drop [Pa]
Λ	molar conductivity [S·m^2/mol]
α	permselectivity [-]
β	open ratio [-]
γ	activity coefficient [-]
δ	intermembrane distance [m]
ε	permittivity [F/m]
η_{pump}	pump efficiency [-]
μ	viscosity [Pa·s]

Subscripts

H	high concentration solution
L	low concentration solution
CEM	cation exchange membrane
AEM	anion exchange membrane

Acronyms

RED	reverse electrodialysis
$_4$Ha	Ammonium bicarbonate
ORC	organic Rankine cycle

SGE	salinity gradient energy
IEM	ion exchange membrane
CP	concentration polarization
TDEG	thermal-driven electrochemical generator
PMMA	polymethyl methacrylate
CEM	cation exchange membrane
AEM	anion exchange membrane
OCV	open circuit voltage

Author details

Deok Han Kim, Byung Ho Park, Kilsung Kwon, Longnan Li and Daejoong Kim*

*Address all correspondence to: daejoong@sogang.ac.kr

Department of Mechanical Engineering, Sogang University, Seoul, Republic of Korea

References

[1] Oluleye G, Jobson M, Smith R, Perry SJ. Evaluating the potential of process sites for waste heat recovery. Applied Energy. 2016;**161**:627-646

[2] Lu H, Price L, Zhang Q. Capturing the invisible resource: Analysis of waste heat potential in Chinese industry. Applied Energy. 2016;**161**:497-511

[3] Hung TC, Shai TY, Wang SK. A review of organic Rankine cycles (ORCs) for the recovery of low-grade waste heat. Energy. 1997;**22**:661-667

[4] Chen H, Goswami DY, Stefanakos EK. A review of thermodynamic cycles and working fluids for the conversion of low-grade heat. Renewable and Sustainable Energy Reviews. 2010;**14**:3059-3067

[5] Elsheikh MH, Shnawah DA, Sabri MFM, Said SBM, Hassan MH, Bashir MBA, et al. A review on thermoelectric renewable energy: Principle parameters that affect their performance. Renewable and Sustainable Energy Reviews. 2014;**30**:337-355

[6] Tritt TM. Thermoelectric phenomena, materials, and applications. Annual Review of Materials Research. 2011;**41**:433-448

[7] Alam H, Ramakrishna S. A review on the enhancement of figure of merit from bulk to nano-thermoelectric materials. Nano Energy. 2013;**2**:190-212

[8] Lecompte S, Huisseune H, van den Broek M, De Schampheleire S, De Paepe M. Part load based thermo-economic optimization of the organic Rankine cycle (ORC) applied to a combined heat and power (CHP) system. Applied Energy. 2013;**111**:871-881

[9] Mondejar ME, Ahlgren F, Thern M, Genrup M. Quasi-steady state simulation of an organic Rankine cycle for waste heat recovery in a passenger vessel. Applied Energy. 2016; in the press

[10] Luo X, Cao X, Mo Y, Xiao K, Zhang X, Liang P, et al. Power generation by coupling reverse electrodialysis and ammonium bicarbonate: Implication for recovery of waste heat. Electrochemistry Communications. 2012;**19**:25-28

[11] Mikhaylin S, Bazinet L. Fouling on ion-exchange membranes: Classification, characterization and strategies of prevention and control. Advances in Colloid and Interface Science. 2016;**229**:34-56

[12] Daniilidis A, Herber R, Vermaas DA. Upscale potential and financial feasibility of a reverse electrodialysis power plant. Applied Energy. 2014;**119**:257-265

[13] Logan BE, Elimelech M. Membrane-based processes for sustainable power generation using water. Nature. 2012;**488**:313-319

[14] McGinnis RL, McCutcheon JR, Elimelech M. A novel ammonia–carbon dioxide osmotic heat engine for power generation. Journal of Membrane Science. 2007;**305**:13-19

[15] Nam JY, Cusick RD, Kim Y, Logan BE. Hydrogen generation in microbial reverse-electrodialysis electrolysis cells using a heat-regenerated salt solution. Environmental Science and Technology. 2012;**46**:5240-5246

[16] Cusick RD, Kim Y, Logan BE. Energy capture from thermolytic solutions in microbial reverse-electrodialysis cells. Science. 2012;**335**:1474-1477

[17] McCutcheon JR, McGinnis RL, Elimelech M. Desalination by ammonia–carbon dioxide forward osmosis: Influence of draw and feed solution concentrations on process performance. Journal of Membrane Science. 2006;**278**:114-123

[18] McGinnis RL, Elimelech M. Energy requirements of ammonia-carbon dioxide forward osmosis desalination. Desalination. 2007;**207**:370-382

[19] Bevecqua M, Carubia A, Cipollina A, Tamburini A, Dedesco M, Micale G. Performance of a RED system with ammonium hydrogen carbonate solutions. Desalination and Water Treatment. 2016:1-12

[20] Kwon K, Park BH, Kim D. Parametric study of reverse electrodialysis using ammonium bicarbonate solution for low-grade waste heat recovery. Energy Conversion and Management. 2015;**103**:104-110

[21] Geise GM, Cassady HJ, Paul DR, Logan BE, Hickner MA. Specific ion effects on membrane potential and the permselectivity of ion exchange membranes. Physical Chemistry Chemical Physics. 2014;**16**:21673-21681

[22] Geise GM, Hickner MA, Logan BE. Ionic resistance and permselectivity tradeoffs in anion exchange membranes. ACS Applied Materials and Interfaces. 2013;**5**:10294-10301

[23] Geise GM, Hickner MA, Logan BE. Ammonium bicarbonate transport in anion exchange membranes for salinity gradient energy. ACS Macro Letters. 2013;**2**:814-817

[24] Geise M, Curtis AJ, Hatzell MC, Hickner MA, Logan BE. Salt concentration differences alter membrane resistance in reverse electrodialysis stacks. 2014:36-39

[25] Veerman J, Saakes M, Metz SJ, Harmsen GJ. Reverse electrodialysis: A validated process model for design and optimization. Chemical Engineering Journal. 2011;**166**:256-268

[26] Tedesco M, Cipollina A, Tamburini A, Bogle IDL, Micale G. A simulation tool for analysis and design of reverse electrodialysis using concentrated brines. Chemical Engineering Research and Design. 2014;**93**:441-456

[27] Huang W, Walker WS, Kim Y. Junction potentials in thermolytic reverse electrodialysis. Desalination. 2015;**369**:149-155

[28] Tedesco M, Cipollina A, Tamburini A, van Baak W, Micale G. Modelling the reverse electrodialysis process with seawater and concentrated brines. Desalination and Water Treatment. 2012:1-21

[29] Veerman J, de Jong RM, Saakes M, Metz SJ, Harmsen GJ. Reverse electrodialysis: Comparison of six commercial membrane pairs on the thermodynamic efficiency and power density. Journal of Membrane Science. 2009;**343**:7-15

[30] Baker RW. Membrane Technology and Applications. 2nd ed. John Wiley & Sons Ltd.; 2004. pp. 53-58

[31] Bard AJ, Faulkner LR. Electrochemical Methods Fundamentals and Applications. 2nd ed. John Wiley & Sons Inc; 2001. pp. 44-86

[32] Kwon K, Han J, Park BH, Shin Y, Kim D. Brine recovery using reverse electrodialysis in membrane-based desalination processes. Desalination. 2015;**362**:1-10

[33] Hong JG, Zhang W, Luo J, Chen Y. Modeling of power generation from the mixing of simulated saline and freshwater with a reverse electrodialysis system: The effect of monovalent and multivalent ions. Applied Energy. 2013;**110**:244-251

[34] Weinstein JN, Leitz FB. Electric power from differences in salinity: The dialytic battery. Science. 1976;**191**:557-559

[35] Clampitt BH, Kiviat FE. Energy recovery from saline water by means of electrochemical cells. Source. 2015;**194**:719-720

[36] Jagur-Grodzinski J, Kramer R. Novel process for direct conversion of free energy of mixing into electric power. Industrial and Engineering Chemistry Process Design and Development. 1986;**25**:443-449

[37] Veerman J, Post JW, Saakes M, Metz SJ, Harmsen GJ. Reducing power losses caused by ionic shortcut currents in reverse electrodialysis stacks by a validated model. Journal of Membrane Science. 2008;**310**:418-430

[38] Lacey RE. Energy by reverse electrodialysis. Ocean Engineering. 1980;**7**:1-47

[39] Dlugolecki P, Nymeijer K, Metz S, Wessling M. Current status of ion exchange membranes for power generation from salinity gradients. Journal of Membrane Science. 2008;**319**:214-222

[40] Vila J, Gines P, Pico JM, Franjo C, Jimenez E, Varela LM, et al. Temperature dependence of the electrical conductivity in EMIM-based ionic liquids: Evidence of Vogel–Tamman–Fulcher behavior. Fluid Phase Equilibria. 2006;**242**:141-146

[41] Hosseini SM, Madaeni SS, Khodabakhshi AR. The electrochemical characterization of ion exchange membranes in different electrolytic environments: Investigation of concentration and ph effects. Separation Science and Technology. 2012;**47**:455-462

[42] Xu T, Hu K. A simple determination of counter-ionic permselectivity in an ion exchange membrane from bi-ionic membrane potential measurements: Permselectivity of anionic species in a novel anion exchange membrane. Separation and Purification Technology. 2004;**40**:231-236

[43] Sata T. Ion exchange membrane: Preparation, characterization, modification and application. The Royal Society of Chemistry. 2004:102-104

[44] Hong JG, Zhang B, Glabman S, Uzal N, Dou X, Zhang H, et al. Potential ion exchange membranes and system performance in reverse electrodialysis for power generation: A Review. Journal of Membrane Science. 2015

[45] McCormick P, Pellegrino J, Mantovani F, Sarti G. Water, salt, and ethanol diffusion through membranes for water recovery by forward (direct) osmosis processes. Journal of Membrane Science. 2008;**325**:467-478

[46] Wenzlaff A, Boddeker KW, Hattenbach K. Pervaporation of water-ethanol through ion exchange membranes. Journal of Membrane Science. 1985;**22**:333-344

[47] Długołęcki P, Anet B, Metz SJ, Nijmeijer K, Wessling M. Transport limitations in ion exchange membranes at low salt concentrations. Journal of Membrane Science. 2010;**346**: 163-171

[48] Tuan LX, Buess-Herman C. Study of water content and microheterogeneity of CMS cation exchange membrane. Chemical Physics Letters. 2007;**434**:49-55

[49] Bastug T, Kuyucak S. Temperature dependence of the transport coefficient of ions from molecular dynamics simulations. Chemical Physics Letters. 2005;**408**:84-88

[50] Wood JA, Benneker AM, Lammertink RG. Temperature effects on the electrohydrodynamic and electrokinetic behaviour of ion-selective nanochannels. Journal of Physics: Condensed Matter. 2016;**28**:1-9

[51] Hatzell MC, Logan BE. Evaluation of flow fields on bubble removal and system performance in an ammonium bicarbonate reverse electrodialysis stack. Journal of Membrane Science. 2013;**446**:449-455

[52] Długołecki P, Ogonowski P, Metz SJ, Saakes M, Nijmeijer K, Wessling M. On the resistances of membrane, diffusion boundary layer and double layer in ion exchange membrane transport. Journal of Membrane Science. 2010;**349**:369-379

[53] Pawlowski S, Sistat P, Crespo JG, Velizarov S. Mass transfer in reverse electrodialysis: Flow entrance effects and diffusion boundary layer thickness. Journal of Membrane Science. 2014;**471**:72-83

[54] Vermaas DA, Guler E, Saakes M, Nijmeijer K. Theoretical power density from salinity gradients using reverse electrodialysis. Energy Procedia. 2012;**20**:170-184

Edited by Enhua Wang

This book on organic Rankine cycle technology presents nine chapters on research activities covering the wide range of current issues on the organic Rankine cycle. The first section deals with working fluid selection and component design. The second section is related to dynamic modeling, starting from internal combustion engines to industrial power plants. The third section discusses industrial applications of waste heat recovery, including internal combustion engines, LNG, and waste water. A comprehensive analysis of the technology and application of organic Rankine cycle systems is beyond the aim of the book. However, the content of this volume can be useful for scientists and students to broaden their knowledge of technologies and applications of organic Rankine cycle systems.

Published in London, UK

IntechOpen

ISBN 978-1-83881-773-2